

**EFFECT OF PROCESS PARAMETERS OF TUNGSTEN  
INERT GAS WELDING ON THE WELD QUALITY OF  
AUSTENITIC STAINLESS STEEL**

Thesis submitted by  
**SUBHAS CHANDRA MOI**

**Doctor of Philosophy (Engineering)**

**Mechanical Engineering Department  
Faculty Council of Engineering & Technology  
Jadavpur University  
Kolkata, India**

**2019**

**JADAVPUR UNIVERSITY  
KOLKATA-700032, INDIA**

**INDEX NO.: 292/14/E**

**1. Title of the Thesis:**

**“Effect of Process Parameters of Tungsten Inert Gas Welding on the Weld Quality of Austenitic Stainless Steel”**

**2. Name, Designation & Institution of the Supervisors:**

**Dr. Asish Bandyopadhyay**

Professor,  
Mechanical Engineering Department,  
Jadavpur University,  
Kolkata-700032  
India

**Dr. Pradip Kumar Pal**

Ex-Professor,  
Mechanical Engineering Department,  
Jadavpur University,  
Kolkata-700032  
India

**Dr. Ramesh Rudrapati**

Assistant Professor  
Mechanical Engineering Department  
Hawassa University, Hawassa – Ethiopia

**3. List of Publications:**

- I. Subhas Chandra Moi, Asish Bandyopadhyay, Pradip Kumar Pal, "Parametric Optimization of TIG Welding Process on Mechanical Properties of 316L Stainless Steel Using RSM", Advances in Materials, Mechanical and Industrial Engineering, Lecture Notes on Multidisciplinary Industrial Engineering, Springer Nature Switzerland, Chapter-15, pp. 315 - 336, 2019.

- II. S. C. Moi, R. Rudrapati, A. Bandyopadhyay, P. K. Pal, “Design Optimization of Welding Parameters for Multi-response Optimization in TIG welding Using RSM based Grey Relational Analysis”, *Advances in Computational Methods in Manufacturing, Lecture Notes on Multidisciplinary Industrial Engineering*, Springer Nature Singapore, Chapter-17, pp. 193-203, 2019.
- III. Subhas Chandra Moi, Pradip Kumar Pal, Asish Bandyopadhyay, Ramesh Rudrapati, “Determination of tungsten inert gas welding input parameters to attain maximum tensile strength of 316L austenitic stainless steel”, *Journal of Mechanical Engineering – Strojnícky časopis*, Vol. 68, No 3, pp. 231-248, 2018.
- IV. Subhas Chandra Moi, Pradip Kumar Pal, Asish Bandyopadhyay, Ramesh Rudrapati, “Effect of heat input on the mechanical and metallurgical characteristics of TIG welded joints”, *Journal of Mechanical Engineering (JMechE)*, Vol. 16(2), pp. 29-40, 2019.
- V. S. C. Moi, R. Rudrapati, A. Bandyopadhyay, P. K. Pal, “Parametric studies on TIG welding of 316L stainless steel by RSM and TLBO,” *Materials Science Forum - Trans Tech Publications*, Vol. 969, pp. 744-749, 2019.
- VI. Subhas Chandra Moi, Pradip Kumar Pal, Asish Bandyopadhyay, “Design Optimization of TIG Welding Process for AISI 316L Stainless Steel”, *International Journal of Recent Technology and Engineering (IJRTE)*, Vol. 8(2), pp. 5348-5354, 2019.
- VII. Subhas Chandra Moi, Ramesh Rudrapati, Pradip Kumar Pal, Asish Bandyopadhyay, “Analysis of impact behaviour of TIG weldment by using hybrid RSM and CSO”, *Journal of Mechanical Engineering – Strojnícky časopis*, Vol. 69, No 4, 2019. **(Accepted)**
- VIII. S. C. Moi, R. Rudrapati, P. K. Pal, A. Bandyopadhyay, “Design optimization of process parameters for tig welding of type 316l austenitic stainless steels”, *Journal of Mechanical Engineering, Bratislava* (Under Review).
- IX. S. C. Moi, R. Rudrapati, P. K. Pal, A. Bandyopadhyay, “Statistical and mathematical modeling of tungsten inert gas welding of 316L stainless steel,” *Advances in Materials and Processing Technologies*, Taylor and Fransis journal (Communicated).


#### **4. List of Patents: NIL**

## **5. List of Presentations in National/ International Conferences:**

- I. S. C. Moi, P. K. Pal, A. Bandyopadhyay, “Optimization of TIG welding process parameters on tensile properties of 316l stainless steel using RSM”, INCOM18: Proceedings of the 1<sup>st</sup> International Conference on Mechanical Engineering, Jadavpur University, Kolkata, India, January 4 - 6, 2018, pp 468-472.

**DEPARTMENT OF MECHANICAL ENGINEERING**  
**FACULTY OF ENGINEERING & TECHNOLOGY**  
**JADAVPUR UNIVERSITY**  
**KOLKATA, INDIA**


*This is to certify that the thesis entitled "Effect of Process Parameters of Tungsten Inert Gas Welding on the Weld Quality of Austenitic Stainless Steel" submitted by Shri Subhas Chandra Moi, who got his name registered on 9<sup>th</sup> April, 2014 for the award of Ph.D. (Engineering) degree of Jadavpur University is absolutely based upon his own work under the supervision of Prof. Asish Bandyopadhyay, Prof. Pradiip Kumar Pal and Dr. Ramesh Rudrapati, that neither his thesis nor any part of the thesis has been submitted for any degree/ diploma or any other academic award any where before.*



14/5/19

---

**Prof. Asish Bandyopadhyay**  
Professor,  
Mechanical Engineering Department  
Jadavpur University, Kolkata, India



14-5-19

---

**Prof. Pradiip Kumar Pal**  
Ex-Professor,  
Mechanical Engineering Department  
Jadavpur University, Kolkata, India

Professor  
Dept. of Mechanical Engineering  
Jadavpur University, Kolkata-32



**Dr. RAMESH RUDRAPATI**  
ASSISTANT PROFESSOR  
MECHANICAL ENGG DEPT  
HAWASSA UNIVERSITY  
ETHIOPIA

EX-Professor  
Dept. of Mechanical Engineering  
Jadavpur University, Kolkata-32

---

**Dr. Ramesh Rudrapati**  
Assistant Professor,  
Department of Mechanical Engineering  
Hawassa University, Hawassa - Ethiopia

# Acknowledgement

---

Pursuing Ph.D. work is both painful and enjoyable experience. It's just like climbing a high peak, step by step, accompanied with bitterness, hardships, frustration, encouragement, trust and with so many people's kind help. When author found himself at the top enjoying the beautiful scenery, he has realized that it is, in fact, teamwork that gets him there. Though it will not be enough to express his gratitude in words to all those people who helped him, author would still like to convey his many, many thanks to all these people.

First of all, the author feels great pleasure in expressing his sincere gratitude towards his thesis supervisors, Dr. Asish Bandyopadhyay, Professor, Mechanical Engineering Department, Jadavpur University, Kolkata; Dr. Pradip Kumar Pal, Ex-Professor, Mechanical Engineering Department, Jadavpur University, Kolkata and Dr. Ramesh Rudrapati, Assistant Professor, Mechanical Engineering Department, Hawassa University, Hawassa-Ethiopia, for their invaluable guidance, suggestions and encouragement provided throughout the period of this thesis work.

The author is indebted to Dr. Gautam Nandi and Dr. Sanjib Acharya, faculty members of Mechanical Engineering Department, Jadavpur University, for their invaluable help and advice to this thesis work from time to time.

The author is grateful to Prof. Gautam Mazumdar, The Head, Mechanical Engineering Department, Jadavpur University for giving encouragement for completing this thesis work. The author expresses special thanks to Dr. Dipankar Bose, faculty member and Tapas Pal, staff member of Mechanical Engineering Department, National Institute of Technical Teachers Training and Research, Kolkata, West Bengal, for their unconditional help and support from time to time.

Moreover, author would like to thank all the researchers in this field whose published literatures have greatly helped him in getting an insight towards the experimental work and acquire a lot of knowledge from these publications.

The author feels that the thesis would not have been completed without the efforts rendered by Shri Pradip Kumar Pal, FFDA Laboratory, Jadavpur University, Shri Rabindra Nath Bose, staff member of Mechanical Engineering Department, Jadavpur University. The author would like to convey thanks to Dr. Nikhil Kumar, Ex-Research Fellow of Mechanical Engineering Department, Jadavpur University for his constant support and help.

Next, I would also like to express my gratitude to Dr. Prosenjit Das, Sr. Scientist, Dr. Sudip Kumar Samanta, Sr. Principal Scientist and Sk. Tanbir Islam, Technical Assistant of CSIR-

Central Mechanical Engineering Research Institute, Durgapur, West Bengal for their unconditional support and help for all the time.

Finally, last but certainly not the least, the author gratefully recalls his beloved parents and brother for their valuable inspiration and support. The author would like to thank to his wife and son for their patience and constant support without which this work couldn't be completed.

*Subhas Chandra Moi*

*Dedicated To My Loving Parents*



## SYNOPSIS

Welding is a versatile means of metal fabrication process. Selecting suitable welding technique with appropriate levels of the input process parameters is the primary goal for any welding practitioner for obtaining the desired quality of the joint with cost effectiveness.

Tungsten inert gas (TIG) welding is one of the efficient joining techniques and it is very often used for the joining of the austenitic stainless steels and other types of steels, due to its capability to create high quality weld joints with excellent mechanical properties and bead appearance. Austenitic stainless steels have excellent mechanical properties and used for making different industrial components. The austenitic stainless steel possesses good mechanical properties: formability, ductility and weldability, toughness, corrosion resistance and high tensile strength at elevated temperature which are desired for various industrial applications like nuclear industry, baseline for the jackets of the 'cable-in-conduit' conductors, ship building, food processing, petrochemical, storage tanks, pressure cups, furnace equipments, etc.

The performance of TIG welding depends on the proper selection of input parameters, because like other welding techniques, it is also a multi factor fabrication technique. There are many factors which can vary/may be varied during the process and each of the factors may influence the quality of the weld. Some of the factors may influence very significantly and some not so very significantly. So, selection of welding process parameters can play crucial role to obtain desired weld joint quality and joint quality is assessed in terms of characteristics like joint strength, hardness, ductility, bending strength, impact properties, endurance limit under fatigue condition, etc.. Thus, each of the various welding techniques need to be studied and is being studied still by the investigators. Directly or indirectly all such studies aim at achieving the desired characteristics of the welded joint and controlling the process in such a way that the intended level of quality is attained. The literature survey done in the present context, illustrates the same, and points towards the fact that more is to be investigated, analyzed, learnt in respect of various aspects of welding so the control of the process becomes easier and predictive – producing the joint characteristics as demanded by the user.

All the points mentioned above are true and applicable for TIG welding of stainless steel, also. Though welding of stainless steel is not a new or emerging area of research, the specific problems related to welding of stainless steel – their various grades, and finally, control of the process parameters and the process to achieve the desired results remain a challenge to the researchers, and to the persons directly engaged in fabrication/welding of stainless steel components and structures. This becomes evident from the literature survey which indicates that people are still searching for more precise control of the process with predictive results.

Extensive research, covering wide ranges of different factors – directing towards various aspects, by many investigators – will ultimately create a reliable, precise data bank and knowledge accumulation. Further, use of different optimization techniques for same field in manufacturing by various researchers requires to be converged by analysis of the results coming out from different optimization approaches, which can only be possible through continued research.

Study of TIG welding of austenitic stainless steel under varied input parameters is still an important and useful area of research. Various aspects are involved in this respect. Work has indeed been done to some extent, by the researchers, each emphasizing or considering certain specific aspects. Study involving a wider range of aspects may prove to be challenging: for example study and analysis of individual and interaction effects of the input parameters on various respects including response to fatigue loading, responses like bending characteristics, hardness at different zones, weld width, ultimate tensile strength, yield strength, percentage elongation and impact strength. Process optimization, mathematical modeling, microstructural study and analysis at varied welding conditions may also be added in the same study.

In the present study, therefore, the effects of TIG welding process parameters such as welding current, welding speed and gas flow rate on the weld joint quality of 316L austenitic stainless steel have been investigated. Experimental runs have been conducted by a semi automatic TIG welding machine to make square butt welded joints, as per Box-behnken design method of response surface methodology (RSM). After welding the quality of the weld has been judged by visual observation and by X-ray radiography test. Then tensile test, impact test, micro-hardness test, bending test, measurements of weld width and microstructural study have been conducted. In so far tensile test is concerned, both notched tensile test and un-notched/smooth tensile test have been performed. Welding quality responses: ultimate tensile strength (UTS), percentage elongation (PE), yield strength (YS), impact strength (IS), hardness (VHN) and weld width (WW) have been measured for all the welded samples. Further, tensile fracture surfaces of base metal and welded specimens have been analyzed by SEM fractography.

Parametric analysis has been made to identify the influences of the selected input welding parameters on weld responses using statistical analysis of variance (ANOVA) and graphical main and interaction plots. Mathematical modeling of welding responses has been made to develop the mathematical relationships between the input welding variables with each weld response separately with the use of RSM. Two-dimensional contour plots have been made to identify individual and interaction effects of process parameters on output responses (UTS, PE, YS, IS, WW and hardness).

The objective of the study also includes parametric optimization of the TIG welding process for improving the weld joint quality characteristics. In this regard teaching learning-based optimization (TLBO) and desirability function approach (DFA) are used. The optimal parametric conditions are obtained by TLBO for maximization of UTS, PE, YS, IS and hardness, and minimization of weld width separately. Multi-objective optimization for all the responses has been done by grey relational analysis technique. Grey relational grade, compromising all the response characteristics, has been developed. Mathematical model has also been developed to predict the relations between the grey relational grade and input welding parameters by RSM. Parametric optimization has been done for maximizing the GRG (which compromises UTS, PE, YS, IS, hardness and WW) by solving the obtained mathematical models with the use of TLBO and DFA. Comparative analysis has also been made between the optimum welding conditions obtained for predicting welding responses separately and combinedly from two optimization approaches: TLBO and DFA. Confirmatory tests have also been conducted to validate the responses obtained from said optimization techniques.

Further, high cycle fatigue behaviour of the TIG welded joint has been tested, and test result is compared with that of the base material. The relevant plots: S-N curves are generated.

Finally based on the experimental results, their interpretations, discussion and analyses, some useful conclusions are drawn. These can be considered as contributions from the present work.

Few representative figures corresponding to some of the results are shown here:

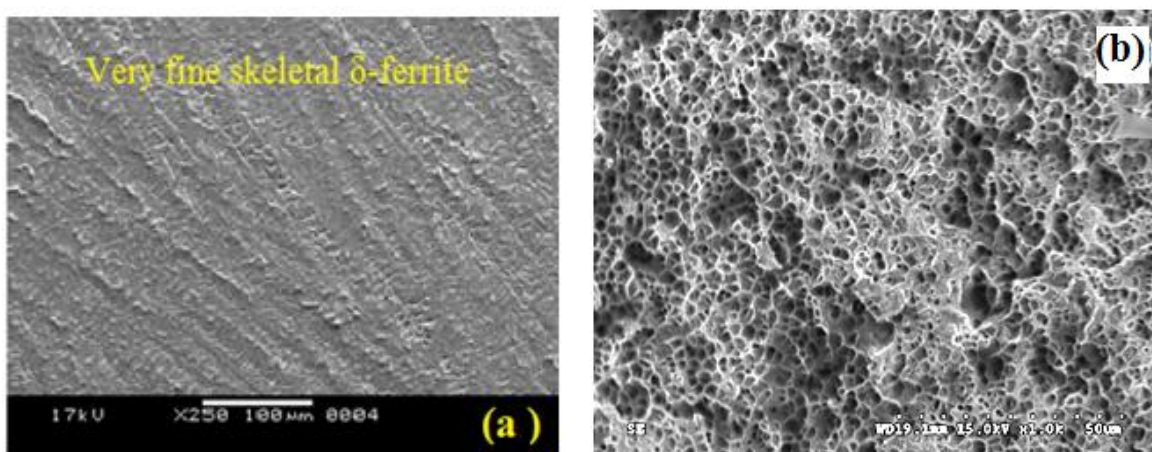


**Fig. 1:** SEM micrographs of one welded specimen: (a) microstructure of weld zone, (b) tensile fracture surface

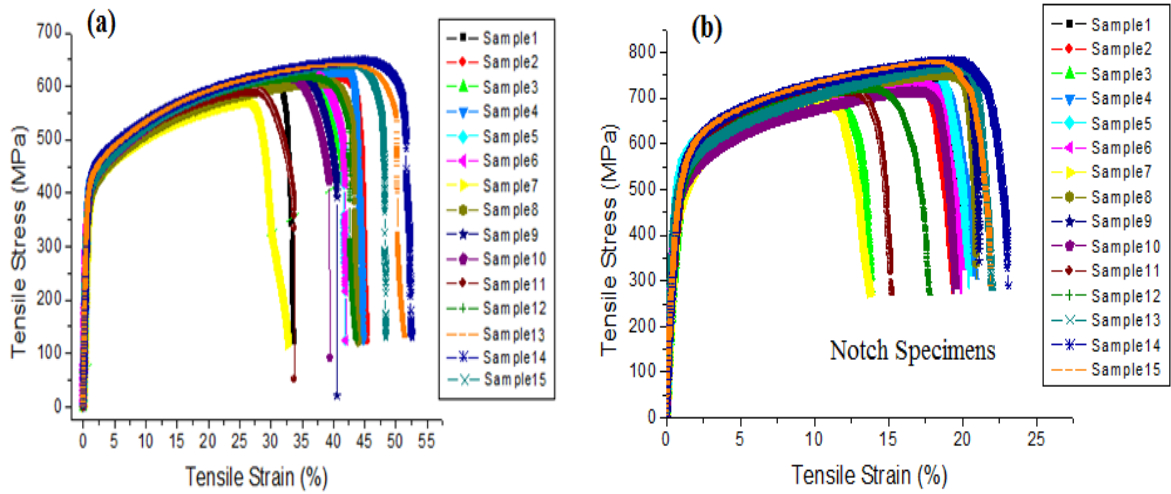


**Fig. 2:** Stress-strain curves (a) for un-notched/smooth specimens (b) for notched specimens

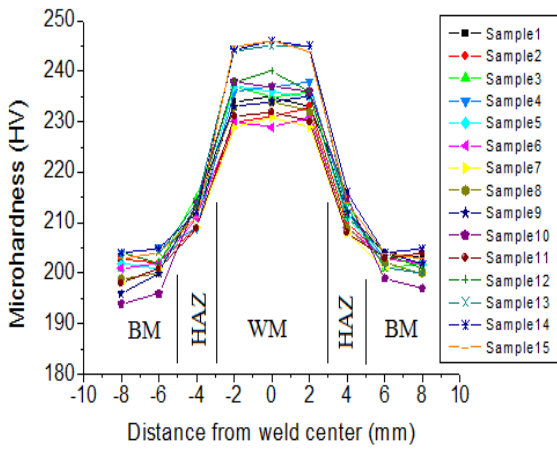


**Fig. 3:** Micro hardness profile of all samples

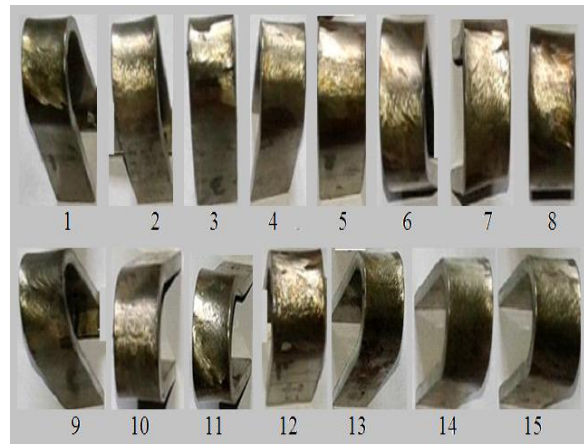


**Fig.4:** Results of bending test

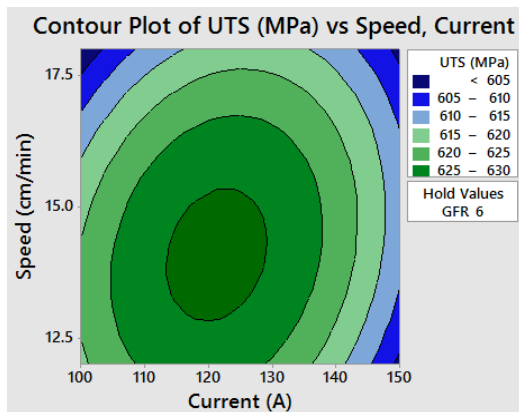


**Fig. 5:** Contour plots of UTS, Speed vs Current

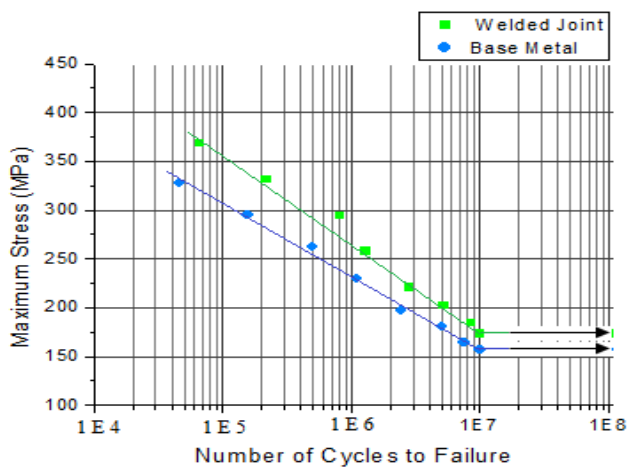


**Fig. 6:** S-N curves for welded joint and base metal

# Table of Contents

---

	<b>Page No.</b>
List of Publications and Presentations from the Thesis	i
Certificate of supervisors'	iv
Acknowledgement	v
Dedication	vii
Synopsis	viii
Table of Contents	xii
List of Figures	xvi
List of Tables	xx
<b>Chapter 1: INTRODUCTION</b>	<b>1</b>
1.1. Tungsten Inert Gas Welding	4
1.2. Types of TIG welding Techniques	7
1.3. TIG Welding System	7
1.4. Input Process Parameters of TIG welding	12
1.5. Output responses of TIG welding	13
1.6. Applications of TIG Welding	14
1.7. TIG Welding of Austenitic Stainless Steels	14
1.8. Microstructure analysis	15
1.9. Design of Experiments	15
1.9.1. Major approaches in design of experiments	15
1.10. Optimization Techniques	17
1.10.1. Desirable function Approach (DFA)	17
1.10.2. Teaching and learning based optimization (TLBO)	17
1.10.3. Grey relational analysis (GRA)	17
1.11. Literature Review	18
1.12. Motivation and objective of the present work	26
<b>Chapter 2: FUNDAMENTALS OF DESIGN OF EXPERIMENT, DATA ANALYSIS AND OPTIMIZATION TECHNIQUES</b>	<b>29</b>
2.1. Some Basic Features of Experimental Design	29
2.2. Step-by-Step Procedure in the Effective Design of an Experiment	30
2.3. Major Approaches to Design of Experiments	31
2.3.1. Factorial design	31
2.3.2. Taguchi method	32
2.3.3. Response surface methodology	32

2.3.4. Analysis of Variance	33
2.4. Optimization techniques for Solving Mathematical Models	35
2.4.1. Teaching learning-based optimization (TLBO)	35
2.4.2. Desirability function analysis (DFA)	37
2.4.3. Grey relational theory	38
2.4.3.1 Grey relational analysis	39
<b>Chapter 3: EXPERIMENTAL PLAN, SETUP AND PROCEDURE</b>	<b>41</b>
3.1. Composition of the Base Material and Filler Material	41
3.2. Input Process Parameters	41
3.3. Response Parameters	42
3.4. Experimental Setup and Procedure	42
3.5. X- Ray Radiography Test	44
3.6. Measurement of weld width	46
3.7. Metallographic Analysis	47
3.8. Micro-hardness Test	48
3.9. Tensile Test	50
3.10. Impact Test	51
3.11. Bending test	52
3.12. Fatigue test	53
<b>Chapter 4: RESULTS AND DISCUSSION</b>	<b>55</b>
4.1. Results and Discussion of Non destructive and Destructive Tests	56
4.1.1. Visual Inspection	56
4.1.2. X-Ray Radiography Test	57
4.1.3. Micro structural analysis	60
4.1.4. Micro hardness Analysis	65
4.1.5. Tensile Behaviour	69
4.1.6. Impact toughness	72
4.1.7. Bending test	73
4.2. Optimization of UTS, PE, YS, IS, VHN and WW for TIG welding of 316L austenitic stainless steel	74
4.2.1. Factor analysis, modeling and optimization of UTS	74
4.2.1.1. Main and interaction effects for UTS	74
4.2.1.2. Mathematical modeling for UTS	75
4.2.1.3. Analysis of variance for UTS	75
4.2.1.4. Model Validation	76
4.2.1.5. Effect of the Parameters on UTS	77
4.2.1.6. Optimization of UTS by TLBO	79
4.2.1.7. Optimization of UTS by DFA	80

4.2.2. Factor analysis, modeling and optimization of PE	80
4.2.2.1. Main and interaction effects for PE	80
4.2.2.2. Mathematical modeling for PE	81
4.2.2.3. Analysis of variance for PE	82
4.2.2.4. Model Validation	82
4.2.2.5. Effect of the Parameters on PE	83
4.2.2.6. Optimization of PE by TLBO	85
4.2.2.7. Optimization of PE by DFA	85
4.2.3. Factor analysis, modeling and optimization of YS	86
4.2.3.1. Main and interaction effects for YS	86
4.2.3.2. Mathematical modeling for YS	87
4.2.3.3. Analysis of variance for YS	87
4.2.3.4. Model Validation	88
4.2.3.5. Effect of the Parameters on YS	88
4.2.3.6. Optimization of YS by TLBO	90
4.2.3.7. Optimization of YS by DFA	90
4.2.4. Factor analysis, modeling and optimization of IS	91
4.2.4.1. Main and interaction effects for IS	91
4.2.4.2. Mathematical modeling for IS	92
4.2.4.3. Analysis of variance for IS	92
4.2.4.4. Model Validation	93
4.2.4.5. Effect of the Parameters on IS	94
4.2.4.6. Optimization of IS by TLBO	96
4.2.4.7. Optimization of IS by DFA	96
4.2.5. Factor analysis, modeling and optimization of hardness	96
4.2.5.1. Main and interaction effects for hardness	96
4.2.5.2. Mathematical modeling for hardness	98
4.2.5.3. Analysis of variance for hardness	98
4.2.5.4. Model Validation	99
4.2.5.5. Effect of the Parameters on hardness	99
4.2.5.6. Optimization of hardness by TLBO	101
4.2.5.7. Optimization of hardness by DFA	101
4.2.6. Factor analysis, modeling and optimization of WW	102
4.2.6.1. Main and interaction effects for WW	102
4.2.6.2. Mathematical modeling for WW	103
4.2.6.3. Analysis of variance for WW	103
4.2.6.4. Model Validation	104
4.2.6.5. Effect of the Parameters on WW	105
4.2.6.6. Optimization of WW by TLBO	107
4.2.6.7. Optimization of WW by DFA	107

4.2.7. Comparative analysis between the optimum welding conditions obtained by TLBO and DFA	107
4.2.8. Confirmatory tests	108
4.3. Multi-objective optimization for TIG welding of austenitic stainless steel	108
4.3.1. Grey relational analysis	108
4.3.2. Factor analysis, modeling and optimization of grey relational grade	109
4.3.2.1. Main and interaction effects for GRG	109
4.3.3.2. Mathematical modeling for GRG	111
4.3.3.3. Analysis of variance for GRG	112
4.3.3.4. Model Validation	113
4.3.3.5. Effect of the Parameters on GRG	113
4.3.4. Optimization by TLBO	114
4.3.5. Optimization by DFA	114
4.3.6. Confirmatory test	115
4.4. Fatigue test of TIG welded joint at optimum parametric condition	116
<b>Chapter 5: CONCLUSIONS AND FUTURE SCOPE OF WORK</b>	<b>123</b>
5.1. Conclusions	123
5.2. Future Scope of Work	127
<b>REFERENCES</b>	<b>129</b>
<b>Appendix-A</b>	<b>143</b>
<b>Appendix-B</b>	<b>145</b>



# List of Figures

---

	<b>Page No</b>
<b>Fig. 1.1:</b> Principle of tungsten inert gas welding	5
<b>Fig. 1.2:</b> Schematic diagram showing the inverter principle of the power sources	8
<b>Fig. 1.3:</b> Three different polarities in TIG welding	9
<b>Fig. 2.1:</b> Flow chart of the teaching learning based optimization (TLBO)	37
<b>Fig. 3.1:</b> Photographic view of experimental setup	44
<b>Fig. 3.2:</b> Schematic diagram of a typical exposure arrangement for X-ray radiography	45
<b>Fig. 3.3:</b> Photographic view of Tool Maker's Microscope	46
<b>Fig. 3.4:</b> Weld bead geometry	47
<b>Fig. 3.5:</b> Semi-automatic polisher and mounted sample after polish	47
<b>Fig. 3.6:</b> Optical microscope	48
<b>Fig. 3.7:</b> Scanning electron microscope	48
<b>Fig. 3.8:</b> Schematic diagram showing positions of micro hardness measurement	49
<b>Fig. 3.9:</b> Micro hardness setup	49
<b>Fig. 3.10:</b> TIG welded sample for tensile test (a) notched specimen (b) smooth specimen	50
<b>Fig. 3.11:</b> Universal testing machine	51
<b>Fig. 3.12:</b> Impact tester machine	52
<b>Fig. 3.13:</b> Impact test specimen	52
<b>Fig. 3.14:</b> TIG welded sample for bending test	53
<b>Fig. 3.15:</b> Bending Tests in Universal Testing Machine	53
<b>Fig. 3.16:</b> Fatigue test specimen	54
<b>Fig. 3.17:</b> Fatigue testing machine	54
<b>Fig. 4.1:</b> Photographic view of welded sample number 1 & 14	57
<b>Fig. 4.2:</b> Image of the X-ray radiography plate (a) sample-14 and (b) sample-7	58
<b>Fig. 4.3:</b> Microstructure of base metal (a) optical microscopy, (b) SEM	60
<b>Fig. 4.4:</b> Optical microstructures of TIG welded joints - (a) sample no.1 (b) sample no.2 (c) sample no. 3 (d) sample no 4 and $a_1, b_1, c_1, d_1$ corresponding weld metals.	61
<b>Fig. 4.5:</b> Optical microstructures of TIG welded joints - (a) sample no. 5 (b) sample no.6 (c) sample no. 7 (d) sample no. 8 and $a_1, b_1, c_1, d_1$ corresponding weld metals	63
<b>Fig. 4.6:</b> Optical microstructures of TIG welded joints - (a) sample no. 9 (b) sample no.10 (c) sample no. 11 (d) sample no. 12 and $a_1, b_1, c_1, d_1$ corresponding weld metals	64
<b>Fig. 4.7:</b> Optical microstructures of TIG welded joints - (a) sample no. 13 (b) sample no.14 (c) sample no. 15 and $a_1, b_1, c_1$ corresponding weld metals	65
<b>Fig. 4.8:</b> SEM micrographs of TIG welded specimens - (a) sample no. 14	

(b) sample no.7 (c) sample no. 2 and a <sub>1</sub> , b <sub>1</sub> , c <sub>1</sub> corresponding weld metals	66
<b>Fig. 4.9:</b> Micro hardness profile of Sample no. 1 to Sample no. 8	67
<b>Fig. 4.10:</b> Micro hardness profile of Sample no. 9 to Sample no. 15	68
<b>Fig. 4.11:</b> Micro hardness profile of all the samples in one frame	69
<b>Fig. 4.12:</b> Stress-strain curves for unnotched specimens of welded samples	70
<b>Fig. 4.13:</b> Stress-strain curves for notched specimens of welded samples	71
<b>Fig. 4.14:</b> Stress-strain curves for notched and unnotched specimens of BM & WM	71
<b>Fig. 4.15:</b> SEM fractograph of tensile fracture surfaces of base metal and welded samples (a) base metal (b) sample no.14 (c) sample no. 7 (d) sample no. 2	72
<b>Fig. 4.16:</b> Typical impact tested welded samples	73
<b>Fig. 4.17:</b> Bend test results of weldments of AISI 316L	73
<b>Fig. 4.18:</b> Main effect plots for UTS	74
<b>Fig. 4.19:</b> Interaction effect plots for UTS	75
<b>Fig. 4.20:</b> Plot of predicted vs. actual results of UTS	77
<b>Fig. 4.21:</b> Contour plots showing combined effects of speed and current on UTS, while GFR hold at a) 6 l/min b) 9 l/min and c) 12 l/min	78
<b>Fig. 4.22:</b> Contour plots showing combined effects of GFR and current on UTS, while speed hold at a) 12 cm/min b) 15 cm/min and c) 18 cm/min	78
<b>Fig. 4.23:</b> Contour plots showing combined effects of GFR and speed on UTS, while current hold at a) 100A b) 125A and c) 150A	79
<b>Fig. 4.24:</b> Optimization plot for UTS	80
<b>Fig. 4.25:</b> Main effect plots for PE	81
<b>Fig. 4.26:</b> Interaction effect plots for PE	81
<b>Fig. 4.27:</b> Plot of predicted vs. actual results of PE	83
<b>Fig. 4.28:</b> Contour plots showing combined effects of speed and current on PE, while GFR hold at a) 6 l/min b) 9 l/min and c) 12 l/min	84
<b>Fig. 4.29:</b> Contour plots showing combined effects of GFR and current on PE, while speed hold at a) 12 cm/min b) 15 cm/min and c) 18 cm/min	84
<b>Fig. 4.30:</b> Contour plots showing combined effects of GFR and speed on PE, while current hold at a) 100A b) 125A and c) 150A	85
<b>Fig. 4.31:</b> Optimization plot for PE	85
<b>Fig. 4.32:</b> Main effect plots for YS	86
<b>Fig. 4.33:</b> Interaction effect plots for YS	86
<b>Fig. 4.34:</b> Plot of predicted vs. actual results of YS	88
<b>Fig. 4.35:</b> Contour plots showing combined effects of speed and current on YS, while GFR hold at a) 6 l/min b) 9 l/min and c) 12 l/min	89
<b>Fig. 4.36:</b> Contour plots showing combined effects of GFR and current on YS, while speed hold at a) 12 cm/min b) 15 cm/min and c) 18 cm/min	89
<b>Fig. 4.37:</b> Contour plots showing combined effects of GFR and speed on YS, while current hold at a) 100A b) 125A and c) 150A	90

<b>Fig. 4.38:</b> Optimization plot for YS	91
<b>Fig. 4.39:</b> Main effect plots for IS	91
<b>Fig. 4.40:</b> Interaction effect plots for IS	92
<b>Fig. 4.41:</b> Plot of predicted vs. actual results of IS	93
<b>Fig. 4.42:</b> Contour plots showing combined effects of speed and current on IS, while GFR hold at a) 6 l/min b) 9 l/min and c) 12 l/min	94
<b>Fig. 4.43:</b> Contour plots showing combined effects of GFR and current on IS, while speed hold at a) 12 cm/min b) 15 cm/min and c) 18 cm/min	95
<b>Fig. 4.44:</b> Contour plots showing combined effects of GFR and speed on IS, while current hold at a) 100A b) 125A and c) 150A	95
<b>Fig. 4.45:</b> Optimization plot for IS	96
<b>Fig. 4.46:</b> Main effect plot for hardness	97
<b>Fig. 4.47:</b> Interaction effects plot for hardness	97
<b>Fig. 4.48:</b> Plot of predicted vs. actual results of hardness	99
<b>Fig. 4.49:</b> Contour plots showing combined effects of speed and current on Hardness, while GFR hold at a) 6 l/min b) 9 l/min and c) 12 l/min	100
<b>Fig. 4.50:</b> Contour plots showing combined effects of GFR and current on Hardness, while speed hold at a) 12 cm/min b) 15 cm/min and c) 18 cm/min	100
<b>Fig. 4.51:</b> Contour plots showing combined effects of GFR and speed on Hardness, while current hold at a) 100A b) 125A and c) 150A	101
<b>Fig. 4.52</b> Optimization plot for hardness	102
<b>Fig. 4.53:</b> Main effect plots for weld width	102
<b>Fig. 4.54:</b> Interaction effect plots for weld width	103
<b>Fig. 4.55:</b> Plot of predicted vs. actual results of WW	104
<b>Fig. 4.56:</b> Contour plots showing combined effects of speed and current on WW, while GFR hold at a) 6 l/min b) 9 l/min and c) 12 l/min	105
<b>Fig. 4.57:</b> Contour plots showing combined effects of GFR and current on WW, while speed hold at a) 12 cm/min b) 15 cm/min and c) 18 cm/min	106
<b>Fig. 4.58:</b> Contour plots showing combined effects of GFR and speed on WW, while current hold at a) 100A b) 125A and c) 150A	106
<b>Fig. 4.59:</b> Optimization plot for WW	107
<b>Fig. 4.60:</b> Main effect plots for GRG	111
<b>Fig. 4.61:</b> Interaction effect plots for GRG	111
<b>Fig. 4.62:</b> predicted vs. actual plot of GRG	113
<b>Fig. 4.63:</b> Contour plots showing combined effects of speed and current on GRG, while GFR hold at a) 6 l/min b) 9 l/min and c) 12 l/min	113
<b>Fig. 4.64:</b> Contour plots showing combined effects of GFR and current on GRG, while speed hold at a) 12 cm/min b) 15 cm/min and c) 18 cm/min	114
<b>Fig. 4.65:</b> Contour plots showing combined effects of GFR and speed on GRG, while current hold at a) 100 A b) 125 A and c) 150 A	114
<b>Fig. 4.66:</b> Optimization plot for GRG	115

<b>Fig. 4.67:</b> S-N curve of welded joint and base metal	118
<b>Fig. 4.68:</b> SEM fractographs showing the fatigue damaged region at different maximum applied stress (a) 184.1MPa (b) 257.74MPa (c) 368.2MPa.	119
<b>Fig. 4.69:</b> Fracture surface morphology of base metal at 164MPa (a) crack initiation (b) crack propagation	120
<b>Fig. 4.70:</b> Fracture surface morphology of welded joint at 184.1MPa (a) crack initiation (b) crack propagation and (c) rapid crack growth before rupture	120
<b>Fig. 4.71:</b> Fracture surface morphology of welded joint at 257.74MPa (a) crack initiation (b) crack propagation and (c) rapid crack growth before rupture	121
<b>Fig. 4.72:</b> Fracture surface morphology of welded joint at 368.2MP (a) crack initiation area (b) & (c) fatigue striation.	122

# List of Tables

---

	<b>Page No.</b>
<b>Table 1.1:</b> Various arc welding processes	6
<b>Table 1.2:</b> Comparison of Shielding Gases	11
<b>Table 3.1:</b> Composition of the base material and filler material	41
<b>Table 3.2:</b> Mechanical properties of base material	42
<b>Table 3.3:</b> TIG welding parameters and theirs levels	43
<b>Table 3.4:</b> Experimental design matrix as per RSM	43
<b>Table 4.1:</b> Results of visual inspection	57
<b>Table 4.2:</b> Results of X-ray radiography test	58
<b>Table 4.3:</b> Measured experimental results	59
<b>Table 4.4:</b> Chemical composition of weld metal	65
<b>Table 4.5:</b> Result of tensile test	70
<b>Table 4.6:</b> Analysis of variance for UTS	76
<b>Table 4.7:</b> Analysis of Variance for PE	82
<b>Table 4.8:</b> Analysis of Variance for YS	87
<b>Table 4.9:</b> Analysis of Variance for IS	93
<b>Table 4.10:</b> Analysis of Variance for Hardness	98
<b>Table 4.11:</b> Analysis of Variance for WW	104
<b>Table 4.12:</b> Obtained optimum TIG welding conditions for all responses by TLBO and DFA	108
<b>Table 4.13:</b> Grey relational generations	109
<b>Table 4.14:</b> Values of $\Delta 0_i$	110
<b>Table 4.15:</b> Grey relational coefficients, grade and ordering	110
<b>Table 4.16:</b> Analysis of Variance for GRG	112
<b>Table 4.17:</b> optimized values of GRG by TLBO and DFA	115
<b>Table 4.18:</b> Multi-objective optimization results	115
<b>Table 4.19:</b> Optimization validation test results	116
<b>Table 4.20:</b> Tensile properties of base metal and its welded joint	117
<b>Table 4.21:</b> Experimental results of fatigue test of welded joint	117
<b>Table 4.22:</b> Experimental results of fatigue test of base metal	118

### **1. INTRODUCTION**

The manufacturing industries are growing quite rapidly for creating components or engineering systems to impart desired combination of properties to the material to perform the intended function in its expected working life. The manufacturing processes involve turning of raw material into finished material (i.e. products) which are intended to be used for some useful purposes. The important manufacturing processes are metal forming, metal cutting, metal joining, etc. These manufacturing processes are applied on raw materials to create variety of parts; but, selection of manufacturing technique is depending on the complexity of geometry of the component and the number of parts to be made, properties of the materials, accuracy of the job etc.

Within the last decades the focus was given to create complex shape parts by joining / welding materials which can withstand ever increasing stresses, temperature, impact strength [1] etc. Welding is well recognized technique all over the world, today as a remarkable versatile means of metal fabrication and repairing purpose of similar or dissimilar materials together permanently with or without application of heat, pressure and filler material [2] ranging from simple constructions to complex systems with high safety requirements. Welding process is efficient, economical and dependable as a means of joining metals [3, 125]. Welding may be performed in air, underwater and space. There are a number of well-established welding processes, but arc welding is still the most popular and widely used welding process among the others, because, of high welding quality, high stability in welding of variety of metals for various industrial applications like ships, bridges, building structures, automobiles, guide way for trains, [4, 5] etc. The most widely used arc welding processes are:

Shielded metal arc (SMA) welding

Tungsten inert gas (TIG) welding

Metal inert gas (MIG) welding and

Submerged arc welding (SAW)

Normally, arc welding process is a very complex operation, as it deals with enormously high temperatures. As a result, it produces severe distortions and high levels of residual stresses, which causes fracture, buckling, corrosion and other type of failures [6, 126]. The primary goal of any welding operation is to make a weldment having the same mechanical properties as the base metal. This may be obtained by protecting the molten weld pool from the atmospheric contamination. In case of gas shielded arc welding, an inert gas is used for shielding the molten weld pool and as a result a strong joint is produced.

TIG welding is basically, an electric arc welding operation which uses non-consumable tungsten electrode, and arc is established between the tip of an electrode and the work piece.

Inert gas (argon, helium etc.) is used to avoid contamination of the weldment with air. It is one of the most widely used technique for joining similar and dissimilar metals compared to other welding processes, due to its capability to create high quality weld joints with excellent mechanical properties and bead appearance [7]. TIG welding process is extensively used in the modern industries such as automobile industry, aircraft, nuclear industry food processing industry, precision manufacturing industry etc. [8]. The quality levels of the weldment can be assessed by various quality performances like bead geometric parameters such as penetration, width and height, deposition efficiency (i.e. ratio of weight of metal deposited to the weight of electrode consumed) and mechanical properties which include hardness, tensile strength, bending strength fatigue strength, [9, 127] etc. Therefore, the proper choice of welding process parameters and its levels are very crucial for obtaining better qualities of welded joint [10, 11]. TIG welding is commonly used method for welding of materials such as stainless steel, mild steel, aluminium, titanium [12] etc.

Stainless steels are consist of a group of high-alloy steels based on the Fe-Cr, Fe-Cr-C and Fe-Cr-Ni systems with minimum of 10.5 wt% chromium content [13, 128]. This level of chromium is sufficient to allow formation of a passive surface oxide to prevent metals from oxidation and corrosion under ambient, noncorrosive conditions [14]. Stainless steels have been becoming good choice for many industrial applications [15] like automobile, marine, naval, pipe, automotive exhaust gas system, chemical industrial equipment, equipment's for power plants [16, 17] etc., due to its quality characteristics like good corrosion resistance, wide range of strength levels, fair formability, aesthetically pleasing appearance etc., compared to traditional materials. In many of the mentioned applications needs joining of stainless-steel materials to make complex parts or desired combinations for usage of various purposes. Almost all stainless steels are weldable with special procedures (if required). But there are significant variations in the weld metal and heat-affected zone microstructure relative to the base materials.

Stainless steels are primarily characterized based on the metallurgical phases, which are predominant. Three phases occur in stainless steels namely martensite, ferrite and austenite. Austenitic stainless steel is the most useful group of stainless steels and it is produced in higher tonnages than any other group. Oil, gas, petrochemical, and nuclear industry employ these materials in many of their equipment because of its non-magnetic material having good corrosion resistance in most environments, formability, ductility and weldability, as well as excellent toughness with high strength [18]. The austenitic stainless steels possess good strength at room temperature. Elements that promote the formation of austenite phase, most notably nickel, are added to these steels in large quantities (generally over 8% by Wt.). Other austenite-promoting elements in stainless steel are C and Cu.

There are a large variety of austenitic stainless steels available, but the 300 series alloys are the oldest and frequently used. Most of these alloys are made based on the 18 Cr - 8 Ni systems, with additional alloying elements or modifications to provide unique/enhanced properties [19].

The austenitic stainless steels type 316LN possesses good mechanical properties: high strength, good corrosion resistance, high ductility and good toughness at low temperatures [20] which desired for various industrial applications like nuclear industry, baseline for the jackets of the 'cable-in-conduit conductors, ship building, food processing and petrochemical [21]. Type 316L is an extra-low carbon version of austenitic chromium nickel stainless steel containing molybdenum that increases corrosion resistance, improves resistance to pitting from chloride ion solutions and provides increased strength at elevated temperatures [22]. The extra low carbon minimizes harmful carbide precipitation due to welding. Austenitic stainless steel is widely using for many industrial applications such as structural support and containment, architectural uses, kitchen equipment, medical products etc. Hence, in the present study austenitic stainless steel has been chosen as a work material.

Today's manufacturing world is consistently trying to achieve a consistent weld quality of the joined parts. Thus, the real challenge lies in control of the process parameters involved which governs the quality of welding [23]. However, TIG welding of austenitic stainless steel, AISI 316L is difficult task, due to corrosion and crack formation resistance. The stainless steel 316L has distinct properties, cheaper cost compared to other steel grades [24] and welding of it is an important area of research. Several aspects need to be explored broadly to develop a sound "knowledge-base" in this area.

In the present work, TIG welding of AISI 316L austenitic stainless steel by varying input process parameters has been investigated through experiments, analysis and optimization. The output responses: ultimate tensile strength (UTS), percentage elongation (PE), yield strength (YS), impact strength (IS), hardness (VHN) and weld width are selected for investigate the welded joint. Higher the better criterion has selected for UTS, PE, YS, IS and hardness (VHN), as maximization of these responses is desired for welded joint. Lower the better criterion is selected for weld width, as minimum weld width is desired for welded joint.

Box-Behnken design of response surface methodology (RSM) and analysis of variance (ANOVA) technique have been utilized for experimentation and analyses of the UTS, PE, YS, IS, hardness and weld width for TIG welding type 316L austenitic stainless steel. Graphical main and interaction plots are also drawn to illustrate the effects of input process parameters on output quality performances. Mathematical modeling has also been addressed for both the responses individually by using response surface methodology (RSM). Direct and interaction effects of process variables on output responses are studied by response contour plots drawn by using RSM approach. Parametric optimization of the TIG welding has also been addressed for each of the responses to predict individually, with use of two different optimization techniques: desirability function approach and teaching learning-based optimization (TLBO) technique. Multi-responses are converted in to single response (Grey relational grade, GRG) by using Grey relational analysis (GRA). Again, mathematical modeling is done between process parameters and GRG. Main and interaction effects plots and contour plots used to determine the significance of input parameters on GRG.



Optimization techniques DFA and TLBO used to solve the mathematical equation of GRG to optimize all the welding responses (UTS, PE, YS, IS, hardness and WW) combinedly. Comparative analysis has also been made among the optimum welding conditions for each responses obtained from DFA and TLBO, to select best optimum welding condition.

Further, high cycle fatigue behaviour of the TIG welded joint (prepared using obtained optimized parametric condition) has been tested, and test result is compared with that of the base material. The relevant plots: S-N curves are generated.

The analysis made in the present work takes into account of the optimization of the process conditions in relation to above mentioned welding responses. The ultimate aim in any manufacturing process is to get the desired output at the least time and at the least expense. This is true even for welding process; to make the process efficient and at the same time economic, the input parameters have to be adjusted. To achieve that, the impact of the parameters and the intensity of impact of each parameter on the output responses have to be understood properly. The trial and error methods can be avoided in future if the variation trends are known properly. The present study is intended to add the knowledge base in TIG welding. So, the process can be controlled more precisely to obtain good weld joint qualities during welding.

## **1.1. Tungsten Inert Gas Welding**

Tungsten inert gas welding, also known as Heliarc tungsten inert gas welding process that was discovered during the Second World War due to the need of the American Aircraft Industry for a technique of joining magnesium and aluminum. Russell Meredith first demonstrated the TIG welding process for the welding of magnesium using a Tungsten electrode and helium as a shielding gas in the late 1930's. This joining technique replaced riveting as a method of building aircraft with aluminum and magnesium components. The heliarc welding has continued to this day with many refinements and name changes, like active TIG welding (A-TIG), dual shield GTAW, guided GTAW, keyhole GTAW and laser-GTAW hybrid processes, but with no change in the fundamentals demonstrated by Meredith. Plasma arc welding also has its origins in the TIG welding process.

In the tungsten inert gas welding, work piece materials are combined together by heating them by an electric arc established between a non-consumable tungsten electrode and the work piece. A filler metal may or may not be used depending upon the joint design. The welding zone including molten metal, tungsten electrode and filler metal is shielded by a stream of inert gas through the welding torch and protects it from the atmosphere contamination. The inert gases normally used in this process are argon and helium. Sometimes a mixture of these gases is also used. The resulting welds have the same chemical integrity as the original base metal. The basic principle of TIG welding process is schematically shown in **Fig. 1.1**.

TIG welding can be done in any welding position and in any modes like manual, semiautomatic and automatic. And it is purely dependent on the availability of the equipment and the type of application. Manual tungsten inert gas welding is a moderately complicated welding method, due to the requirement of high degree of operator skill. Normally in manual TIG welding process requires two hands, since most applications require a filler metal which is fed into the weld area with one hand while operating the welding torch in the other hand. A short arc length is to be maintained, while preventing contact between the tungsten electrode and the work piece material. The arc is usually initialized with a power source with a high frequency generator, which produces an electric spark. This spark is a conductive path for the welding current through the shielding gas and allows the arc to be initiated while the electrode and the work piece are separated, typically about 1.5–3 mm apart.

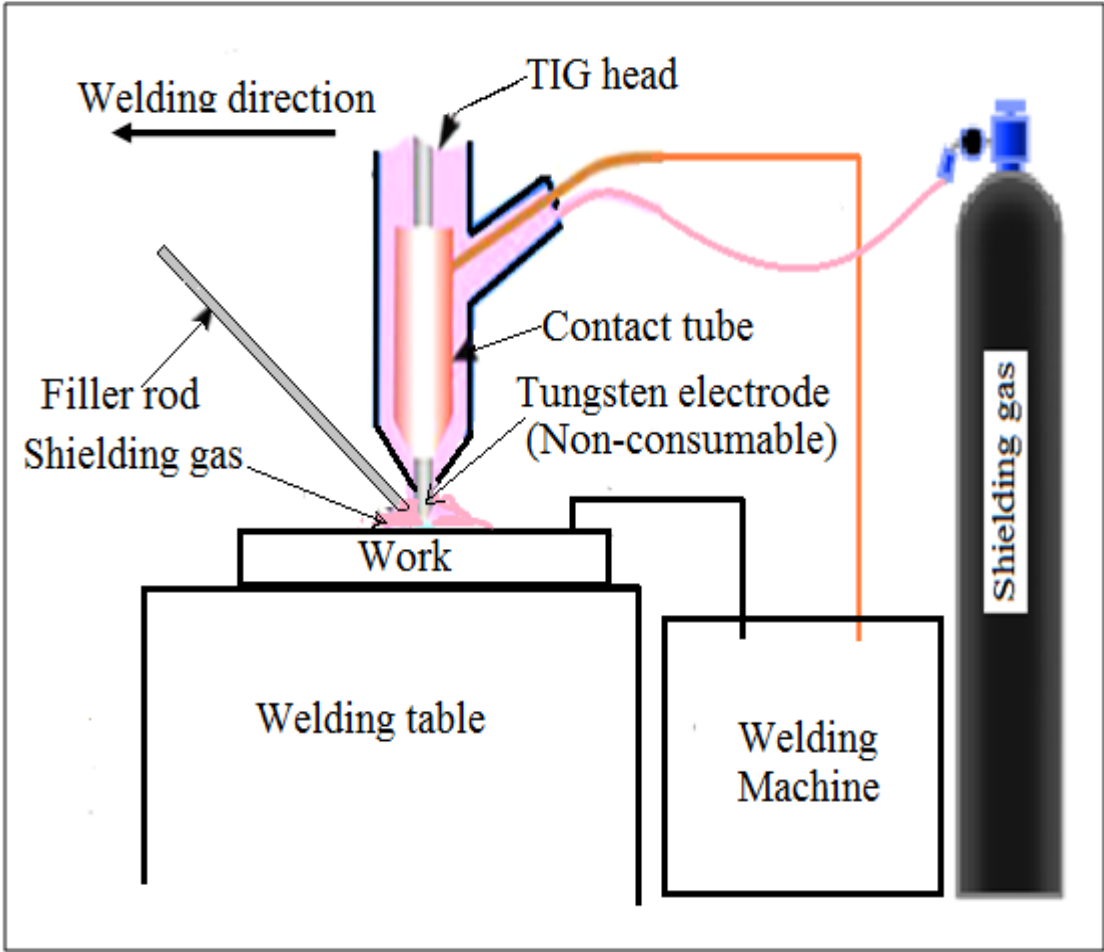


**Fig. 1.1:** Principle of tungsten inert gas welding [25]

Once the arc is struck, the welder moves the torch in a small circle to create a welding pool. The size of the welding pool depends on the size of the electrode and the amount of current. While maintaining a constant separation between the electrode and the work piece, the operator then moves the torch back slightly and tilts it backward about 10–15 degrees from vertical. Filler metal is added manually to the front end of the weld pool as it is needed

Demands placed on metals joints have increased from various viewpoints, such as, environmental concerns, energy saving, high performance, cost saving and so on. The tungsten inert gas welding process was developed in 1941 and its usage is widespread in modern industry, such as aerospace, nuclear, petroleum and chemical industries. The welding of automotive exhaust gas systems, stainless steel pipes, repairing of chemical industries equipment, join high strength reactive metals and alloys such as stainless steel, aluminum and magnesium alloys, nickel alloys, titanium, aluminum, copper, bronze and even gold, can be done by TIG welding process. There are a number of well-established welding processes, but TIG welding is still the most popular and extensively used welding process for the joining ferrous/non ferrous and similar/ dissimilar metals for a wide range of applications [2]. A comparative analysis of the various arc welding processes is listed in **Table 1.1** [129, 130].

**Table 1.1:** Various arc welding processes

<b>Welding Processes</b>	<b>Advantages</b>	<b>Disadvantages / Limitations</b>
Shielded metal arc welding (SMAW)	<ul style="list-style-type: none"> <li>❖ Cheap Portable (no gas required)</li> <li>❖ Versatile (can weld various metals &amp; thicknesses)</li> </ul>	<ul style="list-style-type: none"> <li>❖ Major post-weld cleaning</li> <li>❖ Relatively ‘dirty’ method of welding (sparks/fumes)</li> <li>❖ Requires moderate skill</li> </ul>
Gas metal arc welding (GMAW)	<ul style="list-style-type: none"> <li>❖ higher welding speeds</li> <li>❖ Versatile (can weld various metals &amp; thicknesses)</li> </ul>	<ul style="list-style-type: none"> <li>❖ Requires shielding gas</li> <li>❖ Minor post-weld cleaning</li> </ul>
Tungsten Inert gas welding (TIG)	<ul style="list-style-type: none"> <li>❖ Very high quality and superior welds</li> <li>❖ No post-weld cleaning</li> <li>❖ Versatile (can weld various metals &amp; metal alloys)</li> <li>❖ Yields low distortion and narrow heat affected zone.</li> </ul>	<ul style="list-style-type: none"> <li>❖ Requires shielding gas</li> <li>❖ Low metal deposition rate</li> <li>❖ Requires high degree of operator skill</li> </ul>
Submerged arc welding (SAW)	<ul style="list-style-type: none"> <li>❖ Well suited to welding thick sections</li> <li>❖ High metal deposition rates</li> </ul>	<ul style="list-style-type: none"> <li>❖ Limited to welding in flat position</li> <li>❖ Thin sections are not applicable</li> </ul>
Plasma arc welding (PAW)	<ul style="list-style-type: none"> <li>❖ Higher energy concentration</li> <li>❖ Faster Travel Speeds</li> </ul>	<ul style="list-style-type: none"> <li>❖ Expensive equipment</li> <li>❖ More skill needed than TIG process</li> </ul>

## 1.2. Types of TIG welding Techniques

**Manual Welding:** In manual TIG welding, welder manipulates the welding torch by hand to join the work-metals. In this process called semiautomatic welding, if motorized wire feeder is attached to the torch. This technique requires skilled technician for obtaining better weldments. The equipment's of manual welding is quite inexpensive. This technique is very much useful for joining wide variety of material. This technique is more likely used for welding of stainless-steel pipes and root pass in carbon steel pipes welds.

**Mechanized Welding:** Mechanized welding process requires specialized accessories for conduction of welding operation. Welding parameters may be adjusted according to visual observation of weld made. The basic system of weld machine contains moving and holding wedding torch and work piece. The voltage feedback devices are used to control the arc length as voltage is important variables in TIG welding operation.

**Narrow Groove Welding:** Narrow groove welding is used mainly in TIG cold wire welding process with preparation of narrowed weld joint. Narrow groove welding is limited use to mechanized welding applications, where precise torch location can be maintained [131].

**Automatic Welding:** It is full-fledged automatic welding process; it does not require any welding process parameters adjustment manually and weld observations during welding operation. This process is mostly used for welding of pipes and tubes with the help of orbiting welding heads. The devices attach to the work-metals and move around the circumference fusing the metal. Welding operation this process is controlled by computers. This process can be applied to weld wide variety of materials and features with the use of microprocessors and computer numerical control servo drives.

**TIG Arc Spot Welding:** This welding process is made manually with the use of pistol like holder. The holder contains water cooled gas nozzle and tungsten electrode. Trigger switch is used in this welding technique to control the welding operation. The electrode holder is available to use this process automatic [132].

## 1.3. TIG Welding System

The TIG welding system mainly consists of four fundamental components which are:

- a) AC/DC power source
- b) Welding torch (air/water cooled)
- c) Inert shielding gas (helium, argon or their mixture)
- d) Control unit or arrangement for moving the welding torch as per mode of operation such as manual, semi-automatic, automatic.

**Power source:** Power supplies for TIG welding are generally the constant current type i.e. the current (and thus the heat) remains relatively constant, even if the arc distance and

voltage changes. It is also called a ‘dropper’ because its voltage drops as welding current increases, thus its volt-ampere output curve ‘drips’. The TIG power source can be either AC or DC. Pure tungsten electrode of ball tip shape with DCEN provides good arc stability. Light weight transistorized direct current power sources are currently used, being more stable and versatile than the old thyristor-controlled units. In rectifier-inverter power sources the incoming AC current is rectified and then converted into AC current at a higher frequency than that of the mains supply, in the inverter. Afterwards high voltage AC current is transformed into low voltage AC current suitable for welding, in the transformer, and then rectified, as shown schematically in **Fig. 1.2**. TIG welding with DCEP is preferred for welding of reactive metals like aluminium to take advantage of cleaning action due to development of mobile cathode spots during welding in work piece side.

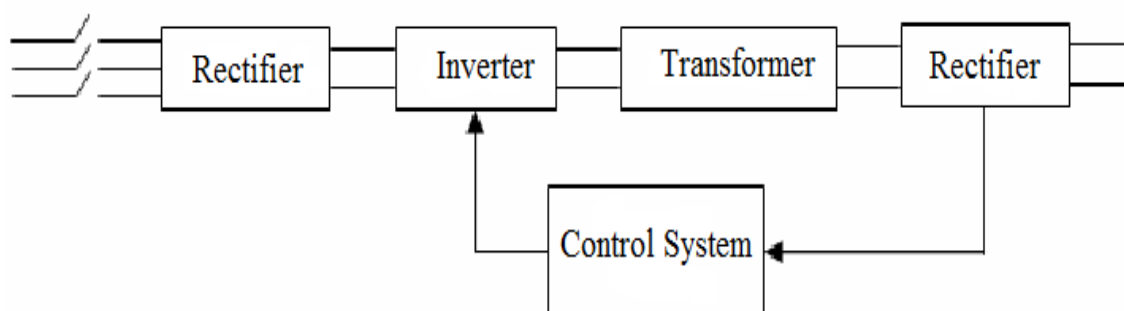


**Fig. 1.2:** Schematic diagram showing the inverter principle of the power sources

**Polarity:** In TIG welding three different polarities are used as shown **Fig. 1.3**, which is as follows:

- i) **Direct Current Electrode Negative (DCEN):** This is also known as straight polarity and it is the most common polarity used in TIG welding. The work piece is connected to positive terminal and the electrode is connected to the negative terminal of the power supply as shown in **Fig.1.3 (a)**. The electrons are emitted from the tungsten electrode and accelerated while travelling through the arc. A significant amount of energy, called the work function, is required for an electron to be emitted from the electrode. When the electron enters the work piece, an amount of energy equivalent to the work function is released. As a result, in TIG welding with DCEN about two-thirds amount of heat is produced at the work piece and about one-third amount of heat is produced at the electrode end. Consequently, a relatively narrow and deep weld is produced.
- ii) **Direct Current Electrode Positive (DCEP):** This is also known as reverse polarity. The electrode is connected to the positive terminal of the power source and work piece to the negative terminal of the power source as shown in **Fig.1.3 (b)**. Now the heating effect of electrons is at the tungsten electrode rather than at the work piece. Consequently, a shallow and wide weld is produced. Moreover, in order to prevent

the electrode tip from melting a large-diameter, water-cooled electrodes may be used. The positive ions of the shielding gas bombard the work piece, knocking off oxide films and producing a clean weld surface. Therefore, DCEP can be used for welding thin sheets of strong oxide-forming materials, where deep penetration is not required.

**iii) Alternating Current (AC):** It is the preferred welding current for most white metals, e.g. aluminium and magnesium. The heat input to the tungsten is averaged out as the AC wave passes from one side of the wave to the other. On the half cycle, where the tungsten electrode is positive, electrons will flow from base material to the tungsten. This will result in the lifting of any oxide skin on the base material. This side of the wave form is called the cleaning half. As the wave moves to the point where the tungsten electrode becomes negative the electrons will flow from the welding tungsten electrode to the base material. This side of the cycle is called the penetration half of the AC wave forms. Reasonably good penetration and oxide cleaning action can both be obtained, as shown in **Fig. 1.3 (c)**.

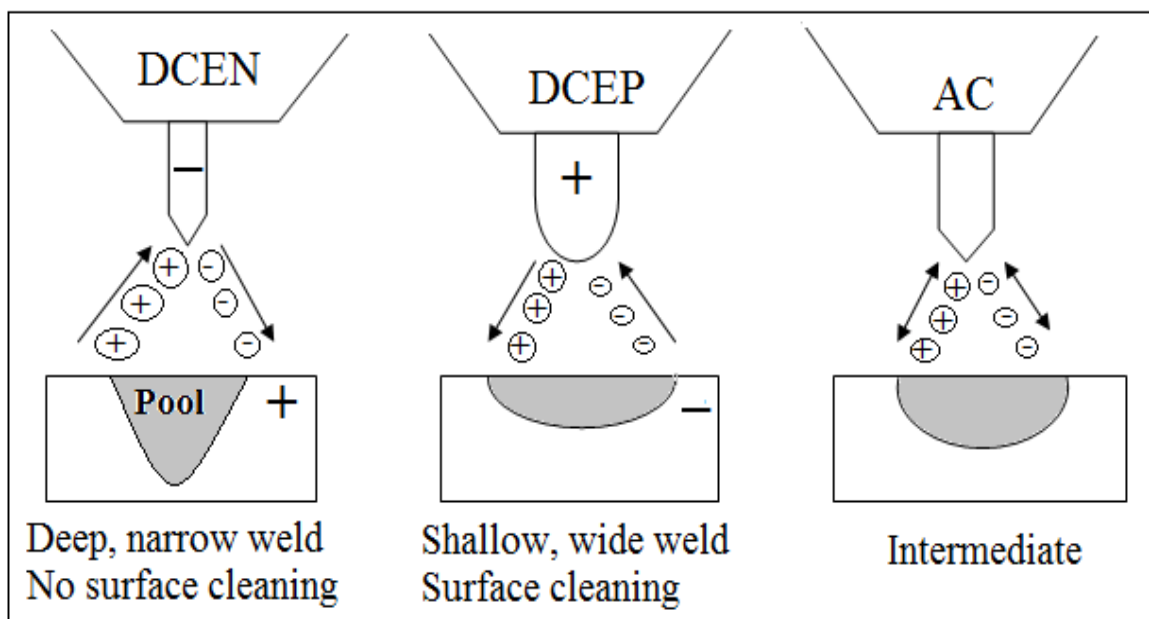


**Fig. 1.3:** Three different polarities in TIG welding [26]

**Welding torch:** TIG welding torches are designed for either manual or automatic operation. These are similar in construction, but the manual torch has a handle while the automatic torch normally comes with a mounting rack. TIG welding torch comprises three main parts which are: non-consumable tungsten electrode, collets and nozzle. Collets are primarily used to hold the tungsten electrode of varying diameter in position. Nozzle helps to form a firm jet of inert gas around the arc, weld pool and tungsten electrode. The diameter of the gas nozzle must be selected in light of expected size of weld pool so that proper shielding of the weld pool can be obtained by forming cover of inert gas. Damaged nozzle does not form uniform stream of inert gas jet around the weld pool. Typical flow rate of shielding inert gas

may vary from 5-50 liters/min. TIG welding torch is generally rated on the basis of their current carrying capacity as it directly affects the weld speed and production rate. Depending upon the current carrying capacity, the welding torch can be either water or air cooled. Air cooling systems are most often used for low-current operations (up to about 200 A), while water cooling is required for high-current welding (up to about 600 A).

The internal metal parts of a torch are made of hard alloys of copper or brass in order to transmit current and heat effectively. The body of the torch is made of heat-resistant, insulating plastics covering the metal components, providing insulation from heat and electricity to protect the welder.

**Electrode:** The electrode which is used in TIG welding is made of tungsten or a tungsten alloy, due to the highest melting temperature among pure metals, at 3,422 °C. So, the electrode is not consumed during welding, but some erosion (called burn-off) can occur. Electrodes can have either a clean finish or a ground finish. Clean finish electrodes have been chemically cleaned, while ground finish electrodes have been ground to a uniform size and have a polished surface, making them optimal for heat conduction. The diameter of the electrode can vary between 0.5 mm and 6.4 mm and their length can range from 75 mm to 610 mm.

Pure tungsten electrodes have poor heat resistance, electron emission and low cost. They find limited use in AC welding of e.g. magnesium and aluminium. Thorium oxide (or thoria) alloy electrodes offer excellent arc performance and starting, making them popular general purpose electrodes. However, it is somewhat radioactive, making inhalation of thorium vapors and dust a health risk, and disposal an environmental risk. Electrodes containing zirconium oxide (or zirconia) increase the current capacity while improving arc stability and starting and increasing electrode life.

**Filler wire:** Almost in all applications of TIG welding filler metals are used, depending upon the thinness of the materials. The filler metal can be fed manually or using some wire feed mechanism. For feeding small diameter filler wire, usually push type wire feed mechanism with speed control device is used. In some cases use of filler metal similar to base metal causes cracking of weld metal especially if its solidification temperature range is wide. Therefore, selection of filler metal should be done after giving full consideration to the following aspects such as mechanical property requirement, metallurgical compatibility, crack tendency of base metal etc.

**Shielding gas:** As with other welding processes such as gas metal arc welding, shielding gases are necessary in TIG welding to protect the welding area from atmospheric gases such as nitrogen and oxygen, which can cause fusion defects, porosity and weld metal embrittlement if they come in contact with the electrode, the arc, or the welding metal. The gas also transfers heat from the tungsten electrode to the metal, and it helps start and maintain a stable arc. Helium, argon or their mixture are commonly used as shielding inert gas for protecting the weld pool depending upon several factors, including the type of

material being welded, joint design, and desired final weld appearance. Argon is the most commonly used shielding gas for tungsten inert gas welding. Nitrogen and hydrogen are sometimes added in argon for specific purposes such as increasing the arc voltage and arc stability. The ionization potential of helium is higher than argon. Therefore, application of helium as shielding gas results in higher arc voltage. As a result it increases the weld penetration in a joint and it also increases the welding speed. Helium has also higher thermal conductivity than argon, so transfer of heat from arc to the base metal increases in case of using Helium. Argon-helium mixtures are also frequently utilized in tungsten inert gas welding, since they can increase control of the heat input while maintaining the benefits of using argon. Normally, the mixtures are made with primarily helium often about 75% or higher and a balance of argon. These mixtures increase the speed and quality of the AC welding of aluminum, and also make it easier to strike an arc. Another shielding gas mixture, argon-hydrogen, is used in the mechanized welding of light gauge stainless steel, but because hydrogen can cause porosity, its uses are limited. Similarly, nitrogen can sometimes be added to argon to help stabilize the austenite in austenitic stainless steels and increase penetration when welding copper. Due to porosity problems in ferritic steels and limited benefits, however, it is not a popular shielding gas additive. **Table 1.2** shows a Comparison of shielding gases used in TIG welding [133, 134, 135].

**Table 1.2:** Comparison of Shielding Gases

<b>Characteristics</b>	<b>Argon</b>	<b>Helium</b>	<b>Argon / Helium Mixes</b>
Travel Speed	Reduced travel speeds	Faster travel speeds	Improved travel speeds over 100% Argon
Penetration	Reduced penetration	Increased penetration	Improved penetration over 100% Argon
Cleaning	Good cleaning action	Less cleaning action	Cleaning properties closer to Argon
Arc Starting	Easier arc starting	Difficult arc starting	Improved arc starting over 100% Helium
Arc Stability	Good arc stability	Less low amperage stability	Improved arc stability over 100% Helium
Arc Cone	Focused arc cone	Flared arc cone	Arc cone shape more focused than Helium
Arc Voltage	Lower arc voltages	Higher arc voltages	Arc voltages between 100% Argon and Helium
Flow Rate	Lower flow rates 10-30 CFH	Higher flow rates (2 times)	Higher flow rates than Argon
Cost	Lower cost and greater availability	Higher cost than Argon	Costs higher than Argon



## 1.4. Input Process Parameters of TIG welding

The welding input process parameters affect the weld bead formed during welding and quality is characterized by weld pool geometry [27]. Therefore, for obtaining optimal weld pool geometry, it is very important to select the proper welding process parameters and their levels. Important process parameters for the TIG welding process which are mostly influence the quality of the weld are discussed in the following paragraph.

**Current:** Welding current is the most important parameter which has direct influence on weld bead shape, depth of penetration, heat input, deposition rate and quality of the weldment. TIG welding uses direct current on electrode negative than the electrode positive, because electrode negative produces higher weld penetration depth and higher travel speed. Besides, reverse polarity produces rapid heating and degradation of the electrode tip, because anode is heated more than cathode in gas tungsten electric arc.

Pulsed DC current with low-frequency (1-10 Hz) is being used to reduce weld distortion and to improve tolerance to joint preparation and to cast-to-cast variations. High-frequency pulsed current (5-30 kHz) improves arc stiffness, increasing penetration depth and maximum welding speed and decreasing formation of porosity in the weld metal. This current is advantageous in automatic welding applications. Welding current can significantly affect the geometrical shape. When welding current increases, the curvature of the pool boundary at the trailing end increases [28].

**Welding Voltage:** The voltage drop between the tip of the tungsten electrode and the base metal is mainly influenced by the type of welding current used. Again the welding current, the arc voltage is proportional to the arc gap length and shielding gas composition [29]. Furthermore, when working with low voltage values a change in arc voltage will affect the heat input to a lesser extent.

**Welding speed:** The effect of the welding speed on the geometrical appearance is slight, although its influence on the pool size is great. Generally arc penetration is inversely proportional to welding speed for the same current and voltage. The size of the molten weld pool geometry is also directly influenced by the welding speed [30]. The increasing welding speed produces a decreasing weld cross section area, and consequently depth of penetration and weld width also reduces. The weld pool becomes teardrop shaped at high welding speeds and elliptical at low welding speeds. Excessive high welding speed increases tendency of undercut, porosity and uneven bead shapes while slower welding speed reduces the tendency to porosity. Normal welding speeds are from 100 to 500 mm/min depending on current, material type and plate thickness.

**Arc length:** The arc length is the distance between the electrode tip and the work-piece. The arc length in TIG welding is usually taken as 1.5 times the electrode diameter. If the arc length increases, the voltage to maintain the arc stability must increase, but the heat input to work-piece decreases due to radiation losses from the column of the arc. Consequently,

weld penetration and cross section area of melted material decrease with increasing arc length. In general, it can be stated that the greater the arc length, the higher is the heat leakage to the surrounding atmosphere which results with inefficient welding heat input/penetration [30].

**Shielding gases:** Shielding gases are used in TIG welding in order to prevent atmospheric contamination of the weld metal. This contamination can produce porosity, weld cracking, scaling and even change in the chemical composition of melted material. Further, shielding gas also has a large influence on the stability of the electric arc. It has a significant influence on the overall performance of the welding system.

Argon is the most used TIG welding shielding gas. It has low ionization potential and is heavier than air, providing an excellent shielding of the molten weld pool. Furthermore it is less expensive than helium, the other inert shielding gas used in the process. Argon is sometimes used in welding of carbon and stainless steels and low thickness aluminum alloy components.

**Electrode vertex angle:** The non-consumable electrode angle influences the weld penetration depth and the weld shape. Electrode angles between 30° and 120° are used. Small angles increase arc pressure and penetration depth but have high tip shape deterioration. Electrode angles from 60° to 120° maintain tip shape for longer periods and give welds with adequate penetration depth-to-width ratio.

## 1.5. Output responses of TIG welding

There are various types of output responses measured in TIG welded joint. A few of them is discussed here. The output responses are those parameters on which quality of TIG welding depends. These are as follows:

**Weld Width:** The quality of TIG weld is greatly influenced by the weld pool geometry because the mechanical properties of the welded joints are strongly dependant on the weld pool geometry. Weld width is a very important factor in determining the quality of welds and it is desirable for obtaining minimum weld bead width in size. If bead width is less, the distortion of welded plates and residual stresses are least.

**Ultimate tensile strength:** This is refers as the maximum amount of tensile stress of the welded joint/material that can withstand before failure take place. Ultimate tensile strength is normally selected as a response parameter to assess weld quality because it is a key mechanical property that can describe weld joint performance.

**Percentage Elongation:** Percent elongation is one way to measure and quantify the ductility of a material as determined by a tension test. Elongation is important in manufacturing as it measures how much bending and shaping a material can withstand without breaking.

**Yield Strength:** Yield strength refers to an indication of maximum stress that can be developed in a material without causing plastic deformation. The value of yield strength is important in the construction of structures, such that the structures are able to perform in the elastic region under normal servicing conditions.

**Hardness:** It can display the elasticity, plasticity and strength of materials. It is an important mechanical property for the weldment. The hardness of the weld indicates that whether the weld metal meets the desired strength requirements or not.

**Impact strength:** It is the resistance of a material to fracture under a sudden impact, or shock load. It is a measure of the toughness of the material. It signifies the product performance, service life, and liability.

## **1.6. Applications of TIG Welding**

TIG welding process can be used to weld almost all metals and metal alloys in use today. It is a particularly effective and economic way for welding light gauge metals (less than 3mm thickness) and for welding metals difficult to weld with the conventional welding process. Gas tungsten arc welding is most commonly used to weld stainless steel and nonferrous materials, such as aluminum and magnesium [136], but it can be applied to nearly all metals, with a notable exception being zinc and its alloys.

The TIG welding process is extensively used in modern industry such as [137, 138, 139]:

- i) Aerospace industry
- ii) Food processing industry
- iii) Precision manufacturing industry
- iv) Automobile industry
- v) Bicycle industry
- vi) Nuclear industry
- vii) Maintenance and repair work

## **1.7. TIG Welding of Austenitic Stainless Steels**

Austenitic stainless steels contain high levels of chromium and nickel and low levels of carbon. The thermal conductivity of austenitic alloys is roughly half that of ferritic alloys. Therefore, the weld heat input that is required to achieve the same penetration is reduced. The molten weld pool of the austenitic stainless steels is commonly more viscous, or sluggish, than ferritic and martensitic alloys. This slows down the metal flow and wettability of welds in austenitic alloys, which may promote lack of fusion defects. Though austenitic stainless steel can be welded by TIG, MIG and other processes, but TIG welding is frequently used for fabrication of austenitic stainless steel.

## 1.8. Microstructure analysis

Microstructure is defined as the structure of a prepared surface or thin foil of a material as revealed by microscope. The microstructure of a material can strongly influence by the physical properties such as strength, toughness, ductility, hardness, corrosion resistance, wear resistance and so on. Weld metallurgy is an important subject. Weld metallurgy is evaluated by study of microstructures. Microstructures at different regions of weldments: weld region, HAZ, and base material give an idea about the quality of weld. Mechanical properties of weld depend upon the phases present in the microstructure, size of the grains, and many other features. In the present work, microstructural studies have been made up to a certain extent.

## 1.9. Design of Experiments

More details of the experimental plan have been discussed in **Chapter–2**. Here only some important points are included. Design of experiments (DOE) is a systematic approach for investigation of a process. A series of structured tests are designed, in which planned changes are made to the input variables of a process. The effects of these changes on a pre-defined output are then assessed. It has more to offer than 'one change at a time' experimental methods, because it allows a judgment on the significance to the output of input variables acting alone, as well as input variables acting in combination with one another.

DOE is a team oriented and variety backgrounds (design, manufacturing and statistics) should be involved when identifying factors and levels and developing the matrix as this is the most skilled part. In order to draw the maximum amount of information a full matrix is needed which contains all possible combinations of factors and levels. If this requires too many experimental runs to be practical, fractions of the matrix can be taken dependent on which effects are of particular interest. The fewer the runs in the experiment the less information is available.

### 1.9.1. Major approaches in design of experiments

**A. Factorial designs:** It allows for the simultaneous study of the effects that several factors may have on a process. When performing an experiment, varying the levels of the factors simultaneously rather than one at a time is efficient in terms of time as well as cost and also allows for the study of interactions between the factors. Interactions are the driving force in many processes. Without the use of factorial experiments, important interactions may remain undetected.

**A1. Full factorial designs:** In a full factorial experiment, responses are measured at all combinations of the experimental factor levels. The combinations of factor levels represent the conditions at which responses will be measured. Each experimental condition is called a run and the response measurement an observation. The entire set of runs is the design.

**A2. General full factorial designs:** In a general full factorial design, the experimental factors can have any number levels. For example, Factor A may have two levels, Factor B may have three levels and Factor C may have five levels. The experimental runs include all combinations of these factor levels. General full factorial designs may be used with small screening experiments, or in optimization experiments.

**A3. Fractional factorial designs:** In a full factorial experiment, responses are measured at all combinations of the factor levels, which may result in a prohibitive number of runs. To minimize time and cost, some of the factor level combinations are excluded. Factorial designs in which one or more level combinations are excluded are called fractional factorial designs. Fractional factorial designs are useful in factor screening because they reduce the number of runs to a manageable size. The runs that are performed are a selected subset or fraction of the full factorial design.

**B. Taguchi design:** Taguchi method is a scientifically disciplined mechanism for evaluating and implementing improvements in products, processes, materials, equipment and facilities. These improvements are aimed at improving the desired characteristics and simultaneously reducing the number of defects by studying the key variables controlling the process and optimizing the procedures or design to yield the best results.

The method is applicable over a wide range of engineering fields that include processes that manufacture raw materials, sub systems, products for professional and consumer markets. In fact, the method can be applied to any process like machining operations, engineering fabrication, computer-aided-design, banking and service sectors etc. Taguchi method is useful for tuning a given process for best results.

**C. Response surface methodology:** Response surface methods are used to examine the relationship between one or more response variables and a set of quantitative experimental variables or factors. These methods are often employed after one has identified a vital few controllable factors and wants to find the factor settings that optimize the response. Response surface methods may be applied where one:

- a) Finds operating conditions that produce the best response.
- b) Finds factor settings that satisfy operating or process specifications.
- c) Identifies new operating conditions that produce demonstrated improvement in product quality over the quality achieved.
- d) Want to develop a mathematical model of the second order response surface with the best fittings.
- e) Tries to find optimal set of experimental parameters that produce a maximum or minimum value of response.

Many response surface applications are sequential in nature in that they require more than one stage of experimentation and analysis. Response surface design can be modeled and visualize response surface patterns by generating the two-dimensional contour plots.

## **1.10. Optimization Techniques**

In the present work, two different optimization techniques / algorithms: desirability function approach (DFA) and teaching and learning based optimization (TLBO) have been used. Grey relational analysis is used to optimize the multiple responses simultaneously. These techniques have been coupled with design of experiments and process optimization has been made. More details of the methods / techniques have been discussed in **Chapter - 2**. Some important points are mentioned here.

### **1.10.1. Desirable function Approach (DFA)**

Derringer and Suich (1980) have proposed a desirability function approach to deal with the multiple performance characteristics. Desirability function approach (DFA) is an effective optimization technique which is effective to identify the input parametric condition to optimize the responses individually and simultaneously also. DFA employs the regression model which obtained from experimental data of each response. In DFA, desirability of each response is defined first. The index number in DFA reflects the desirability of each response, if it is closer to 1 for higher or larger desirability and closer to 0 is for lesser desirability. For all the problems, solving by DFA, desirability value lies between the 0 and 1.

### **1.10.2. Teaching and learning based optimization (TLBO)**

Teaching and learning based optimization (TLBO) is a recently developed heuristic algorithm based on the natural phenomenon of teaching-learning process. It is an intelligent probabilistic algorithm used for solving constrained / unconstrained problems. It does not require any algorithm specific control parameters for efficient working. For example, the effective working of genetic algorithm (GA) requires determination of optimum algorithm specific parameters such as crossover rate and mutation rate. TLBO works on the effect of influence of a teacher on the output of learners in a class. Elitism is a mechanism which is used to replace worst solutions with elite solutions to improve efficiency of the TLBO algorithm.

### **1.10.3. Grey relational analysis (GRA)**

GRA is mainly utilized solve the multi-attribute decision making problems. It considers simultaneously multi objectives simultaneously to identify the best alternative. Data pre-processing steps of GRA can be expressed as:

- ❖ In the GRA, first step is to preprocess the experimental data using higher-the-better and lower-the-better criterions.
- ❖ Normalizing, grey relational co-efficient (GRC)
- ❖ Determination of the grey relational grade (GRG) for each experiment combination

- ❖ Final step is to provide the grades of GRG an ascending order to all factor combinations. Optimal parametric setting can be obtained at which parametric combination possess highest grade value.

### **1.11. Literature Review**

Welding is useful fabricating technique for creating complex structures by joining different parts, as mentioned earlier. Producing better quality weldment is a very important goal for welding investigators and industrialists. TIG welding is multi-input and multi-output variant process. Process parameters and other factors of welding process interact in a complicated manner and effect the weld quality-directly or indirectly. Stainless steels are important materials which using various applications in industries. TIG welding of type 316L stainless steel is an important area of research. Various aspects of TIG welding of different steels were investigated by researchers and investigators. Those aspects include effects of filler rod on weld quality, influences of process parameters and different fluxes, shielding gas on weldment quality, analysis, mathematical modeling and optimization of TIG welding using design of experiments techniques like RSM, analysis of variance, Taguchi method, desirability function approach (DFA), teaching learning based optimization (TLBO), grey relational analysis and other techniques.

Mishra et al. [31] have investigated the TIG and MIG processes for welding of dissimilar mild and stainless-steel materials. Tensile strength has been selected as output response. The experimental results have been compared for different welded joints made by TIG and MIG welding processes, from the results it is identified that TIG welded joints have better physical properties than MIG welded joints. Researchers have stated that TIG welding is more suitable for dissimilar metal welding of mild and stainless steel. Lakshminarayanan et al. [32] have conducted comparative analysis among shielded metal arc welding, gas metal arc welding and gas tungsten arc welding processes to study the tensile and impact properties of the ferritic stainless steel. Researchers have found from their study that gas tungsten arc welding technique is found to be advantageous compared to other welding operations for joining ferritic stainless steels. Bodkhe and Dolas [33] have investigated the effects of process parameters like welding current, torch speed and arc gap on depth of penetration in activated-TIG welding of 304L stainless steel. Durgutlu [34] have studied the effect of mixing H<sub>2</sub> with pure Argon as shielding gas on mechanical properties of welded joint in tungsten inert gas welding of AISI 316L austenitic stainless steels. Maximum tensile strength has been found at Ar-1.5% H<sub>2</sub> gas mixture. Zhu et al. [35] have analyzed the mechanical properties and microstructural characteristics of TIG welded joint of CLAM steel under identical conditions. Rajani et al. [36] have performed experiments to improve the corrosion resistance of TIG welded 316L stainless steel through controlled preheating process. Researchers have found from their study that an increment of preheat temperature improves corrosion behavior of weldments. Rao and Deivanathan [37] have investigated the significance of stainless steel filler material of different grades on welded joint quality of

AISI 310 stainless steel in TIG welding. They have stated from their work that maximum tensile strength is observed with a current of 120A and 309L filler rod. Tseng et al. [38] have made an experimental research work to study the performance of activated TIG welding of 316L austenitic stainless steel with the use of five types of fluxes.

Soltani and Tayebi [39] have conducted comparative analysis of welding of 304L and 316L stainless steels using laser and TIG welding operations. They have considered yield strength, elongation, hardness and weld width as output responses. Researchers have found from their study that TIG welding has produced better weld results compared to laser welding. Molak et al. [40] have carried out experimental work and analyzed the mechanical properties of 316L stainless steel welded joint made by TIG welding process. Thomas et al. [41] have made a comparative analysis on welding of type 316LN stainless steel plates using conventional multi-pass TIG and activated TIG welding. They have found better weld qualities while welding of multi-pass welding of 316LN stainless steel compared to activated-TIG welding. Reddy et al. [42] have made an investigation to study the weldability of AISI 4140 and AISI 316 by TIG welding process with and without using filler metal. For joining this dissimilar metals ER 309L is used as filler material. Hardness and tensile strength have been considered as response parameters for the study.

Tumu et al. [43] have welded the AISI 316L and Duplex 2205 stainless steel using pulsed current gas tungsten arc welding with ER316L and ER309L filler wires. They have carried out macro examination and optical microstructure examinations to check the defect in the weld joints. They have analyzed the tensile strength and percentage elongation of welded samples with varying input parameters. They have mentioned from the study that process parameter selection is crucial for creating better weld joints in TIG welding. Jatimurti et al. [44] have made a research investigation to analyze the relationships between output responses: microstructure and hardness, and welding parameters like welding current and travel speed in TIG welding of type 316L stainless steel. Researchers have stated from their work that lower current and higher travel speed produce fine microstructure and hardness. Kumar and Shahi [45] have studied the impact of varying heat input on the mechanical and metallurgical properties of TIG welded AISI 304 stainless steel joints. The investigators have observed decreasing trend of ultimate tensile strength, micro hardness value of weld metal and HAZ, with increase of welding heat input. Mortazavi et al. [46] have studied the effect of three different heat inputs on microstructure and mechanical properties of dissimilar joints of AISI 316L stainless steel

Notches are very important factors in any structural materials/bodies and the existence of notches or in other words stress concentrations can depreciate the mechanical properties of a material. Notch tensile testing has proven to be a suitable method of testing the tensile properties of welded joints [47]. An experimental analysis have been conducted by Lin et al. [48] for evaluating weld joint qualities such as tensile strength, notch tensile strength, notch tensile ratio and hardness of pure copper materials welded by using friction stir welding and



tungsten inert gas welding. Selvamani and Palanikumar [49] have established empirical relationships to predict ultimate tensile strength, notch tensile strength and percentage elongation of the friction stir welded joints. Anawa and Olabi [50] have analyzed and optimized the notch tensile strength of ferritic and austenitic in laser beam welding process. Analysis of variance and Taguchi method have been used to determine significant parameters which have detrimental effects on output responses and optimize them to produce better welded joint qualities. Karthick et al. [51] have studied notch tensile and impact toughness properties of welded joint of P91 and 316L austenitic stainless steel in shielded metal arc welding. Chu et al. [52] have investigated dissimilar laser welding and joint strength has been evaluated by notch tensile strength and correlated with microstructure and micro hardness. Tsay et al. [53] investigated SP-700 laser welds to assess the influence of post-weld heat treatments on the notched tensile strength of two titanium alloy welds by performing notched tensile tests

There are various optimization methods that can be applied to obtain the desired output performances through the development of mathematical models to specify the relationship between the input parameters and output variables. One of the most widely used methods of optimization is the response surface methodology (RSM), in which the researchers try to approximate the unknown mechanism with an appropriate empirical model [54]. Modeling helps to identify, statistically analyze and optimize the inputs and outputs of any physical system. Optimization techniques like desirability function approach (DFA) and teaching learning-based optimization (TLBO) are found to be efficient to solve the mathematical models and to provide global optimum conditions. Grey relational analysis (GRA) is useful technique to solve the multi-responses simultaneously. The details of reported articles to the literature related to optimization of TIG welding / other manufacturing processes with the use of applications of RSM, RSM and DFA, RSM combined with TLBO, and GRA, etc., are given as follows:

Kiaee and Aghaie-Khafri [55] have investigated the effects of welding process parameters on mechanical properties: tensile strength and hardness in gas tungsten arc welding of A516-70 carbon steel by response surface methodology (RSM). They have found better output responses through experimental analysis and optimization by RSM. Srivastava and Garg [56] have carried out experimental analysis to investigate the effects of the welding process parameters on welding of mild steel plates using gas metal arc welding process by using RSM. The experiments have been planned as per Box Behnken design of RSM. The optimum parametric condition is obtained by RSM. Shukla et al. [57] have developed a quadratic model to analyze the effects of input parameters such as welding current, polarity of electrode and torch angle on depth of penetration of shielded metal arc welding of AISI 1020 welded plates using response surface methodology. An experimental analysis of resistance spot welding based on Box–Behnken design of RSM has been performed by Yue et al. [58]. They have also utilized the applications of RSM to develop a mathematical model between input parameters (i.e. current, electrode force and time) and responses such

shear force, absorption energy and variance of shear force and variance of absorption energy. Singh et al. [59] have developed mathematical models to evaluate the effect of polarity on weld bead geometry in submerged arc welding of mild steel plates and optimized the dimension of weld bead geometry using RSM technique.

A comparative study of pulsed Nd:YAG laser welding of AISI 304 and AISI 316 stainless steels has been reported by Kumar et al. [60] to investigate the effects of laser power, scanning speed and pulse width on the ultimate tensile strength and weld using the empirical models developed by RSM. They have found that among the base materials, 304SS depict better microstructural and mechanical properties than the 316SS for a given parametric condition. Martinez-Conesa et al. [61] have utilized the applications of RSM approach to investigate the significances of process welding variables on bead geometry of butt welded joint in gas metal arc welding. Researchers have obtained improved bead geometry qualities on welded joint. Balasubramanian [62] has established the relationships between the process parameters and the weld bead parameters in pulse current TIG welding. Experimental runs are planned according to Box–Behnken design of response surface methodology. Giridharan and Murugan [63] have optimized pulsed gas tungsten arc welding of AISI 304L stainless steel sheets for obtaining optimal weld pool geometry with full penetration. They have developed a mathematical model to identify the main and interaction effects of pulsed GTAW process parameters on responses. Madadi et al. [64] have carried out experimental research analysis in pulsed TIG weld cladding of stellite alloy on carbon steel by response surface methodology. The mathematical models have been developed to predict hardness and dilution of welded joint. They have found from the analysis that predicted results are much closed to those obtained by experiments. Sen et al. [65] have developed second order regression model by using response surface methodology for optimizing the depth of penetration in gas metal arc welding. Ragavendran et al. [66] have made an experimental investigation in hybrid laser and TIG welding of 316LN stainless steel. Investigators have developed mathematical models to correlate input variables and output responses. Dutta and Pratihari [67] have developed mathematical models for determining input - output relationships in TIG welding process based on conventional regression analysis and neural network and comparisons are also made.

Naik and Reddy [68] have analyzed and optimized process parameters in TIG welding of duplex stainless steel 2205 using analysis of variance and Taguchi method. Tensile strength, hardness and depth of weld have been taken as responses and welding current, time, speed, variation of oxide fluxes, electrode diameter and gas flow rate are the input parameters. Control parameters are optimized to achieve better weld joint properties. Bharath et al. [69] have conducted research analysis on TIG welding of stainless-steel to examine the influences of process parameters such as welding current, welding speed, electrode and root gap, on weld bead of welded joint using ANOVA technique. They have stated from the work that welding speed and current are most significant factors for bending strength and tensile strength respectively.

Vasantharaja and Vasudevan [70] have conducted experimental analysis on activated TIG welding to determine the effects of process welding variables on bead shape parameters: depth of penetration, bead width and heat affected zone width, using RSM and desirability function approach (DFA). The quadratic polynomial mathematical model has been created for optimizing responses for a given set of welding process parameters. Researchers have found better weld joint quality responses with integrated RSM and DFA. Chandrasekhar et al. [71] have conducted an investigation to predict the optimum welding process variables to obtain the maximized depth of penetration (DOP) in hybrid laser -TIG welding of type 316L stainless steels. Multiple regression analysis has been used to postulate the mathematical relationships between the input parameters like laser power, pulse frequency, pulse duration, current and output response (i.e. DOP). The optimum welding condition was determined by solving mathematical model of DOP using genetic algorithm. Joseph and Muthukumar [72] have carried out research analysis to optimize the process parameters of activated tungsten inert gas (A-TIG) welding of AISI 4135 steel. Mathematical relationships between the input parameters such as current, speed, voltage and gas flow rate, and output responses: tensile strength (i.e. ultimate tensile strength) have been developed by using RSM approach. Surface plots are also drawn from the mathematical model of UTS to visualize the factor effects. They have observed from their study that current and voltage are the most significant factor for UTS in A-TIG welded specimen. Finally, optimum welding conditions are obtained by genetic algorithm and simulated annealing.

Nagesh and Datta [73] have applied artificial neural network and genetic algorithm (GA) for predicting the parameters of weld bead geometry by optimizing TIG welding process conditions. They have developed mathematical models between output responses: front height, front width, back height and back width, and with welding process parameters. Optimized welding combination is obtained by GA. An investigation has been done by Ravisankar et al. [74] to study the effect of welding speed and power on residual stresses for a circumferential of butt joint of AISI 304 stainless steel made by TIG welding using numerical simulation. They have observed from the study that with increase of welding speed and power, the longitudinal and circumferential residual stresses are also increases and deteriorate the weldment. Correia et al. [75] have utilized the combined applications of RSM and GA to optimize weld responses in GMAW welding process. Almeida et al. [76] have reported numerical simulation of residual stresses induced by TIG welded joints of AISI 316L. For simulation purpose, researchers have used finite element software, ANSYS and compared the numerical results with the results obtained experimentally. They have found good agreement with simulation results and experimental results.

An investigation has been carried out by Liao et al. [77] to establish the mathematical relationships between process parameters and weld bead geometry in all position TIG welding. Authors have considered RSM design table to conduct experiments. Significance and adequacy of the developed mathematical model has been checked by analysis of variance technique. The influences of welding parameters: welding peak current, welding

velocity, welding duty ratio, and welding position on weld bead geometry have been investigated by graphical main effect plots, and contour and surface plots. Finally, they have applied DFA on experimental data to optimize the TIG welding to enhance the quality of welded joints. Korra et al. [78] have discussed the effects of process parameters on weld bead geometry in activated TIG welding of duplex stainless-steel alloy. Second order mathematical models has been developed by RSM for optimizing performance characteristics: depth of penetration, area of depth of penetration, bead width, bead height, heat-affected zone width, and aspect ratio, for the set of given welding factors: current, torch speed, and arc gap. The significances of input parameters on output responses have been analyzed by generating the contour plots by RSM technique. Multi-response quality characteristics have been optimized simultaneously by using desirability function approach (DFA). They have stated from their work that RSM and DFA is very advantageous for analyzing, modelling and optimizing the multi-objectives in TIG welding operation. Kim et al. [79] have performed an experimental research work on gas metal arc welding of mild steel using RSM along with genetic algorithm and DFA. They have conducted experiments and developed mathematical relation between input and output responses using RSM. Then, they have optimized output responses weld bead height, bead width and penetration using genetic algorithm. They have checked or validated the predicted welding condition obtained by GA with desirability function approach (DFA). They have found from their study that GA had provided global optimum welding condition and same had also been confirmed by DFA.

Teaching-learning based optimization (TLBO) is one of evolutionary and swarm intelligence-based algorithm recently proposed by Rao et al. [80] which works based on natural phenomenon of teaching-learning process. It seems to be a rising star from amongst a number of metaheuristics with relatively competitive performances [81]. Rao and Kalyankar [82] have conducted research work to optimize two conflicting objectives: maximizing production rate and minimum production cost in laser beam welding (LBW). They have used TLBO technique to solve multi-objectives simultaneously. They have compared the obtained optimum results with earlier reported research works and found better results with TLBO. Dikshit et al. [83] have conducted research investigation on high-speed ball-end milling process to optimize the output response using RSM and TLBO. They have postulated the mathematical model to relate input and output parameters relationships using RSM. They have predicted the output response by TLBO. They have also performed confirmatory trails to validate the predicted parametric setting and found satisfactory results from integrated RSM and TLBO optimization approach. Jogi et al. [84] have aimed to study and optimize the process welding parameters (welding current, work piece thickness, voltage and wire feed rate) to optimize weld bead geometry quality characteristics in metal inert gas (MIG) welding of AISI 1018 mild steel by TLBO algorithm. Mathematical models have been developed from experimental data using regression analysis. The generated mathematical equation was solved by TLBO. Researchers were found satisfactory results with TLBO algorithm in optimization of MIG welding of mild steel. Pawar and Rao [85]

have utilized newly developed advanced optimization algorithm, teaching learning-based optimization technique to optimize the process parameters in three machining processes namely abrasive water jet machining, milling and grinding. Rao and Savsani [86] have used TLBO for optimizing input parameters electrolyte concentration, electrolyte flow rate, applied voltage and inter-electrode gap for maximizing the material removal rate (MRR) and for minimizing radial overcut (ROC). They have found improved results by comparing the results obtained by ABC algorithm. Rao and Kalyankar [87] have attempted an investigation for process parameter optimization of modern machining processes ultrasonic machining (USM), abrasive jet machining and wire electrical discharge machining (WEDM) with use of TLBO. Multi response optimization of turning operation of Ti-6Al-4V has been investigated by Sahu and Andhare [88]. Experiments have been carried out with central composite design of RSM and process parameters are optimized using TLBO algorithm and the results are compared with the results of GA. Rudrapati et al. [89] studied influence of turning parameters on surface roughness in CNC lathe. Experiments have been performed according to Box-Behnken design of response surface methodology and mathematical model also developed by RSM to find relationships between the input parameters and output response. Finally, process optimization has been made by teaching learning based optimization algorithm. Patel et al. [90] have applied teaching learning based optimization algorithm to optimize the squeeze casting input-output parameters. The results obtained by TLBO have been compared with evolutionary algorithms (i.e.GA, PSO etc.) and TLBO has been shown outstanding result. Different manufacturing processes, Milling, Drilling, Turning, Grinding and different non-traditional machining processes optimized by the TLBO algorithm are presented in a review paper by Tiwari and Pradhan [91]. The main focus of this review paper is on the optimization of the various manufacturing processes that have been optimized by TLBO algorithm. Kumar et al. [92] have applied teaching-learning-based optimization (TLBO) for the parametric optimization of fabric finishing system of a textile industry. The results of optimization using TLBO are compared with the results obtained by using the genetic algorithm (GA) on the same system. Some improvements in the results are obtained by TLBO algorithm. Sharma et al. [93] have made an experimental investigation to determine the effects of input process parameters: wire feed rate, welding voltage, welding speed and gas flow rate on bead geometry of AISI 430 grade stainless steel in gas metal arc welding (GMAW). Researchers have used hybrid RSM and TLBO to analyze the influences of input welding variables on outcome of the GMAW. Mathematical models were developed, and optimum welding condition was predicted by RSM and TLBO optimization techniques respectively. They have stated that RSM cum TLBO was very advantageous for optimization of bead geometry parameters in GMAW of AISI 430 grade stainless steels.

Apart from the single objective optimization of responses, there are more than one response may require optimizing the simultaneously to obtain the process economics. Analysis and optimization of multi-performance characteristics combinedly is important area of research for any manufacturing process including welding.

Multi response simulation and optimization of TIG welding process of 304 stainless steel have been done by Patil [94]. He has applied newly developed experimental approach which is known as definitive screening design for process improvement. Wahule and Wasankar [95] have carried out experimental research work to optimize the multi-outputs such as tensile strength (TS) and percentage elongation (PE) in TIG welding of SS304 and Fe-410 materials. They have considered grey relational analysis technique to solve multi-objective problem (TS and PE) into single objective problem. Researchers have used analysis of variance tool to study the significances of input parameters on both the output responses. They have stated from their work that input welding parameters are significantly affecting the mechanical properties of welded joint. They have optimized multi-objectives: TS and PE simultaneously by using grey relational analysis. Datta et al. [96] have formulated a mathematical model using grey-based Taguchi method for multi response optimization of welding process parameters on weld bead geometry in submerged arc bead-on-plate welding process. Bahar et al. [97] have conducted analysis on TIG welding of SS316 and MS1020 materials to enhance the welding performance. Welding current, speed and gas flow rate as input parameters and hardness, percentage elongation and UTS as output responses have been selected. Grey relational analysis has been applied to solve the multi-output variables. Factor effects on all the responses have been analyzed by analysis of variance and graphical main effect plots. Optimum input combination has been obtained by grey based Taguchi method. Authors have stated that grey relational analysis is very useful to solve multi-objective problems.

Multi-responses optimization of process parameters in hard turning of AISI 52100 steel through grey relational analysis combination with Taguchi orthogonal array has been done by Panda et al. [98]. The second order mathematical model has also been developed for selection of appropriate process parameters. Model indicates good correlations between the experimental and predicted results. Rizvi and Tewari [99] have applied Taguchi based Grey relational analysis to optimize gas metal arc welding process parameters of AISI304 austenitic stainless steel. They have considered three welding input process parameters such as wire feed rate, arc voltage and shielding gas flow rate. An optimal parametric combination of the welding operation has been obtained through grey relational analysis. Bahar et al. [100] have investigated the process parameters of metal inert gas welding to optimize the hardness and ultimate tensile strength of a weldment between dissimilar materials: mild steel (MS 1020) and stainless steel (SS 316) using Taguchi technique and Grey relational analysis.

Fatigue has become progressively more relevant in developed technology in the areas such as automobile, aircraft, compressor, pump, turbine, nuclear power plants etc. [101] due to cyclic variations of stress, temperature including vibration over a long period of time, thereby reducing the lifetime of structures and components [102, 103]. Today it is often stated that fatigue accounts for at least 90 percent of all service failures due to which occurring mechanical causes. The largest number of weld failures is attributed to either the

high-cycle fatigue caused by flow induced vibration or due to fatigue in general [104]. High cycle fatigue is a typical failure mode in engineering [105]. Again fatigue failure is very sensitive to the influential factors such as specimen size, specimen surface roughness and the inclusion size [106]. Fomin and Kashaev [107] have studied mechanism of internal fatigue crack formation and growth at the early stages of laser beam welded butt joint. Kamaya and Kawakubo [108] have investigated the effect of the mean stress on the fatigue strength of AISI 316 stainless steel and concluded that, in component designs, the mean stress correction does not need to be considered for the load-controlled cyclic loading and for the region where the ratcheting strain is constrained. Vuong [109] has developed a multi-axial high cycle fatigue damage model to predict the total fatigue life of fillet welded joints under various cyclic loads. The very high cycle fatigue behaviour of AISI 310 stainless steel has been investigated by Khan and Wang [110] through the ultrasonic fatigue testing. Pessoa et al. [111] have investigated the effect of loading frequency on the fatigue behaviour of the metastable austenitic stainless steel AISI 304. Ghosh et al. [112] have made an investigation to visualize the welding factor effects on multi-performance characteristics of weld joining in metal inert gas welding of AISI 409 ferritic stainless steel to AISI 316L austenitic stainless steel by using grey relational analysis and Taguchi method. Author have mentioned about effects of welding factors that welding responses are highly depends on the proper selection input parametric combination. Researchers have also stated that grey relational analysis is efficient to deal with multi-responses problems.

## **1.12. Motivation and objective of the present work**

TIG welding has become important joining technique, after invention of non-consumable electrodes with inert gas shield for welding of metals since 1941's. There are different welding methodologies which are developed and come into the use but still TIG welding is comes to the first choice whenever welding stainless steel with good quality and productivity are concerned. This led researchers to the development of TIG welding which could be successfully used to weld almost all metals required for normal fabrication.

In welding, finally objective is to achieve the desired characteristics of the welded joint. The joint quality is assessed in terms of characteristics like joint strength, hardness, ductility, bending strength, impact properties, endurance limit under fatigue condition, etc.. There are so many factors which may influence the quality of the welded joint; some of them are common for many of the welding techniques and some are specific for the particular technique under consideration. Thus, each of the various welding techniques need to be studied and is being studied still by the investigators. Directly or indirectly all such studies aim at achieving the desired properties of the welded joint and controlling the process in such a way the intended level of quality is attained. The literature survey done in the present context and presented in earlier section (**section 1.11**), illustrates the same, and points towards the fact that more is to be investigated, analyzed, learnt in respect of various aspects of welding so the control of the process becomes easier and predictive – producing the joint characteristics as demanded by the user.

All the points mentioned above are true and applicable for TIG welding of stainless steel, also. Though welding of stainless steel is not a new or emerging area of research, the specific problems related to welding of stainless steel – their various grades, and finally, control of the process parameters and the process to achieve the desired results remain a challenge to the researchers, and to the persons directly engaged in fabrication, welding of stainless steel components and structures. This becomes evident from the literature survey which indicates that people are still searching for more precise control of the process with predictive results.

One of the several aspects of importance is process optimization. Though a lot of publications are available and still coming out on process optimization in different fields of manufacturing, a lot more needs to be done. Because each study is done within a range of input parameters, considering variation of selected input parameters, for a specific thickness for work material with one or two different filler materials and emphasizing on certain aspects only. Thus extensive research, covering wide ranges of different factors – directing towards various aspects, by many investigators – will ultimately create a reliable, precise data bank and knowledge accumulation. Further, use of different optimization techniques for same field in manufacturing by the researchers requires to be converged by analysis of the results coming out from varied optimization approaches, which can only be possible through continued research. Teacher-Learning-Based Optimization (TLBO) is a new efficient optimization method.

Further study of TIG welding of austenitic stainless steel under varied input parameters is still an important and useful area of research. Various aspects are involved in this respect. Work has indeed been done to some extent, by the researchers, each emphasizing or considering certain specific aspects. Study involving a wider range of aspects may prove to be challenging: for example study and analysis of individual and interaction effects of the input parameters on various respects including response to fatigue loading, responses like bending characteristics, hardness at different zones, weld width, ultimate tensile strength, yield strength, percentage elongation and impact strength. Process optimization, mathematical modeling, microstructural study and analysis at varied welding conditions may also be added in the same study.

Considering the above, the purpose of the present work is outlined here with the following objectives.

- i. To carry out TIG welding of austenitic stainless steel at varied conditions of input parameters: following RSM experimental design, aiming at parametric influence on the responses.
- ii. To study microstructures of joints at varied input parameters, and to investigate fracture morphology and mechanical properties of the joints.
- iii. To develop mathematical modeling relating responses with the input parameters and to develop contour plots, main and interaction effect plots.



- iv. To optimize the process for various responses individually by two different optimization techniques: DFA and TLBO and multi objective optimization by GRA to optimize all the responses simultaneously.

## **2. FUNDAMENTALS OF DESIGN OF EXPERIMENT, DATA ANALYSIS AND OPTIMIZATION TECHNIQUES**

Scope and motivation of the present work is described in the previous chapter, objective of the present work is also mentioned. To carry out the investigation and the relevant analysis, a set of experiments have been planned. Details of the experimental plan set up and procedure are included in the next chapter i.e. in **Chapter 3**. Here some fundamentals of design of experiments, data analysis techniques and optimization procedures are described. These are relevant to the experimental plan of the present work and subsequent analyses and optimization procedures conducted in the present work.

### **2.1. Some Basic Features of Experimental Design**

The first statistician to consider a formal mathematical methodology for designing experiments was Sir Ronald A. Fisher, in his landmark “The Design of Experiments”. He suggested some important means of experimental design:

- i. **Comparison:** In many fields of study it is hard to reproduce measured results exactly. Comparisons between two or more variables are much more reproducible and are usually preferable. Often one compares against a standard or traditional treatment that acts as baseline.
- ii. **Randomization:** There is an extensive body of mathematical theory that explores the consequences of making the allocation of units to variables by means of some random mechanism such as tables of random numbers. Provided the sample size is adequate, the risks associated with random allocation are calculable and hence can be managed down to an acceptable level. Random does not mean haphazard and great care must be taken that appropriate random methods are used.
- iii. **Replication:** Measurements are usually subject to variation, both between repeated measurements and between replicated processes. Multiple measurements of replicated items are necessary so that the variation can be estimated.
- iv. **Blocking:** It is the arrangement of experimental units into groups (blocks) that are similar to one another. Blocking reduces known but irrelevant sources of variation between units and thus allows greater precision in the estimation of the source of variation under study.
- v. Use of factorial experiments instead of the one-factor-at-a-time method is found to be efficient at evaluating the effects and possible interactions of several factors.

- vi. Analysis of the design of experiments is built on the foundation of the analysis of variance, a collection of models in which the observed variance is partitioned into components due to different factors which are estimated.

## 2.2. Step-by-Step Procedure in the Effective Design of an Experiment

- i. **Selecting the problem:** In order to design an experiment, a problem has to be selected and phrased.
- ii. **Determining dependent variables:** The dependent variables are the variables that are being measured throughout the experiment. There can be many different dependent variables measured during an experiment.
- iii. **Selecting independent variables and their levels:** The independent variables are the variables that are manipulated in the experiment. The number of levels of independent variables determines the number of experimental conditions to be manipulated. This is very important in determining the extent of the scope of the experiment.
- iv. **Selecting the experimental design:** Choice of design involves consideration of sample size, the selection of suitable run order for the experimental trials and determination of whether or not blocking or other randomization is involved. There are several statistical software packages like MINITAB, Design Expert, SPSS etc., by which the choice of experimental design can be decided. The experimenter can enter information about the number of input factors, levels and ranges to the corresponding software package. After entering the suitable data, these programs will either present a selection of designs for consideration or recommend a particular design.
- v. **Performing the experiment:** When conducting the experiment, it is very vital to monitor the process carefully to ensure that everything is being done according to plan. Errors in experimental procedure usually destroy experimental validity. Before conducting the experiment a few trial runs are often helpful which provides information about consistency of experimental material, a check on the measurement system, a rough idea of experimental error and a chance to practice the overall experimental procedure.
- vi. **Statistical analysis of data:** Statistical methods like analysis of variance, signal-to-noise ratio etc. should be used to analyze the experimental data so that results and conclusions are objective rather than judgmental in nature. The data analysis is followed by the hypothesis testing with a particular confidence level. Regression analysis and model adequacy checking are also important analysis techniques.

Design of experiments, or experimental design, is the design of all information-gathering exercises where variation is present, whether under the full control of the experimenter or not. Design of experiments (DOE) is thus a discipline that has very broad application across all the natural and social sciences. It has become one of the most popular statistical techniques since 1990 and is widely employed in various industries and academic fields, depending on the requirements of the situation / problem. By means of this method, optimizing the different process variables is possible and number of required runs would be reduced. It has also become powerful tool in all engineering applications as well.

DOE begins with determining the objectives of an experiment and selecting the process parameters for the study. An experimental design is the laying out of a detailed experimental plan in advance of doing the experiment. Well-chosen experimental designs maximize the amount of information that can be obtained for a given amount of experimental effort. In an experiment, change in one or more process variables is made in order to observe the effect the changes have on one or more response variables. The statistical theory underlying DOE generally begins with the concept of process models. The (statistical) design of experiments is an efficient procedure for planning experiments so that the data obtained can be analyzed to yield valid and objective conclusions.

In this design several discrete or continuous input factors are varied and one or more measured output responses are observed. The output responses are often assumed to be continuous. Experimental data are used to derive an empirical (approximation) model linking the outputs and inputs. These empirical models generally contain first and second-order terms. Sometimes the experiment has to account for a number of uncontrolled factors that may be discrete, such as different machines or operators and some may be continuous (temperature, humidity etc.), also.

## **2.3. Major Approaches to Design of Experiments**

### **2.3.1. Factorial design**

The factorial design is one of the main methods of DOE, in which there two types of experimental designs: full-factorial and fractional factorial. The fractional factorial excludes some of the factor-levels from the full-factorial design to achieve an optimized combination with minimum time and computational cost compared with the full-factorial method. Although the full-factorial design requires a great number of experimental runs, however, it provides very accurate results on the interaction among the factors, so that the conclusions are highly credible and reproducible. Therefore, it is economical for characterizing a complicated process. The most important advantages are that not only the effects of individual parameters but also the relative importance of these parameters concerned in a given process can be obtained and that the interactional effects of two or more variables can also be known. This is not possible in the traditional one-variable-at-a-time experiment.

A design in which every factor appears with every setting of every other factor is called full factorial design. In this design, output responses are measured at all combinations of the input variable levels and it allows investigating the effects of each factor on the response variable. Full factorial designs up to 3 or 4 factors, are very useful in investigating quadratic effects but it is not recommended for 5 or more factors. Three-level design may sometimes require prohibitive number of runs.

### 2.3.2. Taguchi method

Taguchi technique was first proposed by Genichi Taguchi. Taguchi method is a systematic application of design and analysis of experiments for the purpose of designing and improving product quality at minimum cost by reducing the variance. Standard tables, known as orthogonal arrays (OA) are used for constructing the design of experiments in Taguchi method. In orthogonal array experiments are nothing but fractional design of experiments. Signal-to-noise (S/N) ratio technique in Taguchi methodology is used to analyze the experiments. S/N ratios are derived from the quadratic loss function and three of them [Eq. (2.1) - (2.3)] are considered to be standard and widely applicable.

$$\text{Nominal is the best: } S / N = 10 \log \bar{y} / S_y^2 \quad (2.1)$$

$$\text{Smaller is the better: } S / N = -10 \log 1 / n \left( \sum y^2 \right) \quad (2.2)$$

$$\text{Larger is the better: } S / N = -10 \log 1 / n \left( \sum 1 / y^2 \right) \quad (2.3)$$

where,  $\bar{y}$  is the average of observed data,  $s_y^2$  is the variation of 'y',  
n is the number of observations and 'y' is the observed data.

### 2.3.3. Response surface methodology

Response surface methodology (RSM) is one of the important methods in design of experiments for analysis of data; it is a collection of mathematical and statistical techniques that are useful for modeling and analysis of problems in which output response is influenced by several variables (input parameters) and the goal is to find the correlation between the response and the variables. RSM is widely used to identify the optimum process conditions that produce the best quality characteristics [113]. It is an empirical modelization technique devoted to the evaluation of relations existing between a group of controlled experimental factors and the observed results of one or more selected criteria. A prior knowledge of the studied process is thus necessary to achieve a realistic model. This method is often employed to build the mathematical relation between controllable factors (input parameters) and output response. Furthermore, this mathematical model can be used to determine the operating condition that produces best response, satisfies process specifications and identifies new parametric condition that produces improved product quality over the quality achieved. In the RSM, the quantitative form of relationship between the desired response and independent input variables can be represented as follows:

$$Y = f(x_1, x_2, x_3) \quad (2.4)$$

where  $x_1, x_2, x_3$  are input parameters and  $Y$  is the output response which is required to be optimized.

The first-order model is likely to be appropriate when the experimenter is interested in approximating the true response surface over a relatively small region of the independent variable space in a location where there is little curvature in 'f'.

For the case of three independent variables, the first-order model in terms of the coded variables is,

$$Y = \beta_0 + \beta_1 x_1 + \beta_2 x_2 + \beta_3 x_3 \quad (2.5)$$

The form of the first-order model in **Eq. 2.5** is sometimes called a main effects model, because it includes only the main effects of the three variables  $x_1, x_2$  and  $x_3$ . If there is an interaction between these variables, it can be added to the model easily as follows:

$$Y = \beta_0 + \beta_1 x_1 + \beta_2 x_2 + \beta_3 x_3 + \beta_{12} x_1 x_2 + \beta_{13} x_1 x_3 + \beta_{23} x_2 x_3 \quad (2.6)$$

This is the first-order model with interaction. Adding the interaction term introduces curvature into the response function. Often the curvature in the true response surface is strong enough that the first-order model (even with the interaction term included) is inadequate. A second-order model will likely be required in these situations. For the case of three variables, the second-order model is:

$$Y = \beta_0 + \beta_1 (x_1) + \beta_2 (x_2) + \beta_3 (x_3) + \beta_{11} (x_1^2) + \beta_{22} (x_2^2) + \beta_{33} (x_3^2) + \beta_{12} (x_1 x_2) + \beta_{13} (x_1 x_3) + \beta_{23} (x_2 x_3) \quad (2.7)$$

where, all  $\beta$ -s are the coefficients of linear, quadratic and interaction of input parameters  $x_1, x_2$  and  $x_3$ . The term  $\beta_0$  is the intercept term,  $\beta_1, \beta_2$  and  $\beta_3$  are the linear terms,  $\beta_{11}, \beta_{22}$  and  $\beta_{33}$  are the squared terms and  $\beta_{12}, \beta_{13}$  and  $\beta_{23}$  are the interaction terms between the independent / input variables. The  $\beta$ 's are a set of unknown parameters. To estimate the values of these parameters, one must collect data on the system. Because, in general, polynomial models are linear functions of the unknown  $\beta$ 's, one refers to the technique as linear regression analysis. All the beta values and has been calculated based on least squares method.

#### 2.3.4. Analysis of Variance

Analysis of variance (ANOVA) is used to investigate and model the relationship between a response variable and one or more independent variables. It is an appropriate procedure for testing the equality of several means. It is the most useful technique in the field of statistical inference. If, in an experiment there are treatments or different levels of a single factor and 'n' observations have been taken for each level,  $y_{ij}$  represents the  $j^{\text{th}}$  observation taken under the factor level  $i$  and  $y_{i0}$  represents the total of observations under  $i^{\text{th}}$  treatments. Here  $\bar{y}_{i0}$ ,

represents the average of the observations under the  $i^{\text{th}}$  treatment. Similarly,  $y_{\infty}$  represents the grand total of all the observations and  $\bar{y}_{oo}$  represents the grand average of all the observations. Then the total sum of squares is used as a measure of overall variability in the data.

$$SS_T = \sum_{i=1}^a \sum_{j=1}^n (y_{ij} - \bar{y}_{oo})^2 \quad (2.8)$$

$$SS_T = SS_{\text{Treatments}} + SS_{\text{Error}} \quad (2.9)$$

where  $SS_T$  = total sum of squares;  $SS_{\text{Treatments}}$  = sum of squares due to treatments (i.e. between treatments);  $SS_{\text{Error}}$  = sum of squares due to error (i.e. within treatments).

There are ‘N’ total observations. So,  $SS_T$  have N-1 degrees of freedom. There are ‘a’ levels of factor, so  $SS_{\text{Treatments}}$  has a-1 degrees of freedom.

$$MS_{\text{Treatment}} = \frac{SS_{\text{Treatments}}}{a-1} \quad (2.10)$$

$$MS_{\text{Error}} = \frac{SS_{\text{Error}}}{N-a} \quad (2.11)$$

$$F_0 = \frac{SS_{\text{Treatment}}/(a-1)}{SS_{\text{Error}}/(N-a)} = \frac{MS_{\text{Treatment}}}{MS_{\text{Error}}} \quad F_0 > F_{\alpha, a-1, N-a} \quad (2.12)$$

where  $MS_{\text{Treatments}}$  = mean squares due to treatments (i.e. between treatments),

$MS_{\text{Error}}$  = mean squares due to error (i.e. within treatments),

$F_0$  = obtained fishers ratio value through experimental data,

$F_{\alpha, a-1, N-a}$  = standard fishers ratio value at significance level at degree of freedom of factor levels and number of observations ( $\alpha$  = significant level at 5% / 10% etc. i.e. confidence level at 95% / 90% etc.),

a-1 = degree of freedom of factor levels,

N-a = degree of freedom of number of observations.

The analysis of variance summary contains usual sum of squares, degrees of freedom, mean squares, F test statistics and P values. In addition to this, there is some more information in ANOVA table such as R-squared and adjusted R-squared

The quantity R-squared is defined as

$$R^2 = SS_{\text{Model}} / SS_T \quad (2.13)$$

where  $SS_{\text{Model}}$  = sum of squares in the model,

$SS_T$  = total sum of squares

$R^2$  value shows as the proportion of the variability in the data explained by the analysis of variance model. Its value varies between 0 - 1 (i.e.  $0 \leq R^2 \leq 1$ ), with larger value being more desirable. The adjusted  $R^2$  is a variation of the ordinary  $R^2$  statistic that reflects the number of factors in the model.

$$R_{adj}^2 = 1 - \frac{SS_E / df_E}{SS_T / df_T} \quad (2.14)$$

where  $SS_E$  = sum of squares due to error,

$df_E$  = degree of freedom due to error,

$SS_T$  = total sum of squares,

$df_T$  = total degree of freedom,

The adjusted  $R^2$  can actually decrease if non-significant terms are added to a model.

The ANOVA technique is also used to identify the effects of variables on the response(s). In the ANOVA Table, there is a P-value for each independent variable, P value in the model shows whether the variable (i.e. input parameter) is significant or not. If the P-value is less or equal to the selected  $\alpha$ -level (significance level at 5% / 10% etc. i.e. confidence level 95% / 90% etc.), then the effect of that variable is significant. If the P-value is greater than the selected  $\alpha$ -value, then it is considered that the variable is not significant. Sometimes the individual variables may not be significant. If the effect of interaction terms is significant, then the effect of each factor is different at different levels of the other factors.

## 2.4. Optimization techniques for Solving Mathematical Models

### 2.4.1. Teaching learning-based optimization (TLBO)

Teaching-learning-based optimization algorithm (TLBO) is a teaching-learning process inspired algorithm proposed by Rao et al. [80], which is based on the effect of influence of a teacher on the output of learners in a class. The algorithm mimics the teaching-learning ability of teacher and learners in a class room. Teacher and learners are the two vital components of the algorithm and describes two basic modes of the learning, through teacher (known as teacher phase) and interacting with the other learners (known as learner phase). The output in TLBO algorithm is considered in terms of results or grades of the learners which depend on the quality of teacher. So, teacher is usually considered as a highly learned person who trains learners so that they can have better results in terms of their marks or grades. Moreover, learners also learn from the interaction among themselves which also helps in improving their results.

TLBO is population-based method. In this optimization algorithm a group of learners is considered as population and different design variables are considered as different subjects offered to the learners and learners' result is analogous to the fitness value of the optimization problem. In the entire population the best solution is considered as the teacher.



The working of TLBO is divided into two parts, teacher phase and learner phase. Working of both the phase is explained below.

**Teacher phase:** It is first part of the algorithm where learners learn through the teacher. During this phase a teacher tries to increase the mean result of the class room from any value  $M_1$  to his or her level (i.e.  $T_A$ ). But practically it is not possible and a teacher can move the mean of the class room  $M_1$  to any other value  $M_2$  which is better than  $M_1$  depending on his or her capability. Considering  $M_j$  is the mean and  $T_i$  be the teacher at any iteration  $i$ . now  $T_i$  will try to improve existing mean  $M_j$  towards it so the new mean will be  $T_i$  designated as  $M_{new}$  and the difference between the existing mean and new mean is given by [80]:

$$\text{Difference\_Mean}_i = r_i (M_{new} - T_F M_j) \quad (2.15)$$

where  $T_F$  is the teaching factor which decides the value of mean to be changed, and ' $r_i$ ' is the random number in the range  $[0, 1]$ . Value of  $T_F$  can be either 1 or 2 which is a heuristic step and it is decided randomly with equal probability as:

$$T_F = \text{round} [1 + \text{rand} (0, 1)\{2 - 1\}] \quad (2.16)$$

The teaching factor is generated randomly during the algorithm in the range of 1-2, in which 1 corresponds to no increase in the knowledge level and 2 corresponds to complete transfer of knowledge. The in between values indicate the amount of transfer level of knowledge. The transfer level of knowledge can be any, depending on the learners' capabilities. In the present work, process is carried out by considering the values in between 1-2, but any improvement in the results was not observed. Hence to simplify the algorithm the teaching factor is suggested to take either 1 or 2 depending on the rounding up criteria. However, one can take any value of  $T_F$  in between 1-2.

Based on this Difference\_Mean, the existing solution is updated according to the following expression

$$X_{new,i} = X_{old,i} + \text{Difference\_Mean}_i \quad (2.17)$$

where  $X_{new,i}$  = new solution,

$X_{old,i}$  = existing solution / solution in the  $i^{\text{th}}$  iteration

**Learner phase:** It is second part of the algorithm where learners increase their knowledge by interaction among themselves. A learner interacts randomly with other learners for enhancing his or her knowledge. A learner learns new things if the other learner has more knowledge than him or her. Mathematically the learning phenomenon of this phase is expressed below.

At any iteration  $i$ , considering two different learners  $X_i$  and  $X_j$  where  $i \neq j$

$$X_{new,i} = X_{old,i} + r_i (X_i - X_j) \quad \text{if } f(X_i) < f(X_j) \quad (2.18)$$

$$X_{new,i} = X_{old,i} + r_i (X_j - X_i) \quad \text{if } f(X_j) < f(X_i) \quad (2.19)$$

Accept  $X_{new}$  if it gives better function value.

where  $X_i$  and  $X_j$  are two independent learners with different knowledge in the class, those have interact mutually to update their knowledge.

The flow chart of the ETLBO algorithm is shown in **Fig. 2.1**.

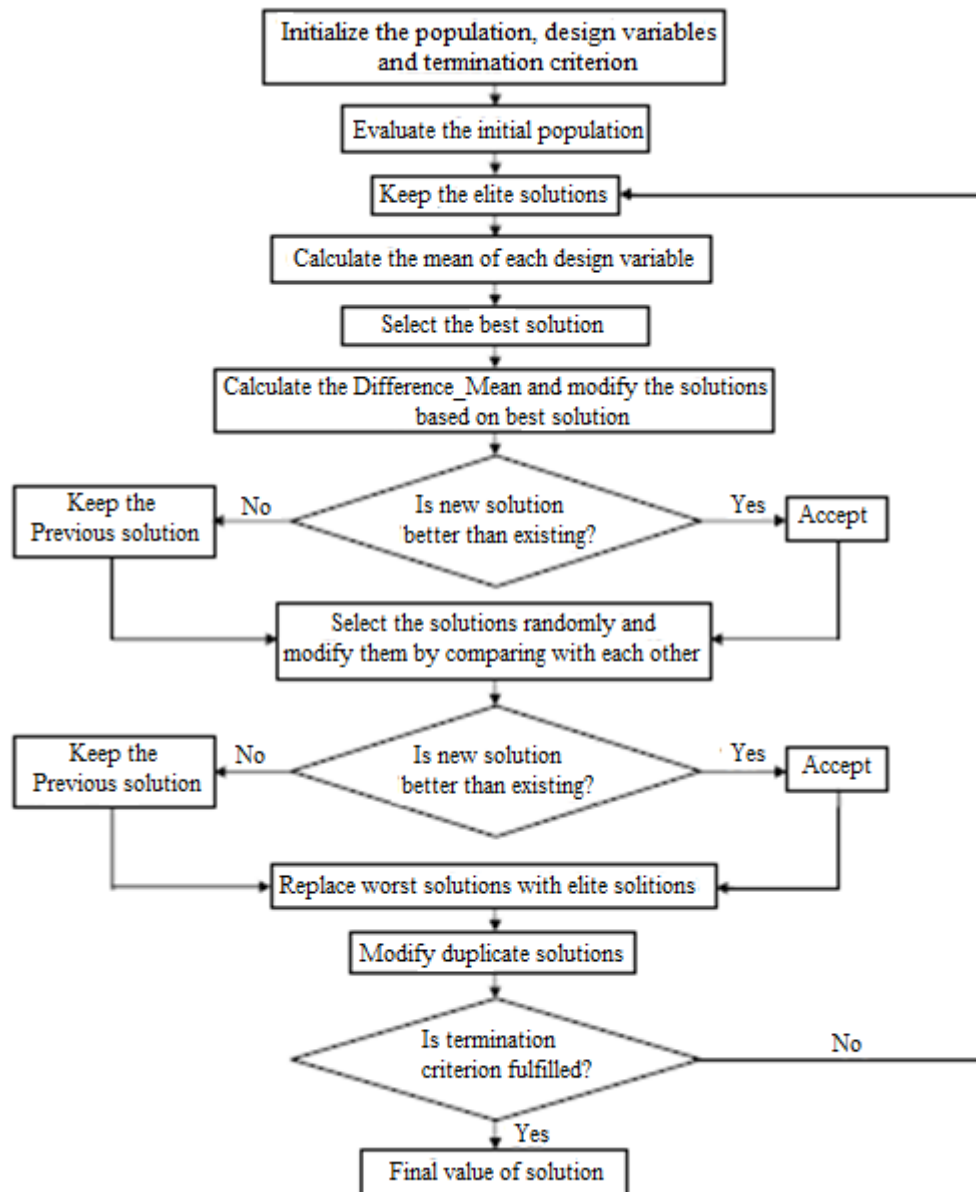


**Fig. 2.1:** Flow chart of the teaching learning based optimization (TLBO)

#### 2.4.2. Desirability function analysis (DFA)

It is an approach in which, individual responses are transformed to corresponding desirability values. Desirability value depends on acceptable tolerance range as well as

target of the response. The general approach is to first convert the response into an individual desirability function  $d_i$ , which may vary over the range  $0 \leq d_i \leq 1$ . If response  $y_i$  meets the goal or target value then  $d_i = 1$  and if response falls beyond the acceptable limit then  $d_i = 0$ . In case of several responses, an overall desirability function is used. The individual desirability is calculated as follows:

$$d_i = f_i(y)^{w_i} \quad (2.20)$$

Where,  $w_i$  is the weight of the function  $f_i(y)$  which depends on the target i.e. whether to minimize or maximize the response. In the expressions given below, 'y' is the response value; U and L are the upper and lower boundaries (i.e. minimum and maximum acceptable values for the response) respectively and T is the target. If the goal of the project is:

To hit target T:

$$f_i(y) = \begin{cases} 0 & y < L \\ \left(\frac{y-L}{T-L}\right) & L \leq y \leq T \\ \left(\frac{U-y}{U-T}\right) & T \leq y \leq U \\ 0 & y > U \end{cases} \quad (2.21)$$

To minimize the response:

$$f_i(y) = \begin{cases} 1 & y < T \\ \left(\frac{U-y}{U-T}\right) & T \leq y \leq U \\ 0 & y > U \end{cases} \quad (2.22)$$

To maximize the response:

$$f_i(y) = \begin{cases} 0 & y < L \\ \left(\frac{y-L}{T-L}\right) & L \leq y \leq T \\ 1 & y > T \end{cases} \quad (2.23)$$

### 2.4.3. Grey relational theory

The grey system theory was first proposed by Deng in 1982 [114]. It is similar to fuzzy technique and is an effective mathematical tool to deal with system analysis characterized by imprecise and incomplete information. The theory is based on the degree of information known. If the system information is unknown, it is called a black system; if the information is fully known, it is called a white system. And a system with information known partially is called a grey system. Deng had also proposed grey relational analysis (GRA) in the grey theory that was proved to be an accurate method for multiple attribute decision making problems. The GRA method is based on the minimization of maximum distance from the ideal referential alternative. The aim of GRA is to investigate the factors that affect the system. The method is based on finding the relationships of both independent and interrelating data series. By finding the GRA mathematically, the grey relational grade

(GRG) can be used to evaluate the relational level between referential series and each comparative series.

The algorithm of GRA is illustrated as follows:

- (1) Calculation of the grey relational generation in which the set of experimental results are normalized in between 0 and 1.
- (2) Calculation of the grey relational coefficients from the normalized data to represent the correlation between the desired and actual experimental data.
- (3) Calculating the grey relational grade by averaging the grey relational coefficients. The grey relational grade is treated as the overall response of the process instead of the multiple responses.
- (4) Performing statistical analysis of variance (ANOVA) for the input parameters with the grey relational grade and find which parameter significantly affects the process performance.

#### 2.4.3.1 Grey relational analysis

**Data pre-processing:** In grey relational analysis, the experimental results are first normalized in the range between zero and unity. This process of normalization is called the “grey relational generation”. The next step is to calculate the grey relational coefficients from the normalized experimental data to express the relationship between the desired and actual experimental data. Then the overall grey relational grade is calculated by averaging the grey relational coefficient corresponding to each selected response. The overall evolution of the multiple responses is based on the grey relational grade. Grey relational analysis converts a multi objective problem into a single objective problem with the objective function of overall grey relational grade. The corresponding level of parametric combination with highest grey relational grade is considered as the optimum parametric combination.

In grey relational analysis, the normalized data corresponding to lower-the-better criterion can be expressed as follows:

$$x_i(k) = \frac{\max y_i(k) - y_i(k)}{\max y_i(k) - \min y_i(k)} \quad (2.24)$$

Larger-the-better:

$$x_i(k) = \frac{Y_i(k) - \min Y_i(k)}{\max Y_i(k) - \min Y_i(k)} \quad (2.25)$$

Where,  $x_i(k)$  is the value after grey relational generation while  $\min y_i(k)$  and  $\max y_i(k)$  are respectively the smallest and largest values of  $y_i(k)$  for the  $k^{\text{th}}$  response. Larger normalized

results correspond to the better performance and the best normalized result should be equal to 1.

**Grey relational co-efficient:** The grey relational coefficients are calculated to express the relationship between the ideal (best = 1) and the actual experimental results. The grey relational coefficient  $\xi_i(k)$  can be calculated as:

$$\xi_i(k) = \frac{\Delta \min + \Delta \max}{\Delta 0_i(k) + r \Delta \max} \quad (2.26)$$

Where,  $\Delta 0_i = \|x_0(k) - x_i(k)\|$  = difference of the absolute value between  $x_0(k)$  and  $x_i(k)$ ;  $\Delta \min$  = smallest value of  $\Delta 0_i$  ;  $\Delta \max$  = largest value of  $\Delta 0_i$  ; and here 'r' is distinguish coefficient which is used to adjust the difference of the relational coefficient, usually 'r' is within the set  $\{0, 1\}$ . The distinguished coefficient weakens the effect of  $\Delta \max$  when it gets too big, enlarging the different significance of the relational coefficient. The suggested value of the distinguished coefficient, r, is 0.5 due to the moderate distinguishing effects and good stability of outcomes.

**Grey relational grade:** Grey relational grade is used to show the relationship among the series in grey relational analysis. The grey relational grade is determined by taking the average of the grey relational coefficient. The grey relational grade can be expressed as follows:

$$\alpha_i = \sum_{k=1}^n \xi_i(k) / n \quad (2.27)$$

where, 'n' is the number of performance characteristics.

**Grey relational ordering:** In relational analysis, the practical meaning of the numerical values of grey relational grades between elements is not absolutely important, while the grey relational ordering between them yields more subtle information. The combination yielding the highest grey relational grade is assigned an order of 1 while the combination yielding the minimum grade is assigned the lowest order.

### 3. EXPERIMENTAL PLAN, SETUP AND PROCEDURE

Experimental plan, procedure and description of the experiments that involved in the present work are presented here. 3 levels - 3 factors Box-Behnken design technique of response surface methodology has been employed to formulate the experimental plan under varied input process parameters with the help of Minitab 17 to indentify the effect of welding parameters on the weld bead geometry, mechanical and metallurgical characteristics and their correlations. In so far weld bead geometry is concerned, weld bead width (WW) has been measured according to standard procedure using Toolmaker’s microscope. The micro structural analysis of base material along with all welded specimens has been carried out by both optical microscopy and scanning electron microscopy (SEM) to assess the grain structure, change in phase fraction, dislocation behavior and precipitation behavior of welded joint. Mechanical properties such as tensile strength: notched tensile strength and unnotched/smooth tensile strength, percentage elongation, yield strength, impact strength, hardness and fatigue strength have been measured to identify the best quality of welded joint. Further, optimization of output responses have been made individually as well as simultaneously to obtain the optimum parametric condition for good joint quality and also analysis-of-variance (ANOVA) has been applied to determine the significant input process parameters in the process. Mathematical models have been developed to correlate the input parameters with output responses.

#### 3.1. Composition of the Base Material and Filler Material

AISI 316L stainless steel plates of 3 mm thickness has been selected as a work piece material for the present study. The 3 mm thick samples of AISI316L are joined by tungsten inert gas welding. No edge preparation is done for these samples. Filler rod has been taken as ER316L stainless steel of diameter 1.6mm. Chemical compositions of the base material and the filler material are examined and the tested results given in **Table 3.1**.

**Table 3.1:** Composition of the base material and filler material

Weight %	C	Mn	Si	S	P	Cr	Ni	Mo	Cu	Fe
AISI 316L	0.026	0.97	0.26	0.012	0.043	16.12	10.08	2.03	0.15	70.31
ER 316L	0.04	1.5	0.45	0.03	0.03	18.2	12.0	2.3	0.75	64.7

#### 3.2. Input Process Parameters

The most influencing parameters which affect weld pool geometry as well as mechanical properties of TIG welded joint are identified through extensive literature survey and previous work done. The common parameters are welding current, arc voltage, electrode

size, wire feed rate, arc travel speed, electrode stick out etc. And further the quality of weld in TIG may be affected due to welding position, electrode composition, edge preparation, the type of gases used and its flow rate. In the present investigation, after careful study the following input process parameters have been selected:

- ❖ Welding current
- ❖ Welding speed
- ❖ Shielding gas flow rate.

### 3.3. Response Parameters

The quality of the weldment is mainly characterized by the weld bead geometry as well as mechanical properties of the welded joint. Keeping all this in mind, the following output parameters have been selected as the response parameters for TIG welding of 316L austenitic stainless steel:

- ❖ Weld width (WW)
- ❖ Hardness (VHN)
- ❖ Ultimate tensile strength (UTS)
- ❖ Percentage elongation (PE)
- ❖ Yield strength (YS)
- ❖ Impact strength (IT)

### 3.4. Experimental Setup and Procedure

In the present experimental work AISI 316L stainless steel plates of size 50 mm x 80 mm x 3 mm have been selected as work piece material which is cut from a rolled sheet and ER316L austenitic stainless steel of diameter 1.6 mm has been used as a filler material. The chemical compositions of the base material and filler material are mentioned earlier in **Table 3.1**. The mechanical properties of the base metal are also listed in **Table 3.2**. The important identified input process parameters are welding current, gas flow rate and welding speed. A large number of trials have been performed on 3 mm thick AISI 316L stainless steel plates to find out the efficient and practicable working limits of TIG welding parameters and this has been done by altering one of the selected parameters while others remain constant. The visual inspection of the samples has been used to identify the working limits of the welding process parameters. The identified welding parameters along with their three levels are shown **Table 3.3**.

**Table 3.2:** Mechanical properties of base material

Ultimate Tensile strength (MPa)	Yield strength (MPa)	Modulus of elasticity (GPa)	Hardness (HV)
609	328	180	204

**Table 3.3:** TIG welding parameters and theirs levels

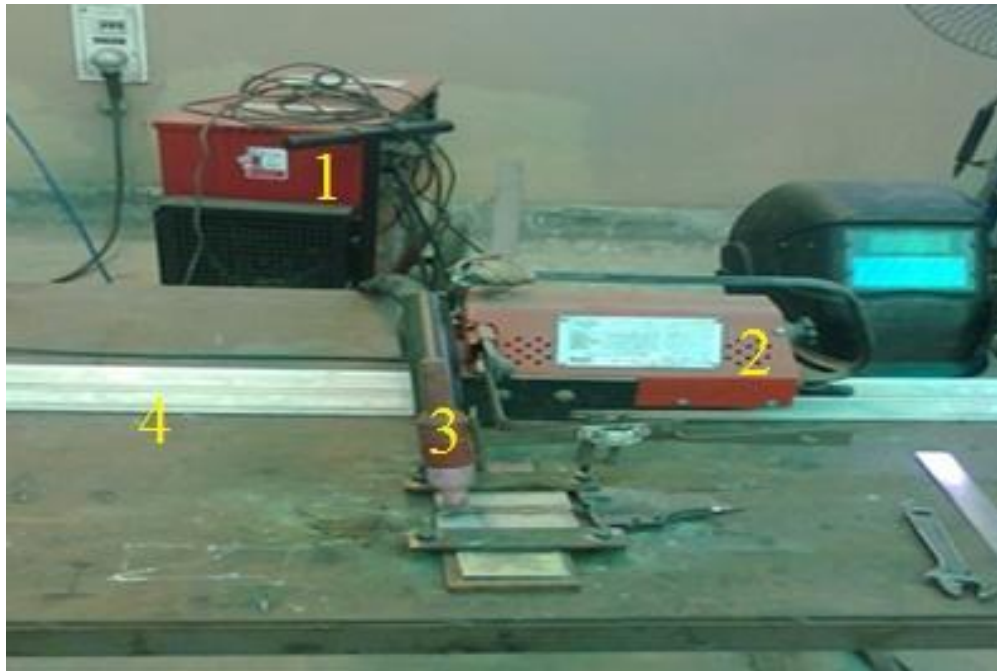
Parameters	Units	Notation	Levels		
			-1	0	+1
Welding current	A	A	100	125	150
Travel Speed	cm/min	B	12	15	18
Gas flow Rate	l/min	C	6	9	12

The statistical software Minitab 17 is applied to develop the experimental plan according to Box-Behnken design technique of RSM under varied input process parameters. The experimental design matrix is shown in **Table 3.4**. All the experiments have been conducted by a semi-automatic TIG welding machine (Model-SUPERGEN320, M/C SR. No-12111097670 and Make-Ador Welding Ltd.). The pictorial view of the experimental unit is shown in **Fig. 3.1**. Here, the TIG torch has been fixed to the travel car to confirm the torch is set at a predetermined angle. The travel car travels on the defined path and can move only straight line direction. Control of current, speed and gas flow rate are done by manually for each run. All plates of size 100 mm x 80 mm x 3 mm and filler rods are cleaned by stainless steel wire brush with acetone for removing the dust, oil, grease and thin oxide coating before welding. Square butt joint configurations have been prepared by tungsten inert gas welding using argon with purity 99.99%, as shielding gas. The welding direction has been taken as normal to the direction of rolling. During welding the work pieces have been placed on copper plate and mechanical clamps are also used for avoiding distortion.

**Table 3.4:** Experimental design matrix as per RSM

Sl. No	Input welding parametric settings		
	Current (A)	Speed (cm/min)	Gas flow rate (l/min)
1	100	12	9
2	150	12	9
3	100	18	9
4	150	18	9
5	100	15	6
6	150	15	6
7	100	15	12
8	150	15	12
9	125	12	6
10	125	18	6
11	125	12	12
12	125	18	12
13	125	15	9
14	125	15	9
15	125	15	9





*1-welding machine, 2-travel car, 3-TIG torch, 4- track*

**Fig. 3.1:** Photographic view of experimental setup

### **3.5. X- Ray Radiography Test**

X-ray radiographic test is a non-destructive testing (NDT) method that uses X-rays to produce a radiograph of a specimen, showing any changes in thickness, defects (internal and external), and assembly details to ensure optimum quality of a product.

X-ray radiographic test usually is suitable for testing welded joints that can be accessed from both sides, with the exception of double-wall signal image techniques used on some pipe. Although this is a slow and expensive NDT method, it is a dependable way to detect porosity, inclusions, cracks, and voids in weld interiors-rays, generated electrically, are penetrating radiation which is differentially absorbed by the material through which it passes; the greater the thickness, the greater the absorption. X-rays also have the property, like light, of partially converting silver halide crystals in a photographic film to metallic silver, in proportion to the intensity of the radiation reaching the film, and therefore forming a latent image. This can be developed and fixed in a similar way to normal photographic film. Material with internal voids is tested by placing the subject between the source of radiation and the film. The voids show as darkened areas, where more radiation has reached the film, on a clear background. In X-radiography the penetrating power is determined by the number of volts applied to the X-ray tube - in steel approximately 1000 volts per inch thickness is necessary. In X-radiography the intensity, and therefore the exposure time, is governed by the amperage of the cathode in the tube. Exposure time is usually expressed in terms of milli ampere minutes. To produce an X-ray radiograph, the film package (comprising film and intensifying screens - the latter being required to reduce the exposure time - enclosed in a light tight cassette) is placed close to the surface of the subject.

The source of radiation is positioned on the other side of the subject some distance away, so that the radiation passes through the subject and on to the film. After the exposure period the film is removed, processed, dried, and then viewed by transmitted light on a special viewer. Various radiographic and photographic accessories are necessary, including such items as radiation monitors, film markers, image quality indicators, darkroom equipment, etc. Where the last is concerned there are many degrees of sophistication, including fully automatic processing units. Also required are such consumable items as radiographic film and processing chemicals. Fig.3.2 illustrates of Radiography Recent developments in radiography permit ‘real time’ diagnosis. Such techniques as computerized tomography yield much important information, though these methods maybe suitable for only investigative purposes and not generally employed in production quality control.

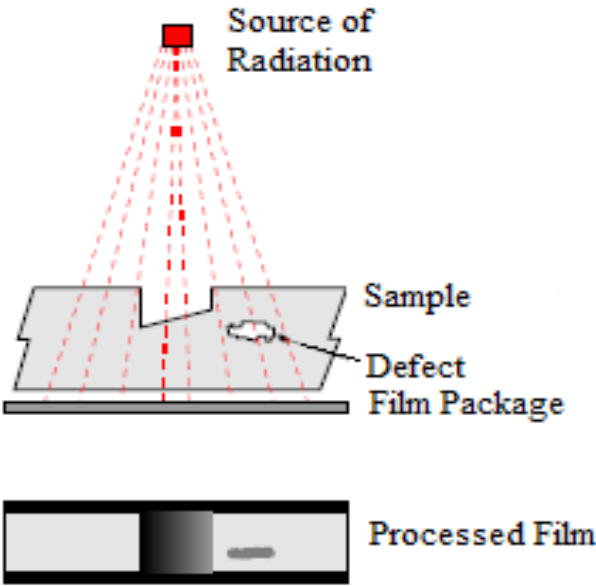


**Fig. 3.2:** Schematic diagram of a typical exposure arrangement for X-ray radiography

**Controlling Radiographic Quality**

One of the methods of controlling the quality of a radiograph is through the use of image quality indicator (IQI). The IQI is used to indicate the quality of the radiographic technique and not intended to be used as a measure of the size of a cavity that can be located on the radiograph. The IQI indicates that a specified amount of change in material thickness will be detectable in the radiograph, and that the radiograph has a certain level of definition so that the density changes are not lost due to unsharpness. Without such a reference point, consistency and quality could not be maintained and defects could go undetected.

X-ray is used to determine the internal soundness of welds. This examination has been done for all 15 welded joints after the visual inspection by XXQ-2005 X-Ray flaw detector. X-ray radiography tests have been done at SKB metallurgical services, Salkia, Howrah111062.

The important specifications of this equipment are as follows:

Voltage:	120 kV
Current:	5 mV
Film:	LASER NDT-7
Sensitivity:	< 2%
SOD:	28"
Screen:	0.15 mm
Technique:	S.W.S.I.
IQI:	ASTM-1A
Exposure time:	30 Sec
Processing temperature:	200C

### 3.6. Measurement of weld width

The weld bead shape is a very important factor in determining the quality of welds. Weld width is directly proportional to the arc current, welding voltage, the diameter of electrode and is inversely proportional to the welding speed. The mechanical properties of welds are affected by the weld bead shape. Hence, its close control is must. The weld bead shape is a very important factor determining the quality. A welding joint is considered to be good or of high quality if weld bead width is minimum in size. If bead width is less, the distortion of welded plates and residual stresses are least.

After X-ray radiography test, all the welded specimens have been cut perpendicular to the direction of welding for measurement of weld bead geometry according to standard procedure using toolmaker's microscope. **Fig. 3.3** shows the photographic view of the Tool Maker's Microscope in which the two dimensional co-ordinate of a point on any specimens can be measured by the microscopic view and the two micrometer system. Weld bead width has been measured for all the welded samples. **Fig. 3.4** shows the elements of weld bead geometry.



**Fig. 3.3:** Photographic view of Tool Maker's Microscope

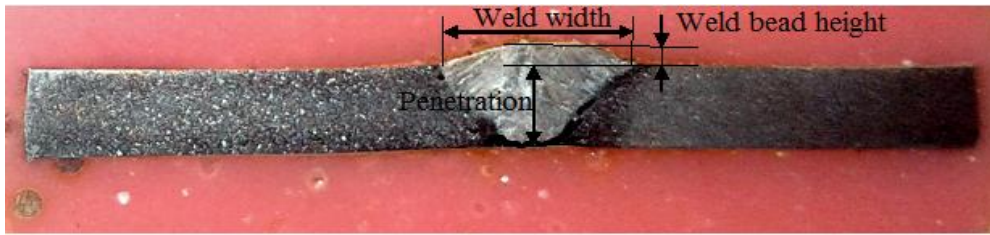


**Fig. 3.4:** Weld bead geometry

### 3.7. Metallographic Analysis

All the welded samples have been prepared for the metallographic examinations to reveal the micro-structural details. Generally the steps involved in preparing such samples are as follows: (i) Cutting (ii) Mounting (iii) Grinding (iv) Polishing and (v) Etching.

At first samples of size nearly 20 mm x 10 mm x 3 mm is cut from TIG welded joints by machining. After mounting and grinding samples are prepared by polishing successively in 80, 120, 220, 320, 400, 1200, 1600, 2000 grade emery papers using semi-automatic polisher (*Make: BUEHLER; Model: ECOMET 3000*) to remove the scratches. **Fig. 3.5** represents the pictorial view of semi-automatic polisher setup and a mounted sample after polish. Thereafter all of the samples are polished by Velvet cloth. After the polishing each of the samples is ready for etching. The compositions of the etchant are 2.4 gm of  $\text{CuCl}_2$ , 10 ml of 99 %  $\text{C}_2\text{H}_5\text{OH}$  and 10 ml of 40% HCl. Micro structural examination has been conducted using an optical microscope (*Make: Leica; Model: DLM2700M*) as shown in **Fig. 3.6**. And micrographs have been taken at different magnifications.

A scanning electron microscope (SEM) (*Make: JEOL; Model: JSM6360*) as shown in **Fig. 3.7** is also used to observe the microstructures of different welded samples. It produces images of a sample by scanning the surface with a focused beam of electrons that interact with atoms in the work sample to produce various signals, which contains information about the sample's surface topography and composition.



**Fig. 3.5:** Semi-automatic polisher and mounted sample after polish



**Fig. 3.6:** Optical microscope



**Fig. 3.7:** Scanning electron microscope

### **3.8. Micro-hardness Test**

Micro-hardness Test is a method of determining a material's hardness or resistance to indentation when test samples are very small or thin, or when small regions in a composite sample or plating are to be measured. Micro hardness is an important mechanical property. It can display the elasticity, plasticity and strength of materials. The aim of hardness testing of welded joints is to identify:

- a) The hardness of the parent metal and make an approximate determination of the materials tensile strength to assure the correct material is being welded.
- b) The hardness of the weld to ensure the weld metal meets or exceeds the strength requirements of the parent metal.
- c) The hardness of the HAZ to ensure the welding heat input, preheat and inter pass temperature has been controlled sufficiently to produce a HAZ with the appropriate strength and toughness.

After micro structural analysis micro-hardness measurement has been performed by Vickers's micro-hardness testing machine (*Make: MATSUZAWA; Model: AMT-X7BFS*) on etched transverse cross section of the welded specimens using a load of 100gf, which is applied for duration of 15s. Nine different locations have been selected for the measurement of micro hardness values as shown in **Fig. 3.8**. These locations are 4 points on the base metal, 2 points on the HAZ zone and 3 points on the weld zone. The micro hardness setup is shown in **Fig. 3.9**.

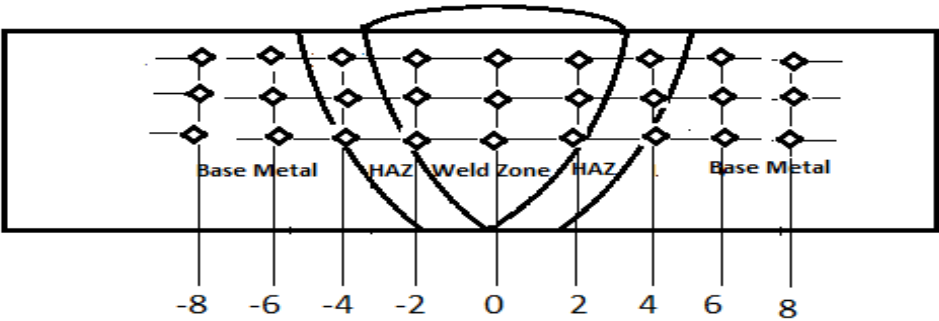


**Fig. 3.8:** Schematic diagram showing positions of micro hardness measurement

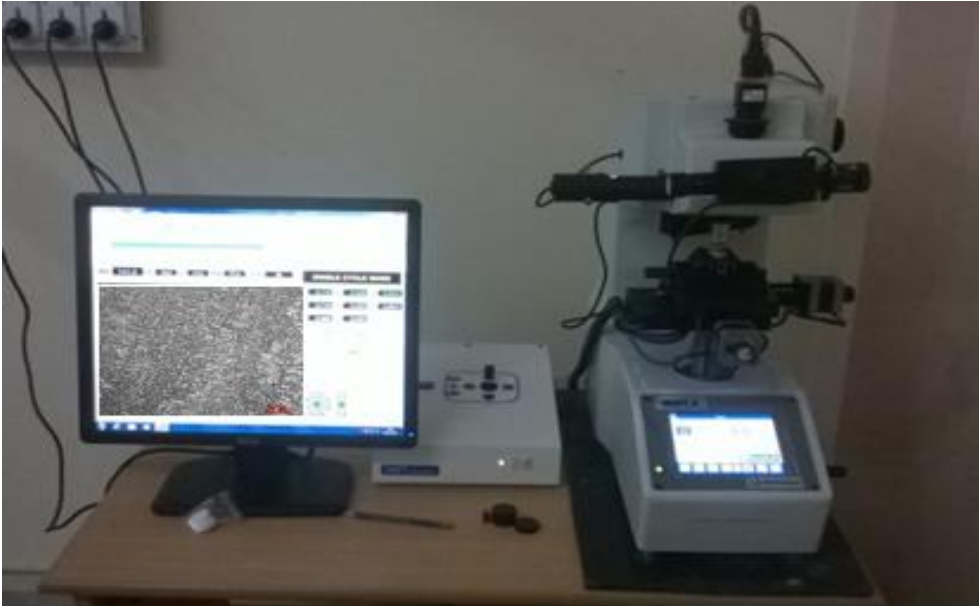


**Fig. 3.9:** Micro hardness setup

### 3.9. Tensile Test

Tensile properties of the welded joints namely ultimate tensile strength, yield strength and ductility (percentage elongation) can be obtained using tensile test which is usually conducted at constant strain rate. The tensile test is a standard test for procedure qualification and is also used to indicate whether the weld strength equals that of the base metal tensile strength or less. Tensile strength has been selected to assess weld quality because it is a key mechanical property that can describe weld joint performance. The ultimate tensile strength of weld joint is important because it is an estimate of maximum load that the weld can support.

Two different types of tensile specimens, notched tensile specimens and smooth /unnotched tensile specimens have been prepared in accordance with ASTM E8M-04 as shown in **Fig. 3.10(a)** and **Fig. 3.10(b)** respectively. The measurement of tensile strength of welded samples have been conducted by Instron universal testing machine (Model- 8801 and capacity-100kN) at a strain rate of 0.001/s to evaluate notched tensile strength (NTS), un-notched tensile strength, percentage elongation and yield strength of base metal as well as TIG welded joints. The pictorial view of universal testing machine setup is shown in **Fig. 3.11**. After tensile test, the fracture surfaces of test specimens of base metal and welded joints have been examined using scanning electron microscope to investigate the fracture morphology.

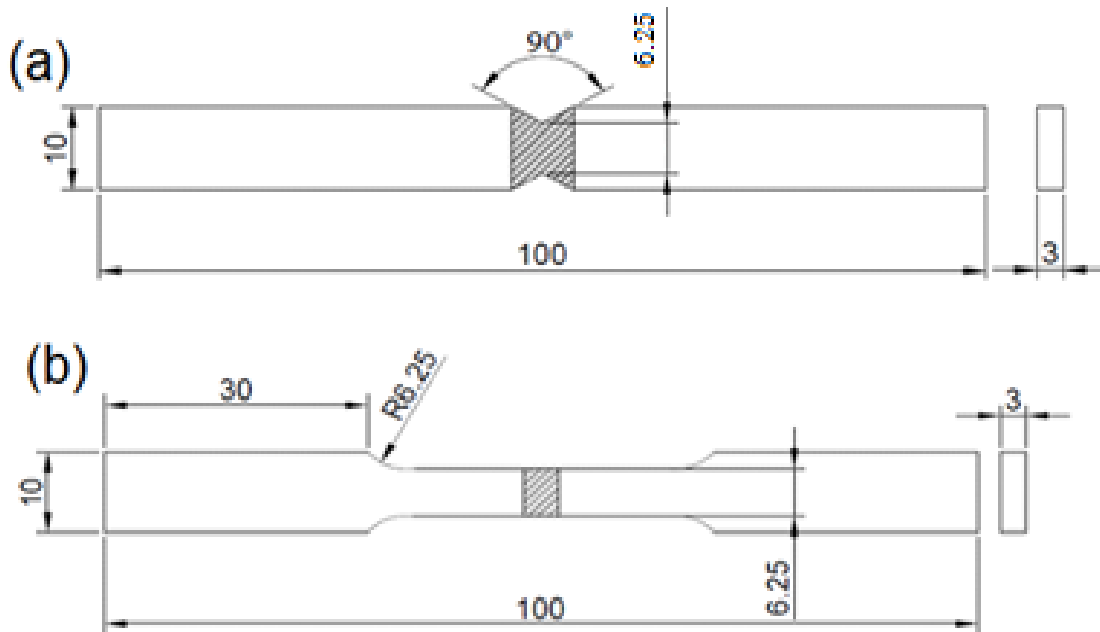


**Fig. 3.10:** TIG welded sample for tensile test (a) notched specimen (b) smooth specimen



**Fig. 3.11:** Universal testing machine

### **3.10. Impact Test**

In actual practice, engineering components during service are subjected to various kinds of load: static and dynamic loads which are classified on the basis of the rate of change in magnitude of load and direction. Dynamic loads are characterized by high rate of change in load magnitude and direction. Reverse happens in case of static loads. A material which possesses a large amount of impact resistance is said to be tough material. Impact strength is the ability to resist high rate of loading. It is the critical property for most of the materials because impact strength is related to the product performance, service life, and liability.

Charpy V-notch impact test is also carried out to evaluate the impact toughness values of all the welded samples along with base metal at room temperature using Impact tester machine (Make-S. D. HARDSON & CO., Model No. SDH/100). The pictorial view of impact tester machine setup is shown in **Fig. 3.12**. The test specimens have been prepared in accordance with ASTM E23 as shown **Fig. 3.13**. V-notches are prepared in the weld zone.





**Fig. 3.12:** Impact tester machine

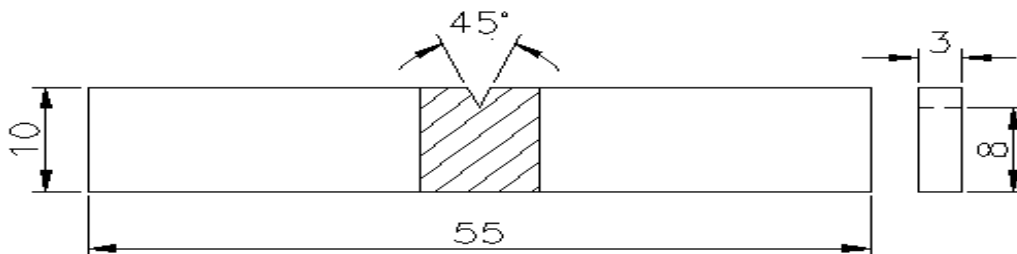


**Fig. 3.13:** Impact test specimen

### 3.11. Bending test

Bending test is one of the most important and commonly used destructive tests to determine the ductility and soundness (for the presence porosity, inclusion, penetration and other macro-size internal weld discontinuities) of the weld joint produced under one set of welding conditions. Bending of the weld joint can be done from face or root side depending upon the purpose i.e. whether face or root side of the weld is to be assessed.

Bending test of all the welded joints have been performed from face side of the weld on Universal Testing Machine (Model No. AI-UTM-600KN, Serial Number 018/2001) using simple compressive or bending load and die of standard size for free and guided bending. The pictorial view of test specimen and universal testing machine setup is shown in **Fig.3.14** and **Fig. 3.15** respectively.

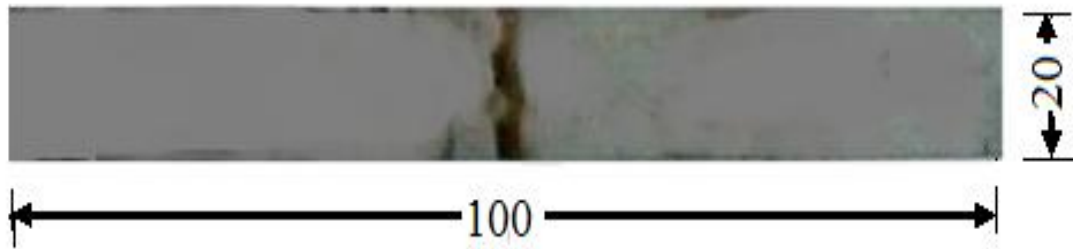


**Fig. 3.14:** TIG welded sample for bending test



**Fig. 3.15:** Bending Tests in Universal Testing Machine

### **3.12. Fatigue test**

Fatigue is the most common cause of failure in welded structures and components, accounting for around 90% of failures that can occur at a fluctuating load well below the yield point of the metal and below the allowable static design stress. There will be little or no deformation at failure. Fatigue, thereby reduces the lifetime of structures and components. High cycle fatigue is a typical failure mode in engineering.

High cycle fatigue behaviour of the welded joints as well as base metals has also been investigated. Fatigue test specimens have been prepared in accordance with ASTM E4 as shown in **Fig. 3.16**. Load-controlled uniaxial fatigue tests have been performed using a Testronic 100KN RUMUL resonant testing machine at room temperature, at stress ratio (R) of 0.1 and at a frequency of 80Hz. The pictorial view of fatigue testing machine setup is shown in **Fig. 3.17**.

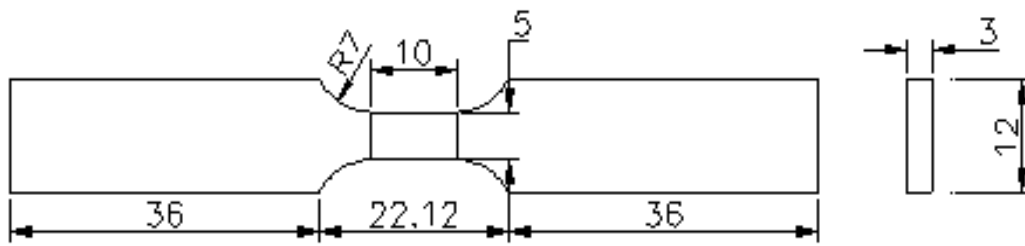


**Fig. 3.16:** Fatigue test specimen



**Fig. 3.17:** Fatigue testing machine

## **4. RESULTS AND DISCUSSION**

Experimental plan, setup and procedure have been discussed in **chapter 3**. The process parameters chosen for the present study are welding current, travel speed and gas flow rate. The process variable with their values at different levels is shown in **Table 3.3**. The selection of the values of the welding input variables is limited by the capacity of the welding set up used in the experimentation as well as recommended combinations depending on work piece properties. The three levels of the each parameter have been selected at an equal spacing. Experimental runs have been conducted on a semi-automatic TIG welding machine to make weld joints of type 316L austenitic stainless steel, as per Box-Behnken design method of RSM as shown in **Table 3.4**. Welding quality responses: ultimate tensile strength (UTS), percentage elongation (PE), yield strength (YS), impact strength (IS), hardness (VHN) and weld width (WW) have been measured for all fifteen welded samples. Bending test has also been performed for all the samples to assess the soundness of the weld quality.

Parametric analysis has been made to study the influences of selected input welding parameters on weld responses using statistical analysis of variance and graphical main and interaction plots. Mathematical modeling of welding responses has been made to develop the mathematical relationships between the input welding variables with each weld response separately with the use of response surface methodology (RSM). Contour plots have developed from the mathematical models to study the direct and interaction effects of process parameters on each response variable. The optimization of weld quality responses has been made by solving the mathematical models of each response to obtain the desired values of response(s), separately for each welding characteristic such as UTS, PE, YS, IS, hardness and WW in TIG welding of 316 L austenitic stainless steel materials using two optimization techniques namely desirability function approach (DFA) and teaching learning based optimization (TLBO) approach.

The optimization of multi-response characteristics simultaneously, is difficult problems due to their different objectives. In the present work, multi-objective of UTS, PE, YS, IS, hardness and WW have been optimized combinedly by converting into single objective function. Grey relational analysis technique has been used to convert the multi objective problem in to single objective problem. Grey relational grade which compromising the all the response characteristics has been developed. Factor analyses have been done by using analysis of variance (ANOVA) technique and graphical main and interaction plots, to study the significances of welding responses on grey relational grade (i.e. for all responses). Mathematical modeling has been made to develop mathematical relations between the grey relational grade and input welding parameters by RSM. Direct and interaction effects of welding input parameters on grey relational analysis has been made by generating contour

plots from the developed mathematical model of Grey relational analysis by using RSM approach. Parametric optimization has been done for maximizing the GRG (which compromises UTS, PE, YS, IS, hardness and WW) by solving the obtained mathematical models with the use of TLBO and DFA.

Comparative analysis has also been made between the optimum welding condition obtained for predicting welding responses separately and combinedly from two optimization approaches: TLBO and DFA. Confirmatory tests have also been done to validate the responses obtained from said optimization techniques.

Finally, high cycle fatigue behaviour of TIG welded joints has been investigated. These welded joints have been made at obtained optimized parametric condition.

## **4.1. Results and Discussion of Non destructive and Destructive Tests**

After welding operation, quality of the weld has been judged, first by visual inspection and then by non-destructive and destructive testing methods. In so far as non-destructive test is concerned, X-ray radiography has been taken up. In case of destructive testing tensile test, hardness test, impact test, and bending test have been conducted. The results of each test and their analysis are discussed in the following sections.

### **4.1.1. Visual Inspection**

A visual inspection examines the quality of weldment such as bead appearance, width and thickness, welding defects like undercut, cracks, pits, and slag inclusions in the surfaces of the welded joints. It is a very easy, simple and economical activity. It does not require any costly equipment. It requires different types of welding gauges, magnifying glass etc. Visual inspection can be done at three stages: Before welding, during welding and after welding. Photographic view of two welded specimens, sample number 1 and sample number 14 are shown in **Fig. 4.1**.

The results of post-weld visual inspection of all the welded samples are listed in **Table 4.1**. The defects observed in the visual inspection in some of the samples include: porosity, little under cut at the end, large reinforcement height, lack of penetration etc. Under certain parametric conditions, almost no defects are found in a few samples like sample numbers 2, 5, 8, 9, 12, 13, 14 and 15. The possible reasons of the defects found in several samples are due to fluctuation of voltage, lack of environmental suitability and due to semi-automatic TIG welding machine set-up etc. Defects may come from any type of inhomogeneity in the base metal as well as filler wire. Porosity may occur due to contaminated surfaces, improper gas shielding, too high arc length etc. [140]. Undercut defect may be caused by inappropriate joint geometry in some of the samples. It may have been resulted because of excessive welding current, and voltage. The combined effects of various welding input parameters can also form undercut defect on weldment [141]. The possible causes for formation of large reinforcement height are: too high welding current, too much root opening

and too much filler metal for the travel speed used [142]. In welding, lack of penetration is one of the main defects which most significantly affect the joint strength of the welded sample. The reasons for lack of penetration are faster travel speed, lower heat input, incorrect selection of welding currents levels, improper cleaning of welding zone, presence of oxides, scale and other impurities which do not allow the deposited metal to fuse accurately with the base metal [143]. Photographic view of all other specimens have been illustrated in Appendix-A.

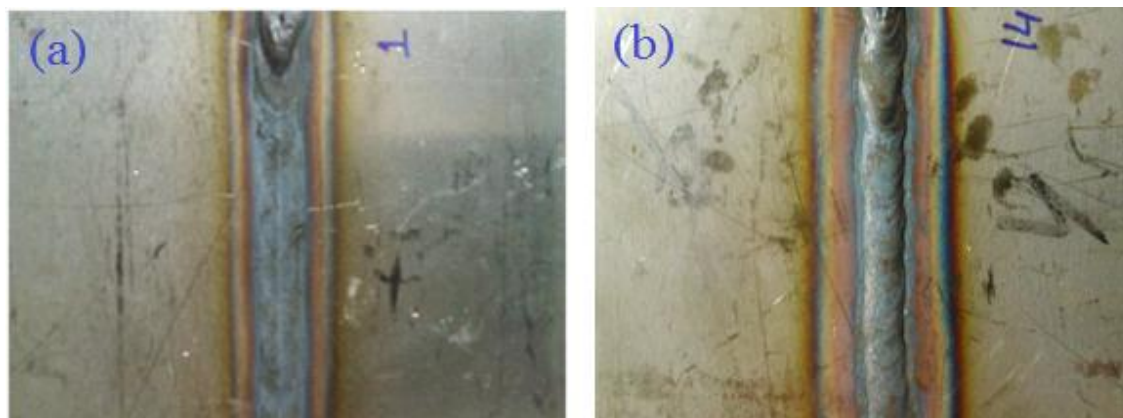


**Fig. 4.1:** Photographic view of welded sample number 1 & 14

**Table 4.1:** Results of visual inspection

EXP. No.	Current (A)	Speed (cm/min)	GFR (l/min)	Observations
1	100	12	9	Large reinforcement height at the starting
2	150	12	9	Uniform penetration & uniform weld bead
3	100	18	9	Lack of penetration at the end
4	150	18	9	Little undercut at the end
5	100	15	6	Good penetration throughout
6	150	15	6	Large reinforcement height
7	100	15	12	Lack of penetration at the end
8	150	15	12	Uniform HAZ width, no defect
9	125	12	6	Good penetration throughout
10	125	18	6	Min. porosity but good penetration throughout
11	125	12	12	Lack of penetration at the end
12	125	18	12	Uniform penetration & uniform weld bead
13	125	15	9	Good penetration throughout
14	125	15	9	Uniform penetration & uniform weld bead
15	125	15	9	Good penetration throughout

#### 4.1.2. X-Ray Radiography Test

X-ray radiography test has been performed for all the 15 welded samples to determine

the internal soundness of the welded joints after the visual inspection by XXQ-2005 X-Ray flaw detector. The image of X-ray radiography of two samples (sample no.14 and sample no.7) is shown in **Fig. 4.2** and the results of X-ray radiography examination is illustrated in **Table 4.2**. It is observed that almost all the welded samples pass through X-ray radiography test with no significant defect remarks. But minimum porosity has been found in sample no.7 and sample no.10. Porosity may create when atmospheric gases are being entrapped in the solidifying metal. The causes of porosity may include lack of shielding gas or too much shielding gas, improper cleanness of the work piece etc.

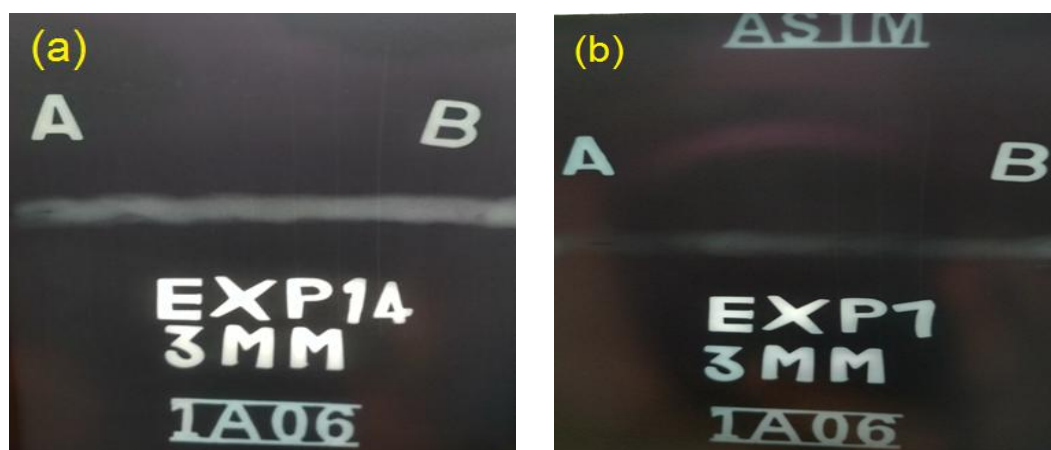


**Fig. 4.2:** Image of the X-ray radiography plate (a) sample-14 and (b) sample-7

**Table 4.2:** Results of X-ray radiography test

EXP. No.	Current (A)	Speed (cm/min)	GFR (l/min)	Observations	Remarks
1	100	12	9	No significant defect	Acceptable
2	150	12	9	No significant defect	Acceptable
3	100	18	9	No significant defect	Acceptable
4	150	18	9	No significant defect	Acceptable
5	100	15	6	No significant defect	Acceptable
6	150	15	6	No significant defect	Acceptable
7	100	15	12	Minimum porosity	Acceptable
8	150	15	12	No significant defect	Acceptable
9	125	12	6	No significant defect	Acceptable
10	125	18	6	Minimum porosity	Acceptable
11	125	12	12	No significant defect	Acceptable
12	125	18	12	No significant defect	Acceptable
13	125	15	9	No significant defect	Acceptable
14	125	15	9	No significant defect	Acceptable
15	125	15	9	No significant defect	Acceptable

Qualities of the joints are further evaluated by other tests and studies, as well. If the results of visual inspection and the results of X-ray radiography test are compared, then some consistency can be observed. It is found from **Table 4.1** & **Table 4.2** that low current is not

the primary cause of lack of penetration, because for sample numbers 1, 3, 5 and 7 also have the current level 100A; but for these samples almost no defect is found. Lack of penetration defect may also come from any irregularities in the base metal or filler wire as mentioned earlier in case of visual inspection. Large electrode angle may also be a possible reason for this type of defect. Any improper welding environment can also affect the weld quality. This may have occurred due to entrapped gas in the weld pool, which could have been avoided by proper selection of gas flow rate and arc gap. A faster travel speed, too small root gap may also be the reasons in such defect [142]. Therefore defects may possibly appear from inappropriate choice of different welding parameters namely current, voltage, arc gap etc. including their ranges also [143]. It is noticed from the tables of Visual as well as radiography examination that almost no welding defects are observed, when welding with middle value of welding current, speed and gas flow rate. It is also found from Visual inspection and X-ray radiographic examination that no significant defect presences in sample numbers 13, 14 and 15. Thus, this is the reason for obtaining higher values of tensile properties of the samples under tensile testing. The image of X-ray radiography of all the welded samples has been illustrated in Appendix-B.

After non-destructive testing, destructive tests like tensile test (un-notched / smooth specimens), hardness test, impact test, bending test have been conducted. The measured output responses are tabulated in **Table 4.3**.

**Table 4.3:** Measured experimental results

Sample No.	Output responses					
	UTS (MPa)	% Elongation	Yield Strength (MPa)	Impact Strength (J)	Hardness (HV)	Weld width (mm)
1	612.13	33.72	316.11	41.5	234	7.61
2	616.42	45.49	374.76	39.0	231	6.78
3	608.48	42.06	370.21	40.5	236	6.22
4	630.37	41.69	377.82	45.5	237	6.35
5	621.26	41.77	340.26	41.0	236	6.81
6	612.91	40.23	364.12	38.5	230	6.64
7	580.61	30.25	309.12	33.5	230	7.37
8	607.69	44.51	370.11	40.0	233	6.82
9	624.15	40.56	274.61	42.0	234	6.83
10	616.24	39.85	355.11	39.5	237	6.18
11	592.42	33.77	300.52	35.0	231	7.44
12	615.88	42.22	292.51	42.5	238	6.24
13	639.42	51.68	344.45	51.0	244	6.55
14	642.64	52.38	370.41	52.0	245	6.54
15	639.67	51.32	350.24	51.5	245	6.56
Base metal	608.88	51.85	328.01	40.0	204	---



### 4.1.3. Micro structural analysis

The micro structural analysis of base material along with all welded specimens has been carried out by optical microscopy and base metal along with three chosen welded specimens have also been carried out scanning electron microscopy (SEM). These specimens are sample no.14, sample no.7 and sample no.2. The selection of these samples for microstructural analysis is based on the obtained responses i.e. the specimens having maximum, minimum and average mechanical properties respectively are considered for the analysis of SEM.

**Fig. 4.3** shows the typical microstructure (both optical microscopy and scanning electron microscopy) of base the metal. The base metal mainly consists of fully austenitic structure along with few annealing twins. Wichan and Loeshpahn [115] are also reported similar result. **Fig. 4.4 – Fig. 4.7** shows the optical microstructures of TIG welded transition zone and weld zone of all the specimens. The base metal (BM), heat affected zone (HAZ) and weld metal (WM) can be easily distinguished. The microstructure of base metal is completely different from weld metals irrespective of input parameters. The fusion zone mainly consists of ferrite and austenite. The white zone refers to austenite and dark zone is ferrite. The micrographs of TIG welded samples show epitaxial columnar dendritic growth at the primary stages of solidification from the fusion boundary towards the weld center. However, grains are found to be coarser in HAZ zone compared to the base metal. This may be attributed to lower cooling rate in the HAZ region. Furthermore weld metals show the presence of lacy  $\delta$  ferrite at the dendrite core surrounded by inter dendritic  $\gamma$ -phase.

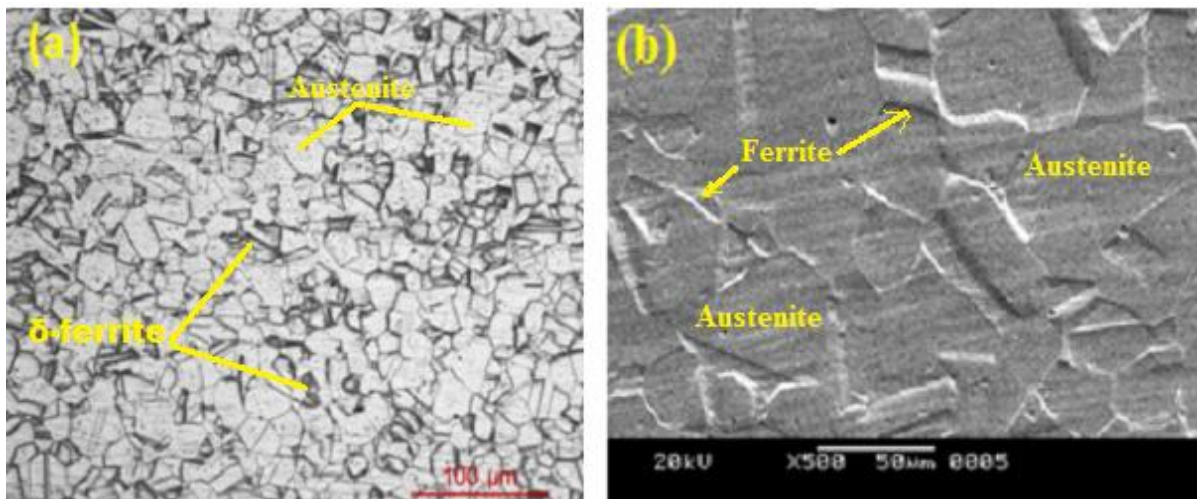


**Fig. 4.3:** Microstructure of base metal (a) optical microscopy, (b) SEM

It is known that increasing welding current, increases the heat input. As heat input increases the molten weld metal takes longer time for solidification. Therefore grain size becomes larger and coarse compare to the samples welded under low welding currents. For higher heat inputs, i.e. slow cooling rates the  $\delta$ -ferrite can have a vermicular morphology with a coarse dendritic structure as shown in **Fig. 4.4 b<sub>1</sub>**. Similar types of grain structures are also found in **Fig. 4.5 (b<sub>1</sub>& d<sub>1</sub>)** under higher welding current due to the slow solidification rate.

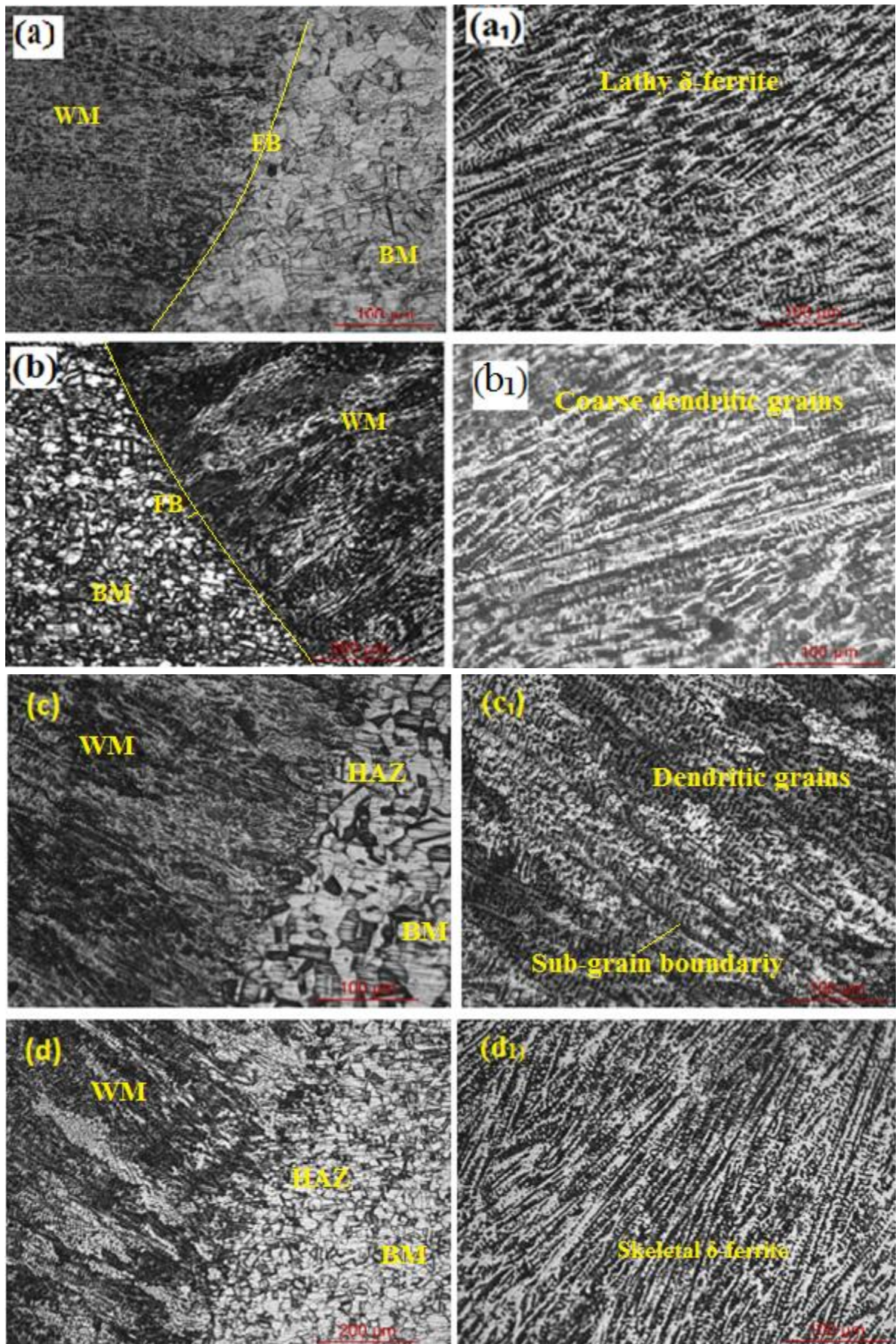


**Fig. 4.4:** Optical microstructures of TIG welded joints - (a) sample no.1 (b) sample no.2 (c) sample no. 3 (d) sample no 4 and a<sub>1</sub>, b<sub>1</sub>, c<sub>1</sub>, d<sub>1</sub> corresponding weld metals.

Increasing welding current as well as welding speed the weld pool changes from elliptical to tear drop shaped. Consequently, the depth of penetration increases rapidly. As welding speed increases the width of heat affected zone becomes very small due to rapid cooling of weld pool. At the same time the dendrite size in the weld zone also reduced because at high speed (low heat input) the weld metal gets less time for the growth of dendrites as illustrated in **Fig.4.4 (d-d<sub>1</sub>)**. Depending on the welding speed, different structures can be observed in the weld region. The heat input and the welding speed can affect the solidification mode of weld metal significantly. The quality of weld is mostly controlled by the solidification manners of the weld metal. It controls weld-metal microstructure, grain structure, mechanical properties etc. The weld metal solidification mode can be explained by the  $Cr_{eq}/Ni_{eq}$  ratio [116]. Chromium and nickel equivalents can be determined on the basis of chemical composition of the investigated weld metal. The chemical composition of weld metal is shown in **Table 4.4**. The  $Cr_{eq}/Ni_{eq}$  ratio is calculated using the Schaeffler formula [14] given below:

$$Cr_{eq} = Cr + Mo + 1.5 Si + 0.5 Nb \quad (4.1)$$

$$Ni_{eq} = Ni + 30 C + 0.5 Mn \quad (4.2)$$

In the present study the  $Cr_{eq}/Ni_{eq} = 1.62$ . Therefore the solidification mode is ferritic-austenitic mode (FA) as  $1.48 \leq Cr_{eq}/Ni_{eq} \leq 1.95$ .



where L is the liquid,  $\delta$  is delta-ferrite and  $\gamma$  is austenite respectively.

At lower welding speed means high solidification constraints, the grains in the innermost part of the weld are oriented longitudinally as a result a nearly circular weld pool may be obtained as noticed in the **Fig. 4.4 (a & b)**. With higher welding speed, the cooling rate is high then the grains will grow at a faster rate and it cover up more area. And smaller equiaxed grains structure is formed as illustrated in **Fig. 4.6b<sub>1</sub>**. From **Fig. 4.5c<sub>1</sub>** and **Fig. 4.6c<sub>1</sub>**, it is observed that larger grain growth is obtained under higher shielding gas flow rate due to the rapid solidification rate. As the shielding gas flow rate increases the grain structure becomes coarser and more distinct. The most favorable result is achieved at a gas flow rate of 9 l/min.

The SEM micrographs of chosen welded specimens are illustrated in **Fig. 4.8**. Both optical and SEM micrographs exhibit similar types of results. The weld zone of sample no. 14 exhibits a very fine skeletal  $\delta$ -ferrite along with grain, sub grain and migrated boundaries in plain austenitic matrix due to moderate heat input and moderate cooling rate. The weld sample no.7 consists of  $\delta$ -ferrite in the form of dendritic lathy  $\delta$ -ferrite at the dendrite core surrounded by inter dendritic  $\gamma$ -phase due to low welding heat inputs, i.e. high cooling rates. The microstructure of the weld, sample no. 2 depicts a coarse equiaxed grains structure

which has been formed due to the decomposition of dendritic grains in plain austenitic matrix and coarse HAZ zone is also formed.

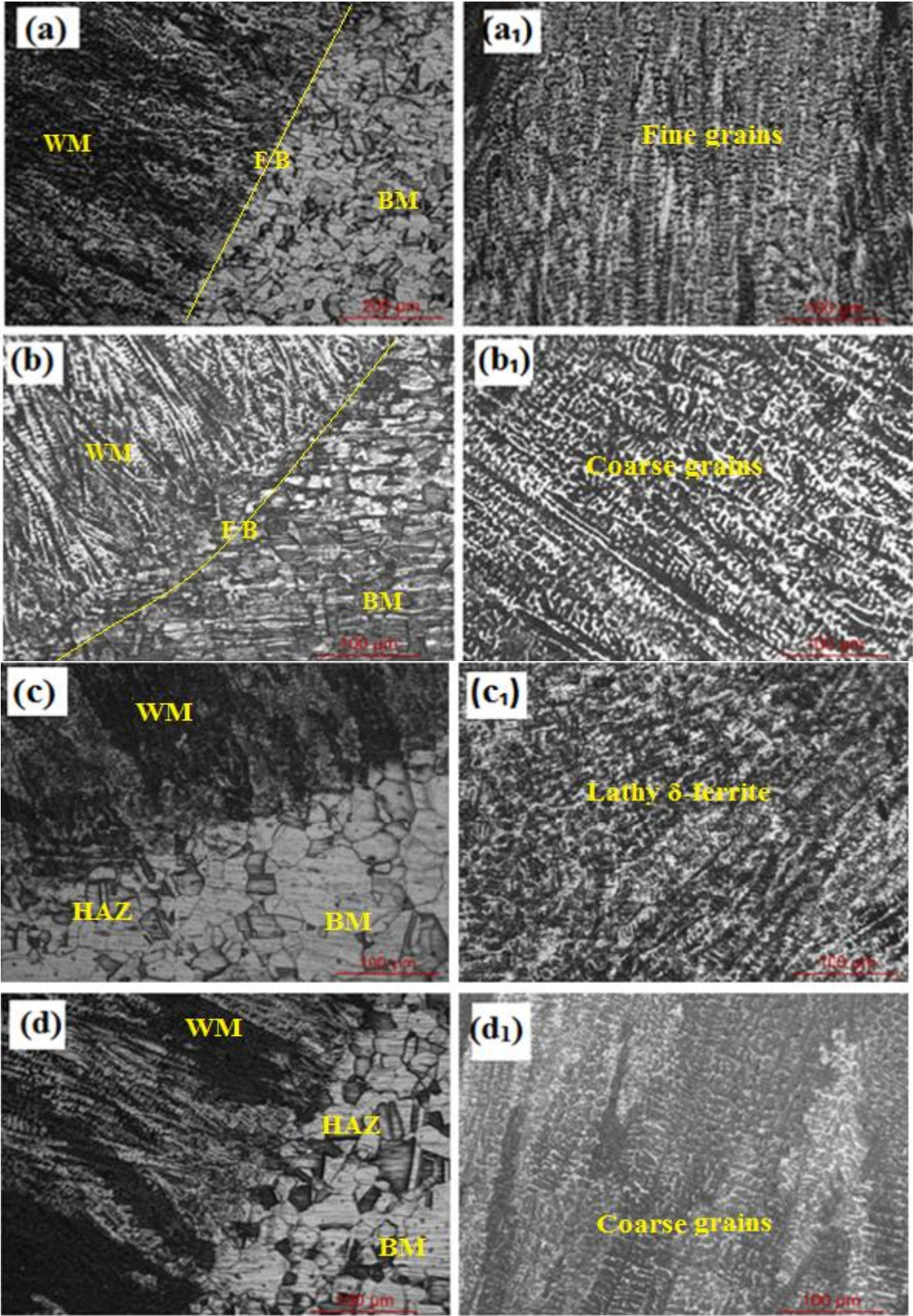


**Fig. 4.5:** Optical microstructures of TIG welded joints - (a) sample no. 5 (b) sample no.6 (c) sample no. 7 (d) sample no. 8 and a<sub>1</sub>, b<sub>1</sub>, c<sub>1</sub>, d<sub>1</sub> corresponding weld metals

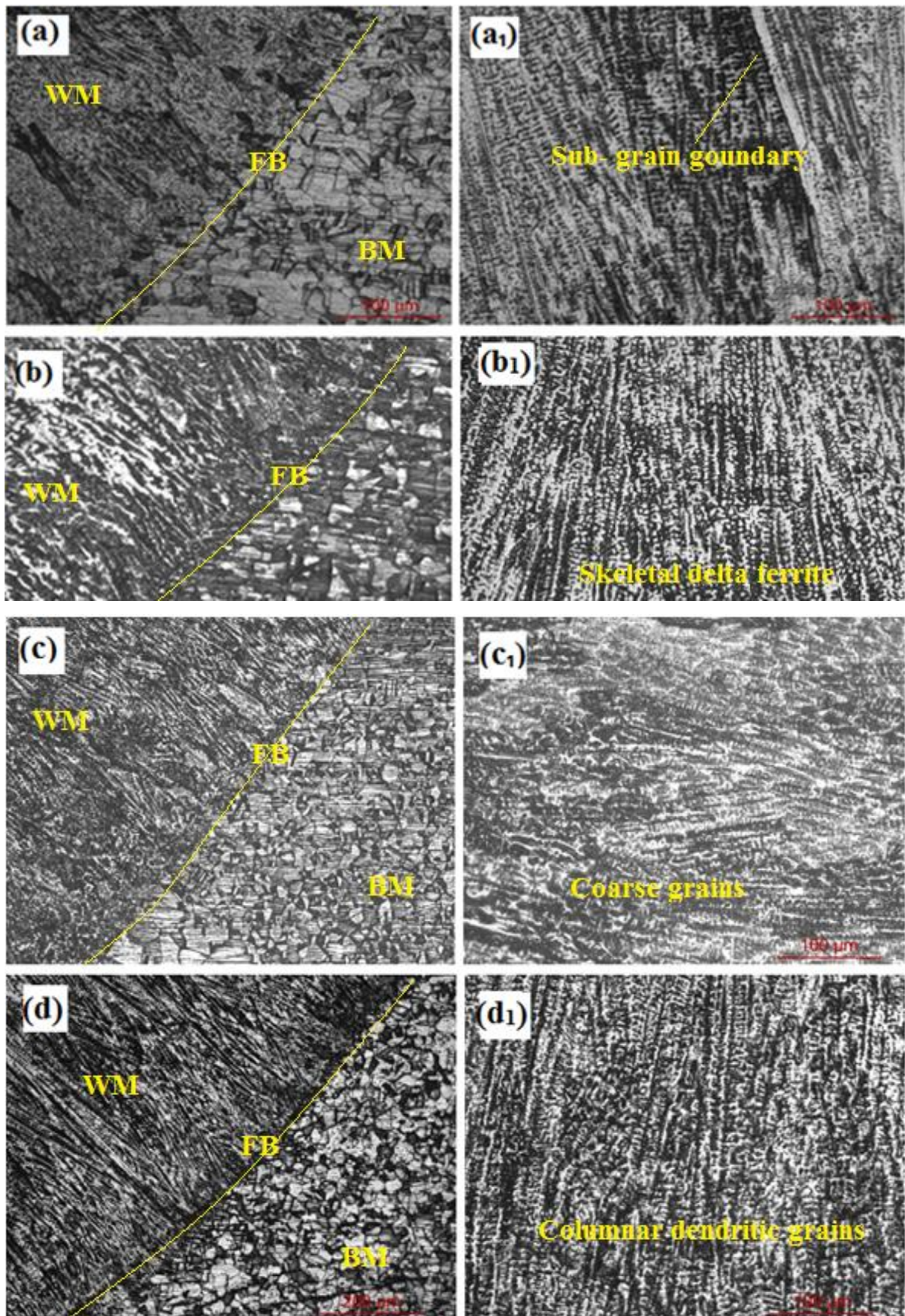


**Fig. 4.6:** Optical microstructures of TIG welded joints - (a) sample no. 9 (b) sample no.10 (c) sample no. 11 (d) sample no. 12 and a<sub>1</sub>, b<sub>1</sub>, c<sub>1</sub>, d<sub>1</sub> corresponding weld metals

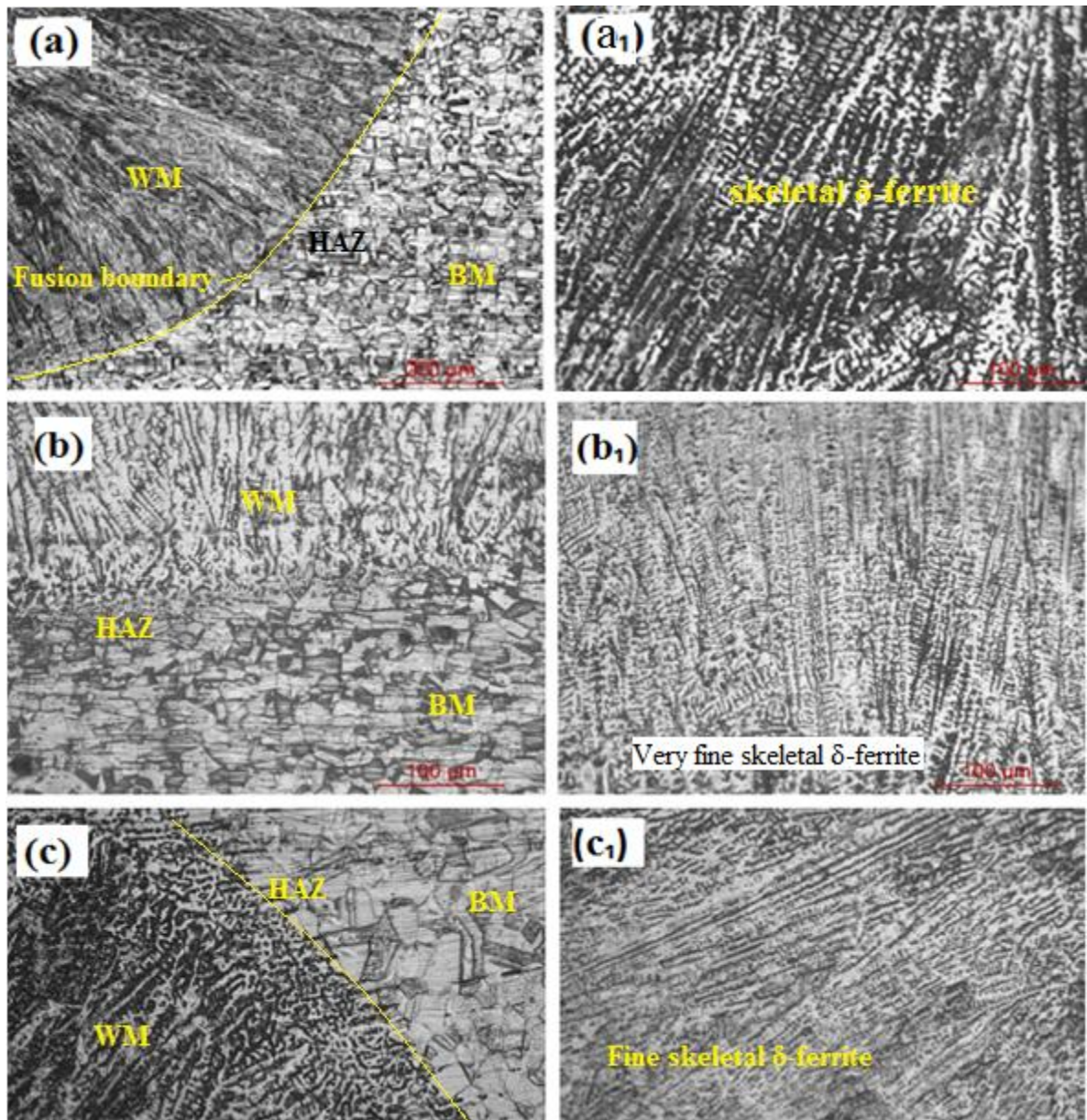


**Fig. 4.7:** Optical microstructures of TIG welded joints - (a) sample no. 13 (b) sample no.14 (c) sample no. 15 and a<sub>1</sub>, b<sub>1</sub>, c<sub>1</sub> corresponding weld metals

**Table 4.4:** Chemical composition of weld metal

Alloy element	C	Mn	Si	S	P	Cr	Ni	Mo	Fe
Weld Metal	0.031	1.41	0.33	0.021	0.034	17.23	10.88	2.23	Bal.

#### 4.1.4. Micro hardness Analysis

The micro hardness values of all the joints across the fusion zone (horizontal direction) have been measured and the average hardness values of 316L stainless steel weld metals are listed in **Table 4.3**. **Fig. 4.9** and **Fig.4.10** represents the micro-hardness profile of all the welded samples. From these figures the consistency of the trend is found for most of the samples. It is also noticed that all TIG welded joints exhibits higher micro-hardness value at

welded zone/ fusion zone when compared with the HAZ and base metal irrespective of welding input parameters used. Similar result has been reported by buddu et.al. and Kumar et.al. [117, 118]. The micro hardness value increases towards the fusion zone as the indenter passes from base metal to weld center. It is found that the micro hardness value ranges from 194-214HV at base metal, 208 - 216HV at HAZ region and 230 - 245 HV at weld region. Variations in the base metal hardness may be due to some impurities and inhomogeneity present in the base metal. Sample no.14 depicts the highest hardness value (~245HV) and sample no. 7 shows the lowest hardness value (~230HV) in the weld zone. The variation in hardness values in different weld samples may be induced by their microstructure refinement due to their different solidification rates of the weld pool. The weld sample no. 7 has lower  $\delta$ -ferrite content and relatively coarse grain structure. The sample no.14 having relatively higher hardness values due to higher  $\delta$ -ferrite content and having relatively finer grain structure.

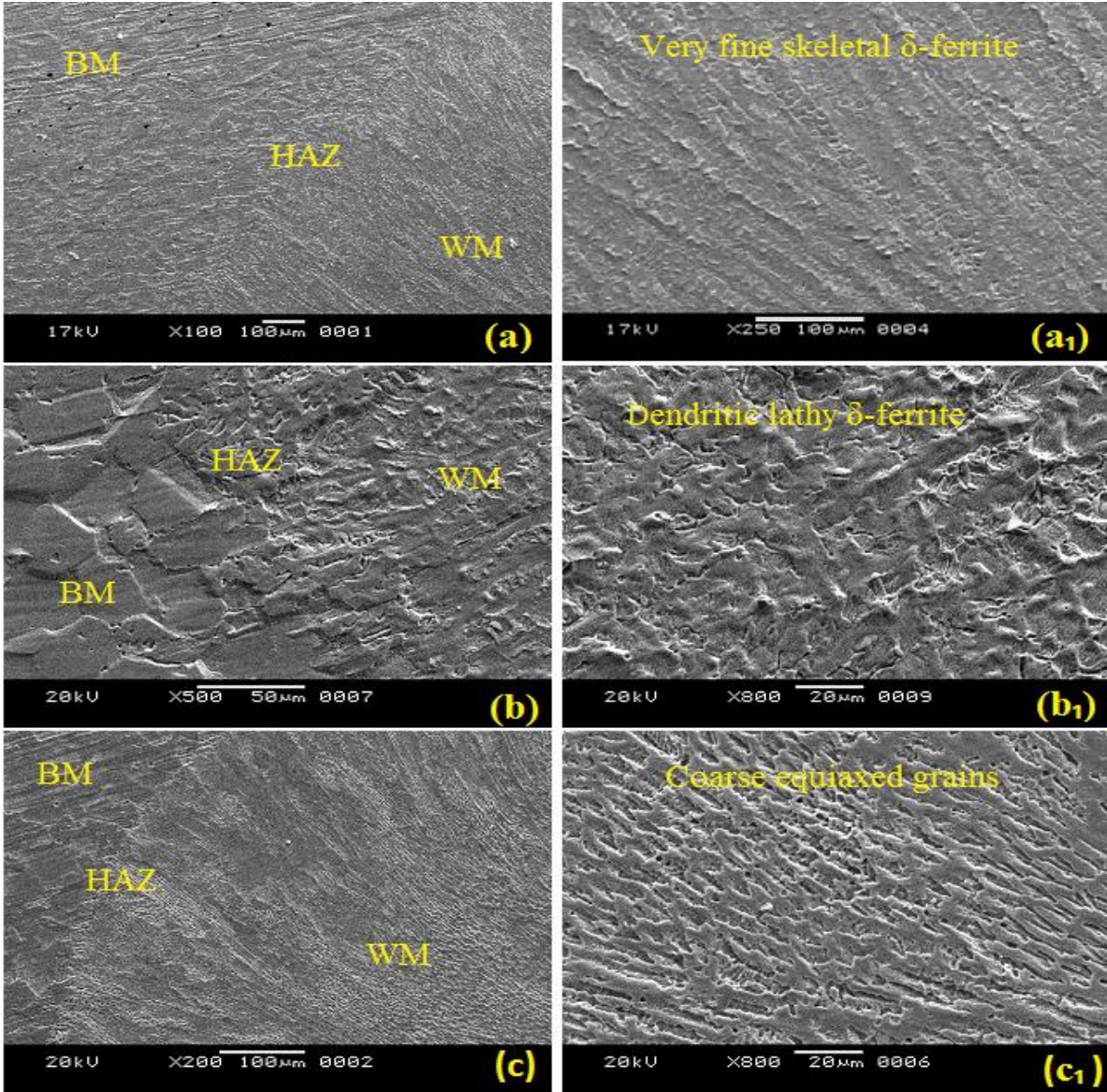


**Fig. 4.8:** SEM micrographs of TIG welded specimens - (a) sample no. 14 (b) sample no.7 (c) sample no. 2 and a<sub>1</sub>, b<sub>1</sub>, c<sub>1</sub> corresponding weld metals

It is observed that at higher value of heat input the micro hardness value of the weldment becomes lower. This may be due to decomposition of base metal and lower  $\delta$ -ferrite content and relatively coarse grain structure as seen in the sample no. 2, 6, 8 and 11. The weld samples numbers 12, 13, 14 and 15 having relatively higher  $\delta$ -ferrite at the dendrite core and relatively fine grain structure due to faster cooling rate, results in higher hardness values.

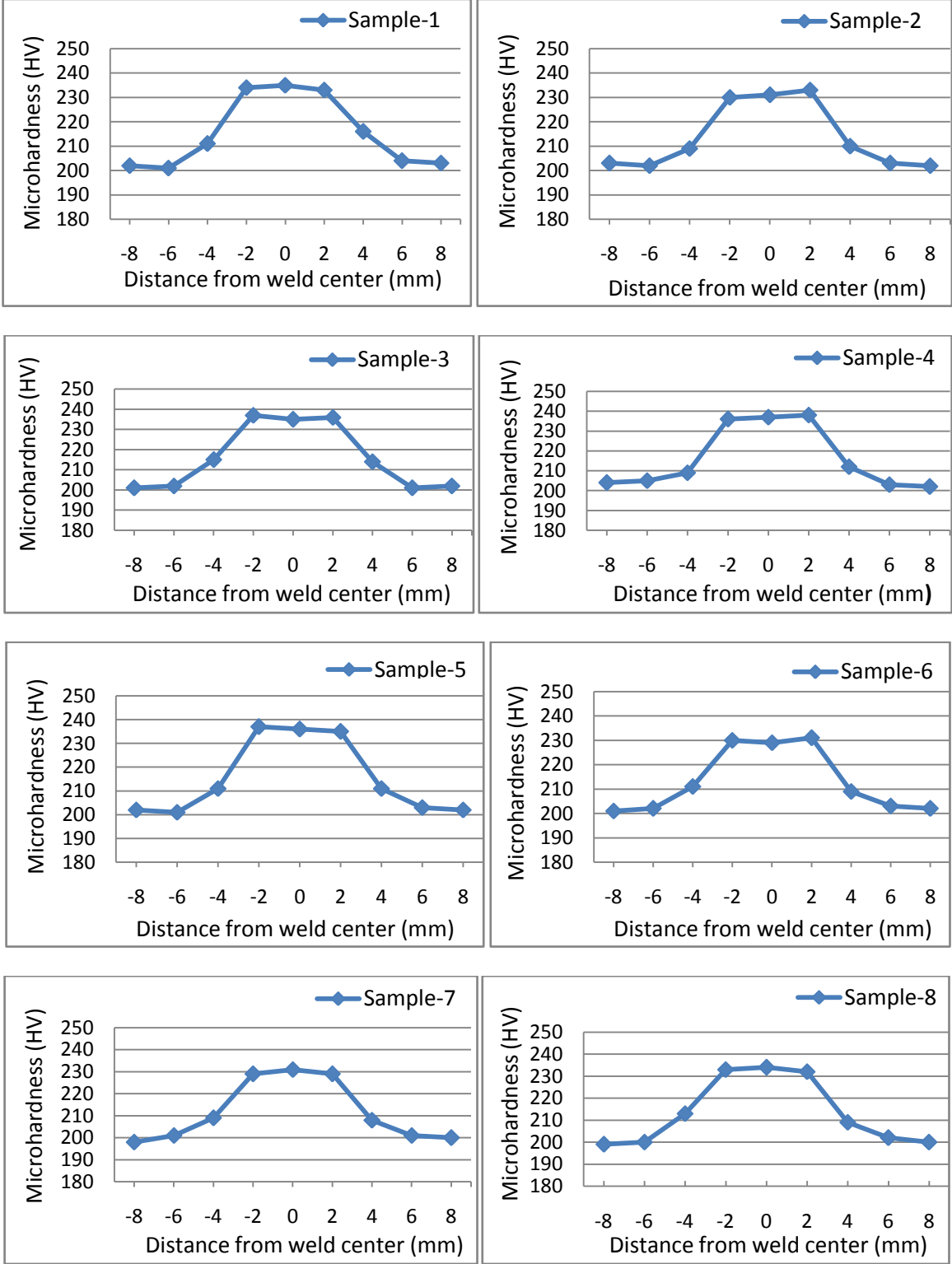


**Fig. 4.9:** Micro hardness profile of Sample no. 1 to Sample no. 8



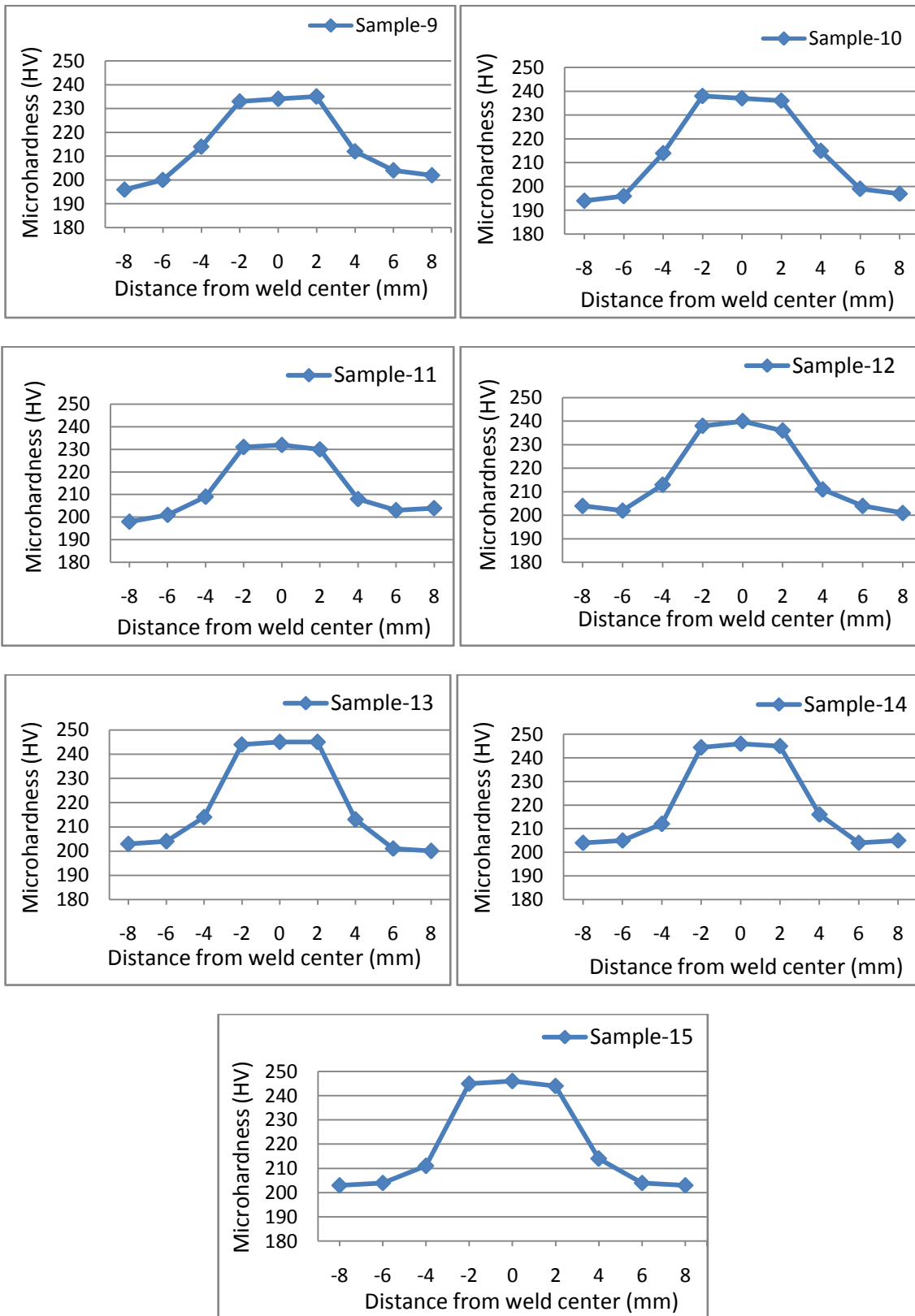


**Fig. 4.10:** Micro hardness profile of Sample no. 9 to Sample no. 15

**Fig.4.11** shows the Micro hardness profile of all welded specimens in one frame. From this figure it is clear that a consistent trend is found for all the samples. Sample no. 14 and 15 shows highest micro hardness value and sample no.7 depicts lowest value.

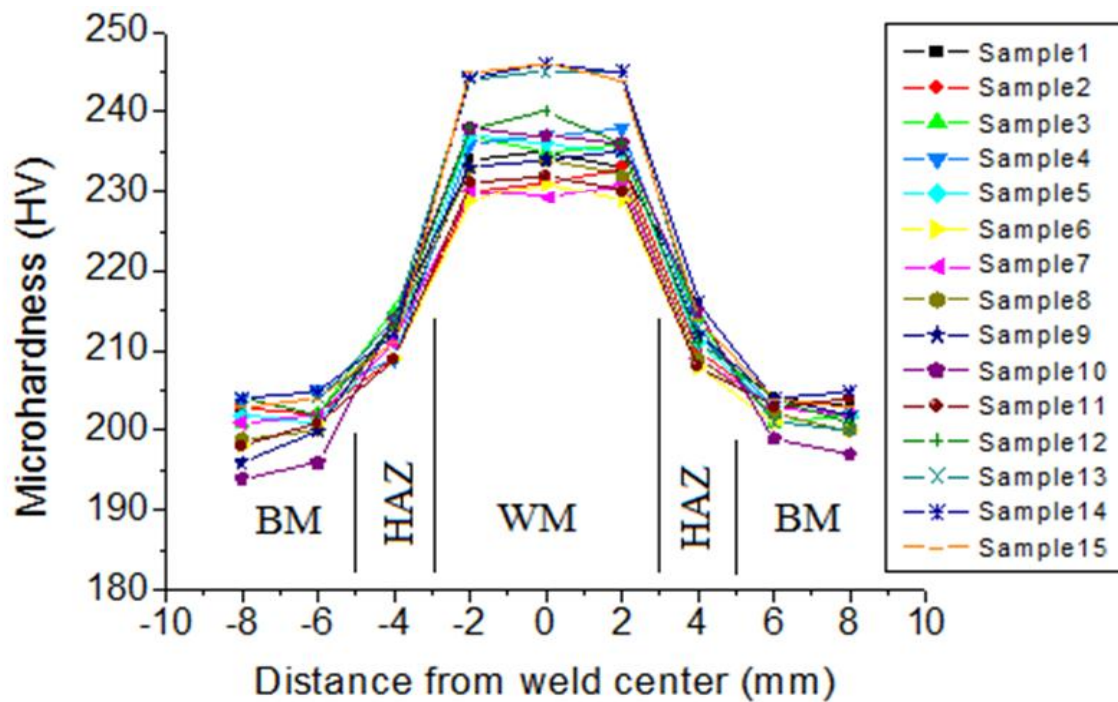


Fig. 4.11: Micro hardness profile of all the samples in one frame

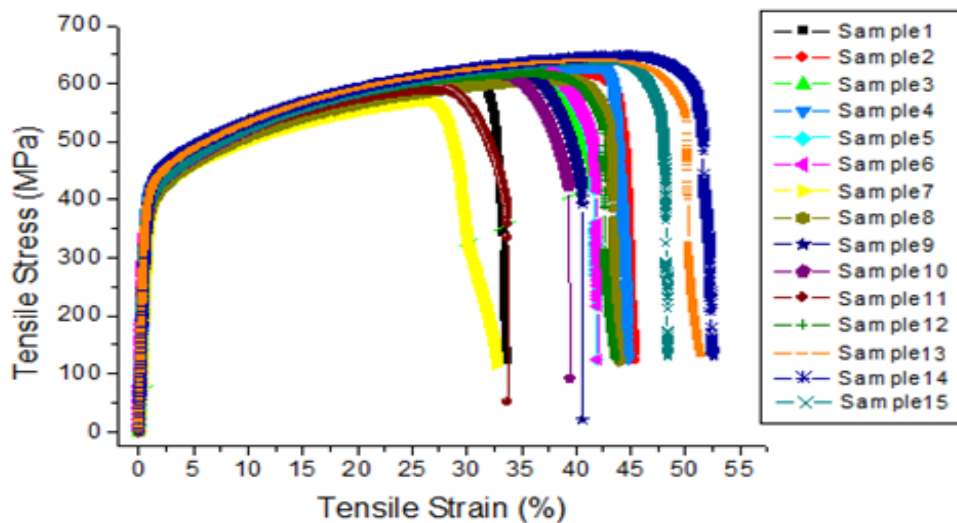
#### 4.1.5. Tensile Behaviour

The uniaxial tensile test of all the welded samples along with base metal has been carried out to evaluate the joint strength for both notched and un-notched specimens at room temperature. The result of tensile test of un-notched/smooth specimens is already listed in **Table 4.3**. A comparative study between the results of tensile test of notched specimens as well as un-notched/smooth specimens is listed in **Table 4.5**. All the welded samples are fractured at HAZ-BM interface regardless of the welding input parameters except sample no. 7 and sample no. 11 for un-notched tensile specimens. But the base metal is fractured at the centre of the gauge length. From **Table 4.5** it is found that sample no. 7 shows minimum joint strength in both cases i.e. notched and un-notched specimens, whereas sample no. 14 depicts maximum joint strength in both cases. Notched tensile specimens exhibit higher tensile strength compared to un-notched tensile specimens for all the TIG welded samples. This may be due to the failure of notch specimens from welded portion where fine grain structures have been observed as evidenced by the micro structure. In case of un-notch specimens, the failures have occurred in HAZ zone having coarse structure [48, 53]. Weld sample no. 7 has slightly more yield strength (YS) than that of base metal, whereas sample no. 11 shows slightly lower YS compared to base metal for smooth specimens. In so far as percentage elongation is concerned, weld sample no. 14 represents the highest value compared to the other welded samples for both notched and un-notched specimens. The notch strength ratio (NSR) is also calculated as the ratio of notched tensile strength (NTS) to un-notched / smooth tensile strength (UTS) and it is tabulated in the **Table 4.5**. It is found that the NSR is greater than unity for all the welded joints, even for base metal also. Similar result has been reported by Lin et al. and Lakshminarayanan et al. [48,119]. This indicates that the TIG welded joints are insensitive to notches or geometric discontinuities and this implies that AISI 316L welded joints fall under “notch ductile materials” category.

**Table 4.5:** Result of tensile test

Sample no.	Un-notched/smooth specimens			Notched specimens			NSR
	UTS (MPa)	YS (MPa)	PE	NTS (MPa)	YS (MPa)	PE	
1	612.13	316.11	33.72	727.22	424.94	19.23	1.19
2	616.42	374.76	45.49	728.42	497.93	18.91	1.18
3	608.48	370.21	42.06	685.69	454.19	14.25	1.13
4	630.37	377.82	41.69	736.75	488.75	21.35	1.17
5	621.26	340.26	41.77	763.87	493.88	20.12	1.23
6	612.91	364.12	40.23	731.54	477.69	19.62	1.19
7	580.61	309.12	30.25	680.24	386.84	14.35	1.17
8	607.69	370.11	44.51	752.32	478.94	20.36	1.23
9	624.15	274.61	40.56	765.68	481.67	21.65	1.23
10	616.24	355.11	39.85	709.94	439.99	18.05	1.15
11	592.42	300.52	33.77	707.25	368.88	17.11	1.19
12	615.88	292.51	42.22	721.65	435.43	18.35	1.17
13	639.42	344.45	51.68	770.63	465.36	22.68	1.21
14	642.64	370.41	52.38	783.27	471.69	23.18	1.22
15	639.67	350.24	51.32	775.23	469.84	22.51	1.21
BM	608.88	328.01	51.85	658.4	362.25	32.20	1.08

The stress-strain curves for all the samples for both smooth and notched specimens of welded joints are shown in **Fig. 4.12** and **Fig. 4.13** respectively. Again, a comparative stress-strain curve for both notched and un-notched specimens of selected (maximum and minimum strength) welded joints along with base metals are also shown in **Fig. 4.14**. The sample no. 14 exhibits much higher tensile strength and higher ductility than others due to formation of very fine skeletal  $\delta$ -ferrite grains in the weld region, moderate precipitation and smaller dendrite size [120]. The reason of lowest tensile strength obtained by sample no. 7 is formation of coarse grains structure in the weld zone and higher dendrite size. This is in line with the micro-hardness data.

**Fig. 4.12:** Stress-strain curves for un-notched specimens of welded samples

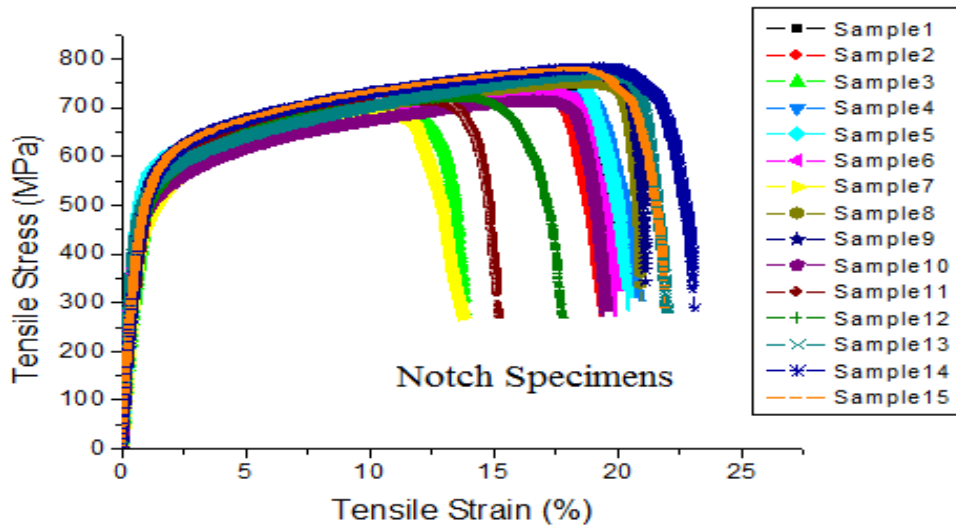


**Fig. 4.13:** Stress-strain curves for notched specimens of welded samples

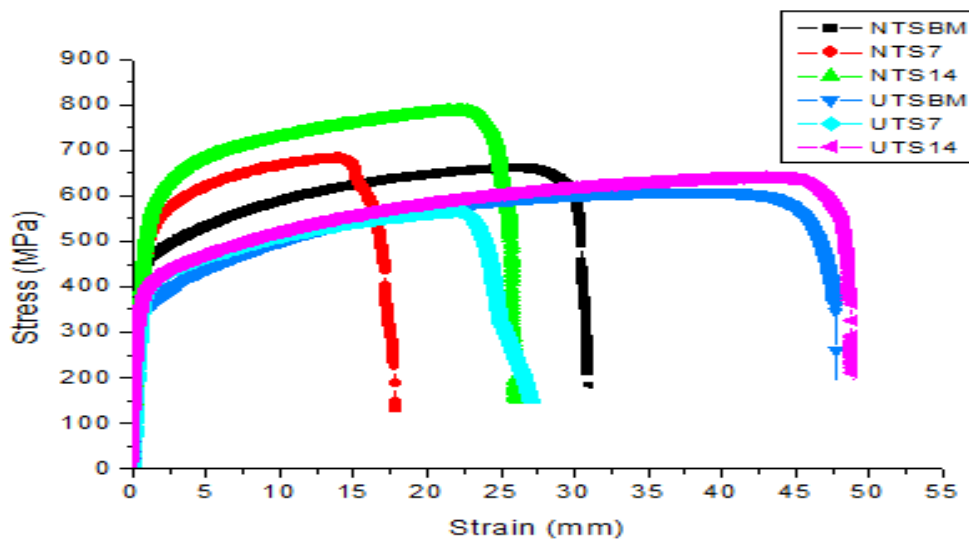


**Fig. 4.14:** Stress-strain curves for notched and un-notched specimens of BM & WM

The surface morphology of tensile fractured specimens of base metal and three chosen welded joints (sample no. 14, sample no. 7 and sample no. 2) have been examined using scanning electron microscope and the obtained result is shown in **Fig. 4.15**. High magnification fracture morphology of base metal is presented in **Fig. 4.15 (a)**. The fracture surfaces consist of many equiaxed dimples of varying size and shape, micro voids and voids. There is no surface cracks are observed. These are the characteristics of mode of ductile fracture. **Fig. 4.15 (b)-(d)** shows high magnification SEM fractograph of weld samples prepared using different input parameters. Significant disparity is observed in the surface morphology, like size and shape of the dimples, surface cracks etc. among this TIG welded samples. It is may be due to different cooling rate for the different weldments. High heat input, results in slow cooling rate and it will take longer time for solidification. As a result it produces coarse grain, hence coarse dimples.

It is noticed from SEM fractographs that a large number of very fine and shallow dimples are observed and no surface cracks are also visible in sample no.14. This is the reason for its

highest tensile strength and percentage elongation. This is in line with the metallographic results. The sample no. 14 consists of a large number of very fine skeletal  $\delta$ -ferrite in plain austenitic matrix. An increase in the  $\delta$ -ferrite content leads to an increase in the strength [121, 122]. In case of sample no.7, it consists of coarse dimples and voids. Some crack boundaries are also observed here. Whereas, elongated dimples with voids are found in sample no 2 due to high heat input [123]. Some cracks are also noticed here. It is also observed that small dimples are surrounded by the large ones in all the specimens.

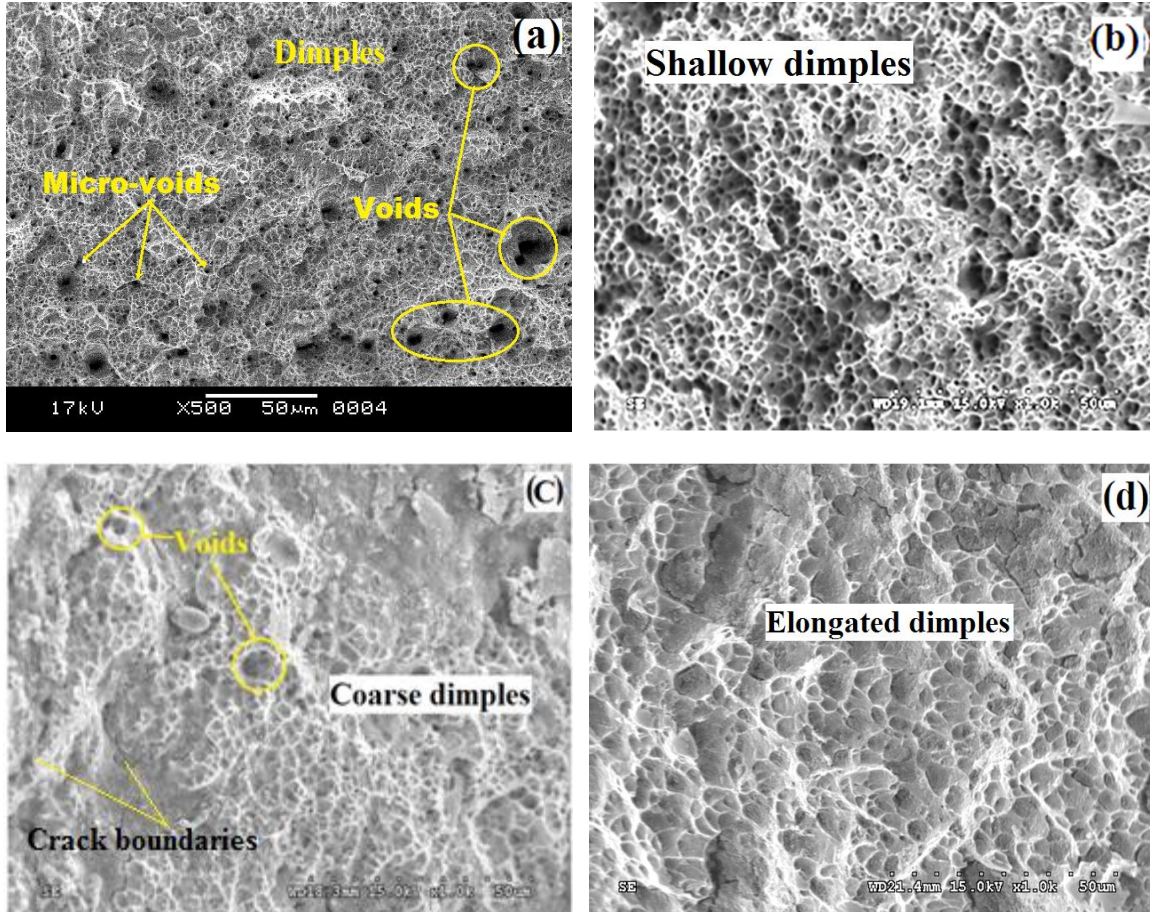


**Fig. 4.15:** SEM fractograph of tensile fracture surfaces of base metal and welded samples (a) base metal (b) sample no.14 (c) sample no. 7 (d) sample no. 2.

#### 4.1.6. Impact toughness

Charpy V-notch impact test is also carried out to evaluate the impact toughness values of all TIG welded samples at room temperature. The test specimens have been prepared in accordance with ASTM E23 and the tested samples are shown in **Fig. 4.16**. V-notches are prepared exactly midpoint of the base metal and center of the weld zone for welded joints. The results of Charpy V-notch impact test are listed in **Table 4.3**. The results indicate that for most of the samples, impact energy is satisfactory. From **Table 4.3** it is found that under some parametric conditions of welding current, welding speed and shielding gas flow rate, impact strength are remarkably good as compared to base metal. For welded samples, it is within the range of 33.5J – 52J. The impact toughness of base metal is found to be 40

Joules, which is comparatively lower than the weld sample no.13, 14 and 15 but comparatively higher than the sample no. 7 and the sample no. 11. Sample number 14 exhibits the highest impact toughness value (52J) and the enhancement in impact toughness value is approximately 30% compared to the base metal value due to presence of fine grain structure as compare to sample no. 11, whereas sample no.7 has coarsest grain structure as a result lowest toughness has been observed [51].

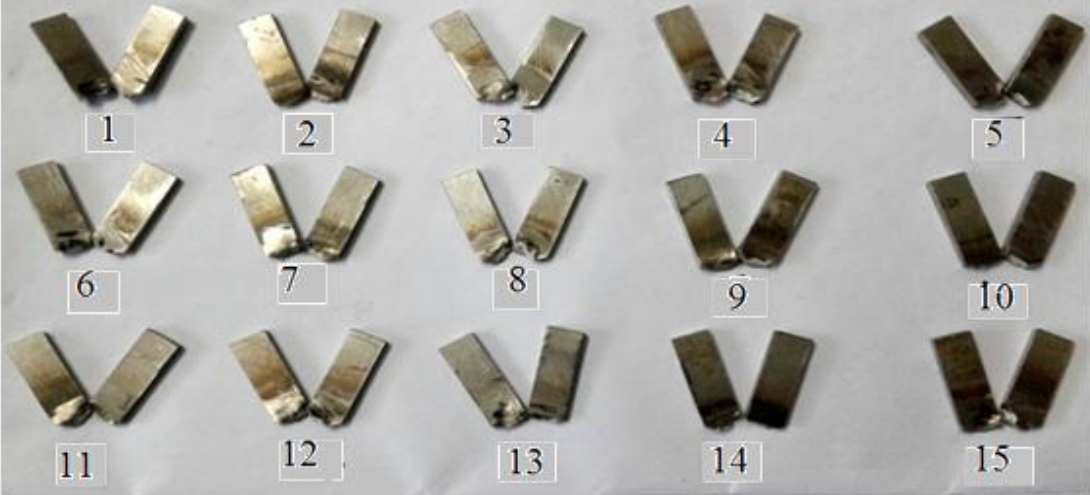


**Fig. 4.16:** Typical impact tested welded samples

**4.1.7. Bending test**

Bending test of all the welded joints have been carried out until 180° from face side of the weld on Universal Testing Machine to ensure the ductility and soundness of the welded joints. The result indicates that no cracks or failure has been observed visually in the bended area of all the welded samples (**Fig. 4.17**) except sample no.11. In this sample small crack has been observed and it is running across the weld region. It is may be due to coarse grain structure as observed in the microstructure [144].



**Fig. 4.17:** Bend test results of weldments of AISI 316L

## 4.2. Optimization of UTS, PE, YS, IS, VHN and WW for TIG welding of 316L austenite stainless steel

The experimental runs are performed according to Box-Behnken design of RSM and output response characteristics are measured and given in **Table 4.3**. The data shown in **Table 4.3** has been used to evaluate the performance of TIG welding of 316L austenitic stainless steel.

### 4.2.1. Factor analysis, modeling and optimization of UTS

#### 4.2.1.1. Main and interaction effects for UTS

The main and interaction effect plots for UTS are made and shown in **Fig. 4.18** and **Fig. 4.19** respectively. MINITAB statistical software version 17 is utilized for this purpose. The main effect plots are very useful to compare the effects of input parameters on response variable. The significance of the factors and also individual effects on output responses can be evaluated from these plots. From the main effect plots (**Fig. 4.18**), it is noted that UTS is increasing and then decreasing with increase of all welding parameters (welding current, welding speed and gas flow rate). The higher the difference between the minimum and the maximum limits in each factor is, the higher the effect on corresponding response variable. From the **Fig. 4.18**, it is found that gas flow rate is dominant factor for UTS, next welding current and followed by welding speed.

**Fig. 4.19** shows the interaction effects of process parameters on response variable, UTS. The non-parallelism of the lines in each case indicated that some amount of interaction exists between the two factors, whereas intersecting lines give an indication of strong interaction. **Fig. 4.19** reveals that interaction effects of process parameters are most significant. Analysis has been continued for modeling and optimization of UTS using RSM combined with teaching and learning based optimization (TLBO) and desirability function approach (DFA).

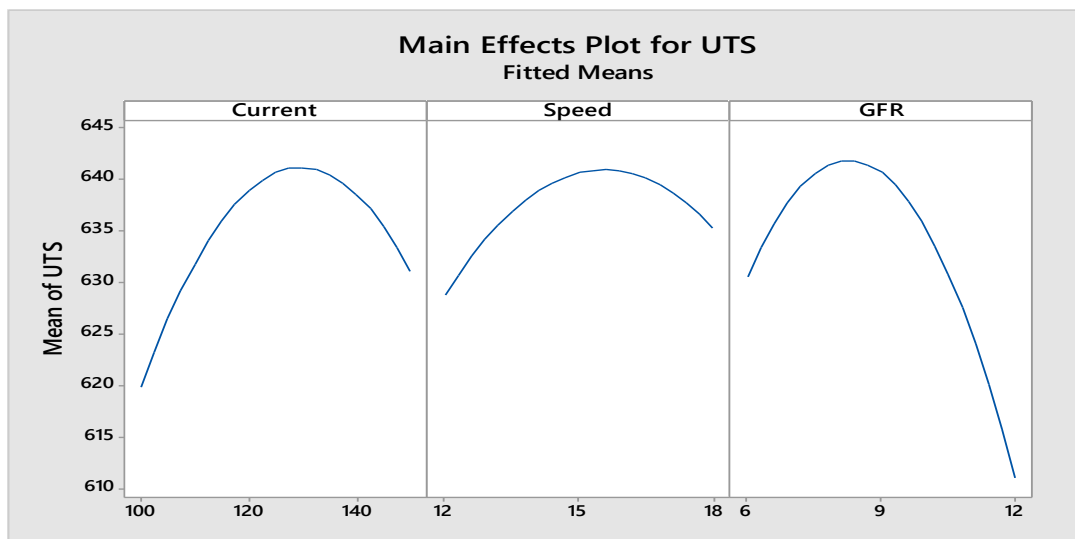


**Fig. 4.18:** Main effect plots for UTS

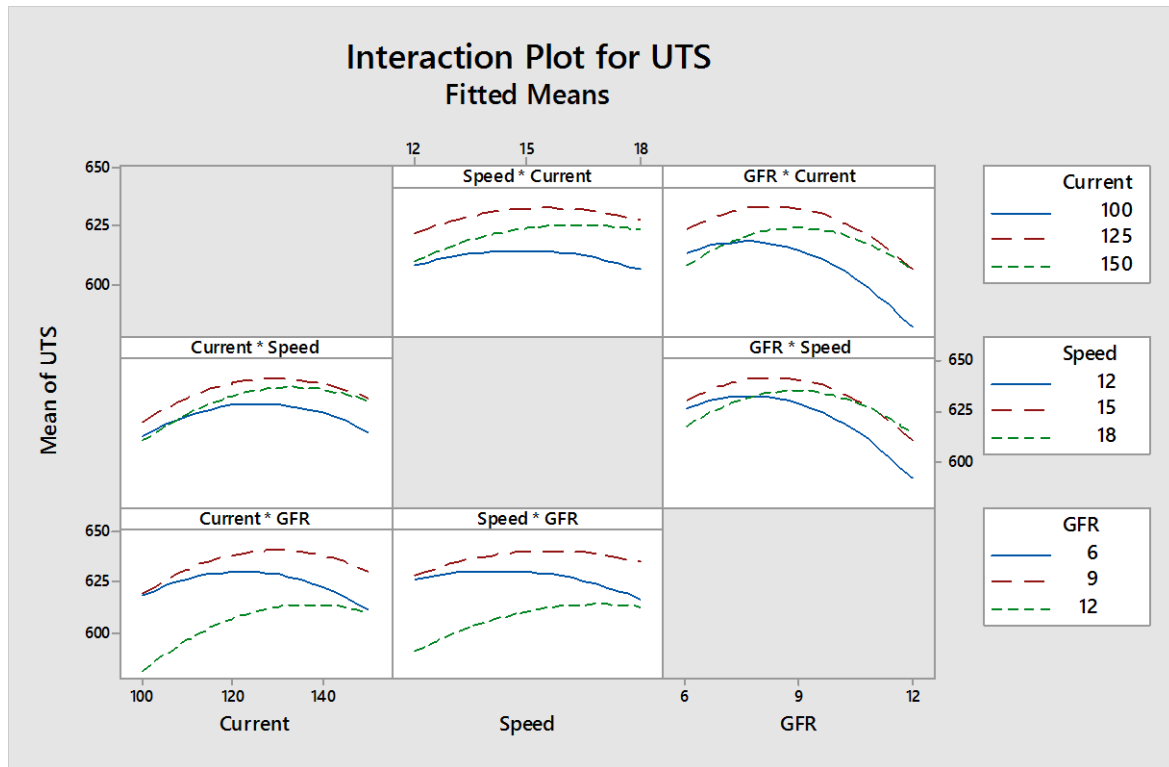


**Fig. 4.19:** Interaction effect plots for UTS

#### 4.2.1.2. Mathematical modeling for UTS

Response surface methodology from MINITAB 17 software is applied on experimental data for developing the second-order response surface model for output response, UTS. Mathematical model for UTS is obtained in terms of current (A), welding speed (B) and gas flow rate (C). The basic second order quadratic model is given in **Eq.2.7**. The relationship for input parameters and UTS is shown in **Eq. 4.3**. All the betas are coefficients of linear, quadratic and interaction of input parameters A, B and C. The term  $\beta_0$  is the intercept term,  $\beta_1$ ,  $\beta_2$  and  $\beta_3$  are the liner terms,  $\beta_{11}$ ,  $\beta_{22}$  and  $\beta_{33}$  are the squared terms, and  $\beta_{12}$ ,  $\beta_{13}$  and  $\beta_{23}$  are the interaction terms between the independent / input variables. All the beta values have been directly obtained from MINITAB 17 software, based on least squares method using experimental data as shown in **Table 4.3**. The final mathematical model is developed by considering un-coded values (un-coded values are the values such as current (A) = 100, 125 and 150 A, speed (B) = 12, 15 and 18 cm/min and gas flow rate (C) = 6, 9 and 12 l/min.

$$\begin{aligned}
 Y_{\text{UTS}} = & 214.6 + 4.338 \text{ Current} + 14.52 \text{ Speed} + 8.55 \text{ GFR} - 0.02423 \text{ Current*Current} \\
 & - 0.954 \text{ Speed*Speed} - 2.202 \text{ GFR*GFR} + 0.0587 \text{ Current*Speed} \\
 & + 0.1181 \text{ Current*GFR} + 0.871 \text{ Speed*GFR}
 \end{aligned}
 \tag{4.3}$$

#### 4.2.1.3. Analysis of variance for UTS

ANOVA test is carried out to determine the dependency of welding quality response, UTS on selected process parameters: current, speed and gas flow rate. The ANOVA test is



conducted at larger is the better criterion and the results of ANOVA test are shown in **Table 4.6** for UTS (where DF is degree of freedom, F variance ratio and P significant factor).

The ANOVA test is performed at a significance level of 5% i.e., confidence level of 95%. Since P values given in **Table 4.6** are less than 0.05, the developed model is significant. According to the other hypothesis, if at least one of these coefficients is equal to zero, the model will be accepted; it is seen from **Table 4.6** that this hypothesis is confirmed. From the ANOVA table (**Table 4.6**) of UTS, it is found that direct effect of gas flow rate and square combination of current\*current, and gas flow rate\*gas flow rate is most significant on UTS as its P values are zero. The individual effects of current and speed, squared combinations of speed\*speed and their interaction effects of current - speed, current - gas flow rate and speed - gas flow rate are significant for UTS as their P values are less than 0.05, as found from the **Table 4.6**.

The correlation coefficient R-square value for the experimental result obtained is 0.9900 (99.00%) for UTS which shows a good correlation the experimental results possess, whereas adjusted R- square values of UTS is 0.9720 (97.20%) which also indicates good correlation.

**Table 4.6:** Analysis of variance for UTS

Source	DF	Adj SS	Adj MS	F-Value	P-Value	Remarks
<b>Model</b>	<b>9</b>	<b>4009.91</b>	<b>445.55</b>	<b>54.96</b>	<b>0.000</b>	<b>Significant</b>
<b>Linear</b>	<b>3</b>	<b>1095.36</b>	<b>365.12</b>	<b>45.04</b>	<b>0.000</b>	<b>Significant</b>
<b>Current</b>	<b>1</b>	<b>252.11</b>	<b>252.11</b>	<b>31.10</b>	<b>0.003</b>	<b>Significant</b>
<b>Speed</b>	<b>1</b>	<b>83.53</b>	<b>83.53</b>	<b>10.30</b>	<b>0.024</b>	<b>Significant</b>
<b>GFR</b>	<b>1</b>	<b>759.72</b>	<b>759.72</b>	<b>93.71</b>	<b>0.000</b>	<b>Significant</b>
<b>Square</b>	<b>3</b>	<b>2277.27</b>	<b>759.09</b>	<b>93.63</b>	<b>0.000</b>	<b>Significant</b>
<b>Current*Current</b>	<b>1</b>	<b>846.44</b>	<b>846.44</b>	<b>104.41</b>	<b>0.000</b>	<b>Significant</b>
<b>Speed*Speed</b>	<b>1</b>	<b>272.18</b>	<b>272.18</b>	<b>33.57</b>	<b>0.002</b>	<b>Significant</b>
<b>GFR*GFR</b>	<b>1</b>	<b>1450.21</b>	<b>1450.21</b>	<b>178.88</b>	<b>0.000</b>	<b>Significant</b>
<b>2-Way Interaction</b>	<b>3</b>	<b>637.28</b>	<b>212.43</b>	<b>26.20</b>	<b>0.002</b>	<b>Significant</b>
<b>Current*Speed</b>	<b>1</b>	<b>77.44</b>	<b>77.44</b>	<b>9.55</b>	<b>0.027</b>	<b>Significant</b>
<b>Current*GFR</b>	<b>1</b>	<b>313.82</b>	<b>313.82</b>	<b>38.71</b>	<b>0.002</b>	<b>Significant</b>
<b>Speed*GFR</b>	<b>1</b>	<b>246.02</b>	<b>246.02</b>	<b>30.35</b>	<b>0.003</b>	<b>Significant</b>
<b>Error</b>	<b>5</b>	<b>40.54</b>	<b>8.11</b>			
<b>Lack-of-Fit</b>	<b>3</b>	<b>34.12</b>	<b>11.37</b>	<b>3.54</b>	<b>0.228</b>	<b>Not Significant</b>
<b>Pure Error</b>	<b>2</b>	<b>6.42</b>	<b>3.21</b>			
<b>Total</b>	<b>14</b>	<b>4050.44</b>				

Model Summary: R-Sq = 99.00%, R-Sq(adj) = 97.20%, R-sq(pred)= 86.17%

#### 4.2.1.4. Model Validation

The soundness of the developed model of UTS has also been checked by predicted vs. actual plot. **Fig. 4.20** shows the relationship between the actual and predicted values of response for UTS. This figure also indicates that the developed model is adequate and predicted results are in good agreement with measured data.

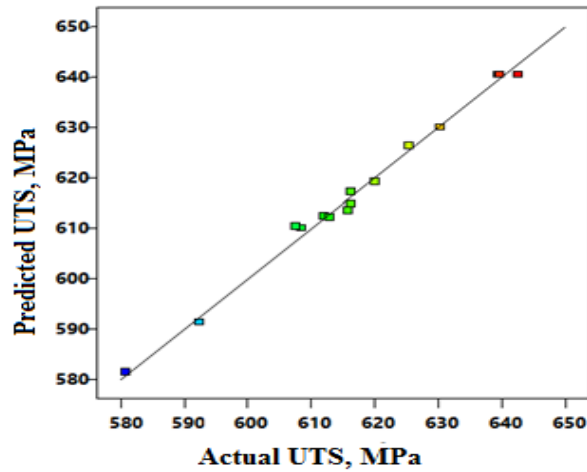


**Fig. 4.20:** Plot of predicted vs. actual results of UTS

#### 4.2.1.5. Effect of the Parameters on UTS

The contour plots are drawn based on mathematical models (Eq. 4.3) as established through RSM to illustrate the effects of the input variables, individually and combinedly on output responses for UTS in Fig. 4.21 - Fig. 4.23. The contour plots show the variations of response variable due to change in the levels of two input variables while the other input parameter is held constant at particular level i.e. level 1, level 2 and level 3.

The contour plots shown in Fig. 4.21, present the combined effects of input process parameters on UTS for speed vs current, while gas flow rate is held constant at their respective lowest, medium and highest values i.e. 6 l/min, 9 l/min and 12 l/min. Fig. 4.22 shows the influences of welding input variables: GFR vs. current on UTS, while speed hold at their respective lowest, medium and highest values. Fig. 4.23 represents the influence of GFR vs. speed on UTS, while welding current hold at their respective lowest, medium and highest values.

The shape of the corresponding contour plot indicates whether interactions among the input parameters influence the response significantly or not. An elliptical nature of the contour plots indicates that the interactions between the input parameters significantly influence the response. If the curvature in the contour lines is more, interaction effect is more. Comparatively straighter contour lines showing small or no curvature indicate lesser / no interaction effect. Fig. 4.21 – Fig 4.23 reveals that interaction effects of input welding parameters are prominent because contour lines show considerable curvature / slope.

The contour plots not only reveal interaction effects of input parameters but also give optimal input parameters from which desired response can be obtained. The maximum tensile strength of the joint is exhibited by the dark green colour area in the contour plot. Any parametric combination within this area provides better UTS values in comparison to other regions. From contour plots, it is noticed that, UTS first increases steadily then decreases with further increasing in the levels of the welding current, speed and GFR. UTS is found to be maximum, almost at the medium levels of welding current, speed and GFR.

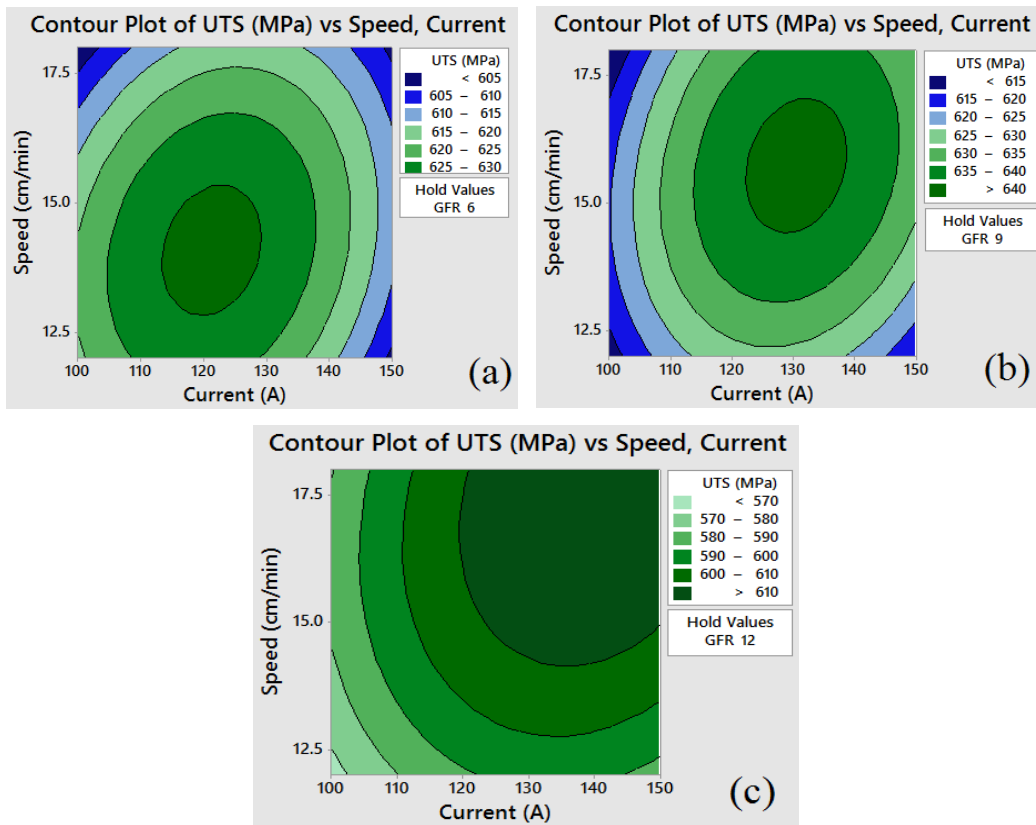


**Fig. 4.21:** Contour plots showing combined effects of speed and current on UTS, while GFR hold at a) 6 l/min b) 9 l/min and c) 12 l/min

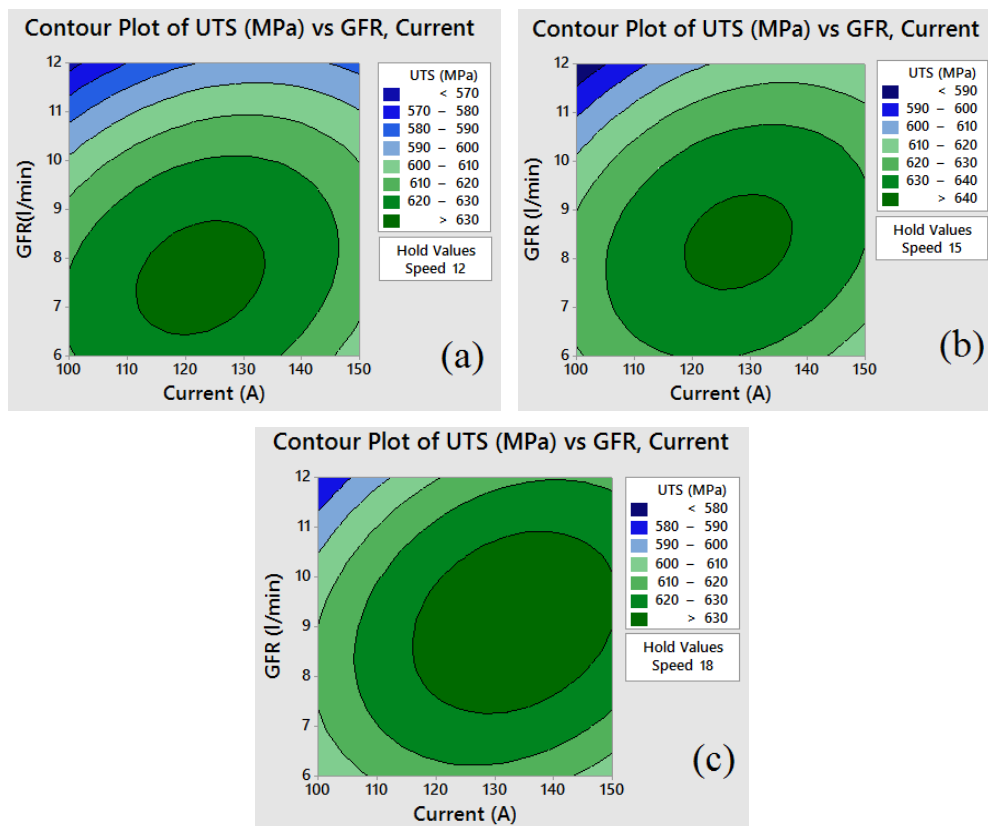


**Fig. 4.22:** Contour plots showing combined effects of GFR and current on UTS, while speed hold at a) 12 cm/min b) 15 cm/min and c) 18 cm/min

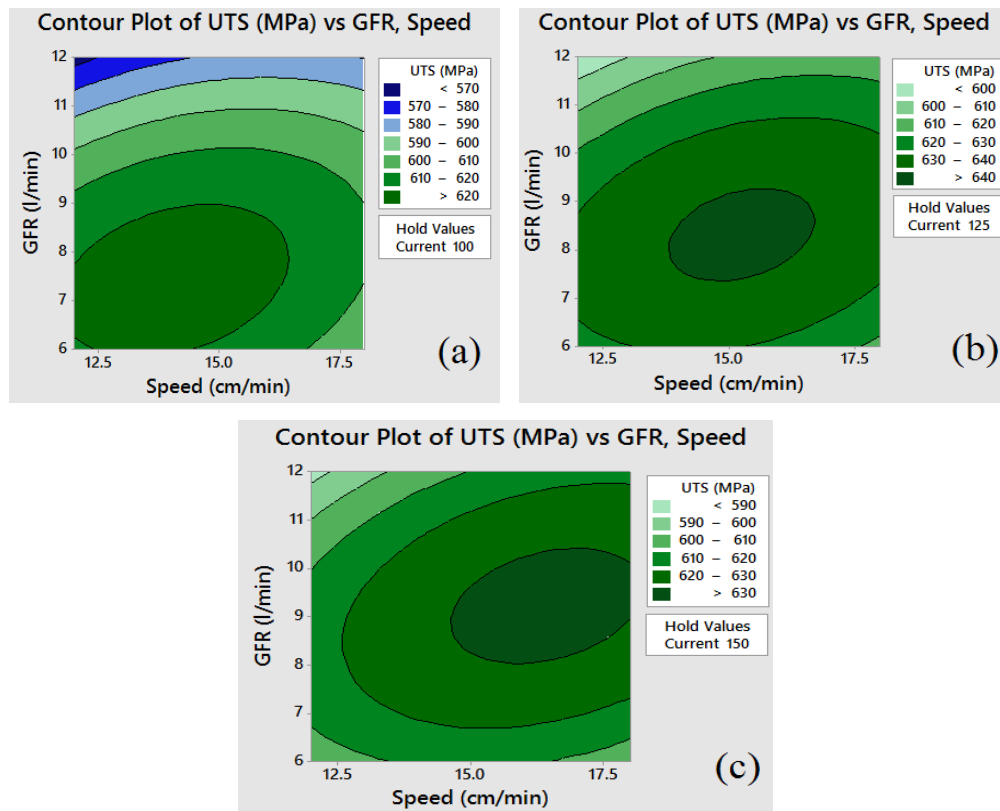


**Fig. 4.23:** Contour plots showing combined effects of GFR and speed on UTS, while current hold at a) 100A b) 125A and c) 150A

#### 4.2.1.6. Optimization of UTS by TLBO

TLBO is used to obtain the optimum welding conditions by solving the mathematical model of UTS as given in Eq. 4.3 for seeking maximization of UTS. The implementation steps of the TLBO are summarized below:

- Step 1: Initialize the population (i.e. learners') and design variables of the optimization problem (i.e. number of subjects offered to the learner) with random generation and evaluate them.
- Step 2: Select the best learner of each subject as a teacher for that subject and calculate mean result of learners in each subject.
- Step 3: Evaluate the difference between current mean result and best mean result according to Eq. 2.15 by utilizing the teaching factor (TF).
- Step 4: Update the learners' knowledge with the help of teacher's knowledge according to Eq. 2.17.
- Step 5: Update the learners' knowledge by utilizing the knowledge of some other learner according to Eq. 2.18 and Eq. 2.19.
- Step 6: Repeat the procedure from step 2 to 5 till the termination criterion is met.

The TLBO code is run in MATLAB environment and optimum welding setting and predicted response is obtained in first run itself. The obtained maximized UTS = 642.13

Mpa at welding condition of current (A) = 128.79 A, speed (B) = 15.39 cm/min and gas flow rate (C) = 8.42 l/min. the same optimum condition is also shown in **Table 4.12**.

**4.2.1.7. Optimization of UTS by DFA**

The optimization plot is drawn (**Fig. 4.24**) by using MINITAB software by considering maximization of the responses. UTS has to be maximized to improve the mechanical properties of welded specimen. So, **Eq. 2.23** is used here. Calculation of desirability values is taken care by MINITAB software and it finally provides the optimum welding condition for the desired / maximized values of responses. The factor setting in the plot denotes optimum welding condition and ‘y’ value denotes optimum response value. Obtained optimum parametric setting and corresponding response values are: maximized UTS = 642.13 Mpa at welding condition of current (A) = 128.79 A, speed (B) = 15.39 cm/min and gas flow rate (C) = 8.42 l/min. the same optimum condition is also shown in **Table 4.12**.

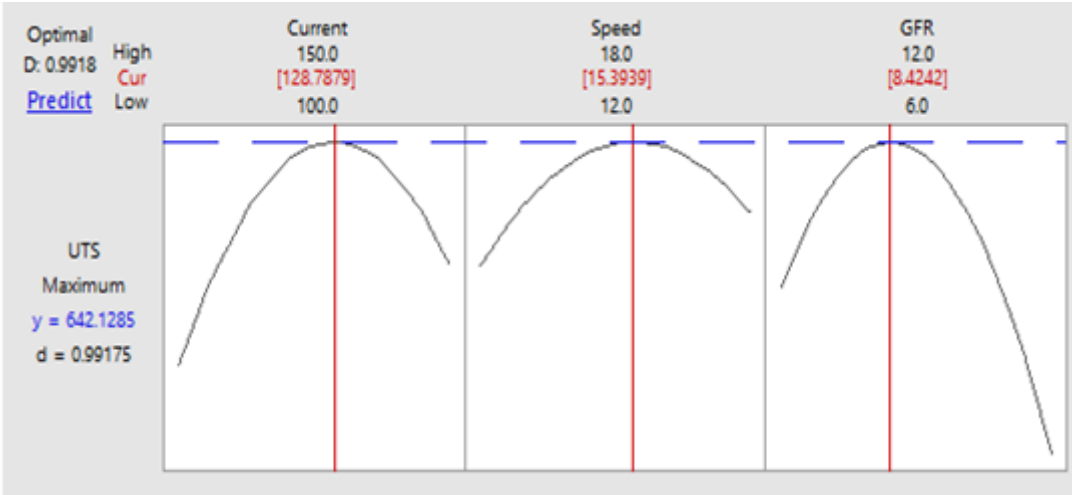


**Fig. 4.24:** Optimization plot for UTS

**4.2.2. Factor analysis, modeling and optimization of PE**

**4.2.2.1. Main and interaction effects for PE**

The main and interaction plots are drawn and shown in **Fig. 4.25** and **Fig. 4.26** respectively, using experimental data of percentage elongation (PE) (**Table 4.3**) and evaluation has made as like procedure given in section 4.2.1.1. It is noted from the **Fig. 4.25** that PE is increasing and then decreasing with increase of all welding parameters (current, speed and gas flow rate). The higher the difference between the minimum and the maximum limits in each factor is, the higher the effect on corresponding response variable. From the **Fig. 4.25**, it is found that welding current is dominant factor for PE, next is welding speed and followed by gas flow rate.

Interaction effect plots for PE are shown in **Figs. 4.26**. Interaction effects plots reveals that interaction effects are most significant for PE, as non-parallelism lines and intersecting lines are present in each pair of parameters as found from **Figs. 4.26**.

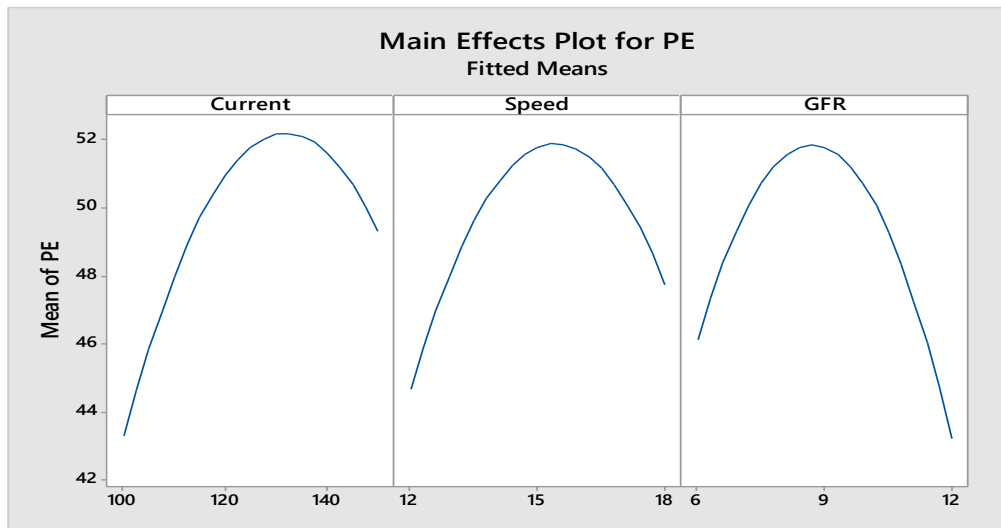


Fig. 4.25: Main effect plots for PE

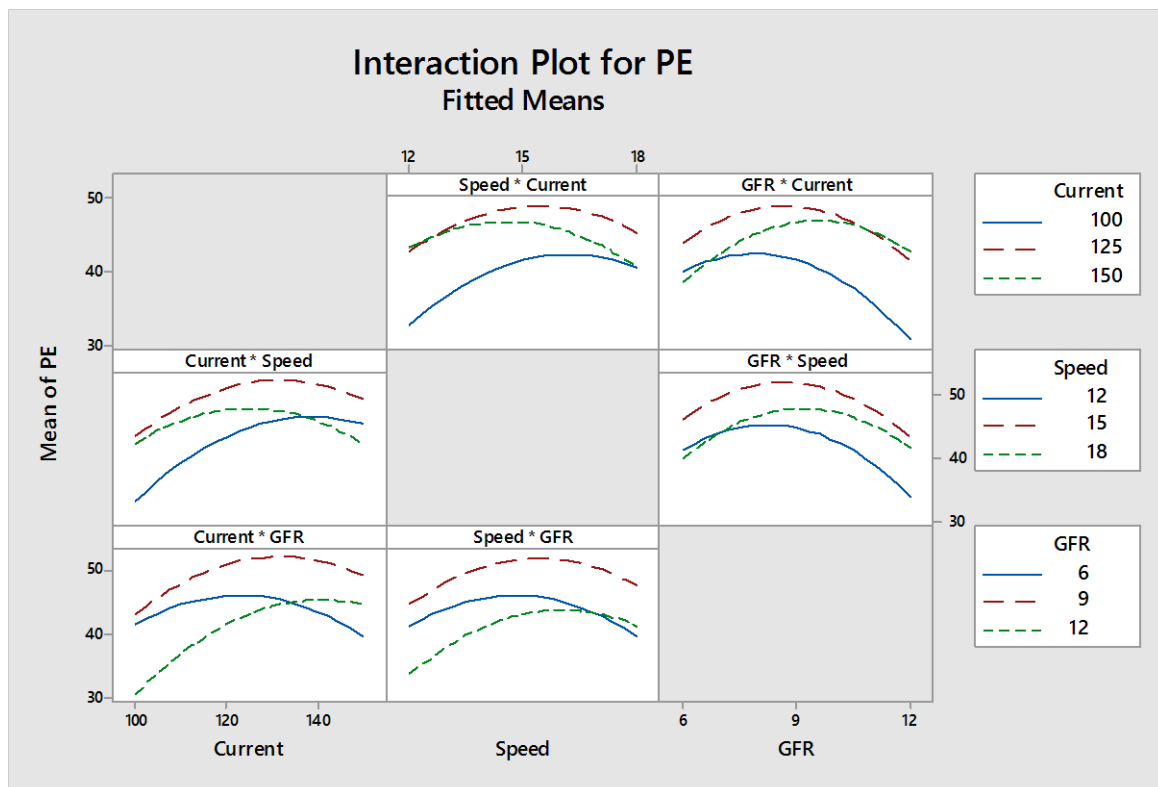


Fig. 4.26: Interaction effect plots for PE

#### 4.2.2.2. Mathematical modeling for PE

The mathematical relationships between the welding input parameters and welding response PE is made by RSM approach by following the procedure given in Section 4.2.1.2. The obtained mathematical equation is given in Eq. 4.4.

$$\begin{aligned}
 Y_{PE} = & -289.3 + 2.446 \text{ Current} + 21.85 \text{ Speed} + 3.36 \text{ GFR} - 0.008771 \text{ Current*Current} \\
 & - 0.6191 \text{ Speed*Speed} - 0.7913 \text{ GFR*GFR} - 0.04047 \text{ Current*Speed} \\
 & + 0.05267 \text{ Current*GFR} + 0.2544 \text{ Speed*GFR}
 \end{aligned}
 \tag{4.4}$$

### 4.2.2.3. Analysis of variance for PE

The statistical tool analysis of variance (ANOVA) is made for PE using MINITAB 17 software and given in **Table 4.7**. The evolution of results of ANOVA for PE is made as like ANOVA of UTS. The hypothesis is confirmed form ANOVA table (**Table 4.7**) of PE, as more than one term in the table is zero.

The results of ANOVA as shown in **Table 4.7**, it is found that individual effects of current (A) and the squared combinations of current (A) \* current (A), speed (B) \* speed (B) and gas flow rate (C)\* gas flow rate (C) and interaction effects of current (A) \* gas flow rate (C) are most significant for PE, as its P values are zero. The direct effects of speed (B), gas flow rate (C) and interaction effects of current (A) \* speed (S) and speed (B) \* gas flow rate (C) are significant for PE, because, its P values are less than 0.05 as found from **Table 4.7**.

The correlation coefficient R-square value for the experimental result obtained is 99.48% for PE which shows a good correlation the experimental results possess, whereas adjusted R-square value is 98.54% also indicates good correlation.

**Table 4.7:** Analysis of Variance for PE

Source	DF	Adj SS	Adj MS	F-Value	P-Value	Remarks
<b>Model</b>	9	587.950	65.328	106.30	0.000	Significant
<b>Linear</b>	3	108.566	36.189	58.88	0.000	Significant
Current	1	72.722	72.722	118.33	0.000	Significant
Speed	1	18.850	18.850	30.67	0.003	Significant
GFR	1	16.994	16.994	27.65	0.003	Significant
<b>Square</b>	3	359.153	119.718	194.79	0.000	Significant
Current*Current	1	110.949	110.949	180.53	0.000	Significant
Speed*Speed	1	114.622	114.622	186.50	0.000	Significant
GFR*GFR	1	187.267	187.267	304.71	0.000	Significant
<b>2-Way Interaction</b>	3	120.231	40.077	65.21	0.000	Significant
Current*Speed	1	36.845	36.845	59.95	0.001	Significant
Current*GFR	1	62.410	62.410	101.55	0.000	Significant
Speed*GFR	1	20.976	20.976	34.13	0.002	Significant
<b>Error</b>	5	3.073	0.615			
Lack-of-Fit	3	2.492	0.831	2.86	0.270	Not significant
Pure Error	2	0.581	0.291			
<b>Total</b>	14	591.023				

Model Summary: R-Sq = 99.48%, R-Sq(adj) = 98.54%, R-sq(pred) = 93.03%

### 4.2.2.4. Model Validation

The plot, predicted vs. actual values of response for PE is shown in **Fig. 4.27**. This figure indicates that the developed model is adequate and predicted results are in good agreement with measured data.

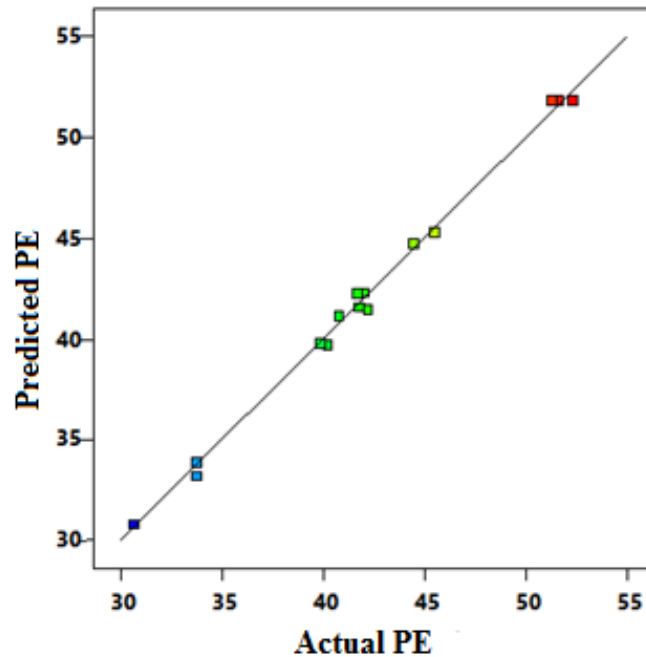


**Fig. 4.27:** Plot of predicted vs. actual results of PE

#### 4.2.2.5. Effect of the Parameters on PE

The contour plots are drawn from the mathematical model of PE (Eq. 4.4) using RSM application to explore the significance of welding process parameters on PE. The contour plots for PE are shown in Fig. 4.28 – Fig. 4.30. The contour plots shown in Fig. 4.28, present the effect of input process parameters on PE for speed vs current, while gas flow rate is held constant at their respective lowest, medium and highest values. Fig. 4.29 shows the influences of welding input variables: GFR vs. current on PE, while speed hold at their respective lowest, medium and highest values. Fig. 4.30 represents the influence of GFR vs. speed on PE, while welding current hold at their respective lowest, medium and highest values.

From the contour plots given in Fig. 4.28 – Fig. 4.30, it is found that direct and interaction effects of process welding parameters are most significant for percentage elongation of welded joint of 316 L stainless steel in TIG welding operation, as the lines in the contour plots are elliptical / curvature in nature. As mentioned earlier that elliptical / curvature lines in contour plots indicates the effects of process parameters on responses. The dark green color area in the contour plot gives idea of process parametric combinations where PE can be maximized. It is observed that percentage elongation is maximum at the medium levels of welding input parameters: welding current, speed and GFR. The cooling rate decreases with increase in heat input at low welding speed. This in turn will take longer time for solidification. As a result, it produces coarse grain, hence low percentage elongation. Welding current has a significant effect on PE. At lower welding current, the percentage elongation of the welded joint is lower. When current is increased the PE is also increased and reached its maximum value as it forms uniform penetration.



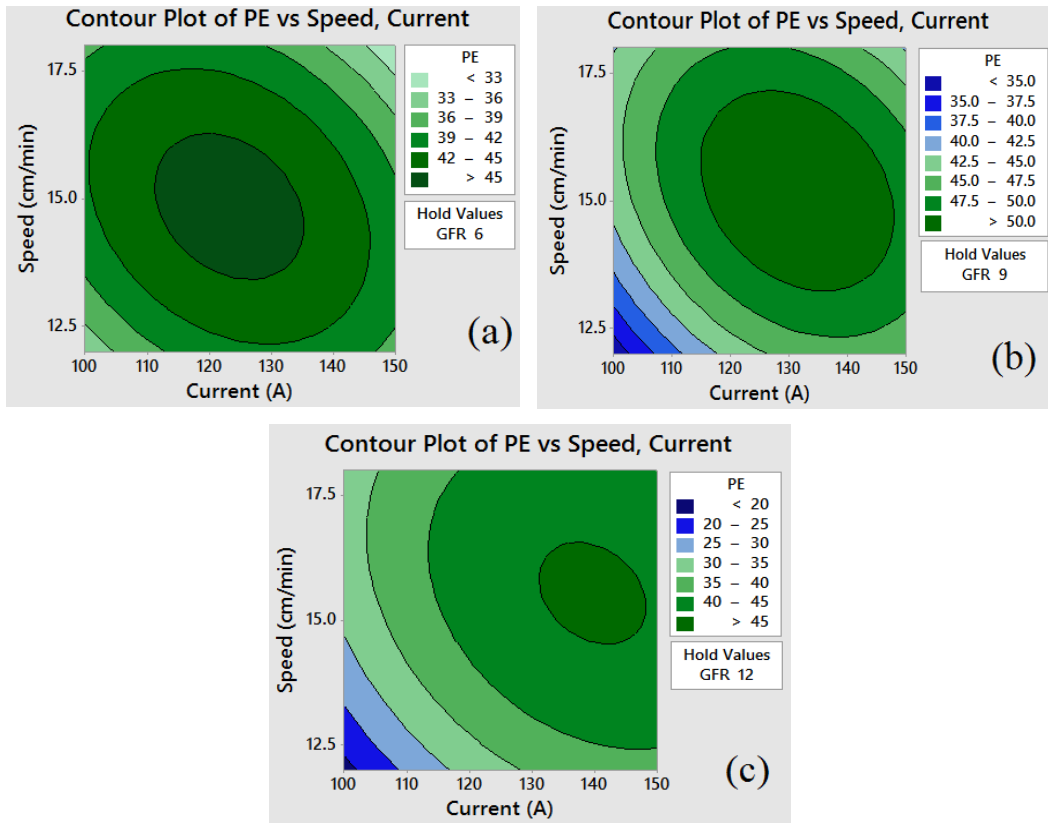


**Fig. 4.28:** Contour plots showing combined effects of speed and current on PE, while GFR hold at a) 6 l/min b) 9 l/min and c) 12 l/min

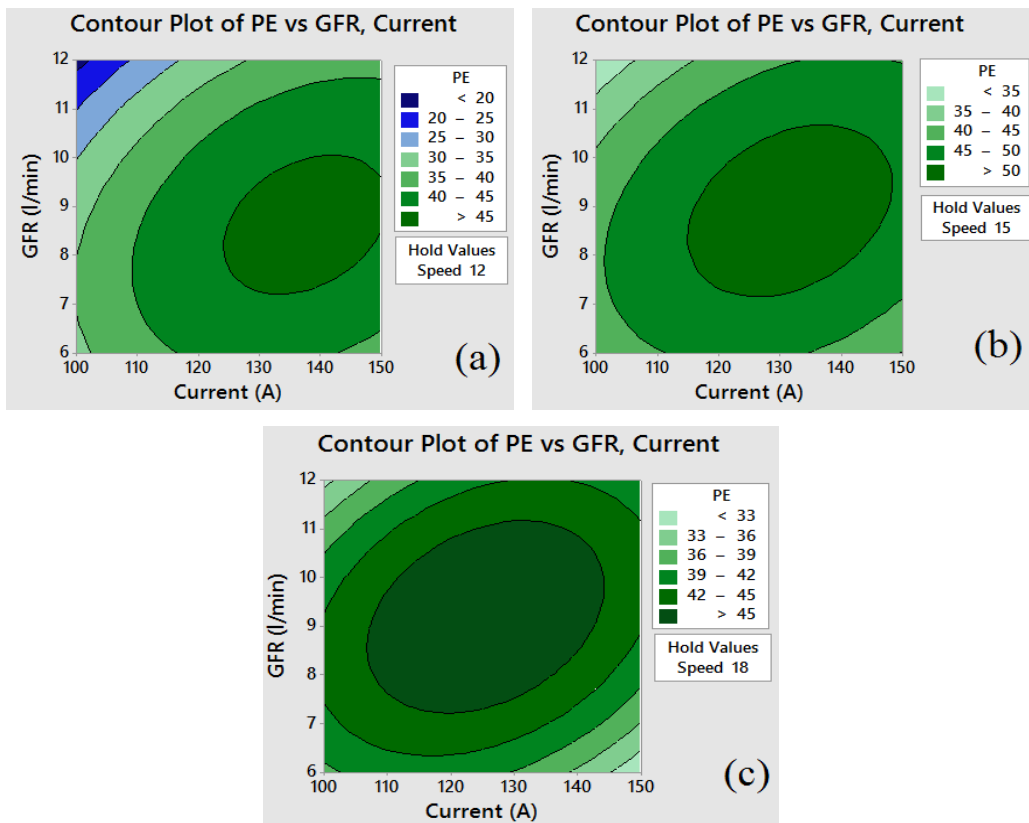


**Fig. 4.29:** Contour plots showing combined effects of GFR and current on PE, while speed hold at a) 12 cm/min b) 15 cm/min and c) 18 cm/min

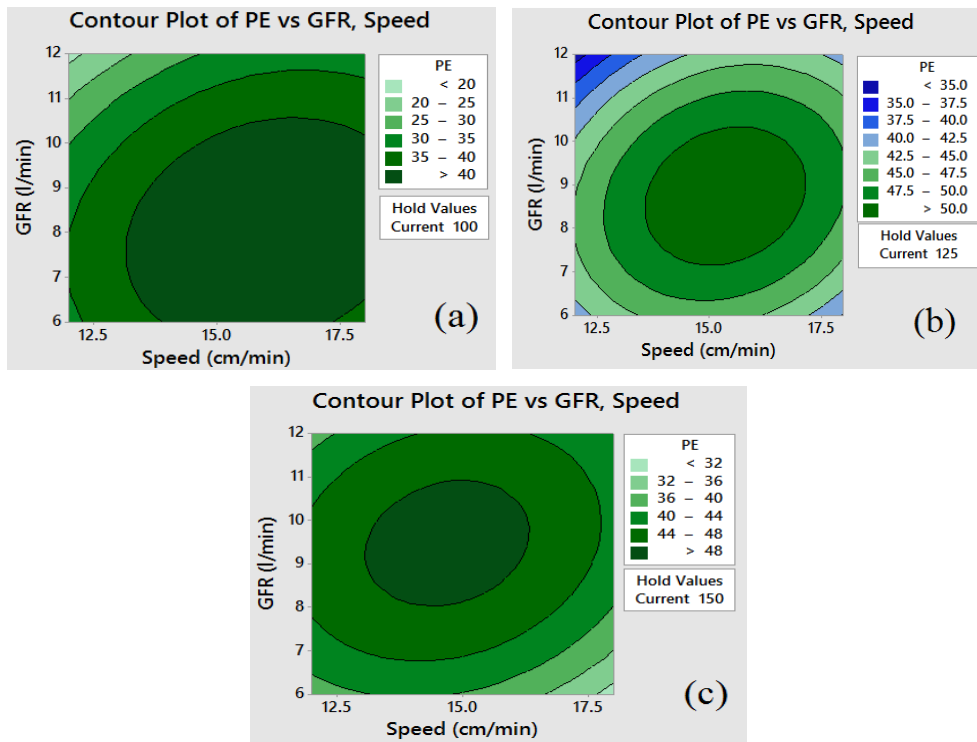


**Fig. 4.30:** Contour plots showing combined effects of GFR and speed on PE, while current hold at a) 100A b) 125A and c) 150A

#### 4.2.2.6. Optimization of PE by TLBO

The optimization of PE is carried out by using TLBO algorithm. The procedural steps mentioned in sec. 4.2.1.6 are used to predict the PE. The obtained optimum welding condition is: current (A) = 131.31 A, speed (B) = 15.21 cm/min and gas flow rate (C) = 8.91 l/min and corresponding PE = 52.23. The same predicted welding condition and output response is given in Table 4.12.

#### 4.2.2.7. Optimization of PE by DFA

The same procedure of DFA to optimize the UTS, as given in section 4.2.1.7 is used to predict the PE and optimization plot is drawn and shown in Fig. 4.31. Obtained optimized welding combination is: current (A) = 131.31 A, speed (B) = 15.21 cm/min and gas flow rate (C) = 8.91 l/min and corresponding PE = 52.23. Obtained optimal condition(s) is also shown in Table 4.12.

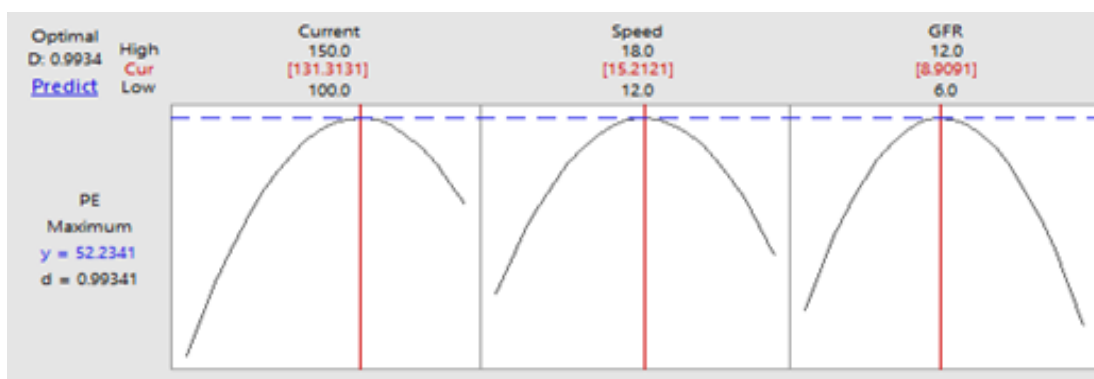


**Fig. 4.31:** Optimization plot for PE

### 4.2.3. Factor analysis, modeling and optimization of YS

#### 4.2.3.1. Main and interaction effects for YS

From the experimental data of yield strength (YS) as given in **Table 4.3**, main and interaction plots are made and shown in **Fig. 4.32** and **Fig. 4.33**. From the main effect plots (**Fig. 4.32**), it is found that YS is decreasing and then increasing with increase of current and with increase of speed and gas flow rate parameters YS is increasing first and then decreasing. From the **Fig. 4.32**, it is found that current is dominant factor for YS as higher the difference between minimum and maximum limits of current compare to other two factors, next is speed and followed by gas flow rate.

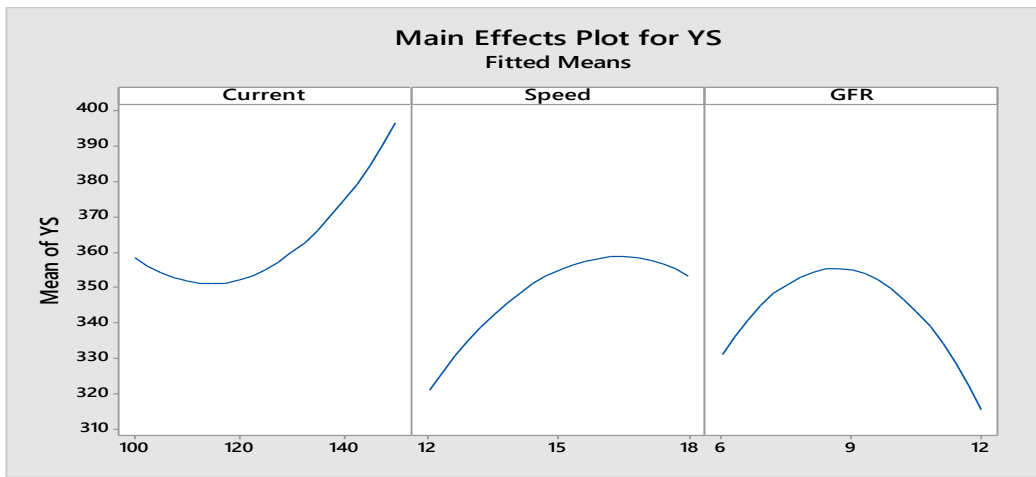


**Fig. 4.32:** Main effect plots for YS

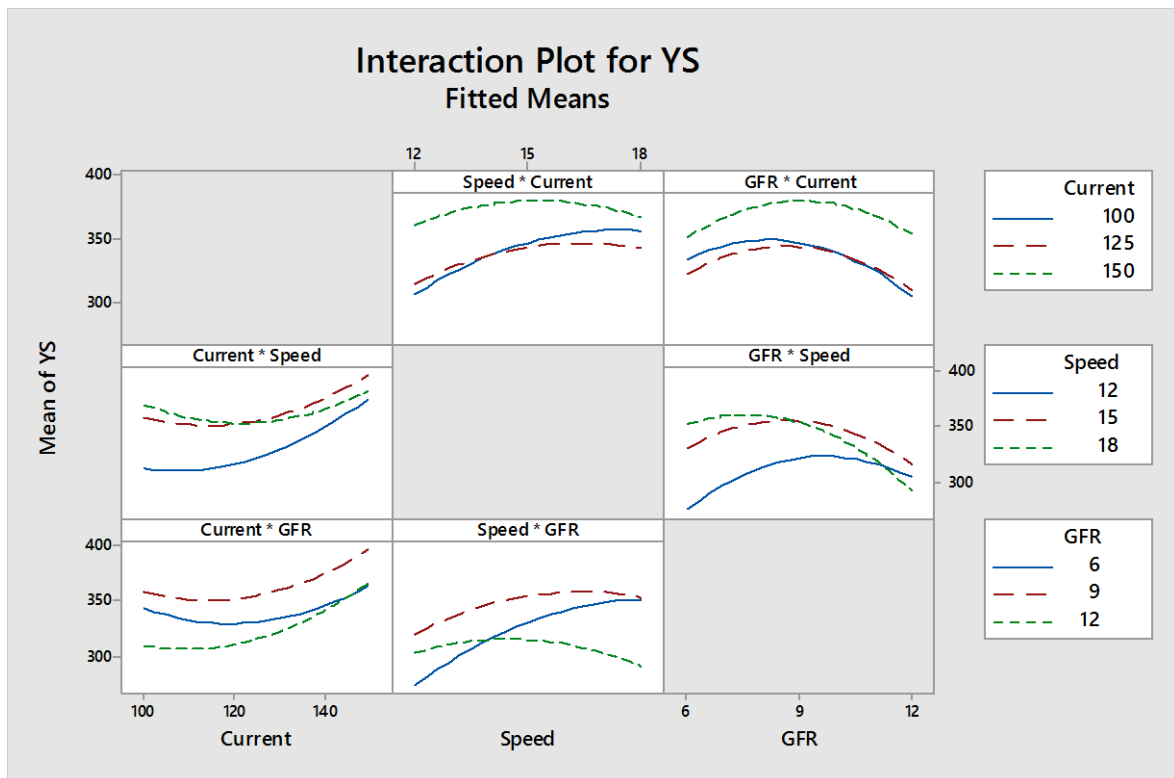


**Fig. 4.33:** Interaction effect plots for YS

The interaction effects between the process welding parameters vs. YS are depicted in **Fig. 4.33**. From the **Fig. 4.33**, it is identified that interaction effects are most significantly influencing the YS because of non-parallelism lines and intersecting lines present in each pair of input variables.

#### 4.2.3.2. Mathematical modeling and contour plots for YS

The mathematical relationships between the welding input parameters and welding response YS is made by RSM approach by following the procedure given in **section 4.2.1.2**. The obtained mathematical equation is given in **Eq. 4.5**.

$$Y_{YS} = - 476 - 6.79 \text{ Current} + 108.0 \text{ Speed} + 82.0 \text{ GFR} + 0.03593 \text{ Current*Current} \\ - 1.974 \text{ Speed*Speed} - 3.509 \text{ GFR*GFR} - 0.1701 \text{ Current*Speed} \\ + 0.1238 \text{ Current*GFR} - 2.459 \text{ Speed*GFR} \quad (4.5)$$

#### 4.2.3.3. Analysis of variance for YS

Analysis of variance is performed on experimental data of YS as given in **Table 4.3** and given in **Table 4.8**. The same procedure followed for conducting ANOVA of YS as given in **section 4.2.1.3**. The developed model is significant at 95% confidence level as P value of the model is less than 0.05.

It is found from **Table 4.8** that direct and square combinations effects of all input welding parameters, are significant on YS as its P values are less than 0.05, except gas flow rate. The interaction effects of current - speed, speed - gas flow rate is significant for YS as their P values are less than 0.05. The interaction effect of current\*gas flow rate is not significant at 95% confidence level, as found from the **Table 4.8**.

**Table 4.8:** Analysis of Variance for YS

Source	DF	Adj SS	Adj MS	F-Value	P-Value	Remarks
<b>Model</b>	9	15463.8	1718.20	18.65	0.002	Significant
<b>Linear</b>	3	5433.4	1811.15	19.66	0.003	Significant
Current	1	2854.3	2854.28	30.98	0.003	Significant
Speed	1	2101.1	2101.14	22.81	0.005	Significant
GFR	1	478.0	478.02	5.19	0.072	Not Significant
<b>Square</b>	3	7075.9	2358.63	25.60	0.002	Significant
Current*Current	1	1861.5	1861.48	20.21	0.006	Significant
Speed*Speed	1	1164.8	1164.84	12.64	0.016	Significant
GFR*GFR	1	3683.3	3683.30	39.98	0.001	Significant
<b>2-Way Interaction</b>	3	2954.4	984.81	10.69	0.013	Significant
Current*Speed	1	651.3	651.27	7.07	0.045	Significant
Current*GFR	1	344.7	344.66	3.74	0.111	Not Significant
Speed*GFR	1	1958.5	1958.51	21.26	0.006	Significant
<b>Error</b>	5	460.6	92.13			
Lack-of-Fit	3	89.2	29.74	0.16	0.915	Not Significant
Pure Error	2	371.4	185.71			
<b>Total</b>	14	15924.4				

Model Summary: R-sq =97.11%, R-sq(adj)= 91.90%, R-sq(pred)= 85.79%

The correlation coefficient R-square value for the experimental result obtained is 0.9711 (97.11%) for YS which shows a good correlation the experimental results possess, whereas adjusted R-square values of YS is 0.9190 (91.90%) also indicates good correlation.

**4.2.3.4. Model Validation**

The relationship between the actual and predicted values of response for YS is shown in **Fig. 4.34**. This figure shows that the developed model is adequate and predicted results are in good agreement with measured data.

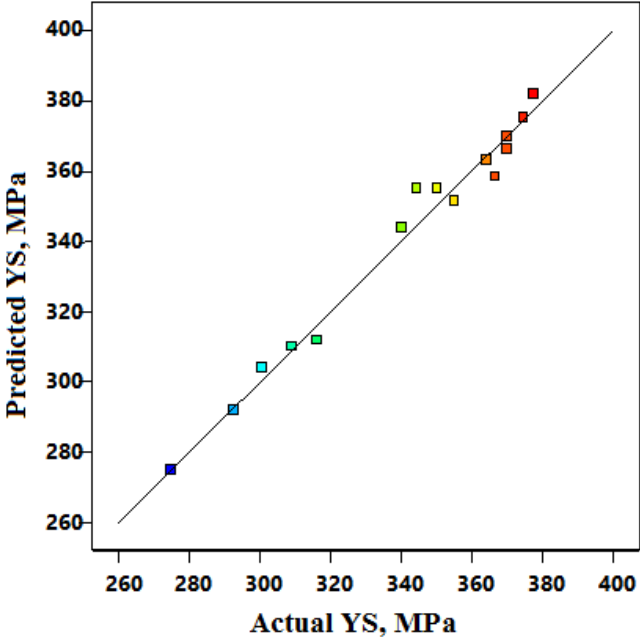


**Fig. 4.34:** Plot of predicted vs. actual results of YS

**4.2.3.5. Effect of the Parameters on YS**

The contour plots are drawn from the **Eq.4.5** and shown in **Fig. 4.35 – Fig. 4.37** using RSM application. The contour plots shown in **Fig. 4.35**, present the effect of input process parameters on YS for speed vs current, while gas flow rate is held constant at their respective lowest, medium and highest values. **Fig. 4.36** shows the influences of welding input variables: GFR vs. current on YS, while speed hold at their respective lowest, medium and highest values. **Fig. 4.37** represents the influence of GFR vs. speed on YS, while welding current hold at their respective lowest, medium and highest values.

From the contour plots given in **Fig. 4.35 – Fig. 4.37**, it is identified that yield strength is adversely affected by input welding parameters, as bent lines / curved lined / elliptical nature lines in the plots.

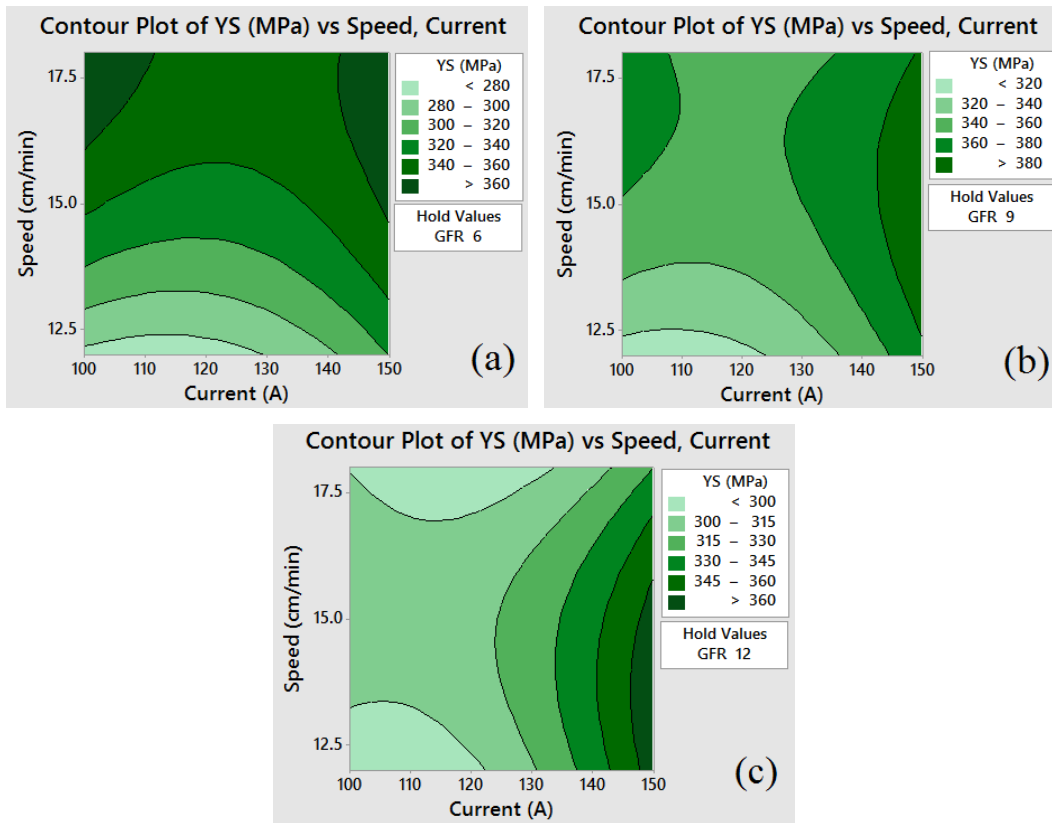


**Fig. 4.35:** Contour plots showing combined effects of speed and current on YS, while GFR hold at a) 6 l/min b) 9 l/min and c) 12 l/min

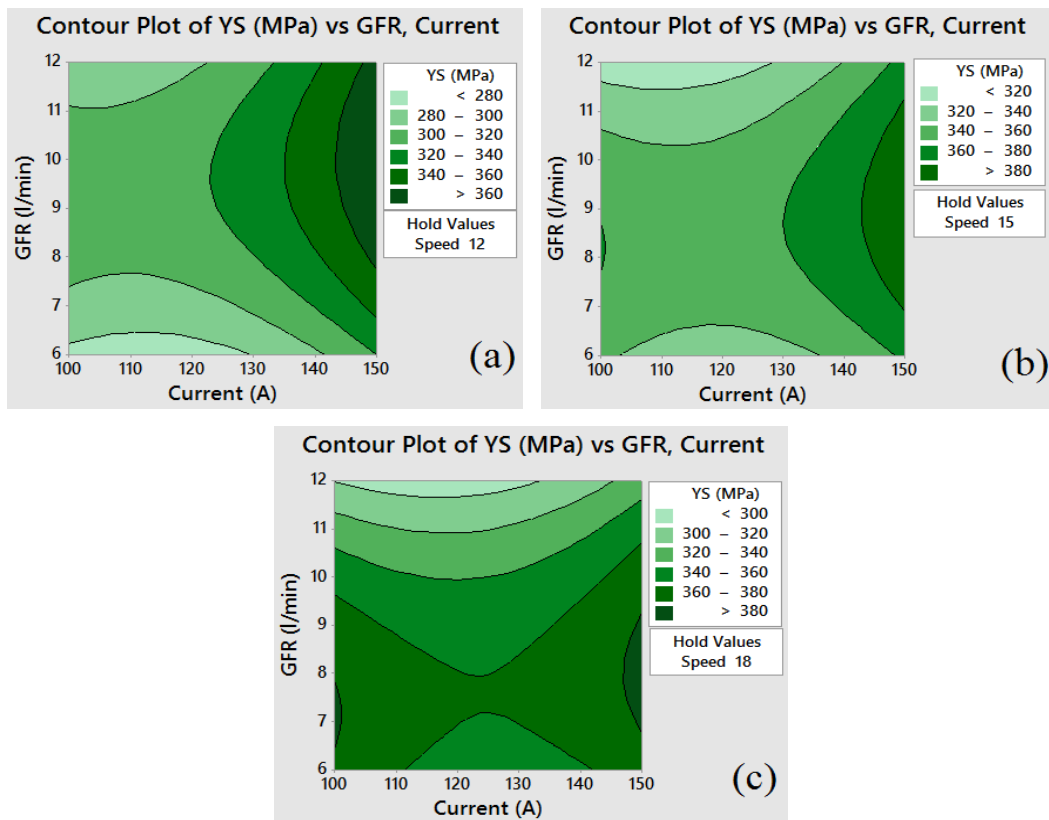


**Fig. 4.36:** Contour plots showing combined effects of GFR and current on YS, while speed hold at a) 12 cm/min b) 15 cm/min and c) 18 cm/min

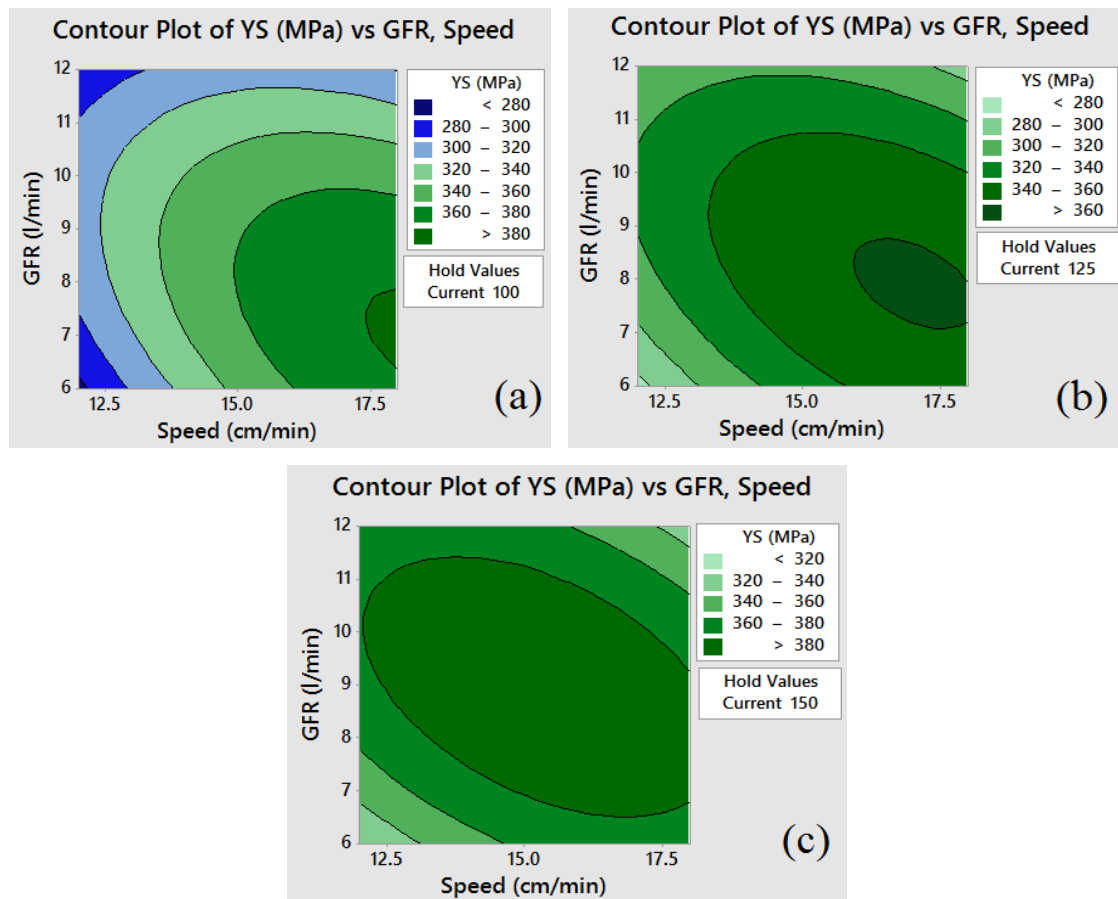


**Fig. 4.37:** Contour plots showing combined effects of GFR and speed on YS, while current hold at a) 100A b) 125A and c) 150A

#### 4.2.3.6. Optimization of YS by TLBO

The optimization of YS is carried out by using TLBO algorithm by using execution steps of TLBO as given in **section 4.2.1.6**. The obtained optimum welding combination is: current (A) = 150 A, speed (B) = 15.33 cm/min and gas flow rate (C) = 8.97 l/min and corresponding YS = 396.55 MPa. The predicted welding condition and output response is shown in **Table 4.12**.

#### 4.2.3.7. Optimization of YS by DFA

The execution steps of DFA for obtaining the optimum conditions are already discussed in **section 4.2.1.7**, the same has been followed in case of optimization of YS. The obtained optimal setting is (**Fig. 4.38**): current (A) = 150 A, speed (B) = 15.33 cm/min and gas flow rate (C) = 8.97 l/min and corresponding YS = 396.55 MPa. The optimal welding condition as well as maximized YS is predicted by DFA and given in **Table 4.12**.

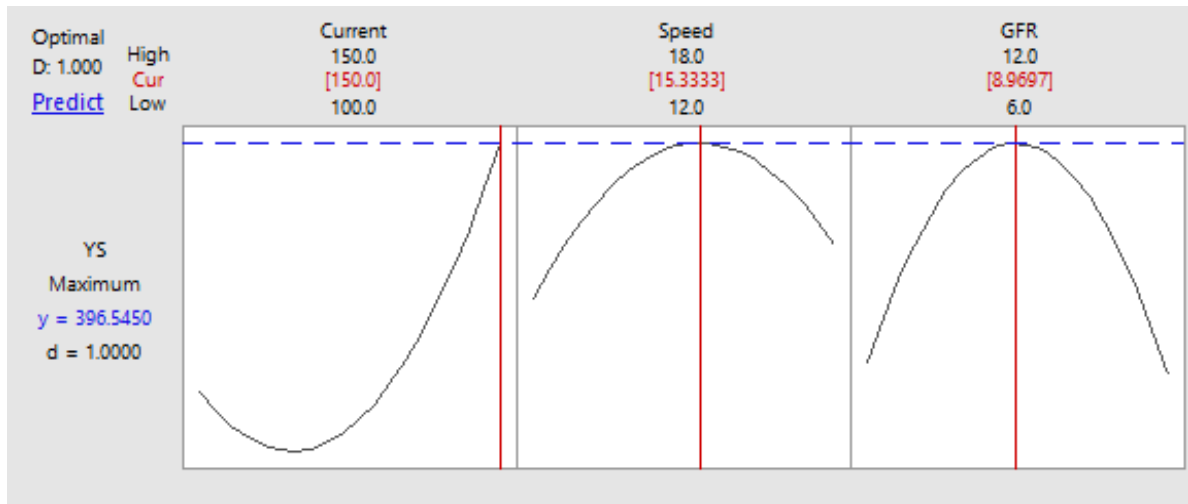


Fig. 4.38: Optimization plot for YS

#### 4.2.4. Factor analysis, modeling and optimization of IS

##### 4.2.4.1. Main and interaction effects for IS

The main and interaction effects of welding parameters vs. impact strength (IS) are illustrated in Fig. 4.39 – Fig.4.40. Analyzing the main effect plots as shown Fig. 4.39, it is found that IS is increasing and then decreasing with increase of all welding input parameters (current, speed and gas flow rate). From the Fig. 4.39, it is found that welding speed is dominant factor for IS, because of higher difference between maximum and minimum limits of welding speed, compare to other parameters, next important factor is GFR and followed by current.

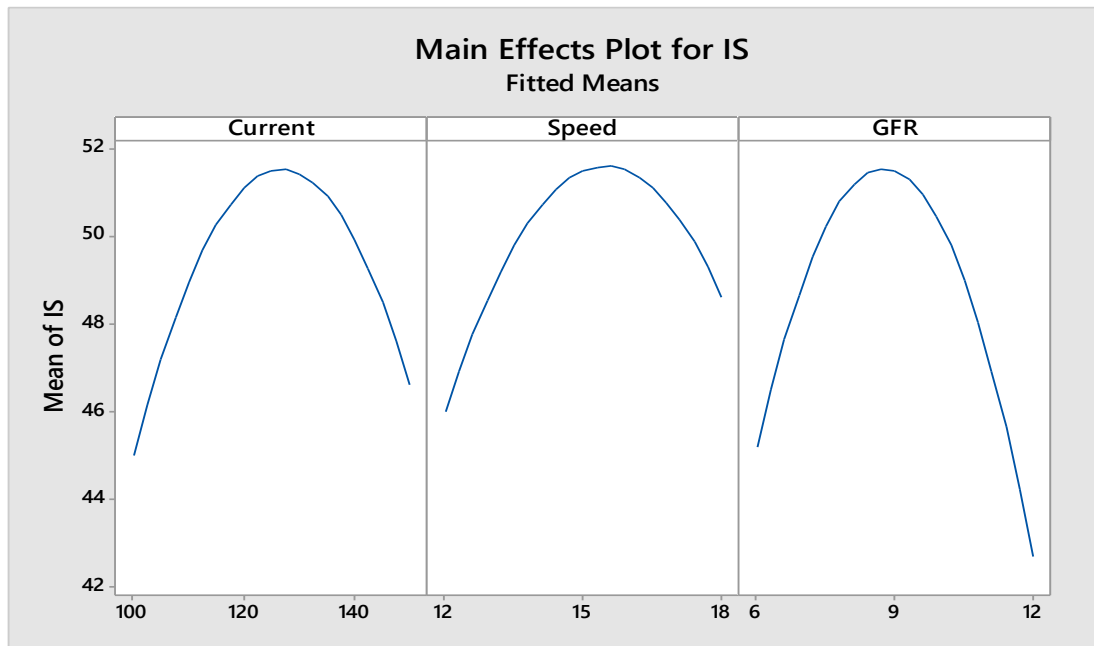
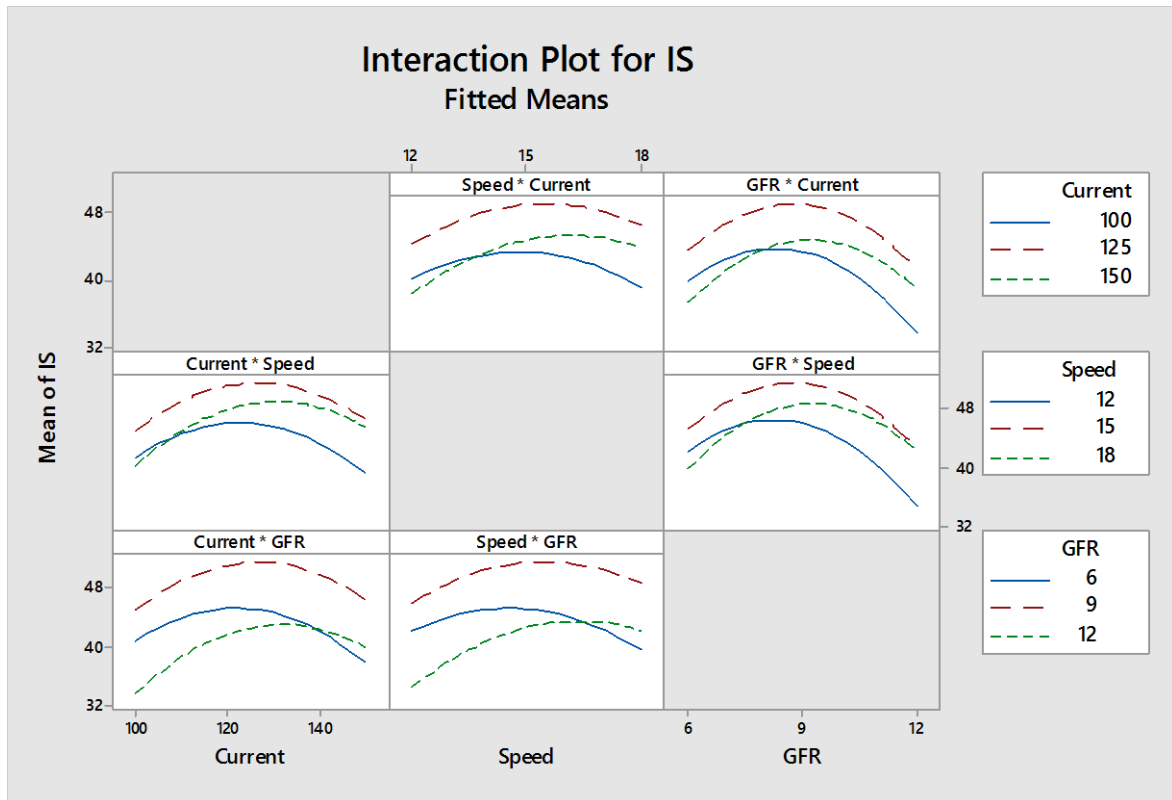


Fig. 4.39: Main effect plots for IS





**Fig. 4.40:** Interaction effect plots for IS

**Fig. 4.40** illustrates the interaction effects of process parameters vs. response variable, IS. The non-parallelism of the lines and intersecting lines in each case of parameters indicates that interaction effects of process parameters are most significant for IS.

#### 4.2.4.2. Mathematical modeling for IS

The mathematical relationship between the welding input parameters and welding quality response IS is made by RSM approach by following the procedure given in **Section 4.2.1.2**. The obtained mathematical equation is given in **Eq. 4.6**.

$$\begin{aligned}
 Y_{IS} = & -152.2 + 1.663 \text{ Current} + 8.77 \text{ Speed} + 6.792 \text{ GFR} - 0.009100 \text{ Current*Current} \\
 & - 0.4653 \text{ Speed*Speed} - 0.8403 \text{ GFR*GFR} + 0.02500 \text{ Current*Speed} \\
 & + 0.03000 \text{ Current*GFR} + 0.2778 \text{ Speed*GFR}
 \end{aligned}
 \tag{4.6}$$

#### 4.2.4.3. Analysis of variance for IS

ANOVA for impact strength (IS) is made and shown in **Table 4.9** as following the steps given in **section 4.2.1.3**. The hypothesis is confirmed from ANOVA table (**Table 4.9**) of IS, as more than one term in the table are zero.

It can be concluded from **Table 4.9** that the individual (current, speed and gas flow rate), square combinations (current\*current, speed\*speed, gas flow rate\*gas flow rate) and interaction (current\*speed, current\*gas flow rate and speed\*gas flow rate) effects of input parameters are most significant on IS as its P values are less than 0.05, even it is found to be zero in most of the cases.

**Table 4.9:** Analysis of Variance for IS

Source	DF	Adj SS	Adj MS	F-Value	P-Value	Remarks
Model	9	438.087	48.676	185.43	0.000	Significant
Linear	3	31.563	10.521	40.08	0.001	Significant
Current	1	5.281	5.281	20.12	0.006	Significant
Speed	1	13.781	13.781	52.50	0.001	Significant
GFR	1	12.500	12.500	47.62	0.001	Significant
Square	3	347.212	115.738	440.90	0.000	Significant
Current*Current	1	119.437	119.437	455.00	0.000	Significant
Speed*Speed	1	64.745	64.745	246.65	0.000	Significant
GFR*GFR	1	211.168	211.168	804.45	0.000	Significant
2-Way Interaction	3	59.312	19.771	75.32	0.000	Significant
Current*Speed	1	14.063	14.063	53.57	0.001	Significant
Current*GFR	1	20.250	20.250	77.14	0.000	Significant
Speed*GFR	1	25.000	25.000	95.24	0.000	Significant
Error	5	1.313	0.263			
Lack-of-Fit	3	0.813	0.271	1.08	0.513	Not Significant
Pure Error	2	0.500	0.250			
Total	14	439.400				

Model Summary: R-Sq = 99.70%, R-Sq (adj) = 99.16%, R-sq(pred)= 96.79%

The correlation coefficient R-square value for the experimental result obtained is 0.9970 (99.70%) for IS which shows a good correlation the experimental results possess, whereas adjusted R- square values of IS is 0.9916 (99.16%) also indicates good correlation.

#### 4.2.4.4. Model Validation

**Fig. 4.41** shows the relationship between the actual and predicted values of response for impact strength. This figure also indicates that the developed model is adequate and predicted results are in good agreement with measured data.

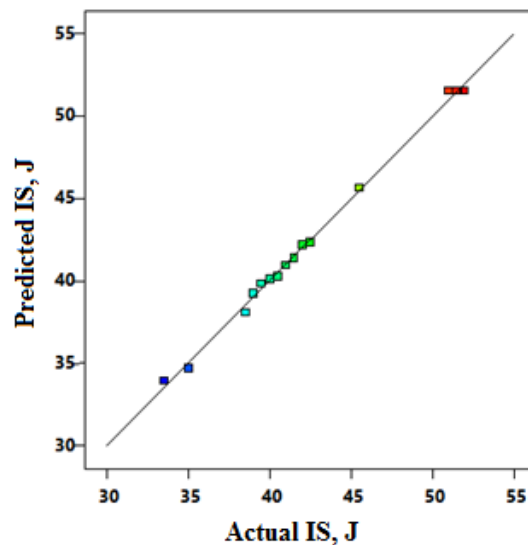


**Fig. 4.41:** Plot of predicted vs. actual results of IS

#### 4.2.4.5. Effect of the Parameters on IS

The contour plots for IS are prepared and given in **Fig. 4.42** – **Fig. 4.44** by using **Eq. 4.6** with the help of RSM approach. The contour plots shown in **Fig. 4.42**, present the effect of input process parameters on IS for speed vs current, while gas flow rate is held constant at their respective lowest, medium and highest values. **Fig. 4.43** shows the influences of welding input variables: GFR vs. current on IS, while speed hold at their respective lowest, medium and highest values. **Fig. 4.44** represents the influence of GFR vs. speed on IS, while welding current hold at their respective lowest, medium and highest values.

From the contour plots of IS as given in **Fig. 4.42** – **Fig. 4.44**, it is found that direct and interaction effects of all welding parameters are most significant as all lines in the given plots are elliptical in nature.

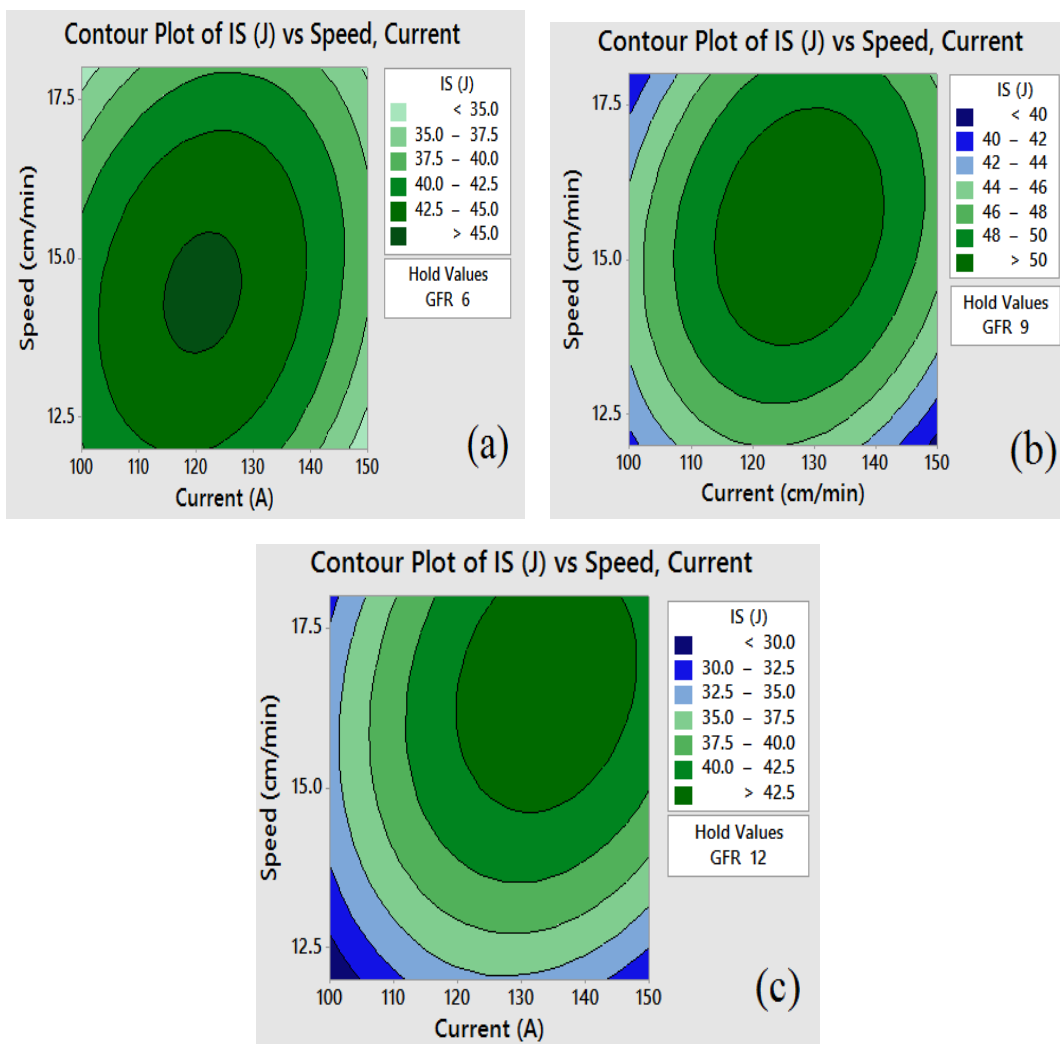


**Fig. 4.42:** Contour plots showing combined effects of speed and current on IS, while GFR hold at a) 6 l/min b) 9 l/min and c) 12 l/min

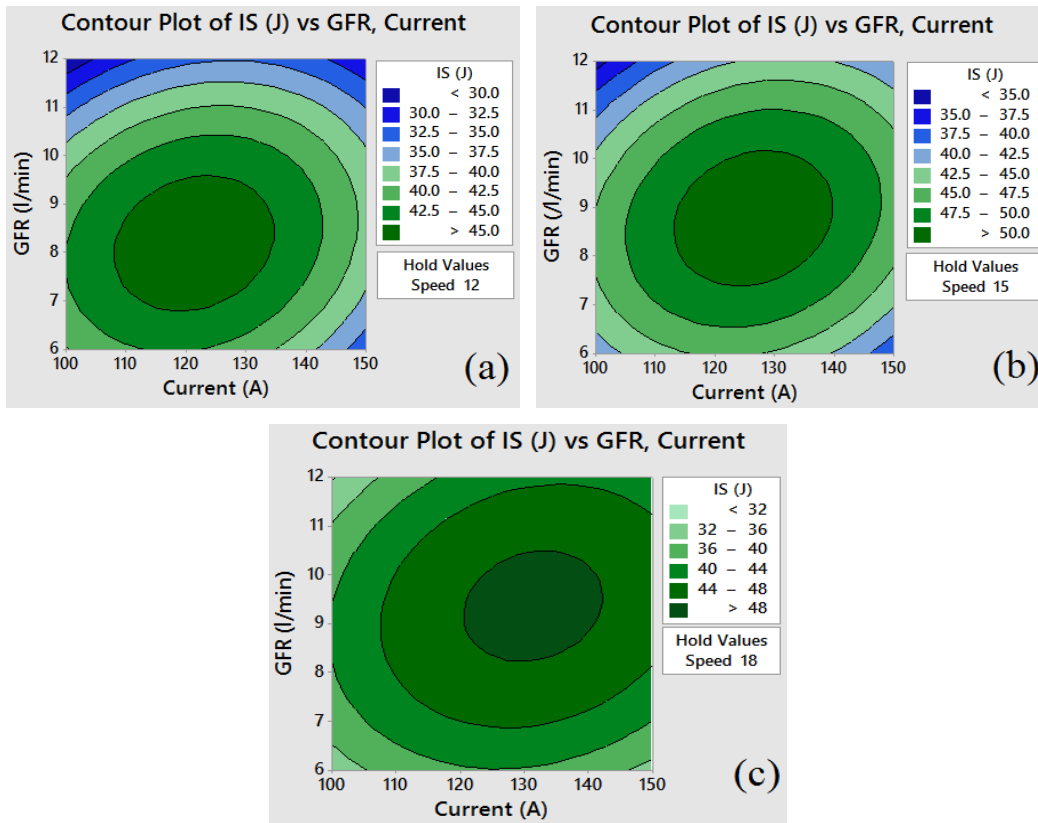


**Fig. 4.43:** Contour plots showing combined effects of GFR and current on IS, while speed hold at a) 12 cm/min b) 15 cm/min and c) 18 cm/min

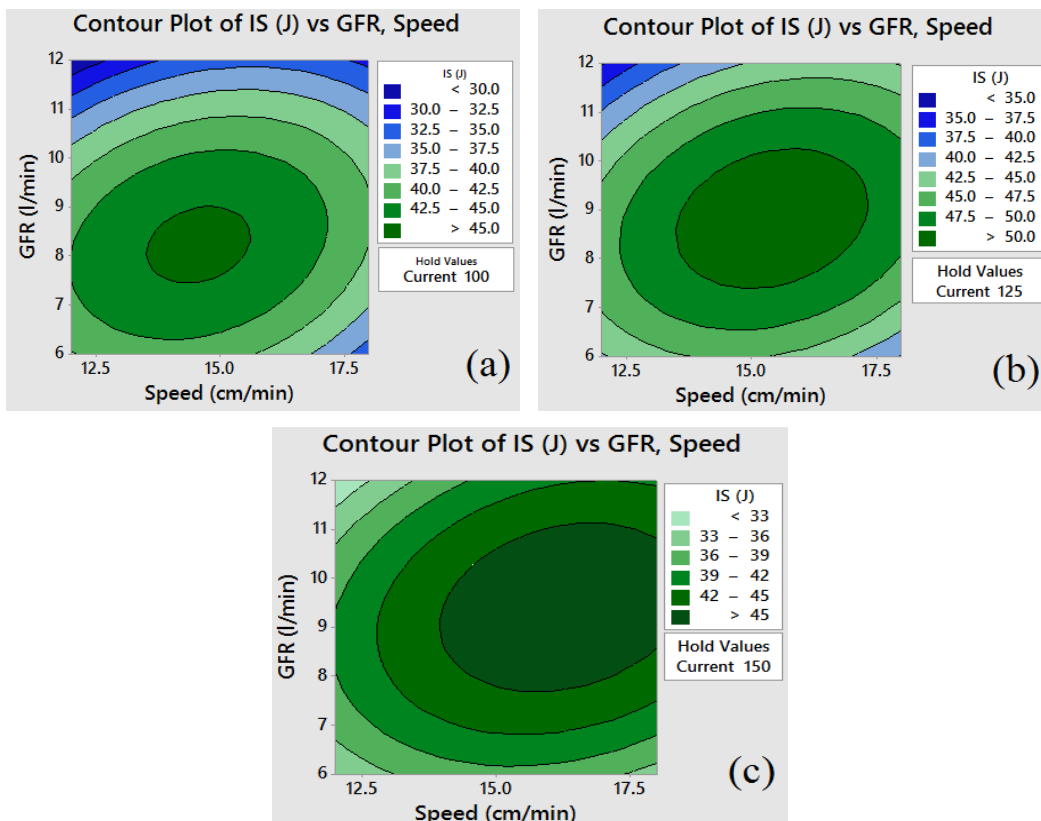


**Fig. 4.44:** Contour plots showing combined effects of GFR and speed on IS, while current hold at a) 100A b) 125A and c) 150A

#### 4.2.4.6. Optimization of IS by TLBO

The optimization of IS is carried out by using TLBO algorithm by using execution steps of TLBO as given in **section 4.2.1.6**. The obtained optimum welding combination is: current (A) = 127.27A, speed (B) = 15.52 cm/min and gas flow rate (C) = 8.85 l/min and corresponding IS =51.67 J. The predicted welding condition and output response is shown in **Table 4.12**.

#### 4.2.4.7. Optimization of IS by DFA

The execution steps of DFA for obtaining the optimum conditions are already discussed in **section 4.2.1.7**, the same has been followed in case optimization IS. The optimal welding condition as well as maximized IS predicted from optimization plot (**Fig. 4.45**) drawn by DFA is: current (A) = 127 A, speed (B) = 15.52 cm/min and gas flow rate (C) = 8.85 l/min and corresponding IS = 51.67 J. The obtained optimal setting is also given in **Table 4.12**.

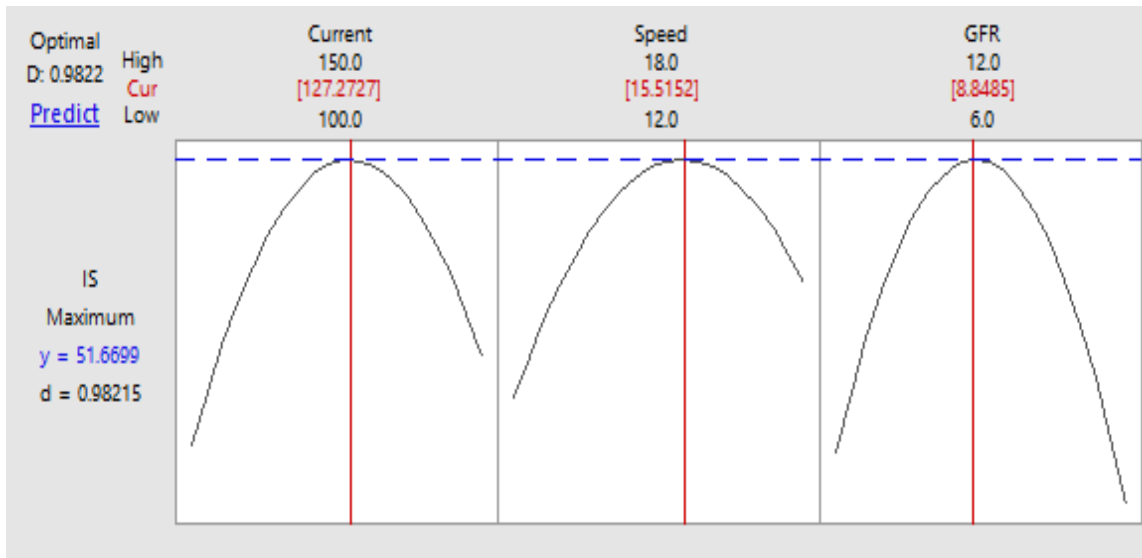


**Fig. 4.45:** Optimization plot for IS

#### 4.2.5. Factor analysis, modeling and optimization of hardness

##### 4.2.5.1. Main and interaction effects for hardness

The main and interaction effects of welding parameters vs. hardness (VHN) are shown in **Fig. 4.46** and **Fig. 4.47** respectively. From the main effect plots of hardness (VHN) as given **Fig. 4.46**, it is identified that hardness is increasing and then decreasing with increase of all welding parameters (current, speed and gas flow rate). By studying the differences between the minimum and maximum limits each as given in **Fig. 4.46**, it is noted that speed is most significant factor for hardness. Welding current and gas flow rate have equal importance on hardness.

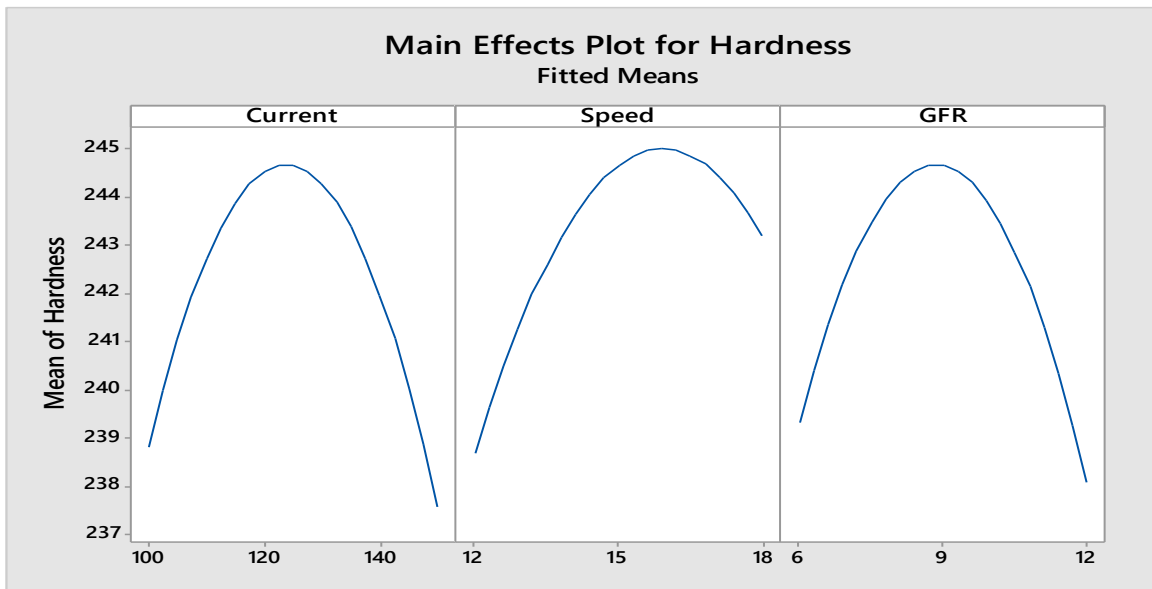


**Fig. 4.46:** Main effect plot for hardness

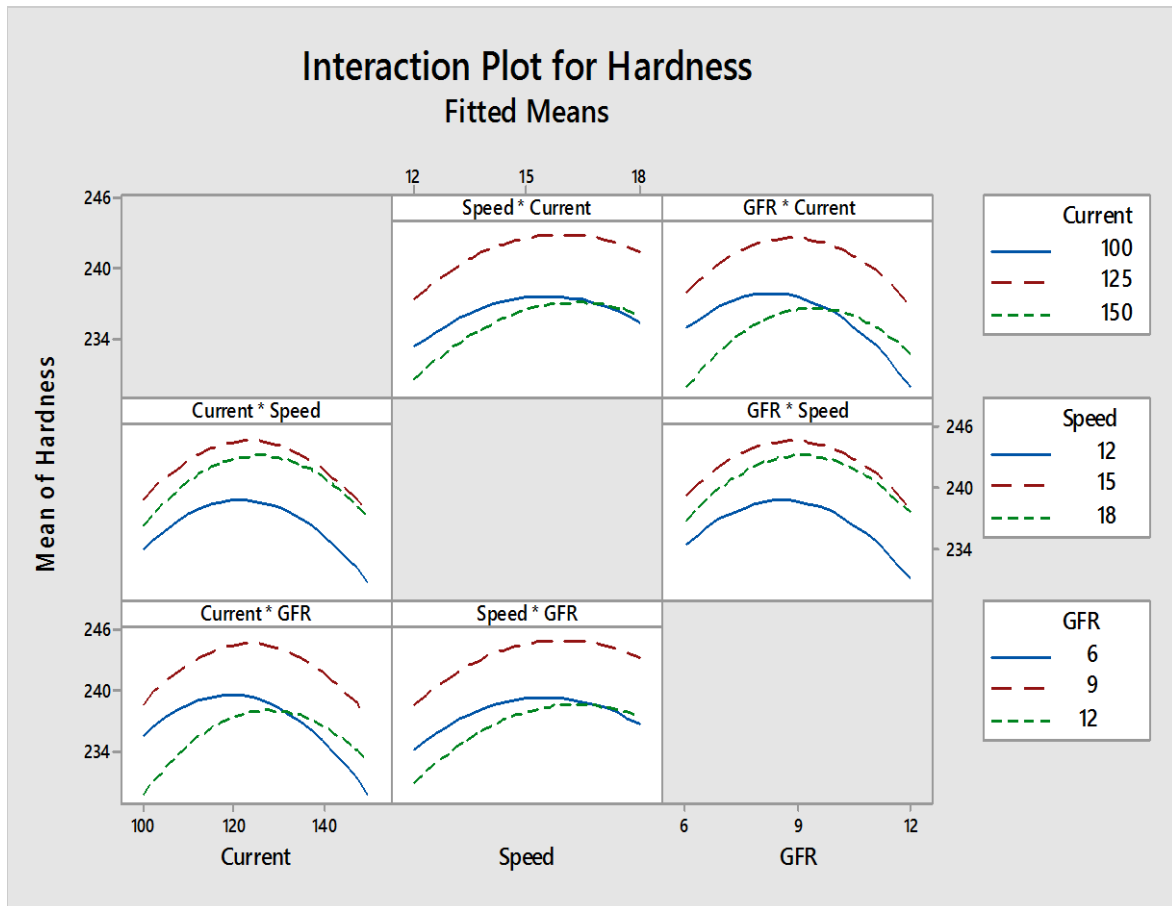


**Fig. 4.47:** Interaction effects plot for hardness

**Fig. 4.47** shows the interaction effects of process parameters vs. hardness (VHN). **Fig. 4.47** reveals that interaction effects of process parameters are most significant for hardness as non-parallelism lines and intersecting lines present in the plots.

#### 4.2.5.2 Mathematical modeling for hardness

The mathematical relationship between the welding input parameters and hardness (VHN) is made by RSM approach by following the procedure given in **Section 4.2.1.2**. The obtained mathematical equation is given in **Eq. 4.7**.

$$Y_{\text{Hardness}} = 4.4 + 2.088 \text{ Current} + 10.44 \text{ Speed} + 6.292 \text{ GFR} - 0.010333 \text{ Current*Current} - 0.4120 \text{ Speed*Speed} - 0.6620 \text{ GFR*GFR} + 0.01333 \text{ Current*Speed} + 0.03000 \text{ Current*GFR} + 0.1111 \text{ Speed*GFR} \quad (4.7)$$

#### 5.2.5.3 Analysis of variance for hardness

ANOVA for hardness is made and shown in **Table 4.10**. The hypothesis is confirmed from ANOVA table (**Table 4.10**) of hardness (VHN), as more than one term in the table is more than zero.

It can be concluded from **Table 4.10** that the individual effect of speed, square combinations (current\*current, speed\*speed, gas flow rate\*gas flow rate) and interaction effects of current\*gas flow rate are most significant for hardness (VHN) as its P values are zero. Direct effects of current and gas flow rate, and interaction effects of current\*speed and speed\*gas flow rate are also significant for hardness (VHN) as their P values are less than 0.05.

**Table 4.10:** Analysis of Variance for Hardness

Source	DF	Adj SS	Adj MS	F-Value	P-Value	Remarks
<b>Model</b>	<b>9</b>	<b>369.517</b>	<b>41.057</b>	<b>144.91</b>	<b>0.000</b>	<b>Significant</b>
<b>Linear</b>	<b>3</b>	<b>46.750</b>	<b>15.583</b>	<b>55.00</b>	<b>0.000</b>	<b>Significant</b>
Current	1	3.125	3.125	11.03	0.021	Significant
Speed	1	40.500	40.500	142.94	0.000	Significant
GFR	1	3.125	3.125	11.03	0.021	Significant
<b>Square</b>	<b>3</b>	<b>294.517</b>	<b>98.172</b>	<b>346.49</b>	<b>0.000</b>	<b>Significant</b>
Current*Current	1	154.006	154.006	543.55	0.000	Significant
Speed*Speed	1	50.776	50.776	179.21	0.000	Significant
GFR*GFR	1	131.083	131.083	462.65	0.000	Significant
<b>2-Way Interaction</b>	<b>3</b>	<b>28.250</b>	<b>9.417</b>	<b>33.24</b>	<b>0.001</b>	<b>Significant</b>
Current*Speed	1	4.000	4.000	14.12	0.013	Significant
Current*GFR	1	20.250	20.250	71.47	0.000	Significant
Speed*GFR	1	4.000	4.000	14.12	0.013	Significant
<b>Error</b>	<b>5</b>	<b>1.417</b>	<b>0.283</b>			
Lack-of-Fit	3	0.750	0.250	0.75	0.615	Not Significant
Pure Error	2	0.667	0.333			
<b>Total</b>	<b>14</b>	<b>370.933</b>				

Model Summary: R-Sq = 99.62%, R-Sq(adj) = 98.93% , R-sq(pred) 96.36%

The correlation coefficient R-square value for the experimental result obtained is 0.9962 (99.62%) for hardness which shows a good correlation the experimental results possess,

whereas adjusted R-square values of hardness is 0.9893 (98.93%) also indicates good correlation.

#### 4.2.5.4. Model Validation

**Fig. 4.48** shows the relationship between the actual and predicted values of response for hardness. From this figure it is observed that the developed model is adequate and predicted results are in good agreement with measured data.

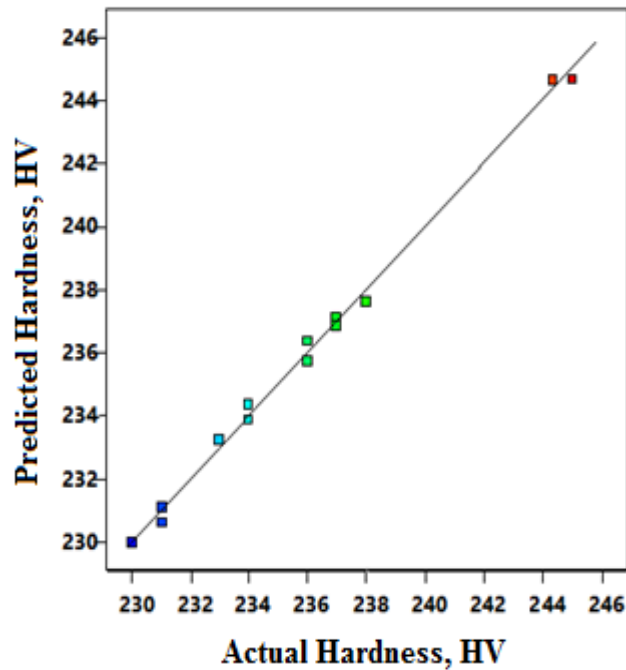


**Fig. 4.48:** Plot of predicted vs. actual results of hardness

#### 4.2.5.5. Effect of the Parameters on Hardness

The contour plots for hardness (VHN) are prepared and given in **Fig. 4.49 – Fig.4.51** by using **Eq. 4.7** with the help of RSM approach. The contour plots shown in **Fig. 4.49**, present the effect of input process parameters on hardness for speed vs current, while gas flow rate is held constant at their respective lowest, medium and highest values. **Fig. 4.50** shows the influences of welding input variables: GFR vs. current on hardness, while speed hold at their respective lowest, medium and highest values **Fig. 4.51** represents the influence of GFR vs. speed on hardness, while welding current hold at their respective lowest, medium and highest values.

From the contour plots of hardness (VHN) as given in **Fig. 4.49 – Fig. 4.51**, it is found that direct and interaction effects of all welding parameters are most significant as all lines in the given plots are elliptical in nature.



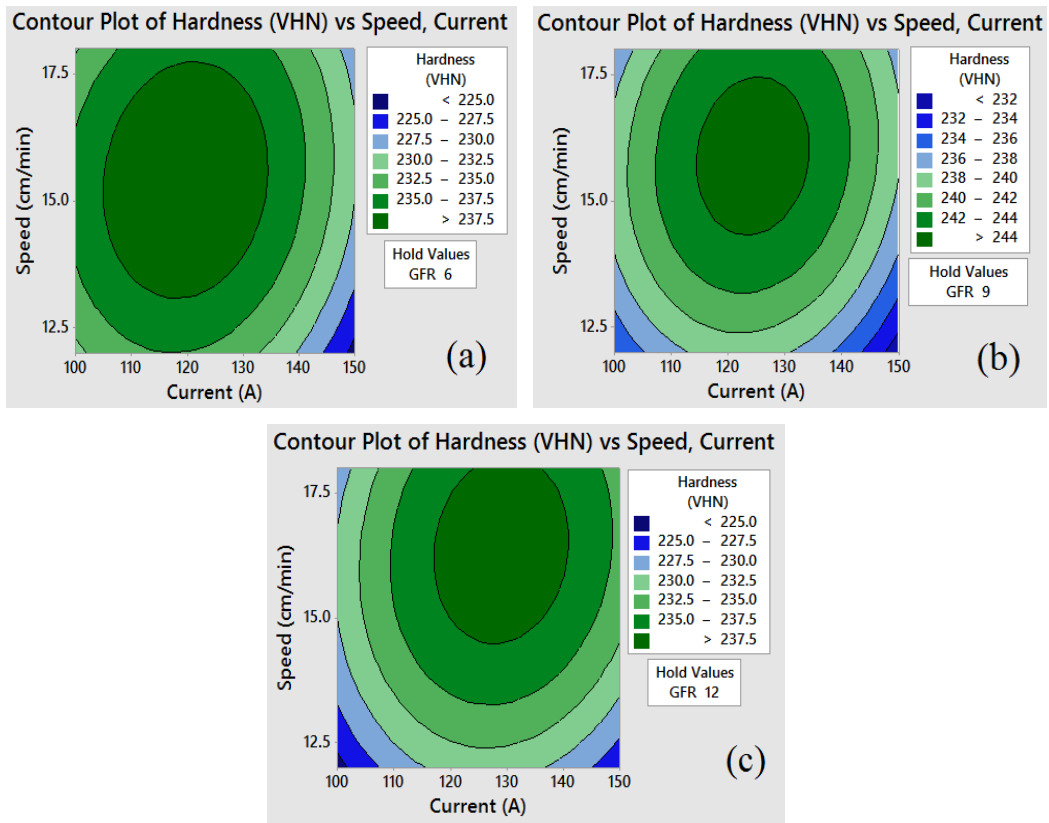


**Fig. 4.49:** Contour plots showing combined effects of speed and current on Hardness, while GFR hold at a) 6 l/min b) 9 l/min and c) 12 l/min

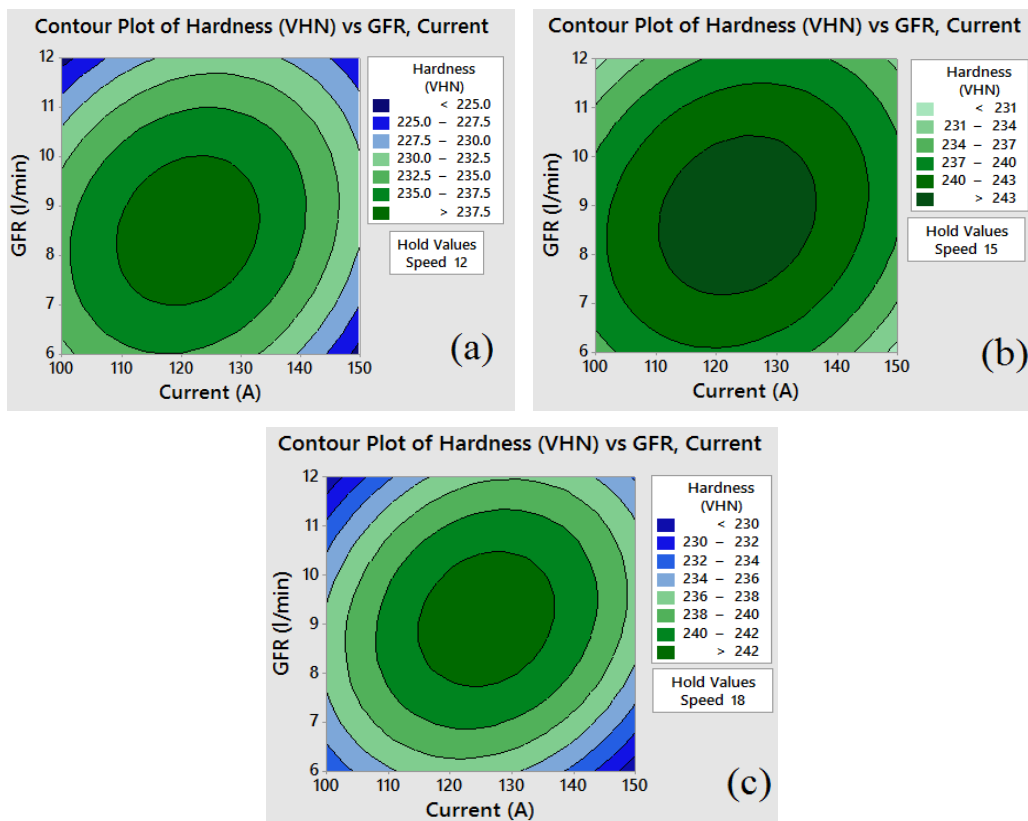


**Fig. 4.50:** Contour plots showing combined effects of GFR and current on Hardness, while speed hold at a) 12 cm/min b) 15 cm/min and c) 18 cm/min

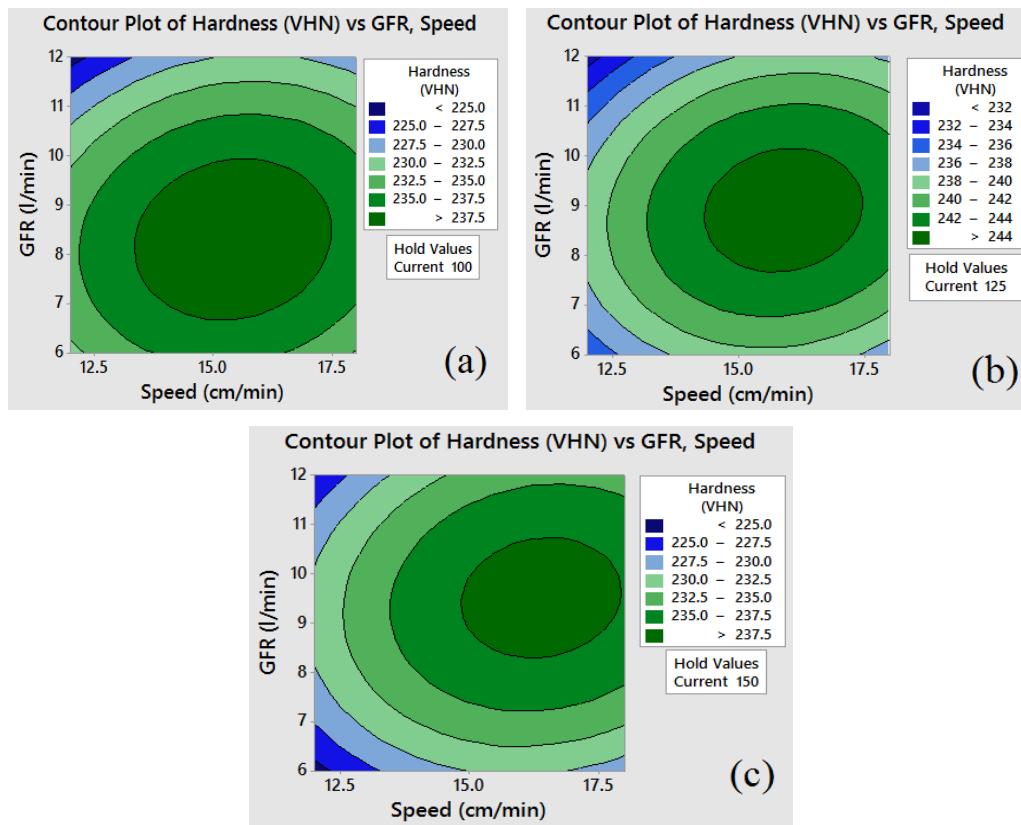


**Fig. 4.51:** Contour plots showing combined effects of GFR and speed on Hardness, while current hold at a) 100A b) 125A and c) 150A

#### 4.2.5.6. Optimization of hardness by TLBO

The optimization of hardness is carried out by using TLBO algorithm by using execution steps of TLBO as given in section 4.2.1.6. The obtained optimum welding combination is: current (A) = 124.24 A, speed (B) = 15.88 cm/min and gas flow rate (C) = 8.91 l/min and corresponding hardness (VHN) = 24.01. The predicted welding condition and output response is shown in Table 4.12.

#### 4.2.5.7. Optimization of hardness by DFA

The execution steps of DFA for obtaining the optimum conditions are already discussed in section 4.2.1.7, the same has been followed in case optimization hardness (VHN). The obtained optimal setting from optimization plot (Fig. 4.52) is: current (A) = 124.24 A, speed (B) = 15.88 cm/min and gas flow rate (C) = 8.91 l/min and corresponding hardness (VHN) = 245.01 MPa and the same optimal welding condition as well as maximized hardness is given in Table 4.12.

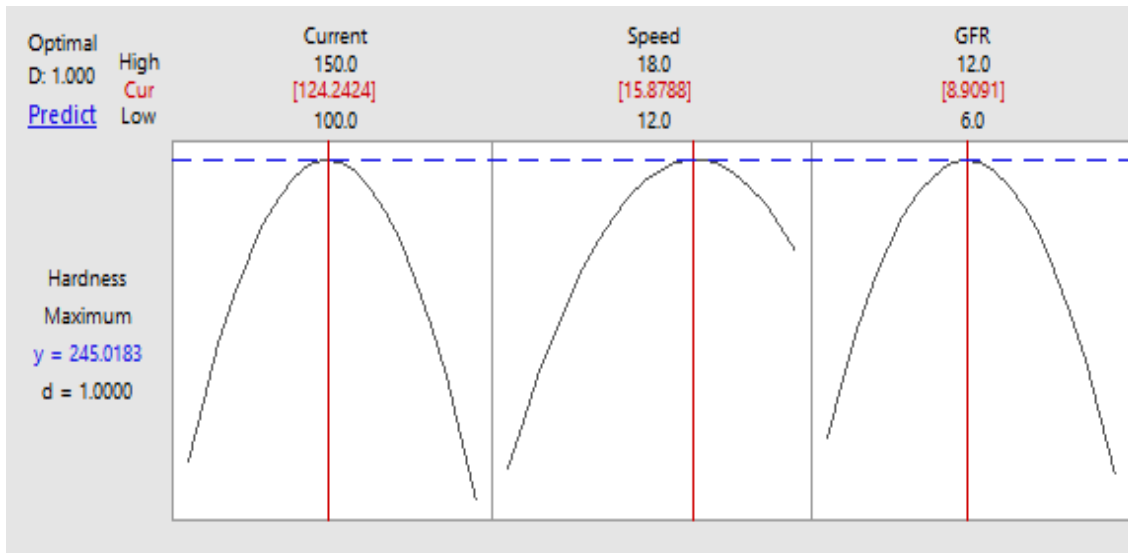


**Fig. 4.52:** Optimization plot for hardness

#### 4.2.6. Factor analysis, modeling and optimization of WW

##### 4.2.6.1. Main and interaction effects for WW

The main and interaction plots are made and given in **Figs. 4.53** and **Fig.4.54** respectively using experimental data of weld width (WW) as shown in **Table 4.3**. From the main effect plots (**Fig. 4.53**), it is found that WW is increasing with increase of gas flow rate (C) and it is decreasing drastically with increase of speed (B). With increase of current, weld width is decreasing and then increasing slightly. From the **Fig. 4.53**, it is found that speed (B) is dominant factor for WW, as difference between the minimum and maximum limits of factors are more for speed compared to other parameters, next is current (A) and followed by gas flow rate (C).

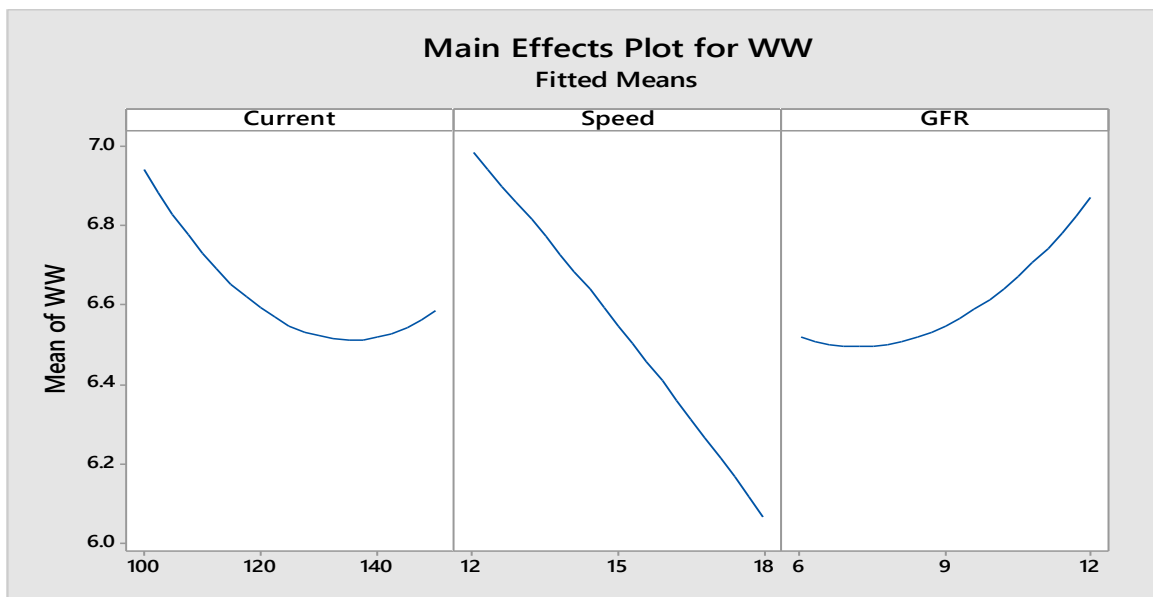


**Fig. 4.53:** Main effect plots for weld width

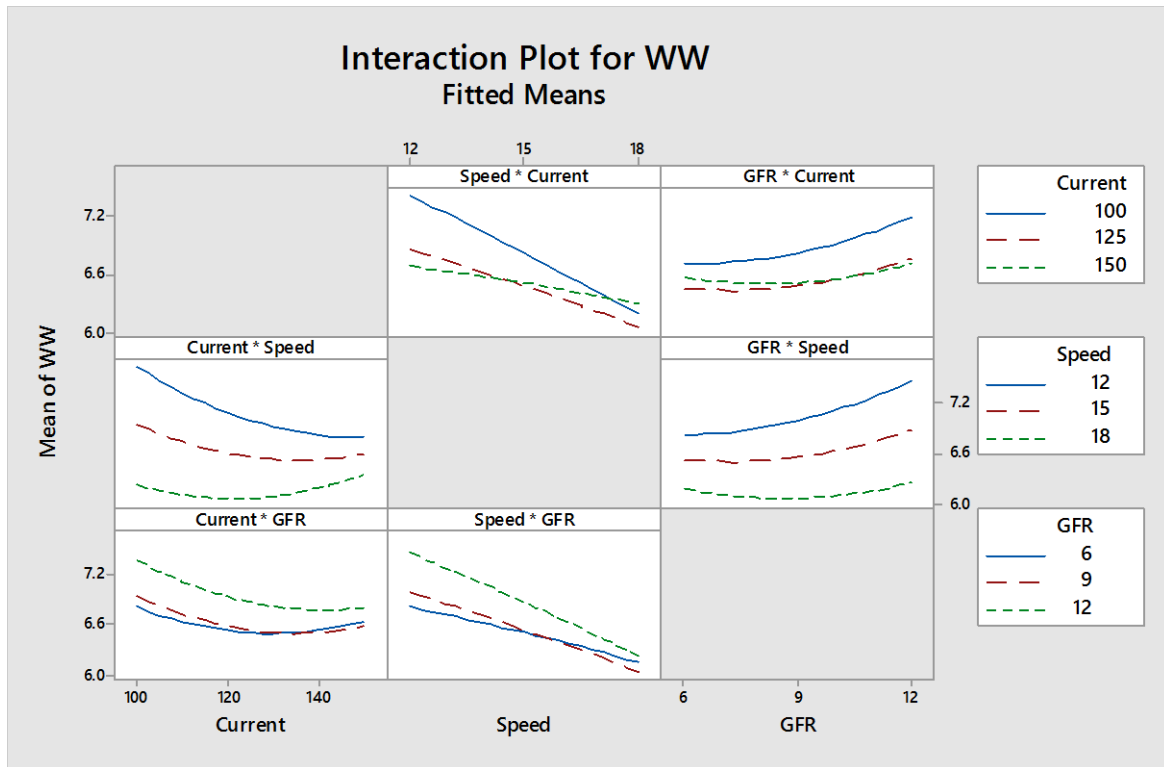


**Fig. 4.54:** Interaction effect plots for weld width

**Fig. 4.54** depicts the interaction effects of process parameters vs. weld width (WW). The non-parallelism of the lines in each case and intersecting lines in **Fig. 4.54** indicates that interaction effects of process parameters are most significant for WW.

#### 4.2.6.2. Mathematical modeling for WW

The mathematical relationships between the welding input parameters and welding response WW is made by RSM approach by following the procedure given in **Section 4.2.1.2**. The obtained mathematical equation is given in **Eq. 4.8**.

$$\begin{aligned}
 Y_{WW} = & 17.781 - 0.12920 \text{ Current} - 0.3363 \text{ Speed} + 0.1537 \text{ GFR} + 0.000342 \text{ Current*Current} \\
 & - 0.002639 \text{ Speed*Speed} + 0.016250 \text{ GFR*GFR} + 0.00320 \text{ Current*Speed} \\
 & - 0.001267 \text{ Current*GFR} - 0.015278 \text{ Speed*GFR}
 \end{aligned} \quad (4.8)$$

#### 4.2.6.3 Analysis of variance for WW

ANOVA for WW is made and shown in **Table 4.11**. The hypothesis is confirmed from ANOVA table (**Table 4.11**) of weld width (WW), as more than one term in the table is more than zero.

It is noted from **Table 4.11** that the individual effects and interaction effects of all process parameters and square combinations of current\*current, and gas flow rate\*gas flow rate are most significant for obtaining minimized weld width (WW) as their P values are zero. The square combination of speed\*speed is significant for WW as its P value is less than 0.05.

**Table 4.11:** Analysis of Variance for WW

Source	DF	Adj SS	Adj MS	F-Value	P-Value	Remarks
Model	9	2.76672	0.30741	1576.48	0.000	Significant
Linear	3	2.18417	0.72806	3733.63	0.000	Significant
Current	1	0.25205	0.25205	1292.56	0.000	Significant
Speed	1	1.68361	1.68361	8633.91	0.000	Significant
GFR	1	0.24851	0.24851	1274.42	0.000	Significant
Square	3	0.24042	0.08014	410.97	0.000	Significant
Current*Current	1	0.16870	0.16870	865.12	0.000	Significant
Speed*Speed	1	0.00208	0.00208	10.68	0.022	Significant
GFR*GFR	1	0.07898	0.07898	405.00	0.000	Significant
2-Way Interaction	3	0.34212	0.11404	584.83	0.000	Significant
Current*Speed	1	0.23040	0.23040	1181.54	0.000	Significant
Current*GFR	1	0.03610	0.03610	185.13	0.000	Significant
Speed*GFR	1	0.07562	0.07562	387.82	0.000	Significant
Error	5	0.00097	0.00019			
Lack-of-Fit	3	0.00077	0.00026	2.58	0.291	Not Significant
Pure Error	2	0.00020	0.00010			
Total	14	2.76769				

Model Summary R-Sq = 99.96%, R-Sq(adj) = 99.90%, R-sq(pred) 99.54%

The correlation coefficient R-square value for the experimental result obtained is 0.9996 (99.96%) for weld width (WW) which shows a good correlation the experimental results possess, whereas adjusted R- square values of hardness is 0.9990 (99.90%) also indicates good correlation.

#### 4.2.6.4. Model Validation

**Fig. 4.55** shows the relationship between the actual and predicted values of response for WW. This figure indicates that the developed model is adequate and predicted results are also in good agreement with measured data.

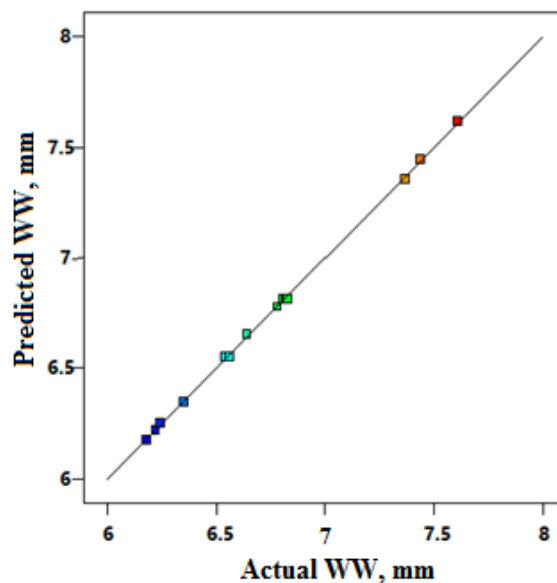


**Fig. 4.55:** Plot of predicted vs. actual results of WW

#### 4.2.6.5. Effect of the Parameters on WW

The contour plots for weld width (WW) are drawn and given in **Fig. 4.56 – Fig.4.58** by using **Eq. 4.8** with the help of RSM approach. The contour plots shown in **Fig. 4.56**, present the effect of input process parameters on WW for speed vs current, while gas flow rate is held constant at their respective lowest, medium and highest values. **Fig. 4.57** shows the influences of welding input variables: GFR vs. current on WW, while speed hold at their respective lowest, medium and highest values. **Fig. 4.58** represents the influence of GFR vs. speed on WW, while welding current hold at their respective lowest, medium and highest values.

From the contour plots of weld width (WW) as given in **Fig. 4.56 – Fig. 4.58**, it is found that direct and interaction effects of all welding parameters are most significant as all lines in the given plots are elliptical nature / curved / bend.

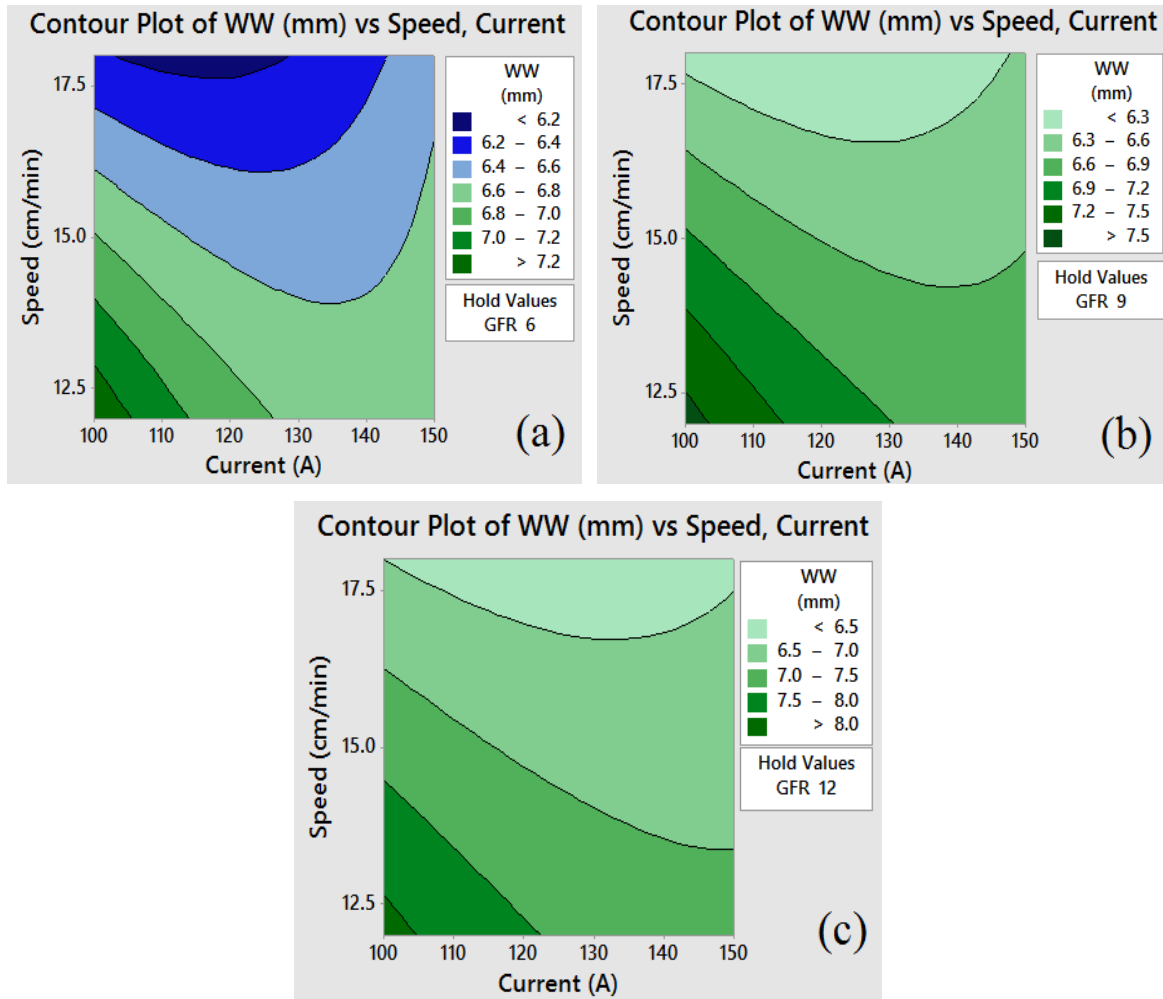


**Fig. 4.56:** Contour plots showing combined effects of speed and current on WW, while GFR hold at a) 6 l/min b) 9 l/min and c) 12 l/min

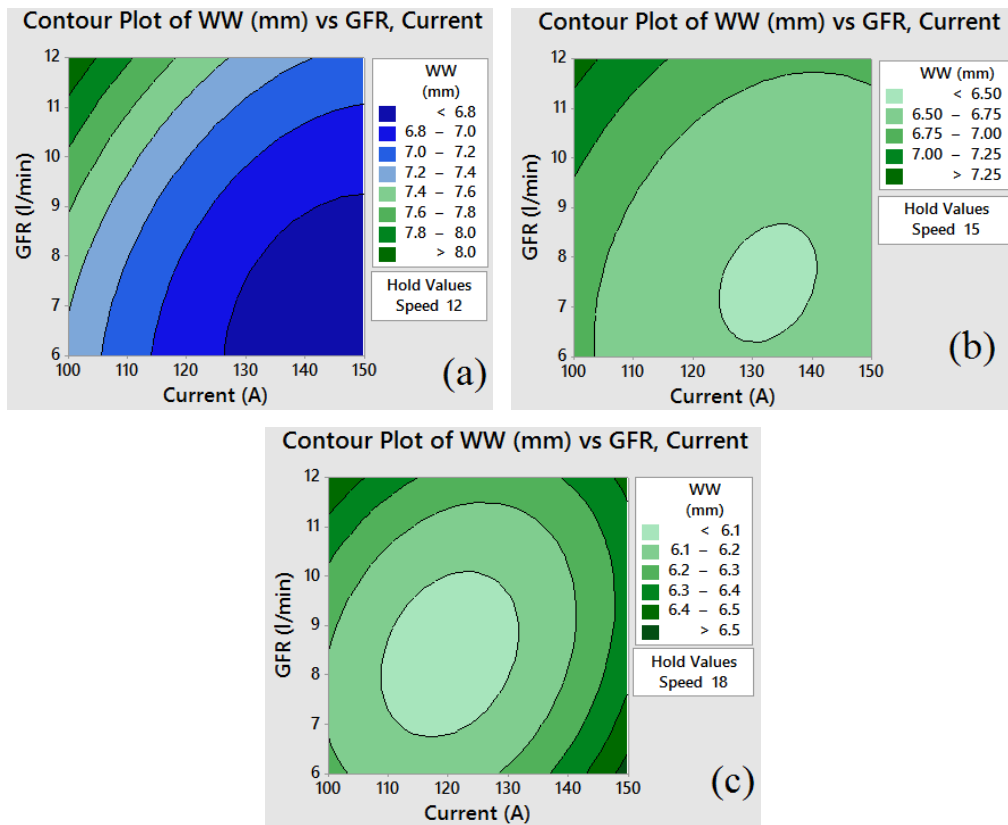


**Fig. 4.57:** Contour plots showing combined effects of GFR and current on WW, while speed hold at a) 12 cm/min b) 15 cm/min and c) 18 cm/min

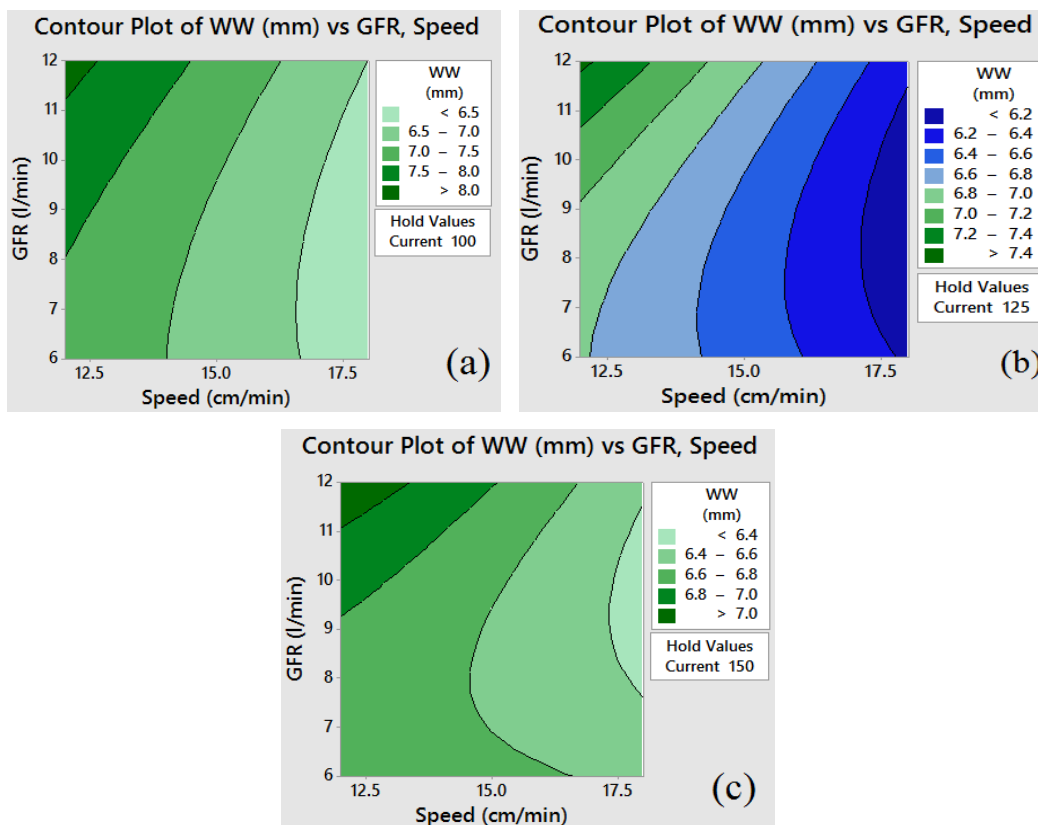


**Fig. 4.58:** Contour plots showing combined effects of GFR and speed on WW, while current hold at a) 100A b) 125A and c) 150A

#### 4.2.6.6. Optimization of WW by TLBO

The optimization of WW is carried out by using TLBO algorithm by using execution steps of TLBO as given in **section 4.2.1.6**. The obtained optimum welding combination is: current (A) = 120.20 A, speed (B) = 18 cm/min and gas flow rate (C) = 8.42 l/min and corresponding minimized weld width = 6.05 mm. The predicted welding condition and output response is also shown in **Table 4.12**.

#### 4.2.6.7. Optimization of WW by DFA

Details of DFA are given earlier and the optimization procedure for execution of DFA from optimization tool in MINITAB software is already given in **section 4.2.1.7**. Weld width needs to be minimized; therefore, **Eq. 2.22** is used in the present case of minimization of weld width. Obtained optimal condition(s) from optimization plot (**Fig. 4.59**) is: current (A) = 120.20 A, speed (B) = 18 cm/min and gas flow rate (C) = 8.42 l/min and corresponding WW = 6.05 mm, the same parametric condition is also given in **Table 4.12**.

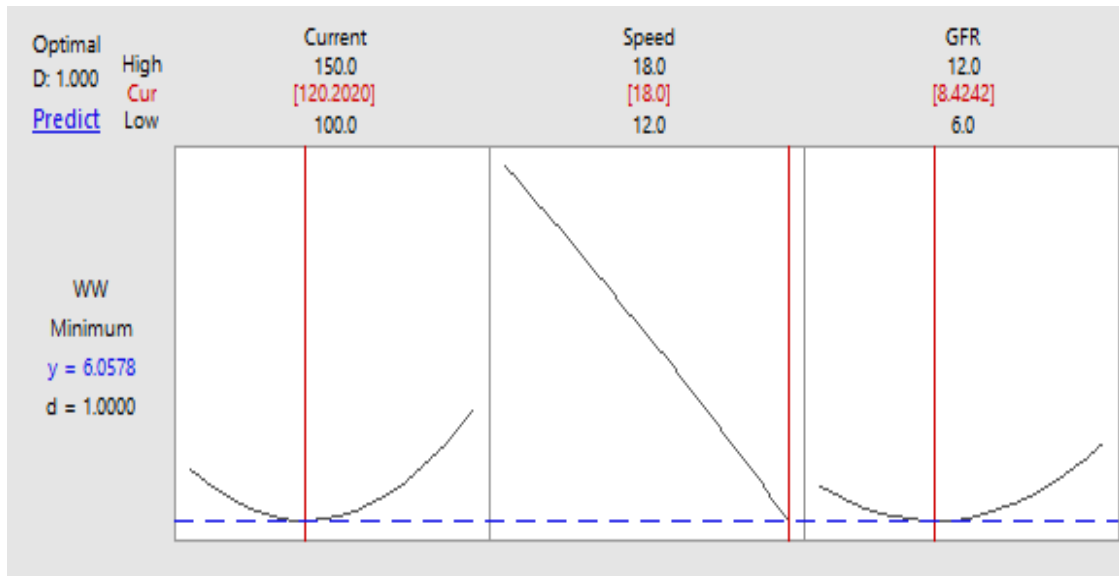


**Fig. 4.59:** Optimization plot for WW

#### 4.2.7. Comparative analysis between the optimum welding conditions obtained by TLBO and DFA

Comparative analysis is made between the predicted parametric conditions and corresponding response variables obtained by TLBO and DFA for UTS, PE, YS, IS, hardness and weld width. From the **Table 4.12**, it is found that obtained optimum welding conditions and corresponding responses values for all the weld quality responses are same for both the techniques i.e. TLBO and DFA. From the results as given in **Table 4.12**, it is stated that both the techniques used in the present work are efficient to optimize welding conditions for TIG welding of type 316L stainless steel materials.



**Table 4.12:** Obtained optimum TIG welding conditions for all responses by TLBO and DFA

Input parameters	UTS		PE		YS		IS		Hardness		WW	
	TLBO	DFA	TLBO	DFA	TLBO	DFA	TLBO	DFA	TLBO	DFA	TLBO	DFA
Welding current (A)	128.79	128.79	131.31	131.31	150	150	127.27	127.27	124.24	124.24	120.20	120.20
Welding speed (cm/min)	15.39	15.39	15.21	15.21	15.33	15.33	15.52	15.52	15.88	15.88	18	18
Gas flow rate (l/min)	8.42	8.42	8.91	8.91	8.97	8.97	8.85	8.85	8.91	8.91	8.42	8.42
Optimized response value	642.13 MPa	642.13 MPa	52.23	52.23	396.55 MPa	396.55 MPa	51.67 J	51.67 J	245.01 HV	245.01 HV	6.05 mm	6.05 mm

#### 4.2.8. Confirmatory tests

Confirmatory experiments are conducted to verify the optimum welding conditions as shown in **Table 4.12** obtained from the TLBO and DFA. From the results of confirmatory tests, it is found that optimal results are good agreement with the initial experimental runs (**Table 4.3**).

#### 4.3. Multi-objective optimization for TIG welding of austenite stainless steel

Good mechanical properties on welded joints of any welding operation are primary aim of industrialists. Mechanical properties are characterized by ultimate tensile strength (UTS), percentage elongation (PE), yield strength (YS), impact strength (IS), hardness (VHN) and weld width (WW) which demanded in many engineering and domestic applications. But, optimization of multiple objectives is not straight forward and much more complicated than of single performance characteristics. For that grey relational analysis has been used to convert multiple optimization problems into single objective optimization problem. To solve the multi-responses: UTS, PE, YS, IS, hardness and WW in the present work, Grey relational analysis is then coupled with statistical technique analysis of variance to identify the significant welding variables on responses i.e. grey relational grade. RSM technique has been employed to develop mathematical relational between grey relational grade and input welding parameters. Then obtained mathematical model of grey relational grade has been solved by using TLBO and desirability function approach (DFA).

##### 4.3.1. Grey relational analysis

Grey relational analysis has been conducted on experimental data to translate multi-responses into single objective problem by following the steps mentioned earlier. In the present work, UTS, PE, YS, IS, hardness must be maximized to enhance the mechanical properties and weld width (WW) needs to be minimized to reduce the material requirement. As mentioned above, in GRA, first step is to preprocess the data. Here, **Eq. 2.25** is used to preprocess the data of UTS, PE, YS, IS, hardness. And **Eq. 2.24** is used to process the experimental data of weld width. The pre-processing data is given in **Table 4.13**. **Eq.2.26**

has been used to calculate the grey relational coefficient. The  $\Delta_0i$  values and Grey relational values are given in **Tables 4.14** and **Table 4.15** respectively. Finally, **Eq. 2.27** has been used to determine the grey relational grade by averaging the grey relational coefficients of all the responses. Grey relational ordering has been made to grey relational grade values. The GRG values and ordering are given in **Table 4.15**.

**Table 4.13:** Grey relational generations

S. No	Grey relational generation					
	UTS	PE	YS	IS	Hardness	WW
1	0.508141222	0.156800723	0.402093	0.432432	0.2667	0
2	0.577301306	0.68865793	0.970352	0.297297	0.0667	0.5804
3	0.449298726	0.533664709	0.926267	0.378378	0.4000	0.9720
4	0.802192488	0.516945323	1	0.648649	0.4667	0.8811
5	0.655328067	0.520560325	0.636082	0.405405	0.4000	0.5594
6	0.520715783	0.450971532	0.867261	0.27027	0	0.6783
7	0	0	0.334367	0	0	0.1678
8	0.436562953	0.644374153	0.925298	0.351351	0.2000	0.5524
9	0.701918427	0.465883416	0	0.459459	0.2667	0.5455
10	0.574399484	0.433800271	0.779963	0.324324	0.4667	1
11	0.190391746	0.159060099	0.251042	0.081081	0.0667	0.1189
12	0.568595841	0.540894713	0.173433	0.486486	0.5333	0.9580
13	0.948089634	0.96836873	0.676679	0.945946	0.9333	0.7413
14	1	1	0.928205	1	1	0.7483
15	0.952119942	0.95210122	0.732778	0.972973	1	0.7343

### 4.3.2. Factor analysis, modeling and optimization of grey relational grade

#### 4.3.2.1. Main and interaction effects for GRG

The main and interaction plots are drawn using Grey relational grade (GRG) as shown in **Table 4.15** utilizing the application of MINITAB 17 software to analyze the factor effects on GRG. The main and interaction plots are given in **Fig. 4.60** and **Fig.4.61** respectively. Evolution of main and interaction plots are made as per procedure given in **section 4.2.1.1**. From the main effect plots of GRG (**Fig. 4.60**), it is found that GRG is increasing and then decreasing with increase of all welding parameters. From the **Fig. 4.60**, it is found by studying the differences between the minimum and maximum of each factor that speed is most influential factor for GRG, next is current and followed by gas flow rate.

The interaction effects of process parameters vs. GRG illustrated in **Fig. 4.61**. The non-parallelism of the lines in each case and intersecting lines indicates that interaction effects of process parameters are most significant for GRG as found in **Fig. 4.61**.

**Table 4.14:** Values of  $\Delta 0i$ 

S. No	$\Delta 0i$ values					
	UTS	PE	YS	IS	Hardness	WW
1	0.491859	0.843199	0.597907	0.567568	0.7333	1
2	0.422699	0.311342	0.029648	0.702703	0.9333	0.4196
3	0.550701	0.466335	0.073733	0.621622	0.6000	0.0280
4	0.197808	0.483055	0	0.351351	0.5333	0.1189
5	0.344672	0.47944	0.363918	0.594595	0.6000	0.4406
6	0.479284	0.549028	0.132739	0.72973	1	0.3217
7	1	1	0.665633	1	1.0000	0.8322
8	0.563437	0.355626	0.074702	0.648649	0.8000	0.4476
9	0.298082	0.534117	1	0.540541	0.7333	0.4545
10	0.425601	0.5662	0.220037	0.675676	0.5333	0
11	0.809608	0.84094	0.748958	0.918919	0.9333	0.8811
12	0.431404	0.459105	0.826567	0.513514	0.4667	0.0420
13	0.05191	0.031631	0.323321	0.054054	0.0667	0.2587
14	0	0	0.071795	0	0.0000	0.2517
15	0.04788	0.047899	0.267222	0.027027	0	0.2657

**Table 4.15:** Grey relational coefficients, grade and ordering

S. No	Grey relational coefficient						GRG	Ordering
	UTS	PE	YS	IS	Hardness	WW		
1	0.50410	0.37225	0.45541	0.46835	0.40541	0.33333	0.42314	13
2	0.54189	0.61626	0.94402	0.4157	0.34884	0.54373	0.56841	7
3	0.47587	0.51742	0.87149	0.44578	0.45455	0.9470	0.61869	5
4	0.7165	0.50862	1	0.58730	0.48387	0.8079	0.68404	4
5	0.59195	0.51050	0.57876	0.45680	0.45455	0.53160	0.52069	11
6	0.51058	0.47663	0.79022	0.40659	0.33333	0.60851	0.52098	10
7	0.33333	0.33333	0.42895	0.33333	0.33333	0.37533	0.35627	15
8	0.47017	0.58437	0.87002	0.43529	0.38462	0.52768	0.54536	9
9	0.62650	0.48350	0.33333	0.48052	0.40541	0.5238	0.47551	12
10	0.5402	0.46896	0.69441	0.42529	0.48387	1	0.60212	6
11	0.38179	0.37287	0.40033	0.35238	0.34884	0.36203	0.36971	14
12	0.53682	0.52132	0.37691	0.49333	0.51724	0.92258	0.56137	8
13	0.90594	0.94050	0.60730	0.90244	0.88235	0.65899	0.81625	3
14	1	1	0.87444	1	1	0.66512	0.92326	1
15	0.91261	0.91258	0.65170	0.94872	1	0.65297	0.84643	2

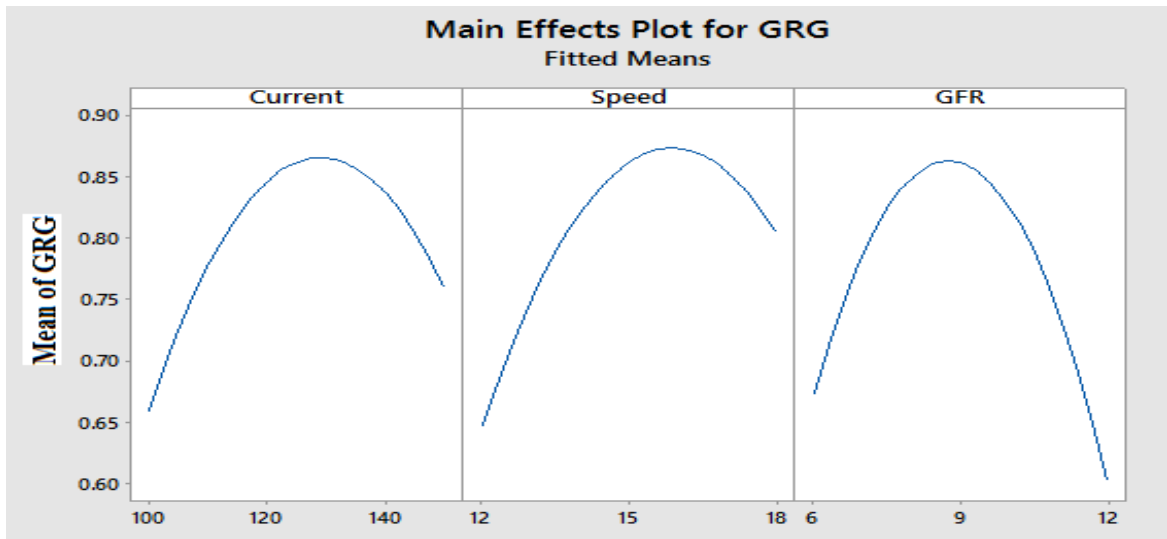


**Fig. 4.60:** Main effect plots for GRG

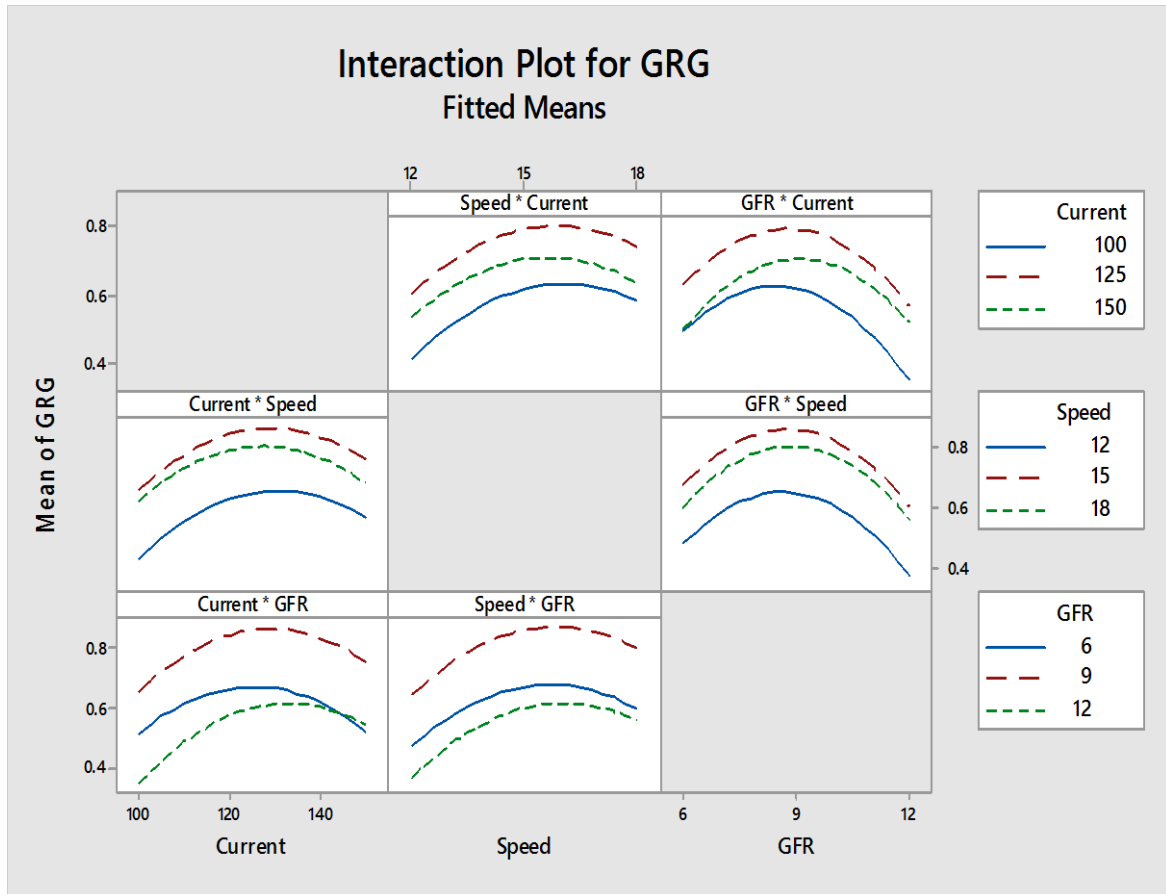


**Fig. 4.61:** Interaction effect plots for GRG

#### 4.3.3.2. Mathematical modeling for GRG

RSM from MINITAB 17 software is applied and mathematical model for grey relational grade. The procedure for developing mathematical relation between input parameters and output response is already discussed in **section 4.2.1.2**. The same procedure has been followed for developing mathematical model(s) for GRG and final mathematical model is given below.

$$Y_{GRG} = - 8.446 + 0.06128 \text{ Current} + 0.4967 \text{ Speed} + 0.3298 \text{ GFR} \\ - 0.000244 \text{ Current*Current} - 0.01511 \text{ Speed*Speed} - 0.02486 \text{ GFR*GFR} \\ - 0.000266 \text{ Current*Speed} + 0.000629 \text{ Current*GFR} + 0.00181 \text{ Speed*GFR} \quad (4.9)$$

#### 4.3.3.3. Analysis of variance for GRG

ANOVA is made for GRG and given in **Table 4.16**. The hypothesis is confirmed from ANOVA table (**Table 4.16**) of grey relational grade (GRG), as more than one term in the table is zero.

It can be concluded from **Table 4.16** that square combination of current\*current (A\*A) and gas flow rate\* gas flow rate (C\*C) are most significant on all the welding responses as its P value is zero. The individual effects of current (A), speed (B) and gas flow rate (C), and square combination of speed\*speed (B\*B), and interaction effects of current – gas flow rate (A\*C) are significant for all welding characteristics as their P values are less than 0.05. Interactions among current-speed and speed-gas flow rate are not significant at 95% confidence level, as found from the **Table 4.16**.

The correlation coefficient R-square value for the experimental result obtained is 0.9844 (98.44%) for GRG shows a good correlation the experimental results possess, whereas adjusted R- square values of GRG is 0.9563 (95.63%) which also reveals good correlation.

**Table 4.16:** Analysis of Variance for GRG

Source	DF	Adj SS	Adj MS	F-Value	P-Value	Remarks
<b>Model</b>	<b>9</b>	<b>0.388599</b>	<b>0.043178</b>	<b>35.07</b>	<b>0.001</b>	<b>Significant</b>
<b>Linear</b>	<b>3</b>	<b>0.079791</b>	<b>0.026597</b>	<b>21.60</b>	<b>0.003</b>	<b>Significant</b>
Current	1	0.020000	0.020000	16.24	0.010	Significant
Speed	1	0.049524	0.049524	40.23	0.001	Significant
GFR	1	0.010267	0.010267	8.34	0.034	Significant
<b>Square</b>	<b>3</b>	<b>0.297242</b>	<b>0.099081</b>	<b>80.48</b>	<b>0.000</b>	<b>Significant</b>
Current*Current	1	0.085737	0.085737	69.64	0.000	Significant
Speed*Speed	1	0.068321	0.068321	55.49	0.001	Significant
GFR*GFR	1	0.184894	0.184894	150.18	0.000	Significant
<b>2-Way Interaction</b>	<b>3</b>	<b>0.011566</b>	<b>0.003855</b>	<b>3.13</b>	<b>0.125</b>	<b>Not Significant</b>
Current*Speed	1	0.001597	0.001597	1.30	0.306	Not Significant
Current*GFR	1	0.008911	0.008911	7.24	0.043	Significant
Speed*GFR	1	0.001058	0.001058	0.86	0.396	Not Significant
<b>Error</b>	<b>5</b>	<b>0.006156</b>	<b>0.001231</b>			
Lack-of-Fit	3	0.000068	0.000023	0.01	0.999	Not Significant
Pure Error	2	0.006088	0.003044			
<b>Total</b>	<b>14</b>	<b>0.394755</b>				

Model Summary: R-Sq = 98.44%, R-Sq(adj) = 95.63%, R-sq(pred) = 96.25%

#### 4.3.3.4. Model Validation

Fig. 4.62 shows the relationship between the actual and predicted values of GRG. This figure indicates that the developed model is adequate.

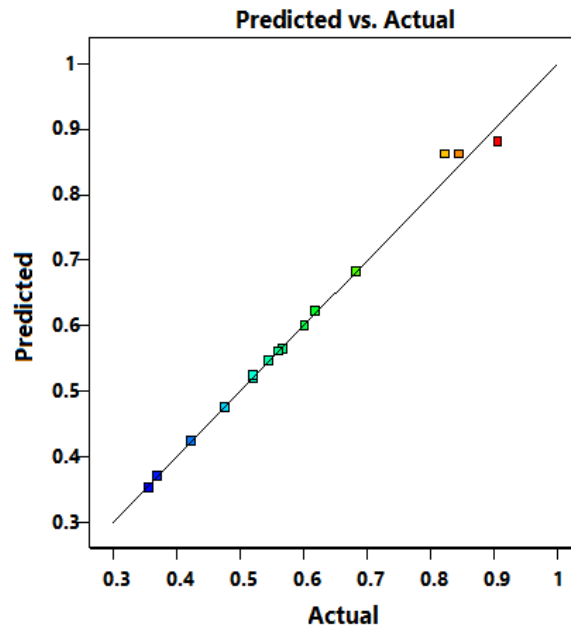


Fig. 4.62: predicted vs. actual plot of GRG

#### 4.3.3.5. Effect of the Parameters on GRG

The contour plots for GRG are made and given in Fig. 4.63 – Fig. 4.65 by using Eq. 4.9 with the help of RSM approach. The contour plots shown in Fig. 4.63, present the effect of input process parameters on GRG for speed vs current, while gas flow rate is held constant at their respective lowest, medium and highest values. Fig. 4.64 shows the influences of welding input variables: GFR vs. current on GRG, while speed hold at their respective lowest, medium and highest values. Fig. 4.65 represents the influence of GFR vs. speed on GRG, while welding current hold at their respective lowest, medium and highest values.

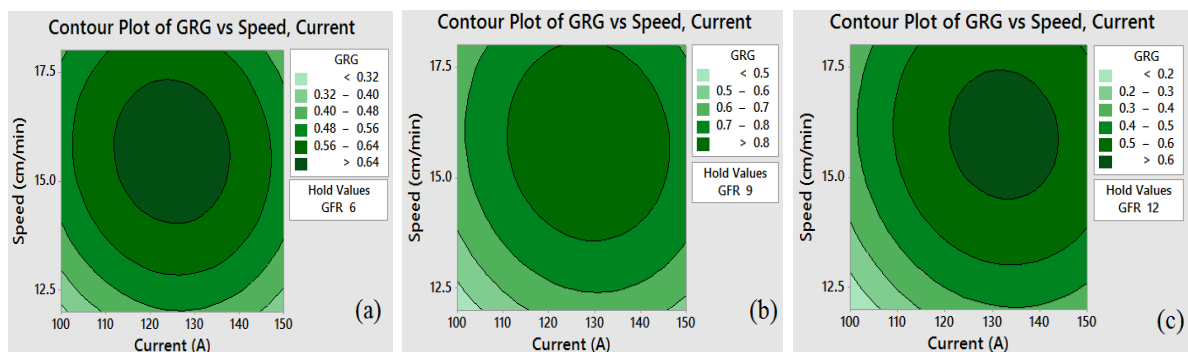
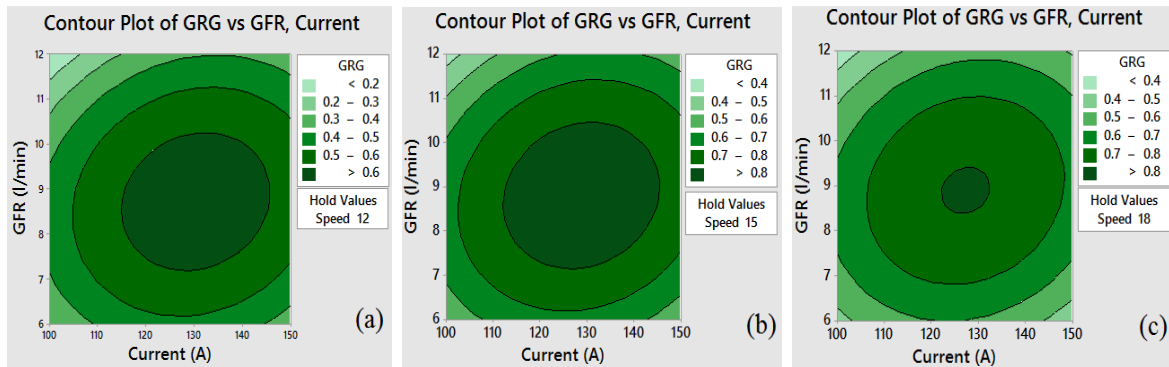
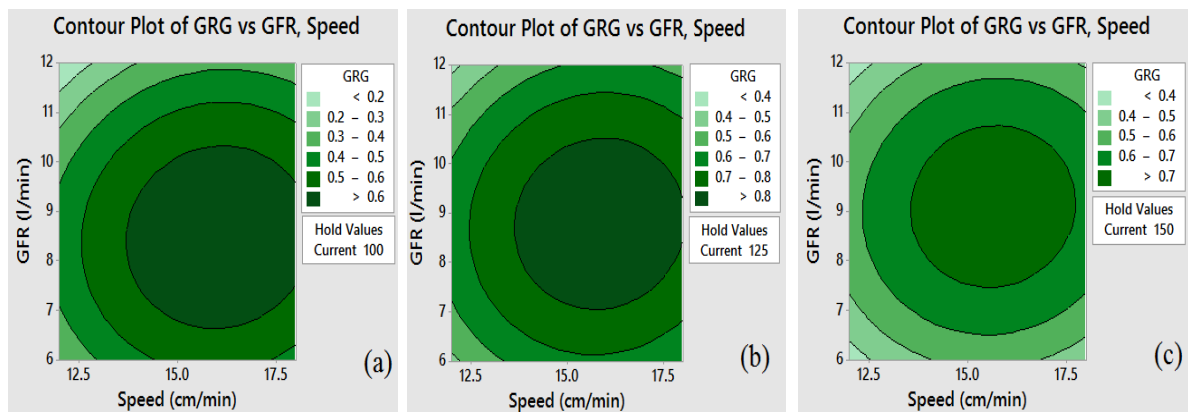


Fig. 4.63: Contour plots showing combined effects of speed and current on GRG, while GFR hold at a) 6 l/min b) 9 l/min and c) 12 l/min

From the contour plots of GRG as given in **Fig. 4.63 – Fig. 4.65**, it is found that direct and interaction effects of all welding parameters are most significant as all lines in the given plots are elliptical in nature.



**Fig. 4.64:** Contour plots showing combined effects of GFR and current on GRG, while speed hold at a) 12 cm/min b) 15 cm/min and c) 18 cm/min



**Fig. 4.65:** Contour plots showing combined effects of GFR and speed on GRG, while current hold at a) 100 A b) 125 A and c) 150 A

#### 4.3.4. Optimization by TLBO

For TIG welding of austenite stainless steel material, optimization by TLBO is carried out using the procedural steps mentioned in **section 4.2.1.6**. The results are shown in **Table 4.17**.

#### 4.3.5. Optimization by DFA

Details of DFA are given earlier and the optimization procedure for execution of DFA from optimization tool in MINITAB software is already given in **section 4.2.1.7**. The same procedure has been followed in the present case to maximize GRG. Optimal conditions are shown in the optimization plot (**Fig. 4.66**). Obtained optimal conditions for GRG is shown in **Table 4.17**.

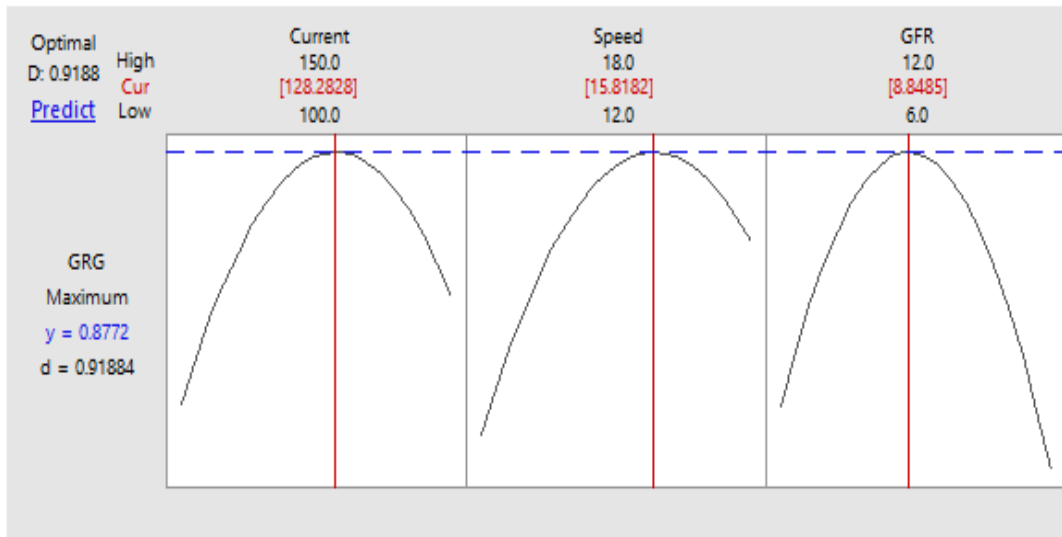


**Fig. 4.66:** Optimization plot for GRG

**Table 4.17:** optimized values of GRG by TLBO and DFA

Input parameters	Predicted welding conditions and GRG	
	By TLBO	By DFA
Welding current (A)	128.43	128.28
Welding speed (cm/min)	15.83	15.82
Gas flow rate (l/min)	8.83	8.85
Maximized GRG	0.88	0.88

The optimized parametric setting values are substituted in mathematical models of UTS (Eq.4.3), PE (Eq. 4.4), YS (Eq.4.5), IS (Eq. 4.6), hardness (Eq. 4.7) and WW (Eq. 4.8) to check the optimized response values and given in Table 4.18. From the Table 4.18, it is found that all response values obtained from multi-objective optimum parametric condition are almost equal to optimum response values obtained from the single objective optimum parametric combination for UTS, PE, IS, hardness and weld width except YS.

**Table 4.18:** Multi-objective optimization results

Input parameters	UTS (MPa)	PE	YS (MPa)	IS (J)	Hardness (HV)	WW (mm)
Welding Current = 128.43 A	641.76	51.98	361.3	51.61	244.82	6.40
Welding Speed = 15.83cm/min						
Gas flow rate = 8.83 (l/min)						

#### 4.3.6. Confirmatory test

The results of optimization obtained have been validated by performing confirmatory experiments. Table 4.19 represents the average results of three confirmatory tests that are conducted at optimum conditions. It is noticed from table that the percentage error between



the predicted and experimental results is very small. This indicates that the optimized TIG welding process parameters can be considered to obtain desired quality of weldment of 316L stainless steel.

**Table 4.19:** Optimization validation test results

Optimum Input parameters	Comparison	Output responses					
		UTS (MPa)	PE	YS (MPa)	IS (J)	Hardness (HV)	WW (mm)
A = 128.43A	Actual	645.56	52.12	368.20	52.56	247.0	6.45
B= 15.83cm/min	Predicted	641.76	51.98	361.30	51.61	244.82	6.40
C= 8.83l/min	Error %	0.59	0.27	1.91	1.84	0.89	0.78

#### 4.4. Fatigue test of TIG welded joint at optimum parametric condition

Fatigue has become progressively more relevant in developed technology in the areas such as automobile, aircraft, compressor, pump, turbine etc. Many of the components used in these areas are subjected to repeated load and temperature variations including vibration. Today it is often stated that fatigue accounts for at least 90 percent of all service failures due to which occurring mechanical causes. So taking this into account, mechanical properties of the welded joint has been evaluated in the study by fatigue test of the samples welded under obtained optimized parametric condition. The largest number of weld failures is attributed to either the high-cycle fatigue caused by flow induced vibration or due to fatigue in general. In order to understand the high cycle fatigue behaviour of 316L austenitic stainless steel and its welded joint, the fatigue limits and the fracture modes have been investigated at room temperature.

A set of new TIG welded joints in square butt joint configuration has been prepared at the obtained optimized parametric condition for further investigation of the quality of the obtained TIG welded joint in terms of high cycle fatigue behaviour of the welded joint and compared with base metal. The average tensile properties of TIG welded joints that are made using obtained optimized parametric condition and base metal are listed in **Table 4.20**. Standard sub size fatigue test specimens have been prepared in accordance with ASTM E466 as shown in **Fig. 2.15**. Before fatigue testing, all specimens have been polished as per the recommendations of ASTM E466. Load-controlled uniaxial fatigue tests have been performed using a Testronic 100KN RUMUL resonant testing machine at room temperature, at stress ratio (R) of 0.1 and at a frequency of 80Hz. The fatigue limit has been determined at maximum stresses in the range of 100% to 40% of yield stress. Fatigue tests have been stopped when specimens are fractured or the fatigue cycles reached  $10^8$  cycles.

**Table 4.20:** Tensile properties of base metal and its welded joint

Sample	Yield stress (MPa)	UTS (MPa)	Elongation (%)
Base metal	328.01	608.88	51.85
TIG welded joint	368.20	645.56	52.12

The results of fatigue test of the welded joint and base metal are recorded and shown in **Table 4.21** and **Table 4.22** respectively in terms of number of cycles to failure. Fatigue test has been started with 100% of yield strength of both welded joint and base metal and thereafter it has been reduced to 90%, 80%, 70% and so on till the fatigue limit is determined. S-N curves for welded joint and base metal have also been plotted from the fatigue test results in terms of maximum stress versus number of cycles to failure, to examine the significant difference of fatigue life at high stress compared to lower stress as shown in **Fig. 4.67**. Best fit curves are also plotted for data analysis.

**Table 4.21:** Experimental results of fatigue test of welded joint

Stress ratio, R	Maximum Stress (MPa)	Minimum Stress (MPa)	Stress Amplitude (MPa)	No of cycles to failure	Remarks
0.1	368.20	36.82	165.69	66880	Failed
	331.38	33.14	149.12	218880	Failed
	294.56	29.46	132.55	816893	Failed
	257.74	25.77	115.99	1290215	Failed
	220.92	22.09	99.42	2808614	Failed
	202.51	20.25	91.13	5260789	Failed
	184.10	18.41	82.85	8506472	Failed
	173.05	17.31	77.87	10005735	Didn't fail
	173.05	17.31	77.87	100000233	Didn't fail

From **Fig. 4.67**, it is observed that the number of cycles to failure or fatigue life increases linearly with decrease of the maximum stress in both welded joint and base metal. It is also observed that the welded joint exhibit slightly higher fatigue limits than the base metal specimens. It is may be due to materials strength as welded joint has higher material strength than base metal. Therefore it may be concluded that the higher the materials strength, the higher the fatigue limit is observed. In the S-N curve, the arrow represents the specimens beyond  $10^7$  cycles do not break even after applied many specimen throughout the tests. From the observation of the S-N curves the fatigue limit is successfully characterized for TIG welded joint, as well as base metal in this investigation and it is found as 173.05MPa for welded joint and 157.44MPa for base metal. Welded joint depicts almost 10% higher fatigue limit compare to base metal. Therefore, the obtained TIG welded joint at optimized parametric condition has passed high cycle test successfully and quality of the welded joint is also improved compared to base metal.

**Table 4.22:** Experimental results of fatigue test of base metal

Stress ratio, R	Maximum Stress (MPa)	Minimum Stress (MPa)	Stress Amplitude (MPa)	No of cycles to failure	Remarks
0.1	328.0	32.20	147.9	48968	Failed
	295.2	29.52	132.84	155896	Failed
	262.4	26.24	118.08	495875	Failed
	229.6	22.96	103.32	1100789	Failed
	196.8	19.68	88.56	2454870	Failed
	180.40	18.04	81.18	5114580	Failed
	164.00	16.40	73.8	7501052	Failed
	157.44	15.74	70.85	10005240	Didn't fail
	157.44	15.74	70.85	100002032	Didn't fail

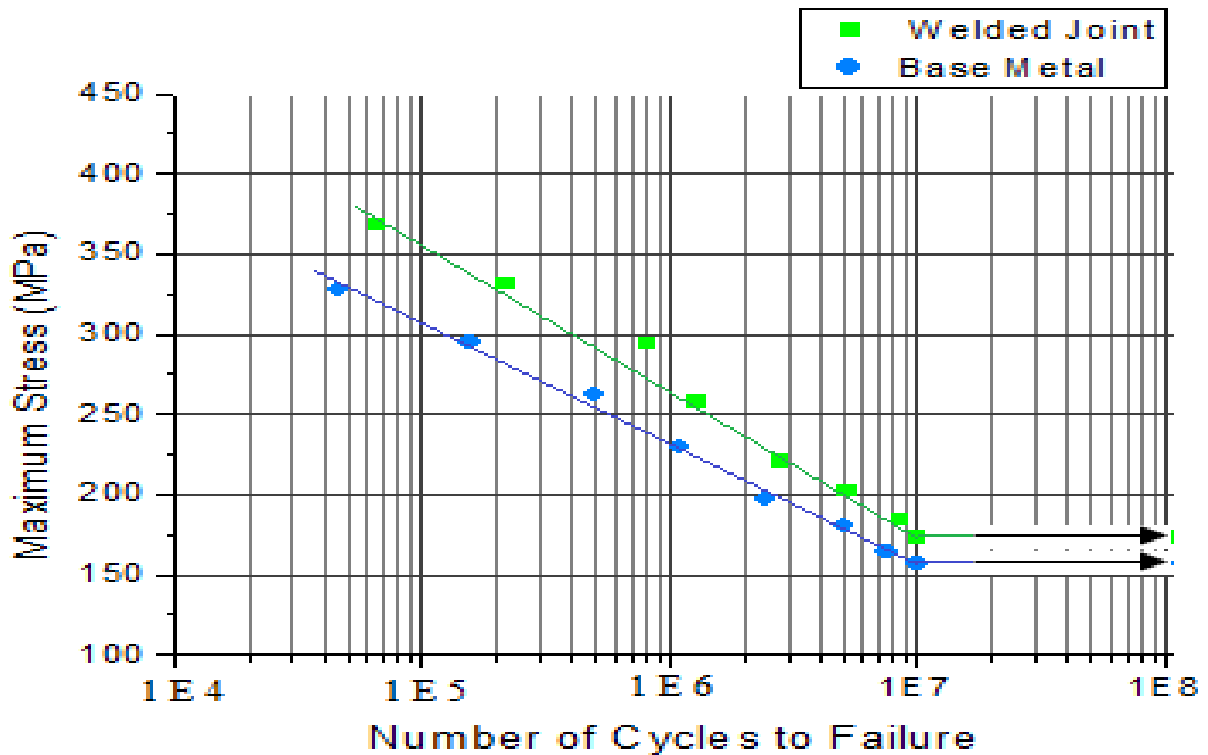


**Fig. 4.67:** S-N curve of welded joint and base metal

The fatigue fracture surfaces are examined by scanning electron microscopy (SEM) to characterize the fracture mode, crack initiation site and the evolution of the fatigue striation structure. **Fig. 4.68** shows the fracture surfaces of TIG welded joint at different maximum applied stress levels. It is observed that the region of fatigue damaged progressively diminished when the maximum applied stress is consecutively increased under constant stress ratio ( $R = 0.1$ ). Similar result has been reported by Huang et al [124]. It may be due to the ligament area could sustain the lower maximum applied stress during the fatigue crack propagation. Thus a fatigue specimen under a lower applied maximum stress led to a larger fatigue damage region and smaller final rupture plastic region. It is also observed that at higher applied stress levels, the specimens exhibit lower fatigue life.

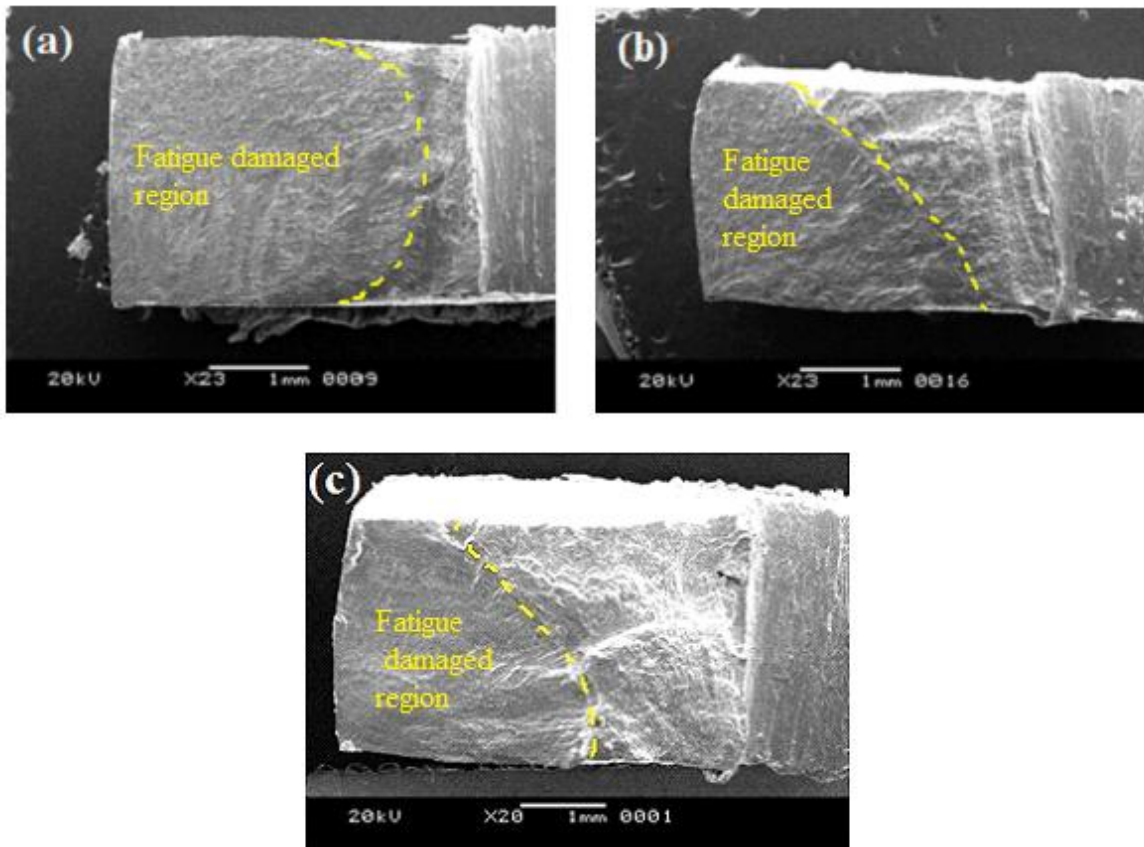


**Fig. 4.68:** SEM fractographs showing the fatigue damaged region at different maximum applied stress (a) at 184.1MPa (b) at 257.74MPa (c) at 368.2MPa.

**Fig. 4.69** represents SEM fractographs of base metal of the specimen failed at  $7.5 \times 10^6$  cycles loaded at 164MPa. **Fig. 4.70** to **Fig. 4.72** illustrates fracture surfaces of TIG welded joint at different maximum applied stress levels. Base metal specimen reveals a clean and not much rough fracture surface, whereas the welded specimens exhibited rough and wavy surfaces. The cracks are found initiating from the surface of welded specimens irrespective of the stress levels and no of cycles before fatigue failure. No fish-eye or subsurface crack initiation is identified. The fracture surfaces are found to be different for the different specimens failed below and above  $10^6$  cycles.

In the process of fatigue fracture three distinct characteristics including crack initiation, crack propagation and instantaneous rupture can be seen clearly. The fatigue crack propagation could be divided into two phases: fatigue crack growth with the characteristic of flat fracture surface and fatigue crack propagated rapidly causing necking and Herringbone characteristic of fracture surface and the fracture surface is very coarse. Furthermore, the fatigue crack could be observed initiating from the side face of the surface. Fatigue striations can be seen clearly. **Fig. 4.70** shows the origin of fatigue cracks and fracture surfaces of the specimen failed at  $8.51 \times 10^6$  cycles loaded at 184.1MPa. A few radial lines are observed around the crack initiation region which may be due to the resistance in crack propagation. Secondary cracks and pores in the subsurface regions as shown in **Fig. 4.70** (c).

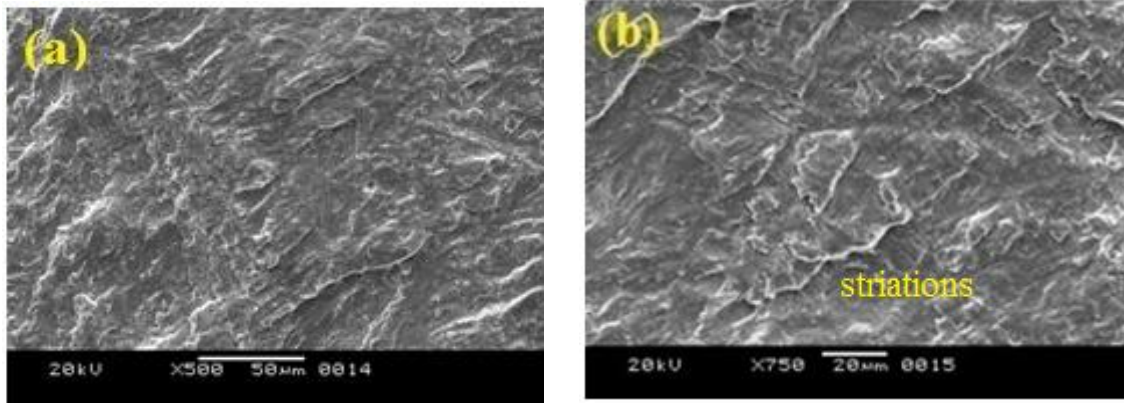


**Fig. 4.69:** Fracture surface morphology of base metal at 164 MPa (a) crack initiation (b) crack propagation

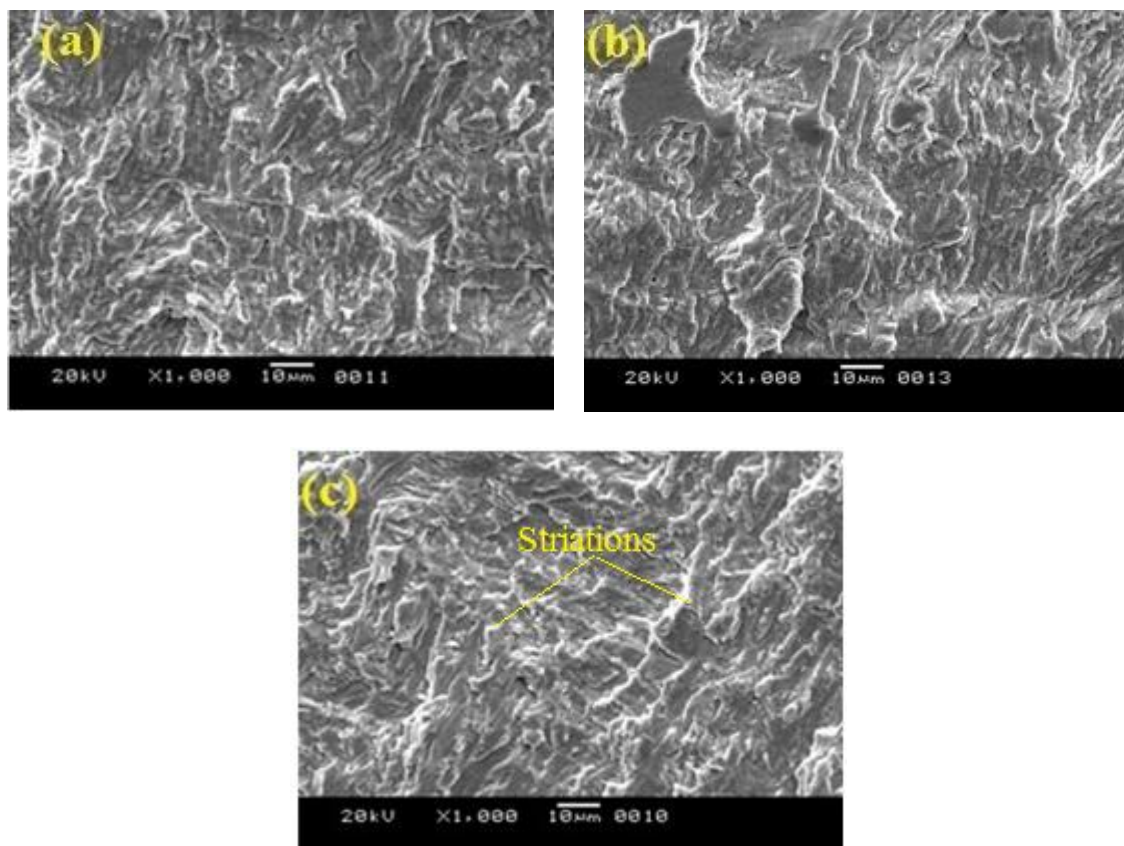
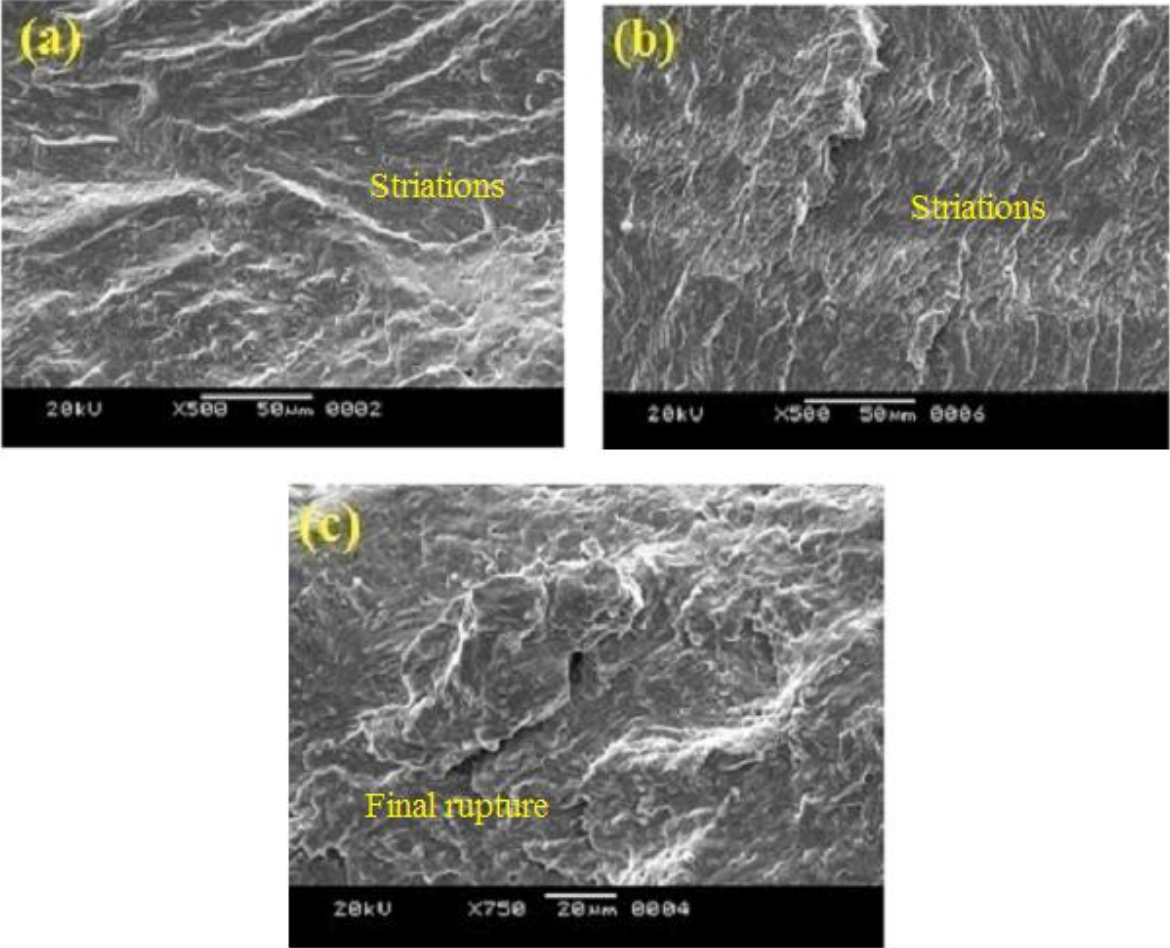


**Fig. 4.70:** Fracture surface morphology of welded joint at 184.1MPa (a) crack initiation (b) crack propagation and (c) rapid crack growth before rupture

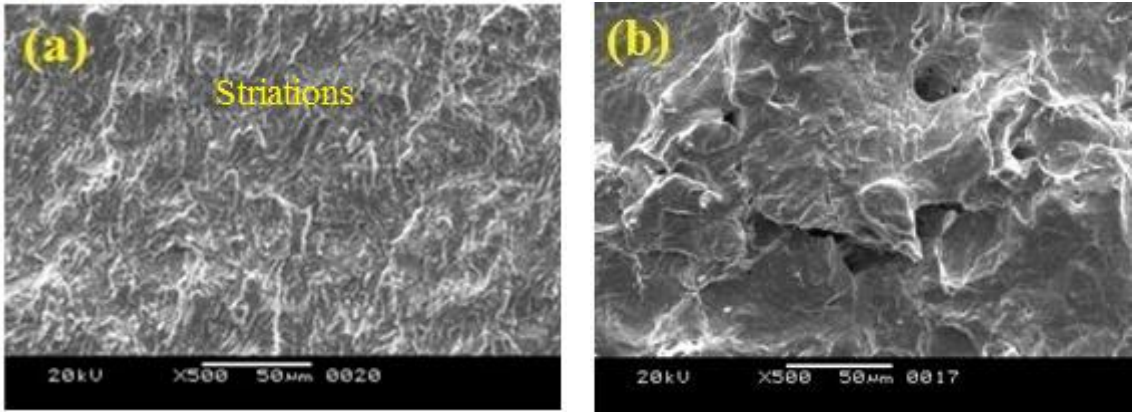
**Fig. 4.71:** shows the fracture surfaces of the welded joint failed at 257.74MPa and  $1.29 \times 10^6$  cycles. Significant disparity is observed in the surface morphology, like size of the facets, fatigue striation structure etc. in the welded specimens failed at different maximum stress levels. **Fig. 4.71(b)** shows fractography of crack propagation area at high magnification and many facets with different size can be found, shown in **Fig. 4.71(c)** which exhibits intergranular crack feature. As seen from the **Fig. 4.69**, the elongated facets are visible for the base metal specimen, when comparing fatigue fracture surfaces between the base metal and the TIG welded specimens. It is obvious that considerably fine facets are dominant in

the welded specimen compared to the base metal specimen, which would result in high fatigue resistance in the welded specimen.

**Fig. 4.72** shows the fractography of crack initiation, crack propagation and rupture areas at high magnification at 368.2MPa and 66880 cycles. It can be seen the cracks initiated at the inclusions of the surfaces of the specimens. Fatigue striations can be seen at the crack propagation area at high magnification as shown in **Fig. 4.72(b)** and **Fig. 4.72(c)**.



**Fig. 4.71:** Fracture surface morphology of welded joint at 257.74MPa (a) crack initiation (b) crack propagation and (c) rapid crack growth before rupture



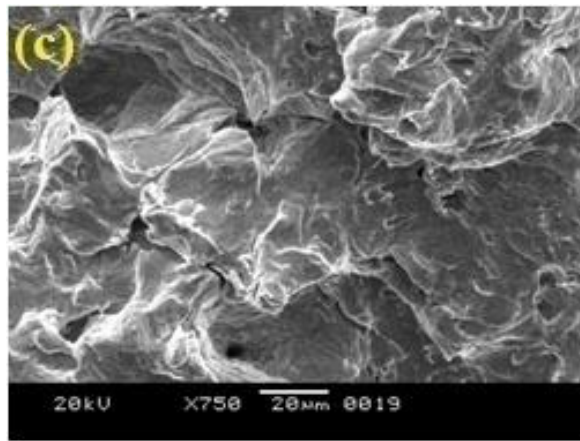


**Fig. 4.72:** Fracture surface morphology of welded joint at 368.2MP (a) crack initiation area (b) & (c) fatigue striation.

## **5. CONCLUSIONS AND FUTURE SCOPE OF WORK**

### **5.1. Conclusions**

In the present work, butt welding of austenitic stainless steel AISI 316L has been prepared by tungsten inert gas (TIG) welding, at varied levels of welding current, welding speed and gas flow rate. The effect of TIG welding input parameters on the quality of the welded joint is investigated. Based on the experimental results, their interpretations, discussion, modeling and analyses, the following points can be concluded:

#### **For destructive and non-destructive test of TIG welded samples**

- i. Some defects like porosity, little under cut at the end, large reinforcement height, lack of penetration etc. are observed in the visual inspection in few samples. However, under certain parametric conditions, almost no defects are found in a few samples.
- ii. From the results of X-ray radiography test, it is observed that almost all the samples pass through X-ray radiography test with no significant defect remarks.
- iii. Fully austenitic structure along with few annealing twins is found in the microstructure of the base metal. The weld solidified in FA (ferritic-austenitic) mode of solidification. Thus, higher  $\delta$ -ferrite content is present in the weld metals.
- iv. The average micro hardness value of all the weld joints is found to be of remarkably higher as compare to those of HAZ zone and base metal irrespective of input process parameters. Higher hardness of the weld metals are the resultant of grain refinement and  $\delta$ -ferrite formation in the weld structure.
- v. It is also found that almost all the welded joints exhibit higher tensile strength than that of the base metal. Both notched and un-notched tensile test exhibit almost similar types of results.
- vi. The NSR is found to be greater than unity for all the welded joints and this indicates that the TIG welded joints are insensitive to notches or geometric discontinuities.
- vii. The welded joint having very fine grain structure along with higher hardness values provides higher tensile properties.
- viii. The surface morphology of tensile specimen (fractured) of welded joints indicates that fracturing mechanism is ductile. A large number of very fine and shallow dimples are observed in SEM fractograph of the joint which shows maximum tensile strength, whereas elongated dimples with voids are found in the joint having minimum strength.
- ix. The results of charpy impact test indicate that for most of the samples, impact energy is satisfactory. Under certain parametric conditions of welding current, welding



speed and gas flow rate, impact strength are remarkably good as compared to base metal.

- x. The results of bending test indicate that almost no cracks or failure have been observed visually in the bended area of all the welded samples.

#### **For UTS for TIG welding of 316L stainless steel**

- i. From the main effect plots of UTS, it is found that response most significantly affected by the gas flow rate parameter compare to other parameters.
- ii. Interaction plots also reveals that interaction effects of process parameter are most significant for UTS.
- iii. By using the welding parameters, the second order response surface model for the UTS is developed by RSM application.
- iv. Contour plots for UTS are drawn from the developed mathematical models. These plots clearly show the interaction effect of input parameters on UTS. The welding conditions satisfying constraints for industrial application can be selected very easily from the contour plot of the developed response models.
- v. From the results of analysis of variance, it is noted that all the process parameters and their squared and interactions, are most significant for UTS.
- vi. Optimum welding condition obtained by TLBO and DFA for maximizing the UTS is: current = 128.79 A, speed = 15.39 cm/min and gas flow rate = 8.42 l/min and corresponding UTS = 642.13Mpa.
- vii. The accuracy optimal result is obtained by TLBO and DFA is same
- viii. Confirmatory test is conducted at optimal condition and found improved UTS as compared to initial experiments.

#### **For PE for TIG welding of 316L stainless steel**

- i. It is found from the main effect plots of PE that welding current is the most important welding parameter which affecting the percentage elongation and it is followed by welding speed and gas flow rate.
- ii. From interaction plots, it is noted that interaction effects of welding input parameters are most significant for PE.
- iii. Mathematical modeling is developed to correlate process parameters with PE by RSM approach
- iv. Contour plots for PE are drawn from the developed mathematical models. These plots are also show the interaction effect of input parameters on PE.
- v. Results of analysis of variance show that all the process parameters directly, its squared combinations and interactions are most significant for PE.
- vi. Optimum PE = 52.23% is obtained by TLBO and DFA at parametric condition of: current = 131.31 A, speed = 15.21 cm/min and gas flow rate = 8.91 l/min

- vii. The accuracy optimal result is obtained by TLBO and DFA is same.
- viii. Confirmatory test has been done optimal condition and found maximized compare to initial experiments.

#### **For YS for TIG welding of 316L stainless steel**

- i. From the main effect plots of YS, it is found that YS most significantly affected by the current parameter compare to other parameters.
- ii. Interaction plots also reveals that interaction effects of process parameter are most significant for both the responses.
- iii. Mathematical modeling is done to correlate process parameters with YS by RSM technique.
- iv. Contour plots for YS are drawn. These plots clearly show the interaction effect of input parameters on the response, YS.
- v. From the results of analysis of variance of YS, it is found that all the process variables, its squared combinations, interactions are significant variables for YS except GFR and interaction effects of current\*gas flow rate.
- vi. Optimal parametric combination obtained by TLBO and DFA for YS is: current = 150 A, speed = 15.33 cm/min and gas flow rate = 8.97 l/min and corresponding YS = 396.55MPa.
- vii. The accuracy optimal result is obtained by TLBO and DFA is same
- viii. Confirmatory test shows the validity of the proposed optimization procedure / techniques.

#### **For IS for TIG welding of 316L stainless steel**

- i. Main effect plots of IS reveals that gas flow rate is most significant factor
- ii. From interaction plots, it is noted that interaction effects of welding parameter have significant effect on IS.
- iii. Mathematical modeling is done by RSM to postulate relationship between process parameters and IS.
- iv. Contour plots for IS are made. These plots show that interaction effects of input parameters are prominent for the response, IS.
- v. Results of analysis of variance show that direct, squared and interaction effects of all process welding parameters are most significant for IS
- vi. Maximum IS value 51.67 J is obtained by TLBO and DFA at parametric condition of current = 127.27A, speed = 15.52 cm/min and gas flow rate = 8.85 l/min
- vii. The accuracy optimal result is obtained by TLBO and DFA is same
- viii. Confirmatory test has been done at optimal condition and found better IS value compare to initial experiments.

### **For hardness (VHN) for TIG welding of 316L stainless steel**

- i. From the main effect plots of hardness, it is found that hardness is most significantly affected by the welding speed compare to other parameters.
- ii. Interaction plots also reveals that interaction effects of process parameter are most significant for both the responses.
- iii. Mathematical modeling is done to correlate process parameters with hardness by RSM technique.
- iv. Contour plots for hardness are drawn. These plots clearly show the interaction effect of input parameters on the response, hardness.
- v. From the results of analysis of variance (ANOVA) of hardness, it is found that all the process variables, its squared combinations, interactions are most significant on hardness.
- vi. Optimal parametric combination obtained by TLBO and DFA for hardness is: current = 124.24 A, speed = 15.88 cm/min and gas flow rate = 8.91 l/min and corresponding hardness = 245.01.
- vii. Confirmatory test shows the validity of the proposed optimization procedure / techniques.

### **For WW for TIG welding of 316L stainless steel**

- i. From the main effect plots of WW, it is found that response, WW most significantly affected by the speed parameter compare to other parameters.
- ii. Interaction plots also reveals that interaction effects of process parameter are most significant for WW.
- iii. By using the welding parameters, the second order response surface models for the WW is developed by RSM application.
- iv. Contour plots for WW are drawn from the developed mathematical models. These plots clearly show the interaction effect of input parameters on WW. The welding conditions satisfying constraints for industrial application can be selected very easily from the contour plot of the developed response models.
- v. From the results of analysis of variance, it is noted that all the process parameters and their squared and interactions, are most significant for WW.
- vi. Optimum welding condition obtained by TLBO and DFA for maximizing the WW is: current = 120.20 A, speed = 18 cm/min and gas flow rate = 8.42 l/min and corresponding minimized weld width = 6.05 mm.
- vii. Confirmatory test is conducted at optimal condition and found improved WW as compared initial experiments.

### **For multi-objective optimization for TIG welding of 316L stainless steel**

- i. From the main effect plots of GRG, it is found that GRG most significantly affected by the speed parameter compare to other parameters.
- ii. Interaction plots also reveals that interaction effects of process parameter are most significant for all the responses.
- iii. Mathematical modeling is done to correlate process parameters with GRG by RSM technique.
- iv. Contour plots for GRG are drawn. These plots clearly show the interaction effect of input parameters on GRG.
- v. From the results of analysis of variance of GRG, it is found that all the process variables, its squared combinations, interactions, except interaction effects of current\*speed and current\*gas flow rate is significant variables for GRG.
- vi. Optimal parametric combination obtained by TLBO and DFA for GRG is: current = 128.43 A, speed = 15.83 cm/min and gas flow rate = 8.83 l/min and corresponding GRG = 0.88
- vii. The percentage error between the predicted results and the results of confirmatory test is found to be less than 2% which validates proposed optimization procedure / techniques.

### **For high cycle fatigue test for base metal and TIG welding of 316L stainless steel**

- i. It is found that at higher stress levels, the specimen exhibited lower fatigue life for both base metal and welded joints. Cracks for base metal are initiated from the surface defects and for welded joint, it is initiated from the surface of the welded zone of the specimens.
- ii. The fatigue limit is successfully characterized for TIG welded joint, as well as base metal in this investigation and it is found as 173.05MPa for welded joint and 157.44MPa for base metal. Welded joint depicts almost 10% higher fatigue limit compare to base metal.
- iii. SEM fractographs of fatigue fracture of the welded joints show that the region of fatigue damaged progressively diminished when the maximum applied stress is consecutively increased under constant stress ratio ( $R = 0.1$ ).

### **5.2. Future Scope of Work**

- ❖ In the present study tungsten inert gas welding of AISI 316L stainless steel has been considered. Investigation may be extended by considering several sets of experiments, in each set thickness of the material being different from the thickness used in the other sets.
- ❖ Investigation may be carried out in respect of other welding processes like, GMAW of AISI 316L stainless steel, as well.

- ❖ Several types of base materials may be considered.
- ❖ Dissimilar welding is another scope of future work.
- ❖ Low cycle fatigue behaviors of welded joints may be investigated
- ❖ Corrosion analysis may be carried out for the welded samples.

## REFERENCES

- [1] O. E. Canyurt, Estimation of welded joint strength using genetic algorithm approach. *International Journal of Mechanical Sciences* 47 (2005) 1249–1261.
- [2] R. S. Parmar, *Welding Processes and Technology*, 2nd edition, Khanna Publications, New Delhi, 1997.
- [3] K. Martinsen, S. J. Hu, B. E. Carlson, Joining of dissimilar materials, *CIRP Annals - Manufacturing Technology*, 64 (2015) 679–699.
- [4] T. Sakthivel, M. Vasudevan, K. Laha, P. Parameswaran, K. S. Chandravathi, M.D. Mathew, A. K. Bhaduri, Comparison of creep rupture behaviour of type 316L(N) austenitic stainless steel joints welded by TIG and activated TIG welding processes, *Materials Science and Engineering: A*, 528(22–23), (2011) 6971-6980.
- [5] M. Dadfar, M. H. Fathi, F. Karimzadeh, M. R. Dadfar, A. Saatchi, Effect of TIG welding on corrosion behavior of 316L stainless steel, *Materials Letters*, 61 (2007) 2343–2346.
- [6] L P. Connor, *Welding handbook-welding processes*, 8th edition, volume-2, American Welding Society, 1991.
- [7] A. Harb, I. Ciuca, R. Ciocoiu, M. Vasile, A. Bibis, B. Rahali, I. Al Hawamda, Effect of TIG welding and manual metal arc welding on mechanical properties of AISI 304 and 316L austenitic stainless-steel sheets, *Key Engineering Materials*, 750 (2017) 26-33.
- [8] A. I. Santillana, C. Boyer, P. F. Pison, A. Foussat, S. A. E. Langeslag, A. T. P. Fontenla, E. M. Ruiz Navas, S. Sgobba, A comparative study of fracture toughness at cryogenic temperature of austenitic stainless-steel welds, *Journal of Materials Engineering and Performance*, 27( 4), (2018) 1995–2002.
- [9] E. Ugur, Melih B, Yugut K, Sueda O. Optimization of weld bead geometry in TIG welding process using grey relation analysis and Taguchi method. *Material Technology*, 43(3), (2009) 43-149.
- [10] Y. S. Tarng, W. H. Yang, Optimisation of the weld bead geometry in gas tungsten arc welding by the Taguchi method, *The International Journal of Advanced Manufacturing Technology*, 14(8), (1998) 549–554.
- [11] S. C. Juang, Y. S. Tarng, Process parameter selection for optimizing the weld pool geometry in the tungsten inert gas welding of stainless steel, *Journal of Materials Processing Technology*, 122(1), (2002) 33-37.

- [12] R. Rudrapati, N. Chowdhury, A. Bandyopadhyay, Parametric optimization of TIG welding process in butt joining of mild steel and stainless steel, *International Journal of Current Engineering and Technology*, (6), (2016) 144-149.
- [13] L. Gardner, The use of stainless steel in structures, *Progress in Structural Engineering and Materials*, 7(2), (2005) 48-55
- [14] J. C. Lippold, D. J. Kotechki, *Welding Metallurgy and Weldability of Stainless Steels*, John Wiley and Sons, New Jersey, (2005)
- [15] D. P. Selvaraj, P. Chandramohan, M. Mohanraj, Optimization of surface roughness, cutting force and tool wear of nitrogen alloyed duplex stainless steel in a dry turning process using Taguchi method, *Measurements*, 49, (2014) 205-215.
- [16] G. Lothongkum, E. Viyanit, P. Bhandhubanyong, Study on the effects of pulsed TIG welding parameters on delta-ferrite content, shape factor and bead quality in orbital welding of AISI 316L stainless steel plate, *Journal of Materials Processing Technology*, 110 (2001) 233–238.
- [17] D. Ahmet, Experimental investigation of the effect of hydrogen in argon as a shielding gas on TIG welding of austenitic stainless steel, *Materials and Design*, 25 (2004) 19–23.
- [18] S. M. Tabatabaeipour, F. Honarvar, A comparative evaluation of ultrasonic testing of AISI 316L welds made by shielded metal arc welding and gas tungsten arc welding processes. *Journal of Materials Processing Technology*, 210 (2010) 1043–1050.
- [19] H. T. Lee, S. L. Jeng, Characteristics of dissimilar welding of alloy 690 to 304L stainless steel, *Science and Technology of Welding & Joining*, 6(4), (2001) 225–234.
- [20] S. Shashi Kumar, N. Murugan, K. K. Ramachandran, Effect of friction stir welding on mechanical and microstructural properties of AISI 316L stainless steel butt joints, *Welding in the World*, (2018) <https://doi.org/10.1007/s40194-018-0621-7>
- [21] A. K. Lakshminarayan, Enhancing the properties of friction stir welded stainless steel joints via multi-criteria optimization, *Archives of Civil and Mechanical Engineering* 16(4), (2016) 605-617.
- [22] R. V. Martins, C. Ohms, K. Decroos, Full 3D spatially resolved mapping of residual strain in a 316L austenitic stainless steel weld specimen, *Materials Science and Engineering: A*, 527 (2010) 4779–4787.

- [23] M. Vasudevan, M. V. Kuppaswamy, A. K. Bhaduri, Optimizing process parameters for gas tungsten arc welding of an austenitic stainless steel using genetic algorithm, *Transactions of the Indian Institute of Metals*, 63( 1), (2010) 1-10.
- [24] N. Ghosh, P. K. Pal, R. Rudrapati, G. Nandi, Parametric optimization of gas metal arc welding process by PCA based Taguchi method on austenitic stainless steel AISI 316L. *Materials Today: Proceedings*, 5 (2018) 1620-1625
- [25] [en.wikipedia.org/wiki/GTAW](http://en.wikipedia.org/wiki/GTAW)
- [26] ASM Handbook, Vol. 6, ASM International, Materials Park, OH, 1993.
- [27] K. Y. Benyounis, A. G. Olabi, Optimization of different welding processes using statistical and numerical approaches – A reference guide, *Advances in Engineering Software* 39 (2008) 483–496.
- [28] N. S. Tsai, T. W. Eager, Distribution of the heat and current fluxes in gas tungsten arcs, *Metallurgical and Materials Transactions B*, 16(4), (1985) 841-846.
- [29] E. Ataman, Effect of GTAW Parameters on Mechanical and Microstructural Properties of Weld Joints of Low Alloy AISI 4130 Steel, MSc Thesis, METU, Ankara, Turkey, 2001.
- [30] K. C. Mills, B. J. Keene, Factors Effecting Variable Weld Penetration, *International Materials Reviews*, (2013) 185-216.
- [31] R. R Mishra, Visnu Kumar Tiwari, S. Rajesha, A study of tensile strength of MIG and TIG welded dissimilar joints of mild steel and stainless steel, *International Journal of Advances in Materials Science and Engineering (IJAMSE)*, 3(2), (2014) 23-32.
- [32] A. K. Lakshminarayanan, K. Shanmugam, V. Balasubramanian, Effect of welding processes on tensile and impact properties, hardness and microstructure of AISI 409M ferritic stainless joints fabricated by duplex stainless steel filler metal, *Journal of iron and steel research International*, 16(5), (2009) 66-72.
- [33] S. C. Bodkhe, D. R. Dolas, Optimization of activated tungsten inert gas welding of 304L austenitic stainless steel, *Procedia Manufacturing*, 20 (2018) 277-282.
- [34] A. Durgutlu, Experimental investigation of the effect of hydrogen in argon as a shielding gas on TIG welding of austenitic stainless steel, *Materials and Design*, 25 (2004) 19-23.
- [35] Q. Zhu, Yu-cheng Lei , Xi-zhang Chen, Wen-jie Ren, Xin Ju, Yi-min Ye, Microstructure and mechanical properties in TIG welding of CLAM steel, *Fusion Engineering and Design*, 86 (2011) 407–411.



- [36] H. R. Zareie Rajani, H. Torkamani, M. Sharbati, Sh. Raygan, Corrosion resistance improvement in Gas Tungsten Arc Welded 316L stainless steel joints through controlled preheat treatment, *Materials and Design*, 34 (2012) 51–57.
- [37] V. Anand Rao, R. Deivanathan, Experimental investigation for welding aspects of stainless steel 310 for the process of TIG welding, *Procedia Engineering*, 97 (2014) 902-908.
- [38] Kuang-Hung Tseng, Chih-Yu Hsu, Performance of activated TIG process in austenitic stainless steel welds, *Journal of Materials Processing Technology*, 211 (2011) 503–512.
- [39] H. M. Soltani, M. Tayebi, Comparative study of AISI 304L to AISI 316L stainless steels joints by TIG and Nd:YAG laser welding, *Journal of Alloys and Compounds*, 767 (2018) 112-121.
- [40] R. M. Molak, K. Paradowski, T. Brynk, L. Ciupinski, Z. Pakiela, K. J. Kurzydowski, Measurement of mechanical properties in a 316L stainless steel welded joint, *International Journal of Pressure Vessels and Piping*, 86 (2009) 43–47.
- [41] M. Thomas, V. P. Raghu, S. R. Ganeshand, M. Vasudevan, High temperature fatigue crack growth rate studies in stainless steel 316L(N) welds processed by A-TIG and MP-TIG welding, 12th International Fatigue Congress, 165 (2018).
- [42] M. P. Reddy, A. A. S. William, M. M. Prashanth, S. N. S. Kumar, K. D. Ramkumar, N. Arivazhagan, S. Narayanan, Assessment of Mechanical Properties of AISI 4140 and AISI 316 dissimilar weldments, *Procedia Engineering*, 75 ( 2014 ) 29 – 33.
- [43] D. P. Tumu, P. Subramani, K. G. Kumar, M. Manikandan, C. G. Mohan, N. Arivazhagan, D. N. Rajan, Investigation on microstructure and tensile properties of dissimilar weld joints between AISI 316l and duplex 2205 stainless steel. *IOP Conf. Series: Materials Science and Engineering* 402 (2018) 1-7.
- [44] W. Jatimurti, F. A. Abdillah, B. A. Kurniawan, R. Rochiem, Effect of current and travel speed variation of TIG welding on microstructure and hardness of stainless-steel SS 316L. *AIP Conference Proceedings*, 1945, 020074 (2018).
- [45] S. Kumar, A. S. Shahi, Effect of heat input on the microstructure and mechanical properties of gas tungsten arc welded AISI 304 stainless steel joints, *Materials and Design*, 32 (2011) 3617-3623.
- [46] E. Mortazavi, R. A. Najafabadi, A. Meysami, Effect of heat input on microstructure and mechanical properties of dissimilar joints of AISI 316L steel and API X70 high-strength low-alloy steel, *Journal of Iron and Steel Research, International*, 24 (12), (2017) 1248-1253,.

- [47] V. Olden, Z. L. Zhang, E. Ostby, B. Nyhus, C. Thaulow, Notch tensile testing of high strength steel weldments, 2nd International Symposium on High Strength Steel, 23-24, April (2002), Verdal, Norway.
- [48] Jau-Wen Lin, Hsi-Cherng Chang, Ming-Hsiu Wu, Comparison of mechanical properties of pure copper welded using friction stir welding and tungsten inert gas welding, *Journal of Manufacturing Processes*, 16, 2 (2014) 296-304.
- [49] S. T. Selvamani, K. Palanikumar, Optimizing the friction welding parameters to attain maximum tensile strength in AISI 1035 grade carbon steel rods, *Measurement*, 53 (2014) 10-21.
- [50] E. M. Anawa, A. G. Olabi, Optimization of tensile strength of ferritic/austenitic laser welded components, *Optics and Lasers in Engineering*, 46 (2008) 571-577.
- [51] K. Karthick, S. Malarvizhi, V. Balasubramanian, S. A. Krishnan, G. Sasikala, Shaju K. Albert, Tensile and impact toughness properties of various regions of dissimilar joints of nuclear grade steels, *Nuclear Engineering and Technology*, 50 (2018) 116-125.
- [52] C. Y. Chu, C. T. Hsieh, L. W. Tsay, Microstructure and notched tensile fracture of Ti-6Al-4V to Ti-4.5Al-3V-2Fe-2Mo dissimilar welds, *Materials and Design*, 63 (2014) 14-19.
- [53] L. W. Tsay , Y. S. Ding , W. C. Chung , C. Chen, Notched tensile strength of SP-700 laser welds, *Materials Letters*, Volume 62(6-7), (2008) 1114-1117.
- [54] A. Kumar, S. Sundarrajan, Optimization of pulsed TIG welding process parameters on mechanical properties of AA 5456 Aluminum alloy weldments, *Journal of Materials and Design*, 30 (2009) 1288-1297.
- [55] N. Kiaee, M. Aghaie-Khafri, Optimization of gas tungsten arc welding process by response surface methodology, *Materials & Design*. 54 (2014) 25-31.
- [56] S. Srivastava, R.K. Garg, Process parameter optimization of gas metal arc welding on IS: 2062 mild steel using response surface methodology, *Journal of Manufacturing Processes*, 25 (2017) 296-305.
- [57] A. A. Shukla, V. S. Joshi, A. Chel, B. A. Shukla, Analysis of Shielded metal arc welding parameter on depth of penetration on AISI 1020 plates using response surface methodology, *Procedia Manufacturing*, 20 (2018) 239-246.
- [58] X. K. Yue, G. Q. Tong, F. Chen, X. L. Ma, X. P. Gao, Optimal welding parameters for small-scale resistance spot welding with response surface methodology, *Science and Technology of Welding and Joining*, 22 (2016) 143-149.

- [59] R. P. Singh, R. K. Garg, D. K. Shukla, Mathematical modeling of effect of polarity on weld bead geometry in submerged arc welding, *Journal of Manufacturing Processes*, 21 (2016) 14–22.
- [60] N. Kumar, M. Mukherjee, A. Bandyopadhyay, Comparative study of pulsed Nd: YAG laser welding of AISI 304 and AISI 316 stainless steels, *Journal of Optics & Laser Technology*, 88 (2017) 24–39.
- [61] E. J. Martinez-Conesa, J. A. Egea, V. Miguel, C. Toledo, J. L. Meseguer-Valdenebro, Optimization of geometric parameters in a welded joint through response surface methodology, *Construction and Building materials*, 154 (2017) 105-114.
- [62] M. Balasubramanian, Prediction of optimum weld pool geometry of PCTIG welded titanium alloy using statistical design, *Engineering Science and Technology, an International Journal*, 19 (2016) 15–21.
- [63] P. K. Giridharan, N. Murugan, Optimization of pulsed GTA welding process parameters for the welding of AISI 304L stainless steel sheets, *The International Journal of Advanced Manufacturing Technology*, 40 (2009) 478–489.
- [64] F. Madadi, F. Ashrafizadeh, M. Shamanian, Optimization of pulsed TIG cladding process of stellite alloy on carbon steel using RSM, *Journal of Alloys and Compounds*, 510 (2012) 71– 77.
- [65] M. Sen, M. Mukherjee, T. K. Pal, Evaluation of correlation between DP-GMAW process parameters and bead geometry, *Welding Journal*, 94 (2015) 265–279.
- [66] M. Ragavendran, N. Chandrasekhar, R. Ravikumar, R. Saxena, M. Vasudevan, A. K. Bhaduri, Optimization of hybrid laser-TIG welding of 316LN steel using response surface methodology (RSM), *Optics and Lasers in Engineering*, 94 (2017) 27-36.
- [67] P. Dutta, D. K. Pratihari, Modeling of TIG welding process using conventional regression analysis and neural network-based approaches, *Journal of Materials Processing Technology*, 184 (2007) 56–68.
- [68] A. Balaram Naik, A. Chennakeshava Reddy, Optimization of tensile strength in TIG welding using the Taguchi method and analysis of variance (ANOVA), *Thermal Science and Engineering Progress*, 8 (2018) 327-339.
- [69] P. Bharath, V. G. Sridhar, M. S. Kumar, Optimization of 316 Stainless Steel Weld Joint Characteristics using Taguchi Technique, *Procedia Engineering*, 97 (2014) 881-891.

- [70] P. Vasantharaja, M. Vasudevan, Optimization of A-TIG welding process parameters for RAFM steel using response surface methodology, *The Journal of Materials: Design and Applications*, 232 (2), (2015) 121-136.
- [71] N. Chandrasekhar, M. Ragavendran, R. Ravikumar, M. Vasudevan, S. Murugan, Optimization of hybrid laser-TIG welding of 316LN stainless steel using genetic algorithm, *Materials and manufacturing processes*, 32 (10), (2017) 1094–1100.
- [72] J. Joseph, S. Muthukumar, Optimization of activated TIG welding parameters for improving weld joint strength of AISI 4135 PM steel by genetic algorithm and simulated annealing, *The International Journal of Advanced Manufacturing Technology*, 93(1–4), (2017) 23–34.
- [73] D. S. Nagesh, G.L. Datta, Genetic algorithm for optimization of welding variables for height to width ratio and application of ANN for prediction of bead geometry for TIG welding process, *Applied Soft Computing*, 10 (2010) 897–907.
- [74] A. Ravisankar, S. Kumar Velaga, Gaurav Rajput, S. Venugopal, Influence of welding speed and power on residual stress during gas tungsten arc welding (GTAW) of thin sections with constant heat input: A study using numerical simulation and experimental validation, *Journal of Manufacturing Processes*, 16 (2014) 200–211.
- [75] D. S. Correia, C. V. Gonçalves, S. S. da Cunha, V. A. Ferraresi, Comparison between genetic algorithms and response surface methodology in GMAW Welding optimization, *Journal of Materials Processing Technology*, 160 (2005) 70–76.
- [76] Diogo F. Almeida, Rui F. Martins, Joao B. Cardoso, Numerical simulation of residual stresses induced by TIG butt-welding of thin plates made of AISI 316L stainless steel, *Procedia Structural Integrity*, 5 (2017) 633-639.
- [77] B. Liao, Y. Shi, Y. Cui, S. Cui, Z. Jiang, Y. Yi, Mathematical Model for Prediction and Optimization of Weld Bead Geometry in All-Position Automatic Welding of Pipes, *Metals*, 8(10), (2018) 756; DOI: 10.3390/met8100756.
- [78] N. Naik Korra, M. Vasudevan, K. R. Balasubramanian, Multi-objective optimization of activated tungsten inert gas welding of duplex stainless-steel using response surface methodology, *The International Journal of Advanced Manufacturing Technology*, 77(1–4), (2015) 67–81.
- [79] D. Kim, S. Rhee, H. Park, Modelling and optimization of a GMA welding process by genetic algorithm and response surface methodology, *International Journal of Production Research*, 40 (2002) 1699-1711.

- [80] R. V. Rao, V. J. Savsani, D. P. Vakharia, Teaching-learning based optimization: A novel method for constrained mechanical design optimization problems, *Computer-Aided Design*, 43 (2011) 303-315.
- [81] C. Matej, S. H. Liu L. Mernik, A note on teaching-learning-based optimization algorithm, *Information Sciences*, 212 (2012) 79-93.
- [82] R. V. Rao, V. D. Kalyankar, Multi-objective multi-parameter optimization of the industrial LBW process using a new optimization algorithm, *Proceedings of the Institution of Mechanical Engineers Part B: Journal of Engineering Manufacture*, 226(6) (2012) 1018-1025.
- [83] M. K. Dikshit, A. B. Puri, Atanu Maity, Empirical modelling of dynamic forces and parameter optimization using teaching-learning-based optimization algorithm and RSM in high speed ball-end milling, *Journal of Production Engineering*, 19(1), (2016) 11-21.
- [84] B. F. Jogi, A. S. Awale, S. R. Nirantar, H. S. Bhusare, Metal Inert Gas (MIG) Welding Process Optimization using Teaching-Learning Based Optimization (TLBO) Algorithm, *Materials today Proceedings*, 5(2), (2018) 7086-7095.
- [85] P. J. Pawar, R.V. Rao, Parameters optimization of machining processes using teaching learning based optimization. *International Journal Advanced Manufacturing Technology*, 67 (2012) 995-1006.
- [86] R. V. Rao, V. J. Savsani, J. Balic, Teaching-learning based optimization algorithm for unconstrained and constrained real-parameter optimization problems, *Engineering Optimization*, 44 (2012) 1447-1462.
- [87] R. V. Rao, V. D. Kalyankar, Parameter optimization of modern machining processes using TLBO algorithm. *Engineering Applications of Artificial Intelligence*, 26 (2013) 524-531.
- [88] N. K. Sahu, A. B. Andhare, Multi objective optimization for improving machinability of Ti-6Al-4V using RSM and advanced algorithms, *Journal of Computational Design and Engineering*, 6 (2019) 1-12.
- [89] R. Rudrapati, P. Sahoo, A. Bandyopadhyay, Optimization of process parameters in CNC turning of aluminium alloy using hybrid RSM cum TLBO approach, *IOP Conference Series: Materials Science and Engineering* 149 (2016) 012039, doi:10.1088/1757-899X/149/1/012039.
- [90] G. C. Manjunath Patel, B. S. Ajith, R. Jonathan, D. S. Allan, M. Aniruddh, M. Ashwith, Teaching learning based optimization of squeeze casting process for quality castings, *IOP Conference Series: Materials Science and Engineering*, 376 (2018) 012112, doi:10.1088/1757-899X/376/1/012112.

- [91] A. Tiwaria, M. K. Pradhan, Applications of TLBO algorithm on various manufacturing processes: A Review, *Materials Today: Proceedings*, 4 (2017) 1644–1652.
- [92] R. Kumar, P. C. Tewari, D. Khanduja, Parameters optimization of fabric finishing system of a textile industry using teaching-learning-based optimization algorithm, *International Journal of Industrial Engineering Computations*, 9 (2018) 221–234.
- [93] G. S. Sharma, S. L. Shinde, R. S. Sayare, Optimization of Process Parameters of GMAW using TLBO Technique, *International Journal of Engineering and Management Research*, 5(2), (2015) 867-872.
- [94] M. V. Patil, Multi response simulation and optimization of gas tungsten arc welding, *applied Mathematical modelling*, 42 (2017) 540-553.
- [95] A. Wahule, K. Wasankar, Multi-response Optimization of Process Parameters of TIG Welding for Dissimilar Metals (SS-304 and Fe-410) using Grey Relational Analysis, *International Research Journal of Engineering and Technology*, 5(6), (2018) 986-993.
- [96] S. Datta, A. Bandyopadhyay, P. K. Pal, Slag recycling in submerged arc welding and its influence on weld quality leading to parametric optimization, *International Journal of Advanced Manufacturing Technology*, 39 (2008) 229–238.
- [97] D. Bahar, A. Venkatesh, B. K. Vinay, T. R. K. P. Siva, Multi objective optimization of TIG welding parameters for joining dissimilar materials. *International Journal of Engineering & Science Research*, 8 (2018) 26-33.
- [98] A. Panda, A. K. Sahoo, A. K. Rout, Multi-attribute decision making parametric optimization and modeling in hard turning using ceramic insert through grey relational analysis: A case study, *Decision Science Letters*, 5 (2016) 581–592.
- [99] S. A. Rizvi, S. P. Tewari, Optimization of gas metal arc welding parameters of SS304 austenitic steel by Taguchi-Grey relational analysis, *Journal of Computational and Applied Research in Mechanical Engineering*, 7 (2), (2018) 189-198.
- [100] D. Bahar, Md. N. Sharif, K. Shravan Kumar, D. Reddy, Optimization of MIG welding process parameters for hardness and strength of welding joint using Grey relational analysis, *International Journal of Research in Advent Technology*, 6(5), (2018) 893-899.
- [101] S. Goyal, R. Sandhya, M. Valsan, K. B. S. Rao, The effect of thermal ageing on low cycle fatigue behaviour of 316 stainless steel welds, *International Journal of Fatigue* 31 (2009) 447–454.

- [102] N. Miura, Y. Takahashi, High-cycle fatigue behavior of type 316 stainless steel at 2880C including mean stress effect, *International Journal of Fatigue*, 28 (2006) 1618–1625.
- [103] G. Fargione, F. Giudice, A. Risitano, The influence of the load frequency on the high cycle fatigue behaviour, *Theoretical and Applied Fracture Mechanics*, 88 (2017) 97–106.
- [104] Y. Ono, T. Yuri, N. Nagashima, H. Sumiyoshi, T. Ogata, N. Nagao, High-cycle fatigue properties of alloy 718 base metal and electron beam welded joint, *Physica Procedia*, 67 (2015) 1028-1035.
- [105] T. Miyazaki, H. Kang, H. Noguchi, K. Ogi, Prediction of high-cycle fatigue life reliability of aluminum cast alloy from statistical characteristics of defects at meso-scale, *International Journal of Mechanical Sciences*, 50 (2), (2008) 152–162.
- [106] Peng Wen-jie Peng, Xue Huan, GE rui, Peng zhou, The influential factors on very high cycle fatigue testing results, *MATEC Web of Conferences* 165, 20002 (2018), *FATIGUE 2018*, <https://doi.org/10.1051/matecconf/201816520002>
- [107] F. Fomin, N. Kashaev, Influence of porosity on the high cycle fatigue behaviour of laser beam welded Ti-6Al-4V butt joints, *Procedia Structural Integrity*, 7 (2017) 415-422.
- [108] M. Kamaya, M. Kawakubo, Mean stress effect on fatigue strength of stainless steel, *International Journal of Fatigue*, 74 (2015) 20–29
- [109] Vuong Nguyen Van Do, The numerical high cycle fatigue damage model of fillet weld joint under weld-induced residual stresses *IOP Conf. Series: Earth and Environmental Science* 143 (2018) 012037 doi :10.1088/1755-1315/143/1/012037
- [110] M. K. Khan, Q. Y. Wang, Investigation of crack initiation and propagation behavior of AISI 310 stainless steel up to very high cycle fatigue, *International Journal of Fatigue*, 54 (2013) 38–46.
- [111] D. F. Pessoa, G. Kirchhoff , M. Zimmermann, Influence of loading frequency and role of surface micro-defects on fatigue behavior of metastable austenitic stainless steel AISI 304, *International Journal of Fatigue*, 103 (2017) 48–59
- [112] N. Ghosh, P. K. Pal, G. Nandi, Parametric optimization of MIG welding on 316L austenitic stainless steel by Grey-Based Taguchi method, *Procedia Technology*, 25 (2016) 1038-1048.
- [113] D. C. Montgomery, R. H. Myers, C. M. Anderson-Cook, *RSM Process and Product Optimization using Designed Experiments*, 3rd ed., Wiley, New York 2011.

- [114] J. Deng, Control problems of grey systems,” in the international journal Systems and Control Letter, 5, (1982) 288-294.
- [115] C. Wichan, S. Loeshpahn, Effect of filler alloy on microstructure, mechanical and corrosion behaviour of dissimilar weldment between AISI 201 stainless steel and low carbon steel sheets produced by a gas tungsten arc welding, Advanced Materials Research, 581-582, (2012) 808-816.
- [116] Sindo Kou, Welding metallurgy, 2nd edition, Hoboken: John Wiley & Sons Inc; 2003.998.
- [117] R.K. Buddu, N. Chauhan, P.M. Raole, Mechanical properties and microstructural investigations of TIG welded 40 mm and 60 mm thick SS 316L samples for fusion reactor vacuum vessel applications, Fusion Engineering and Design, 89 (2014) 3149-3158.
- [118] N. Kumar, M. Mukherjee, A. Bandyopadhyay, Study on laser welding of austenitic stainless steel by varying incident angle of pulsed laser beam, Optics and Laser Technology, 94 (2017) 296-309.
- [119] A K Lakshminarayanan, K Shanmugam, V Balasubramanian, Effect of Autogenous Arc Welding Processes on Tensile and Impact Properties of Ferritic Stainless Steel Joints, Journal of Iron and Steel Research, International, 16(1), 2009, 62-68.
- [120] G. Padmanaban and V. Balasubramanian, Optimization of laser beam welding process parameters to attain Maximum tensile strength in AZ31B magnesium alloy, Optics & Laser Technology, 42 (2010) 1253-1260.
- [121] A. Gigovi-Geki, M. Oru, S. Muhamedagi, Effect of the delta-ferrite content on the tensile properties in nitronic 60 steel at room temperature and 750°C, Materials and technology 46 (5), (2012) 519–523.
- [122] Y. Jun, G. Ming, Z. Xiaoyan, Study on microstructure and mechanical properties of 304 stainless steel joints by TIG, laser and laser-TIG hybrid welding, Optics and Lasers in Engineering, 48 (2010) 512–517,.
- [123] C. Muthusamy, L. Karuppiyah, S. Paulraj, D. Kandasami, R. Kandhasamy, Effect of Heat Input on Mechanical and Metallurgical Properties of Gas Tungsten Arc Welded Lean Super Martensitic Stainless Steel, Materials Research, 19 (3), (2016) 572-579.
- [124] Jiunn-Yuan Huang, Ji-Jung Yeh, Sheng-Long Jeng, Charn-Ying Chen and Roang-Ching Kuo, High-Cycle Fatigue Behavior of Type 316L Stainless Steel, Materials Transactions, 47(2), (2006) 409 – 417.
- [125] G. Shanmugasunda, B. Karthikeyan, P. SanthoshPonvell, V. Vignesh, Optimization of Process Parameters in TIG Welded Joints of AISI 304L -Austenitic Stainless



Steel using Taguchi's Experimental Design Method, *Materials today: Proceedings*, 16(2) (2019) 1188-1195.

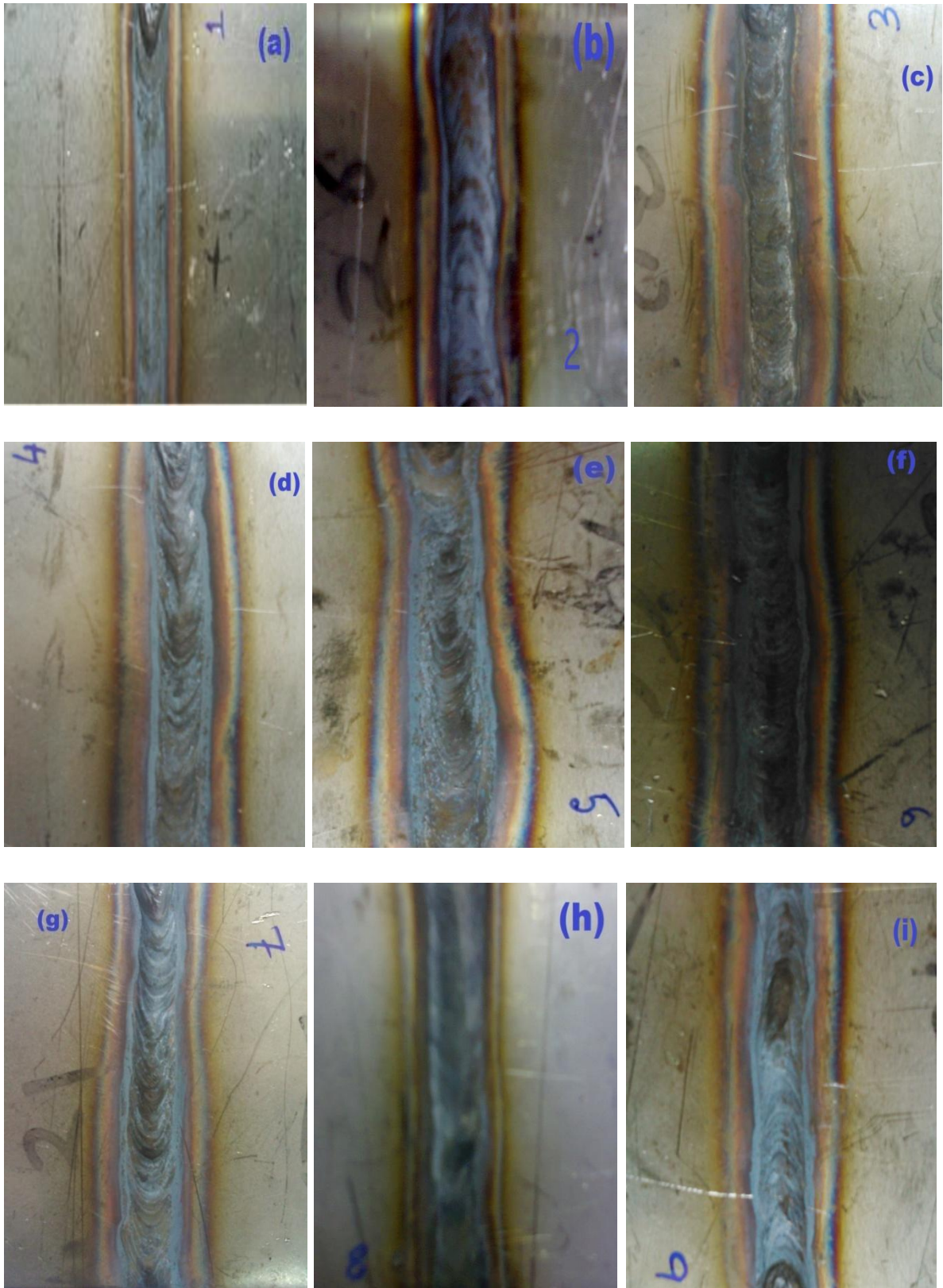
- [126] D. F. Almeida, R. F. Martins, J. B. Cardoso, Numerical simulation of residual stresses induced by TIG butt-welding of thin plates made of AISI 316L stainless steel, *Procedia Structural Integrity*, 5 (2017) 633–639.
- [127] S. Kumar, P. K. Singh, D. Patel, S. B. Prasad, Experimental Investigation and Optimization of Welding Parameters on TIG Welding of Stainless Steel AISI 304 Plates, *Innovation in Materials Science and Engineering*, Springer, (2019) 91-102.
- [128] M. Jurica, Z. Kozuh, I. Garasic, M. Busic, Optimization of the A-TIG welding for stainless steels, *IOP Conf. Series: Materials Science and Engineering*, 329 (2018), 1-9.
- [129] A. Thakur, H. Gebrelibanos, T. Gabrey, Arc Welding Process Selection through a Quality and Costs, *International Journal of Current Engineering and Technology*, 9(3) (2019) 383-394.
- [130] S. A. Vendan, L. Gao, A. Garg, P. Kavitha, D. Gopal, R. Sg, Power Sources and Challenges for Different Arc Welding Processes, *Interdisciplinary Treatment to Arc Welding Power Sources*, Springer (2018) 127-138.
- [131] J. Jun, S. Kim, S. Cho, A Study on Productivity Improvement in Narrow Gap TIG Welding, DOI:10.5781/JWJ.2016.34.1.68.
- [132] W. Zhang, X. Yu, X. Song, X. Lu, Microstructure and mechanical property of stainless steel joints with arc spot welding, *Transactions of the China Welding Institution* 39(12), (2018) 125-128.
- [133] Neelam Vilas Shinde, Martand Tamanacharya Telsang, Effect of Alternate Supply of Shielding Gases of Tungsten Inert Gas Welding on Mechanical Properties of Austenitic Stainless Steel, *Journal of Institution of Engineers (India): Series C*, 97(3), (2016) 299-307.
- [134] J. Zahr, U. Fussel, M. Hertel, M. Lohse, M. Sende and M. Schnick, Numerical and experimental studies of the influence of process gases in TIG welding, *Welding in the World*, 56(3-4), (2012) 85-92.
- [135] H. Zhao, Comparative Research of Helium and Argon Arc Characters, *Journal of Mechanical Engineering* 54(8), (2018) 137-143.
- [136] S. Akellaa, B. R. Kumar, Distortion Control in TIG Welding Process with Taguchi Approach, *Advanced Materials Manufacturing & Characterization*, 3(1) (2013) 199-206.

- [137] A. K. Singh, V. Dey, R. N. Rai, Techniques to improve weld penetration in TIG welding (A review), *Materials Today: Proceedings*, 4 (2017) 1252–1259.
- [138] S.W. Shyu, H.Y. Huang, K.H. Tseng, C.P. Chou, Study of the Performance of Stainless Steel A-TIG Welds, *Journal of Materials Engineering and Performance*, 17(2), (2008) 193-201.
- [139] A.V. Santhana Babu, P. K Giridharan, Productivity improvement in flux assisted TIG welding, *International Journal on Design & Manufacturing Technologies*, 6(2) (2012) 55-62.
- [140] Yiming Huang, Di Wu, Zhifen Zhang, Huabin Chen, Shanben Chen, EMD-based pulsed TIG welding process porosity defect detection and defect diagnosis using GA-SVM, *Journal of Materials Processing Technology* Volume 239, January 2017, Pages 92-102
- [141] Jie Zhu, Jiayou Wang, Na Su, Guoxiang Xu, Maosen Yang, An infrared visual sensing detection approach for swing arc narrow gap weld deviation, *Journal of Materials Processing Technology*, Volume 243, May 2017, Pages 258-268
- [142] N .B. Yahia, T. Belhadj, S. Brag, A. Zghal, Automatic detection of welding defects using radiography with a neural approach, *Procedia Engineering* Volume 10, 2011, Pages 671-679.
- [143] Ioannis Valavanis, Dimitrios Kosmopoulos, Multiclass defect detection and classification in weld radiographic images using geometric and texture features, *Expert Systems with Applications*, Volume 37, Issue 12, December 2010, Pages 7606-7614.
- [144] K. D Ramkumar, D. Mishra, G. Thiruvengatam, S. P Sudharsa, T. H. Mohan, V. Saxena, R. Pandey, N. Arivazhagan, Investigations on the microstructure and mechanical properties of multi-pass PCGTA welding of super-duplex stainless steel, *Bulletin of Materials Science*, 38(4) (2015) 837–846.



## Appendix-A

Photographic views of all the welded samples (sample no.1 to sample no.15) are illustrated below:





## Appendix-B

The images of X-ray radiography of all the welded samples (sample no.1 to sample no.15) are shown below:

